Pertanika Journal of

# SCIENCE & TECHNOLOGY

JST

VOL. 20 (2) JUL. 2012

PERTANIKA JOURNALS

A scientific journal published by Universiti Putra Malaysia Press

## About the Journal

*Pertanika* is an international peer-reviewed journal devoted to the publication of original papers, and it serves as a forum for practical approaches to improving quality in issues pertaining to tropical agriculture and its related fields. *Pertanika* began publication in 1978 as the Journal of Tropical Agricultural Science. In 1992, a decision was made to streamline *Pertanika* into three journals to meet the need for specialised journals in areas of study aligned with the interdisciplinary strengths of the university. The revamped Journal of Science & Technology (JST) aims to develop as a pioneer journal focusing on research in science and engineering, and its related fields. Other *Pertanika* series include Journal of Tropical Agricultural Science (JTAS); and Journal of Social Sciences and Humanities (JSSH).

JST is published in English and it is open to authors around the world regardless of the nationality. It is currently published two times a year, i.e. in January and July.

### Goal of Pertanika

Our goal is to bring the highest quality research to the widest possible audience.

### Quality

We aim for excellence, sustained by a responsible and professional approach to journal publishing. Submissions are guaranteed to receive a decision within 12 weeks. The elapsed time from submission to publication for the articles averages 5-6 months.

### Indexing of Pertanika

Pertanika is now over 33 years old; this accumulated knowledge has resulted in Pertanika journals being indexed in SCOPUS (Elsevier), EBSCO, DOAJ, AGRICOLA, and CABI etc. JST is indexed in SCOPUS, EBSCO, DOAJ and ISC.

### Future vision

We are continuously improving access to our journal archives, content, and research services. We have the drive to realise exciting new horizons that will benefit not only the academic community, but society itself.

We also have views on the future of our journals. The emergence of the online medium as the predominant vehicle for the 'consumption' and distribution of much academic research will be the ultimate instrument in the dissemination of research news to our scientists and readers.

### Aims and scope

Pertanika Journal of Science and Technology aims to provide a forum for high quality research related to science and engineering research. Areas relevant to the scope of the journal include: *bioinformatics, bioscience, biotechnology and biomolecular sciences, chemistry, computer science, ecology, engineering, engineering design, environmental control and management, mathematics and statistics, medicine and health sciences, nanotechnology, physics, safety and emergency management,* and related fields of study.

### Editorial Statement

Pertanika is the official journal of Universiti Putra Malaysia. The abbreviation for Pertanika Journal of Science & Technology is *Pertanika J. Sci. Technol.*

# Editorial Board

2011-2013

## *Pertanika* Editorial Office

Office of the Deputy Vice Chancellor (R&I), 1st Floor, IDEA Tower II, UPM-MTDC Technology Centre
Universiti Putra Malaysia, 43400 Serdang, Selangor, Malaysia
Tel: +603 8947 1622
E-mail: ndeeps@admin.upm.edu.my
URL: http://www.pertanika.upm.edu.my/editorial_board.htm

## Publisher

The UPM Press
Universiti Putra Malaysia
43400 UPM, Serdang, Selangor, Malaysia
Tel: +603 8946 8855, 8946 8854 • Fax: +603 8941 6172
penerbit@putra.upm.edu.my
URL: http://penerbit.upm.edu.my

# Editorial[1]

## Reflections on Graphene: Horses for courses

**THOUGHTS ON GRAPHENE**: Professor Adarsh Sandhu, Electronics-Inspired Interdisciplinary Research Institute, Toyohashi University of Technology, Japan.

The Nobel Prize in Physics for 2010 was awarded 'for groundbreaking experiments regarding the two-dimensional material graphene', and notably, not for the applications of this material that has sparked the imagination of researchers worldwide.

As Andre Geim is quoted as saying in an interview [1] "….the citation, was given for the properties of graphene; it wasn't given for expectations……Ernest Rutherford's 1908 Nobel Prize in Chemistry wasn't given for the nuclear power station….."

Will the new found properties of graphene and its derivatives yield the definitive applications that spawn new industries and create employment opportunities on the scale associated with the semiconductor industry 21st century? Only time will tell. But what are the issues and trends that will determine its destiny? What do we know now may give us a glimpse into the future. First, Graphene is a single layer of carbon with a honeycomb structure. It is inexpensive and easy to produce: mechanical exfoliation, chemical synthesis or vapour phase deposition [2]. It is ambipolar, namely, the charge carrier concentration can be tuned from electrons to holes. It has remarkably high carrier mobility, with charges travelling 10–100 times faster than silicon at room temperature, and exhibits the quantum Hall effect at room temperature, a signature of its 2D nature [3]. The electrical conduction can be switched on and off in bilayers of graphene, thereby, offering possibilities for electron devices similar to field effect transistors. It is transparent, flexible, and has a high thermal conductivity and high Young's modulus, and for the thinnest material known, it has a strong propensity to absorb light, making it an ultra-thin optical quencher [4]. The surface of graphene can be functionalized with a wide range of biochemical species for potential biosensing applications [5].

But the future of graphene is still difficult to predict. For example, as in the early days of the development of silicon and compound semi-conductors, there is still not a consensus about the most useful method for synthesizing graphene. Mechanical exfoliation yields pristine single layered graphene with excellent transport properties, but this approach is not suited for large scale production.

Chemically derived graphene is a promising alternative, not requiring elaborate and expensive gas handling systems or deposition reactors. The quality and size of the resulting graphene flakes, however, are issues, and the search continues for efficient methods to transfer the reduced-graphene oxide to appropriate substrates. With a view to contributing to this and doping aspects of this

particular topic of research, my group at the Electronics-Research Interdisciplinary Research Institute (EIIRIS) at Toyohashi University of Technology recently demonstrated exploiting the charged nature of graphene oxide (GO) to self-assemble GO-flakes at specifically defined regions on patterned substrates followed by reduction with hydrazine to produce r-GO with the necessity to 'hunt' for flakes on substrates [6,7].

Chemical vapour deposition on metal substrates such as copper, nickel, and iron is a front runner for the production of large areas and large volumes of graphene as exemplified by the report by industrial researchers in Korea on large area stretchable transparent electrodes [8]. In spite of this and related reports, however, transferring graphene to useful substrates is proving a challenge. And, intriguingly, substrate-less or suspended graphene shows much better electrical characteristics, but entails a complicated device fabrication process.

Recently, a two groups reported on an economic and environmentally friendly approach that does not require toxic chemicals, where microbials were used to reduce graphene oxide into graphene [9,10]. Inspired by these reports, in 2012 my group at Toyohashi reported on the use of benign microbials extracted from a local riverside for the reduction of GO into high quality graphene [11]. These results are notable as a means of biologically mediated synthesis of graphene for the development of industrial applications of graphene and related compounds.

In addition to industrial applications such as transparent electrodes for touch screens and displays, bio-chemical sensors and ultra-strong light weight composites, more novel applications in the report of boring nanoholes in graphene, then electrostatically pulling biomolecules such as DNA through the tiny hole, and importantly, monitoring fluctuations of the electrical conductivity of the graphene as the DNA goes through for point of measurement DNA sequencing.

But ultimately, the future of graphene related compounds will be determined by a combination of practical applications with water tight intellectual property rights protecting the 2D world. Compared with the silicon and compound semi-conductor industry, the initial investment in research and development of graphene devices is low, which has resulted in huge number of papers from researchers in Asia-Pacific, where funding and infrastructure for research involving expensive vacuum systems and is not as plentiful as their Western counterparts.

But what about patents? Geim did not patent the initial discovery because of insufficient concrete applications and lack of industrial support [1]. Intriguingly, the Manchester group has been surpassed by other inventors in the submission of patents, with surprisingly groups Asian researchers from Kumoh National Institute of Technology, Samsung, and Sungkyunkwan University leading the league of top 10 university inventors [12].

In my view, the future of graphene will be determined by imaginative ideas, innovation, and the resonance of both these boundary conditions with market needs; a classic scenario of horses for courses.

## References


1. Geim, A. (2010). In praise of graphene. Nature Online, 7 October 2010 (doi:10.1038/news.2010.525).
2. Choi, W., Lahiri, I., Seelaboyina, R. & Kang, Y. S., (2010). Synthesis of Graphene and Its Applications: A Review, Critical Reviews. *Solid State and Materials Sciences*, *35*, 52–71.
3. Peres, N.M.R. (2009). The transport properties of graphene (TOPICAL REVIEW), *J. Phys.: Condensed Matter, 21*, 323201–323211.
4. Bonaccorso, F., Sun, Z., Hasan, T. & Ferrari, A.C. (2010). Graphene photonics and optoelectronics. *Nature Photonics, 4*, 611–622.
5. Pumera, M. (2011). Graphene in Biosensing. *Materials Today, 14*, 308.
6. Ishikawa, R., Masashi B.M., Morimoto, Y. & Sandhu, A. (2010). Patterning of Two Dimensional Graphene Oxide on Silicon Substrates. *Jpn. J. Appl. Phys., 49*, 06GC02–06GC05.
7. Ishikawa, R., Masashi B.,M., Morimoto, Y. & Sandhu, A. (2011). Doping graphene films via chemically mediated charge transfer. *Nanoscale Research Letters, 6*(1), 111.
8. Keun, S.K., Zhao, Y., Jang, H., Lee, S.Y., Kim, J.M., Kim, K.S., Ahn, J.H., Kim, P., Choi, J.Y. & Hong, B.H. (2009). Large-scale pattern growth of graphene films for stretchable transparent electrodes. *Nature 457*, 706–710.
9. Everett, C., Sun, Z., Lüttge, A. & Touret, J.M. (2010). Reduction of Graphene Oxide via Bacterial Respiration. *ACS Nano, 4*, 4852– 4856.
10. Wang, G., Qian, F., Saltikov, C.W., Jiao, Y. & Li, Y. (2011). Microbial Reduction of Graphene Oxide by Shewanella. *Nano Research, 4*, 563.
11. Tanizawa, Y., Okamoto, Y., Tsuzuki, K., Nagao, Y., Yoshida, N., Tero, R., Iwasa, S., Hiraishi, A., Suda, Y., Takikawa, H., Numano, R., Okada, H., Ishikawa, R. & Sandhu, A. (2012). Microorganism mediated synthesis of reduced graphene oxide films. *J. Phys.: Conf. Ser., 352*, 012011–012016.
12. Tannock, Q. (2012). Exploiting carbon flatland. *Nature Mat., 11*, 2–5.



**Adarsh Sandhu**, Ph.D
Presidential Advisor on Internationalization
Deputy Director
Electronics-Inspired Interdisciplinary Research Institute (EIIRIS)
Toyohashi University of Technology

Tel/Fax: +81-532-81-5142
E-mail: sandhu@eiiris.tut.ac.jp

1-1 Hibarigaoka Tempaku-cho, Toyohashi City, Aichi Prefecture 441-8580
EIIRIS: http://www.eiiris.tut.ac.jp/
Lab website: http://www.eiiris.tut.ac.jp/sandhulab/


June 11, 2012

Professor Dr Adarsh Sandhu is Deputy Director of the Electronics-Inspired Interdisciplinary Research Institute (EIIRIS), Toyohashi University of Technology. Other responsibilities at Toyohashi include advisor to the president and head of international public relations. He came to Japan in 1985 after receiving a Monbusho Scholarship to study at the Tokyo Institute of Technology and University of Tokyo. Then, in 1986 after completing his doctoral thesis at the University of Manchester, England, he joined Fujitsu Laboratories Ltd., Atsugi, as their first foreign researcher with a permanent position. At Fujitsu, he developed molecular beam epitaxy systems for the growth of III-V compound semi-conductor heterostructures and quantum effect electron devices. Major breakthroughs included the fabrication of the world's first carbon doped base heterojunction bipolar transistor using gas source MBE and ultra-high resolution magnetic field sensors based on HEMT heterostructures.

In 1992, Dr Sandhu took a sabbatical as a visiting scholar at the Cavendish Laboratory, Cambridge University, where he conducted experiments on the transport properties of semiconductor and superconductor interfaces. In April 1995, he left Fujitsu to take up a tenured faculty position at a private university, where he continued to work on condensed matter physics and initiated research on magnetic imaging of ferromagnetic domains by scanning Hall probe microscopy (SHPM). In August 2002, Dr Sandhu accepted a tenured position at the Quantum Nanoelectronics Research Centre, Tokyo Institute of Technology, where his research activities included nano-scanning Hall probe microscopy and development of biosensors based on magnetic labels for rapid medical diagnosis.

Dr Sandhu is a regular visitor at universities in Asia-Pacific, including Tsinghua University and IIT Delhi, and has collaborative projects with several major Japanese corporations. He is also a member of several important Japanese academic societies including the 162 and 175 committee's the Japan Society for the Promotion of Science (JSPS); Japan Society of Applied Physics (JSAP); and Magnetic Society of Japan (MSJ). Dr Sandhu is the founder of the 'JSAP International' newsletter and has authored numerous articles on science and education for Japanese journals. He has the rare distinction of being a member of the Foreign Correspondents Club of Japan (FCCJ), and FCCJ Toastmasters.

Among his research interests are nanomagnetics, with emphasis on two dimensional electron gas heterostructures for the fabrication of high sensitivity Hall sensors and scanning Hall probe microscopy, and exploitation of magnetically induced self-assembly of magnetic nanoparticles for biomolecular recognition and point of care medical diagnostics.

Dr Sandhu is fluent in Japanese—spoken and written, giving lectures on solid-state physics and electromagnetism in the Japanese. He enjoys most sports and outdoor activities and writing about scientific developments in the Asia Pacific region. Dr Sandhu's travels in Asia and observations of the impact of science and technology in this part of the world form a backdrop to his first novel—scheduled for completion in 2012—set in Beijing, Delhi, and Tokyo. Dr Sandhu has served as Editorial Consultant for *Nature Nanotechnology* and *Nature Photonics,* and editor of research highlights for NPG Asia Materials. He is currently the editor of *IOP Asia-Pacific* website - a platform dedicated to highlighting scientific developments in Asia Pacific.

[1] DISCLAIMER
The views expressed in this article are those of the author and do not necessarily represent the views of, and should not be attributed to, the Pertanika Journal or the Pertanika Editorial Board.

**Pertanika Journal of Science & Technology**
**Vol. 20 (2) Jul. 2012**

# Contents

**Selected Articles from World Engineering Congress 2010: Natural Resources and Green Technology**





**Selected Articles from UPM-Malaysian Nuclear Agency Symposium 2011**

Pertanika J. Sci. & Technol. 20 (2): 197 - 203 (2012)

SCIENCE & TECHNOLOGY

Journal homepage: http://www.pertanika.upm.edu.my/

*Short Communications*

# The *h*-index in Elsevier's *Scopus* as an Indicator of Research Achievement for Young Malaysian Scientists

**Yap, C. K.**

*Department of Biology, Faculty of Science, Universiti Putra Malaysia, 43400 Serdang, Selangor, Malaysia*

## HOW TO MEASURE A SCIENTIST'S RESEARCH PERFORMANCE OUTPUT?

If we were given a questionnaire of "How do we measure a researcher as a true scientist? with optional answers like (a) Having a good number of publications, (b) having attending numerous conferences, (c) with a high popularity as always appeared in mass media, and (d) good international networking and good public relations. Options (c) and (d) always come later after option (a) has been achieved, while option (b) can be simply achieved or abstract be accepted for presentation in any conference. Hitherto, publishing in any peer-reviewed journals carry a certain quality since they are highly subjected to peer review evaluation before the paper can be accepted for publication in a journal. Needless to say, those constructive comments given by the reviewers are very crucial in shaping our scientific understanding in our subject area rather than rejection experience (Yap, 2009). Having said so, option (a) will definitely be the best answer. The fact is that option (a) should not be argued whatsoever as the best answer [since publications speaks louder than anything else] and options (a), (b) and (c) are supplementary criteria to option (a) but they are not as vital as option (a).

When we are asked 'What is your scientific research performance or research output?', the answer could always be 'Having a good number of publications.' Then, the next question forwarded is that 'What is the quality and impact of your published papers to the scientific community?' Of course, good and high impact factor journals always accept papers with high novelty in the subject area. Therefore, papers published in good journals are always highly cited and subsequently resulting in high impact (or citations) of the research done to the scientific community. However, the last question is sometimes very subjective and difficult to answer until *h*-index is introduced and discussed among the researchers. This paper aimed to discuss the *h*-index based on Elsevier's *Scopus* database as an indicator of research achievement for young Malaysian scientists.

*Article history:*
Received: 17 January 2011
Accepted: 4 October 2011

*Email address:*
yapckong@hotmail.com (Yap, C. K.)
*Corresponding Author

ISSN: 0128-7680 

When Hirsch (2005) published his popular and highly cited paper entitled, 'An index to quantify an individual's scientific research output in Proceedings of the National Academy of Sciences of the United States of America' in 2005, the paper was cited 681 times in *Scopus* and 1211 times in Google Scholar, as searched on 8 Nov 2010. This shows the tremendous impacts and concerns of many researchers around the world who really care about what is the true or the best measurement of their research performance output. This is due to the fact that recognition of a researcher varies from university to university, both locally and internationally.

*What is h-index?*

The Hirsch's index (*h*-index) by Jorge Hirsch (Hirsch 2005) was introduced as an indicator of lifetime achievement (since the number will not decrease or change once the number is produced) as measured by the number of received citations. Hirsch (2007) proposed the *h*-index as a better alternative to other bibliometric indicators, such as the number of publications, average number of citations, and sum of all citations. The *h*-index is based on a scientist's lifetime citedness (Seglen 1992), which incorporates productivity as well as citation impacts. According to Hirsch (2005), "A scientist has index *h* if *h* of his or her number of papers published over *n* years (*Np*) have at least *h* citations each and the other ($Np - h$) papers have $\leq h$ citations each." Therefore, all the research papers published by a scientist having at least *h* citations are called the 'Hirsch core' (Rousseau, 2006). Those papers in the 'Hirsch core' are the publications within a scientist's publication list that have the greatest visibility or greatest impact, according to Burrell (2007). Meanwhile, Egghe and Rousseay (2006) stated that the *h*-index is an original and simple new measure that incorporates both quantity and visibility of publications.

The introduction of the *h*-index by the physicist Hirsch (2005) as an indicator for quantifying the research output of scientists has since been discussed and studied theoretically and empirically in a number of disciplines (Bornmann & Daniel 2009). Han *et al*. (2010) compared between the journal impact factors and *h*-indices in the journals of reproduction biology computed from the ISI WoS, and found that the *h*-index (2001-2008) exhibited a positive correlation with a five years' Journal Impact Factor (2004-2008) ($r= 0.64$, $p= 0.001$). This clearly shows the relevance of the *h*-index as an indicator of the scientific performance output of researchers.

Thus, the *h*-index is advantageous since the necessary data for calculation are easy to access in the database without the need for any offline data processing (Batista *et al*., 2006). Perhaps, the most comprehensive review on the advantages and limitations of the *h*-index was reported by Costas and Bordons (2007), as presented in Table 1 below.

The *h*-index has already been used by major citation databases to evaluate the academic performance of individual scientists. Although effective and simple, the *h*-index suffers from some drawbacks that limit its use in accurately and fairly comparing the scientific output of different researchers. These drawbacks include information loss and low resolution; the former refers to the fact that in addition to *h*2 citations for papers in the *h*-core, excess citations are completely ignored, whereas the latter means that it is common for a group of researchers to have an identical *h*-index. Zhang (2009) suggested that *e*-index is a necessary *h*-index

Table 1: Advantages and limitations of the *h*-index as reviewed by Costas and Bordons (2007)

| No. | Advantages | Limitations |
|---|---|---|
| 1. | It combines a measure of quantity (publications) and impact (citations) in a single indicator | There are inter-field differences in typical *h* values due to the differences among the fields in productivity and citation practices, so the *h*-index should not be used to compare scientists from different disciplines. |
| 2. | It allows us to characterize the scientific output of a researcher with objectivity, and therefore, may play an important role when making decisions about promotions, fund allocations and awarding prizes. | The *h*-index depends upon the duration of each scientist's career because the pool of publications and citations increases over time, in order to compare scientists at different stages of their career. |
| 3. | It performs better than other single-number criteria that are commonly used to evaluate the scientific output of a researcher (impact factor, total number of documents, total number of citations, citation per paper rate and number of highly cited papers). | Highly cited papers are important for the determination of the *h*-index, but once they are selected to belong to the top *h* papers, the number of citations they receive is not important anymore. |
| 4. | The *h*-index can be easily obtained by anyone with access to the citation databases, such as *Scopus;* in addition, it is also easy to understand. | Since the *h*-index is easily obtained, the authors run the risk of indiscriminate use, such as relying only on it for the assessment of scientists. Research performance is a complex multifaceted endeavour that cannot be assessed adequately by means of a single indicator. |
| 5. | - | The use of the *h*-index could provoke changes in the publishing behaviour of scientists, such an artificial increase in the number of self-citations distributed among the documents on the edge of the *h*-index. |
| 6. | - | There are also technical limitations, such as the difficulty in obtaining the complete output of scientists with very common names, or whether self-citations should be removed or not. Self-citations can increase a scientist's *h*, but their effect on *h* is much smaller than on the total citation count since only self-citations with a number of citations just >*h* are relevant. |

complement, especially for evaluating highly cited scientists or for precisely comparing the scientific output of a group of scientists having an identical *h*-index. The *e*-index as a complementary to *h*-index has been recently supported by Dodson (2009).

Regardless of the limitations listed in Table 1, and with the many different modifications to h-index suggested in the literature, the h-index is still recommended to be used for our young Malaysian scientists. Although the *h*-index may sometimes not reflect the real publication

citation for a researcher, the *h*-index is still a useful supplementary indicator, enrichment for the bibliometric toolset but not a substitution to the advanced indicator and long recognized standard such as Journal Impact Factor (Han *et al*., 2010).

*Why h-index in Elsevier's Scopus database?*

Elsevier's *Scopus* is the largest searchable abstract and citation database of research literature and selected web sources (Rew, 2010) and for this reason, the *Scopus* database was preferred in this paper. Moreover, *Scopus* databases are only based on cited papers while Google Scholar includes not only the cited papers but also the non-cited ones as well (Bar-Ilan *et al*. 2007). Therefore, *Scopus* is theoretically better in terms of quality of papers inclusion in its database although it could still be subjected to arguments and revisions. Bar-Ilan (2008) compared the *h*-indices of a list of highly-cited Israeli researchers based on citation counts retrieved from the Web of Science (WoS), *Scopus* and Google Scholar. In several cases, the results obtained through Google Scholar are considerably different from the results based on the WoS and *Scopus*. Meanwhile, Bar-Ilan *et al*. (2007) found that *Scopus* and the WoS are comparable in terms of the rankings induced. Some of the differences between the different databases are caused by the differing indexing strategies of the databases. Google Scholar does not have a clear policy, but unlike WoS, it indexes books and proceedings as well, and thus, resulting in citing more than journal papers.

*Why h-index for young researchers in Malaysia?*

The 'number of published papers' and the 'values of *h*-index' can show an evolution of how a researcher is recognized as being a true scientist. Perhaps, the saying 'published or perish' should now be upgraded to 'publish in high impact factor journals with potentially getting good h-index in future'. Here, the *h*-index is suggested to be used as an indicator of a researcher's achievement, particularly for young Malaysian scientists, due to four important points discussed below:

1. Most of the young research-based PhD degree holders in Malaysia (graduated in 2000 and after), both trained locally and overseas, are familiar and encouraged to disseminate their research findings to cited international journals as parts of the prerequisite to earn their PhD degrees. As a matter of fact, those researchers who are trained in Malaysian local universities are equally competitive with those trained overseas and are also able to write good scientific papers that are published in international cited journals (personal communication with Dr. Ahmad Zaharin Aris, the youngest PhD degree holder who graduated from Universiti Malaysia Sabah at the age <30).

2. Since *h*-index is highly dependent on the seniority of a researcher, a young researcher should have accumulated citations in order to get a high *h*-index. Of course, this is also continually being affected by several factors such as popularity of the research area, name of the journals and year or time when the paper was first published. Some papers were highly cited when it was newly published but less cited after a period of time. This could be due to the different subject area or field of study. For example, the *h*-index in biological

sciences tends to be higher than that in physics (Hirsch, 2005). Therefore, a range of the *h*-index value should be quantified for a specific field of study when a researcher is qualified to be promoted as an associate professor and a full professorship. Hirsch (2005) suggested that for faculty at major research universities, the *h*-index 12 might be a typical value for advancement to tenure (associate professorship) and that *h*-index 18 might be a typical value for advancement to full professorship.

3. There are only citations received since the year 1996 in *Scopus*. Prior to that, it was rather unfair for the old timer researchers to compare their number of citations or *h*-index with those researchers (usually those of the younger generation) who published their papers after 1996. To exemplify this, a young researcher from Japan named Assoc. Prof. Dr. Takaomi Arai (age < 40 years), who has published 83 papers in *Scopus* with an *h*-index of 16 as compared to a truly recognized academician in Malaysia, an old timer researcher (age > 60 years) named Prof. Dr. Tan Soon Guan (TSG) who has had a total of 119 papers in *Scopus* with an *h*-index of 17 (the above search was done on 26 November 2010 in *Scopus*). The first papers by Arai and TSG in *Scopus* were found to have been published in 1997 and 1976, respectively. Another good comparative example is between an excellent and highly profiled researcher in UPM, Prof. Dr. Yaakob Che Man (age > 50 years) and a young researcher (age < 40 years), Assoc. Prof. Dr. Tan Chin Ping (UPM), who had won the prestigious Prosper.Net-*Scopus* Young Scientist Award in Sustainable Development recently in Shanghai, China, on 5th July 2010 in the category of Agriculture and Food Security. Prof. Yaakob has a total number of 203 papers published in *Scopus* with an *h*-index of 19 while Dr. TCP has 105 publications with an *h*-index of 16. The first papers by Prof. Yaakob and TCP in *Scopus* were found published in 1991 and 1999, respectively (the search in *Scopus* for the last two researchers was done on 3rd December 2010). Therefore, I believe that Prof TSG's and Prof. Yaakob's *h*-indices should have simply reached at least more than 25 if the citations before 1996 were to be fully obtained in *Scopus*.

4. Since the number of publications sometimes does not reflect the impacts of the published works, the *h*-index should be employed to check the impact of the papers published apart from their quantity. Further details of the advantages of the *h*-index can be found in Table 1.

## CONCLUSION

As a final note on this short note paper, I personally foresee the importance of the *h*-index for our Malaysian scientists as a good indicator to quantify an individual's scientific research output (Hirsch, 2005; Bornmann *et al*., 2010). Having reviewed all the above literature, in conclusion, I highly recommend the use of the *h*-index as a better and transparent indicator to complement the number of citations and the number of papers published. Regardless of the criticisms on the accuracy of *h*-index, including not taking into account the citation counts of papers with fewer than *h* citations as reviewed by Bornmann *et al*. (2010), this *h*-index-based bibliometric evaluation should still be ideally and routinely implemented as a must for the promotion committee in evaluating the academic performance of individual scientist, especially the young ones at all universities in Malaysia (be it governmental or non-governmental universities) if

Malaysia was to be recognized as one of the top research-based centre in this region. Certainly, a single indicator can never give more than a rough approximation to an individual's multifaceted profile, and therefore, many other factors should be taken into consideration in combination to evaluating an individual's performance output. This communication paper may potentially shed light to more literature-based studies on the proposed ranges of *h*-index for different academic achievements according to the field of study or subject area.

## ACKNOWLEDGMENTS

I would like to thank Assoc. Prof. Dr. Takaomi Arai and Dr. Ahmad Zaharin Aris for stimulating and useful discussion on this topic.

## REFERENCES

Bar-Ilan, J. (2008). Which *h*-index? – A comparison of WoS, Scopus and Google Scholar. *Scientometrics, 74*(2), 257–271.

Bar-Ilan, J., Levene, M., & Lin, A. (2007). Some measures for comparing citation databases. *Journal of Informetrics, 1*, 26–34.

Batista, P. D., Campiteli, M. G., Kinouchi, O., & Martinez, A. S. (2006). It is possible to compare researchers with different scientific interests? *Scientometrics, 68*, 179-189.

Bornmann, L., & Daniel, H. D. (2009). The state of *h* index research. Is the *h* index the ideal way to measure research performance? *EMBO Reports, 10*(1), 2–6.

Bornmann, L., Mutz, R., & Daniel, H. (2010). The *h* index research output measurement: Two approaches to enhance its accuracy. *Journal of Informetrics, 4*, 407–414.

Burrell, Q. L. (2007). On the *h*-index, the size of the Hirsch core and Jin's *A*-index. *Journal of Informetrics, 1*(2), 170–177.

Costas, R., & Bordons, M. (2007). The h-index: Advantages, limitations and its relation with other bibliometric indicators at the micro level. *Journal of Informetrics, 1*, 193–203.

Dodson, M. V. (2009). Citation analysis: Maintenance of *h*-index and use of *e*-index. *Biochemical and Biophysical Research Communications, 387*, 625–626.

Egghe, L., & Rousseay, R. (2006). An informatric model for the Hirsch-index. *Scientometrics 69,* 121-129.

Han, W., Yu, Q., & Wang, Y. (2010). Comparative analysis between impact factor and *h*-index for reproduction biology journals. *Journal of Animal and Veterinary Advances, 9*(11), 1552-1555.

Hirsch, J. E. (2005). An index to quantify an individual's scientific research output. *Proceedings of the National Academy of Sciences of the United States of America, 102,* 16569–16572.

Hirsch, J. E. (2007). Does the h index have predictive power? *Proceedings of the National Academy of Sciences of the United States of America, 104*(49), 19193–19198.

Rew, D. (2010). Editorial: SCOPUS: Another step towards seamless integration of the world's medical literature. *EJSO, 36*, 2-3.

Rousseau, R. (2006). New developments related to the Hirsch index. *Science Focus, 1*(4), 23–25.

Seglen, P. O. (1992). The skewness of science. *Journal of the American Society for Information Science, 43*(9), 628–638.

Yap, C. K. (2009). Acceptance and rejection of peer-reviewed articles in environmental sciences: My personal publication experience. *Pertanika Journal of Tropical Agricultural Science, 32*(1), 25-27.

Zhang, C. -T. (2009). The *e*-Index, complementing the *h*-Index for excess citations. *PLoS ONE 4*(5): e5429.

Pertanika J. Sci. & Technol. 20 (2): 205 - 219 (2012)

SCIENCE & TECHNOLOGY

Journal homepage: http://www.pertanika.upm.edu.my/

# The Effects of Rainfall Event and Land Use Characteristics on River Basin Hydrological Response: A Case of Sg. Kayu Ara, Malaysia

**Alaghmand, S.[1*], Abdullah, R.[1], Abustan, I.[1], and Vosoogh B.[2]**

*[1]School of Civil Engineering, Universiti Sains Malaysia (USM), Nibong Tebal, 14300, Pulau Pinang, Malaysia*

*[2] Department of Water Engineering, Gorgan University of Agricultural Sciences and Natural Resources, Iran*

## ABSTRACT

As a crucial demand in urban areas, flood risk management has been considered by researchers and decision makers around the world. In this case, hydrological modelling that simulates rainfall-runoff process plays a significant role. This paper quantified the roles of three main parameters in river basin hydrological response, namely, rainfall event duration, rainfall event ARI (magnitude) and land-use development condition. The case study area of this research was Sungai Kayu Ara basin which is located in the western part of Kuala Lumpur, Malaysia. A total of twenty seven scenario were defined for this research, including three different rainfall event durations (60, 120 and 360 minutes), three different ARIs (20, 50 and 100 years) and in three different land-use conditions (existing, intermediate and ultimate). The results of this research indicate that rainfall event duration, rainfall event ARI (magnitude) and land-use development condition have considerable effects of the surface runoff hydrographs in terms of peak discharge and volume.

**Keywords: Hydrological modelling, rainfall duration, rainfall ARI, land-use development, Sungai Kayu Ara**

*Article history:*
Received: 29 January 2010
Accepted: 18 January 2012

*Email addresses:*
sina.wm06@student.usm.my (Alaghmand, S.),
cerozi@eng.usm.my (Abdullah, R.),
ceismail@eng.usm.my (Abustan, I.)
*Corresponding Author

## INTRODUCTION

Water is a basic requirement for sustaining life and development of a society. Nonetheless, proper management, protection and development of water resources are challenges imposed by population growth, increasing pressure on water and land resources by competing usage, and degradation of scarce water resources in many parts of the world.

ISSN: 0128-7680 

River flood is defined as a high flow that exceeds or over-tops the capacity, either the natural or the artificial banks of a stream (Hoyt & Langbein, 1958; Walesh, 1989; Knight & Shiono, 1996; Omen *et al*., 1997; Smith & Ward, 1998). Floods occur due to excessive rain on land, streams overflowing channels or unusually high tides or waves in coastal areas. Some of the most important factors that determine the features of floods are rainfall event characteristics, depth of the flood, velocity of the flow, and duration of the rainfall event (Smith, 1996). Most floods are caused by intense precipitation, in combination with other factors, such as snow melt, inadequate drainage, water-saturated ground or unusually high tides or waves. Floods are the most damaging phenomena that affect both the social and economic aspects of the population (Smith & Ward, 1998).

There is a relationship between urbanization and hydrological characteristics, such as decrease of infiltration, increase of overland flow, increase in frequency and height of flood peak, increase in range of discharge (variability) and decrease lag time. The dangers of floodwaters are associated with a number of different characteristics of the floods, such as depth of water, duration, velocity, sediment load, as well as rate of rise and frequency of occurrence (Kingma, 2002).

In most cases, floods are additionally influenced by human factors. Although these influences are very diverse, they generally tend to aggravate flood hazards by accentuating river flood peaks. Thus, river flood hazards in built environments have to be seen as the consequence of the natural and man-made factors. The factors contributing to river floods can be categorized into three classes, namely; meteorological factors, hydrological factors and human factors, as shown in Table 1.

Hydrological models are regarded as powerful tools for predicting river basin response to rainfall events and assessment of the impacts of parameters such as land-use cover change on river basin hydrology (Whitehead & Robinson, 1993).

Hydrological modelling is a powerful technique of hydrologic system investigation for both the research hydrologists and practicing water resources engineers who are involved in the planning and development of integrated approach for management of water resources. In the recent years, hydrological processes in the river basins have increasingly been studied in order to quantify the possible impacts of changes in land-use, land cover or soil surface conditions and urbanization on river basin hydrological processes, water quality, as well as extreme hydrological events, such as floods and droughts. The objective of the present study was to illustrate the effects of rainfalls and land-use characteristics on hydrological response of a rural basin. To this aim, three factors were considered including rainfall duration, rainfall ARI and percentage of imperviousness. Hydrological response of the river basin to the rainfall and land-use characteristics were evaluated quantitatively based on runoff peak and volume at the outlet of the river basin.

## CASE STUDY

Sungai Kayu Ara basin is the case study in this research, and it is located in Kuala Lumpur, Malaysia. Sungai Kayu Ara basin covers an area of 23.22 $km^2$. The main river of this river basin originates from the reserved highland area of Penchala and Segambut. Sungai Kayu Ara

Table 1: Factors contributing to river floods

| Meteorological factors | Hydrological factors | Human factors |
|---|---|---|
| • Rainfall<br>• Cyclonic storms<br>• Small-scale storms<br>• Temperature<br>• Snowfall and snowmelt | • Soil moisture level<br>• Groundwater level prior to storm<br>• Natural surface infiltration rate<br>• Presence of impervious cover<br>• Channel cross-sectional shape and roughness<br>• Presence or absence of over bank flow, channel network<br>• Synchronization of run-offs from various parts of watershed<br>• High tide impeding drainage | • Surface sealing due to urbanization, deforestation) increase run-off and may be sedimentation<br>• Occupation of the flood plain obstructing flows<br>• Inefficiency or non-maintenance of infrastructure<br>• Too efficient drainage of upstream areas increases flood peaks<br>• Climate change affects magnitude and frequency of precipitations and floods<br>• Urban microclimate may enforce precipitation events |

basin is geographically surrounded within N 3°6′ to N 3°11′ and E 101°35′ to E 101°39′. Fig.1 illustrates the boundaries of Sungai Kayu Ara basin in the western Kuala Lumpur, Malaysia.

The Sungai Kayu Ara basin is a suitable study river basin for this particular research because of the following reasons: firstly, a large part of this particular river basin area is a well developed urban area with different land uses and also high population density (parts of the Kuala Lumpur rural area) that shows the importance of this river basin; secondly, the availability of high density rainfall station network (10 rainfall stations and one water level station), and according to the area of Sungai Kayu Ara basin (23.22 $km^2$), the rainfall station network density is equivalent to 2.3 $km^2$/station, which justifies the minimum requirement of one station per 25 $km^2$ in case of precipitation over small mountainous river basins (Linsley *et al*., 1992); thirdly, the availability of stage discharge curve which has been developed by the DID, Malaysia, and finally, the availability of river basin digital topographic information which can be used in Geography Information System (GIS). This data have been produced by the Department of Survey and Mapping, Malaysia. Table 2 shows the area and the percentage of the coverage types of land-use (Leong, 2007).

## MATERIALS AND METHODS

In this research, HEC-HMS3.1.0 was used as the hydrological model. HEC-HMS3.1.0 is a hydrological model developed by the Hydrologic Engineering Centre of the United States Army Corps of Engineers. In fact, HEC-HMS is a well-known hydrological computer model, which is considered as one of the most utilized hydrological models in water cycle studies (Yawson *et al*., 2005; Cunderlik & Simonovic, 2005; Stehr *et al*., 2008; Ellouze *et al*., 2009). The programme simulates a rainfall-runoff response of a river basin system to a precipitation


Fig. 1: The location and base-map of Sungai Kayu Ara in Malaysia

Table 2: Area and Percentage of the Coverage Types of Land-use in Sungai Kayu Ara Basin

| Types of land-use | Area ($Km^2$) | Coverage percentage (%) |
|---|---|---|
| Rural residential | 1.60 | 6.90 |
| Urban residential | 11.61 | 50.00 |
| Central business district | 1.16 | 5.00 |
| Cultivated land | 3.25 | 14.00 |
| Cleared land | 1.70 | 7.30 |
| Forest | 0.39 | 1.70 |
| Park and lawn | 1.93 | 8.30 |
| Shrub land | 0.21 | 0.90 |
| Miscellaneous | 1.37 | 5.90 |
| Total | 23.22 | 100 |

input by representing the entire river basin as an interconnected system of hydrologic and hydraulic components, which include river basins, streams and reservoirs (HEC-HMS, 2006). Green-Ampt, Snyder unit hydrograph, recession and kinematic wave methods were selected and applied for the rainfall-runoff simulation in Sungai Kayu Ara basin. Some of the inputs were prepared and computed using HEC-GeoHMS, such as river basin sub-division, river network extraction, calculation of area, river basin perimeter, and slope of sub-river basin and river network (Fig. 2).

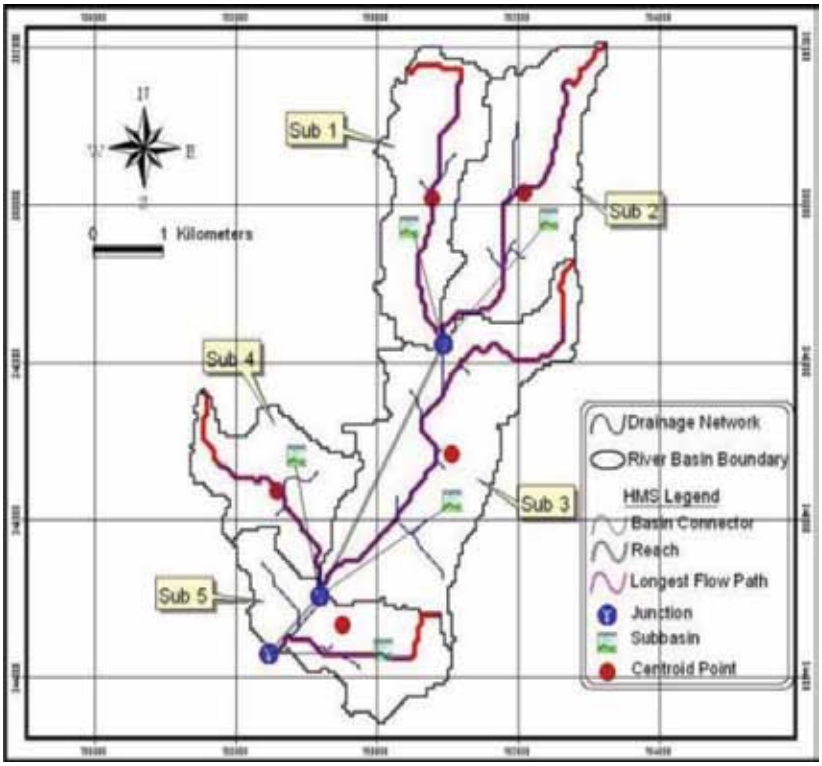


Fig.2: The characteristics of the Sungai Kayu Ara basin generated by HEC-GeoHMS

The identification of the hydrological model in the transformation of rainfall to runoff is related to river basin processes. Therefore, the most important data for hydrological modelling are recorded time series of rainfall and runoff. There were 10 rain gauges installed within the Sungai Kayu Ara river basin. These rain gauges are self-recording and the rainfall data were stored in the built-in data logger memory. Meanwhile, the amount of the recorded rainfall was based on the frequency of the series of tips (tipping budget rain gauges) generated by rainwater. Such information is useful to determine rainfall intensity, rainfall duration and daily total rainfall. The hydrological record was retrieved on site using SRAM (Static Random Access Memory) Card by the DID staff. Furthermore, all data were converted into the Time Dependent Data Processing System (TIDEDA®) in the DID hydrology unit. The software system was developed and supplied by the National Institute of Water and Atmosphere Research of New Zealand (NIWA) and version 1.9 is currently being used. The DID Hydrology Unit, at Jalan Ampang, Kuala Lumpur, was the main reference for extracting the required data in this research. The location for the rain gauges and the water level station at the Sungai Kayu Ara river basin is illustrated in Fig.3. In order to assess the data related to the runoff of the Sungai Kayu Ara river basin, the water level record from station No.3111404 (WL4 in Fig.3) located at Taman Mayang, Damansara was also downloaded from DID. These recorded water stage data were transferred from the water level station to the DID Hydrology Unit through a telemetry system. The stage-discharge data were provided by DID, which were developed using the record at the water level station.

The basic step for the development and application of a model is establishing of the credibility of the model which comprises of sensitivity analysis, calibration and validation processes. The results derived from the sensitivity analysis for the HEC-HMS in Sungai Kayu Ara basin revealed that imperviousness, initial discharge of recession method, peak flow coefficient, lag-time, hydraulic conductivity, moisture deficit and wetting front suction were the most effective on the runoff volume (with more than 5% changes). On the other hand, lag-time, imperviousness, peaking flow coefficient, hydraulic conductivity, moisture deficit, wetting front suction and initial discharge were more important parameters on the runoff peak discharge (with more than 5% change). These parameters must be taken into consideration and focused on during hydrological modelling.

Among the recorded rainfall and water level time series obtained from rainfall and water level stations, 18 rainfall events were selected for calibration and 18 rainfall events for validation process (Fig.3). By applying the 18 calibration rainfall events dataset, the best set of values for each parameter was identified to best represent the hydrologic model of the Sungai Kayu Ara basin. Meanwhile, the credibility of the hydrological model was evaluated using 18 validation rainfall event datasets. The result of the calibration process for one of the calibration events is illustrated in Fig.4.

The established hydrological model for Sungai Kayu Ara basin was simulated based on the rainfall design hyetograph for each ARI (20, 50 and 100 years) and different durations (60, 120 and 360 minutes) in the existing, intermediate and ultimate river basin land-use development

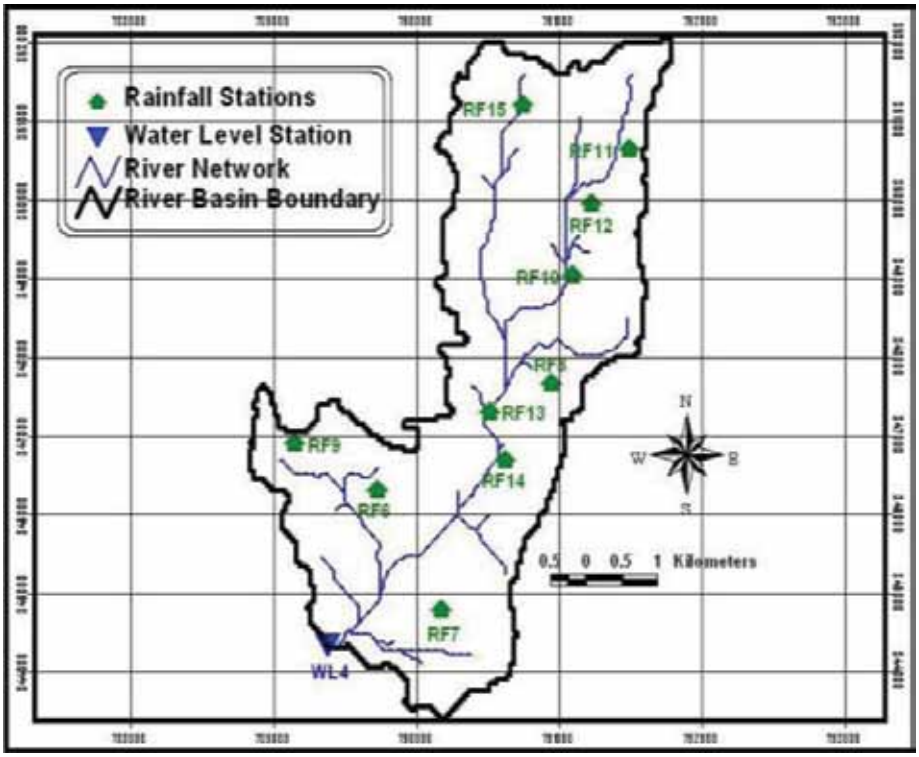


Fig.3: The location of the rainfall and water level stations at Sungai Kayu Ara basin

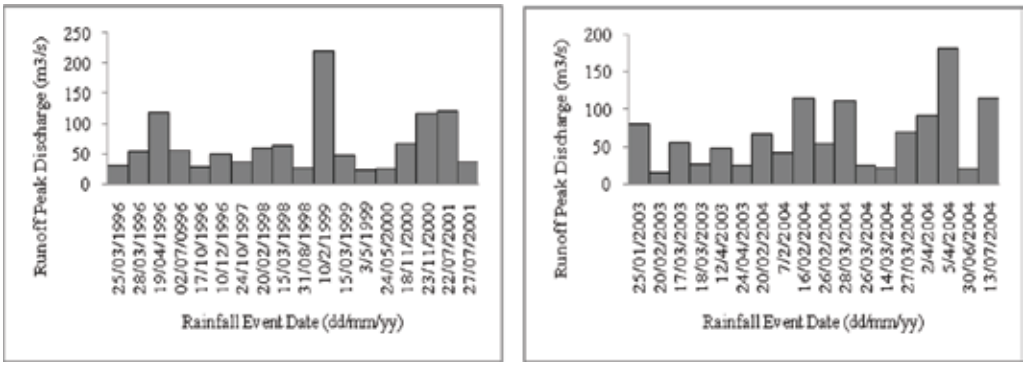


Fig.4: The selected rainfall events for the hydrologic model calibration and validation processes

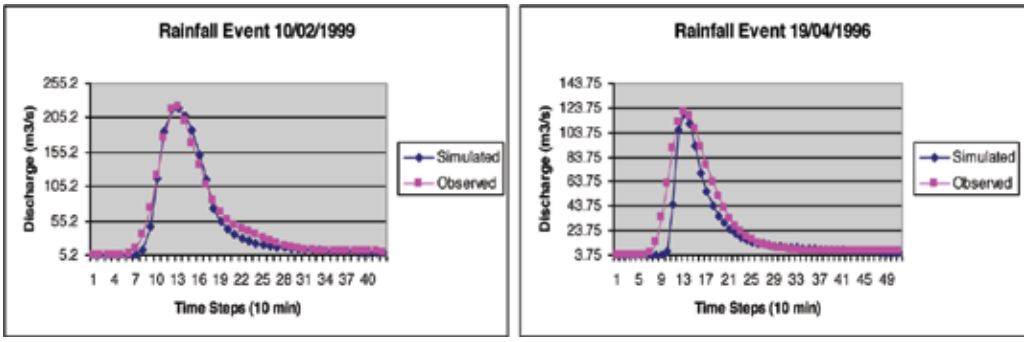


Fig.5: The calibration result for the rainfall event of 10/02/1999 and 19/04/1996

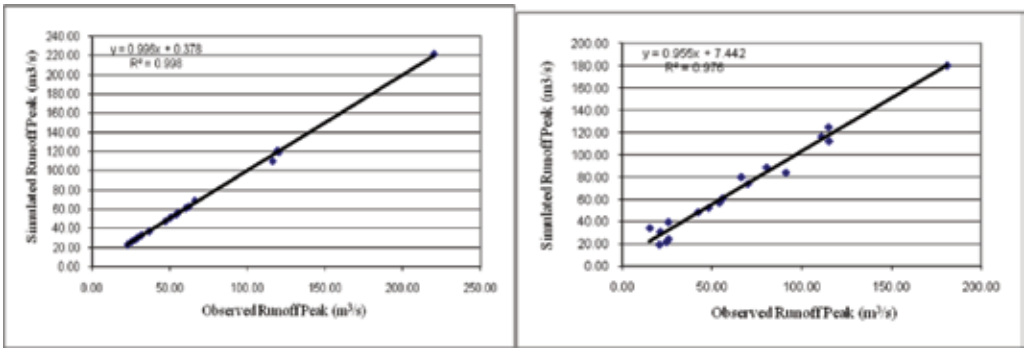


Fig.6: The correlation of the observed and simulated run-off peak discharge in the calibration and validation processes

conditions which were derived based on the storm water management manual (DID, 2000). A total of twenty seven direct run-off hydrographs were produced by the hydrological model. The effects of the different land-use development conditions and the rainfall event characteristics (ARI and duration) were assessed and investigated. Table 3 indicates the total defined study scenarios of this research.

Table 3: Scenarios of the hydrological modelling for Sungai Kayu Ara basin

| Land-use development condition | 20 years ARI | 50 year ARI | 100 year ARI |
|---|---|---|---|
| Existing | 1 hr | 1 hr | 1 hr |
| | 2 hr | 2 hr | 2 hr |
| | 6 hr | 6 hr | 6 hr |
| Intermediate | 1 hr | 1 hr | 1 hr |
| | 2 hr | 2 hr | 2 hr |
| | 6 hr | 6 hr | 6 hr |
| Ultimate | 1 hr | 1 hr | 1 hr |
| | 2 hr | 2 hr | 2 hr |
| | 6 hr | 6 hr | 6 hr |

This research focused on the three scenarios of river basin land-use development conditions, namely, existing, intermediate and ultimate. To this end, three types of the land-use coverage percentages were applied in the HEC-HMS hydrologic model. Table 4 shows the percentage of the imperviousness area in each sub-river basin for each development condition in Sungai Kayu Ara basin.

Finally, the hydrological simulation was applied for three scenarios development conditions (existing, intermediate and ultimate), and each development condition consisted of three different ARIs (20 years, 50 years and 100 years) with three event durations (60 minutes, 120 minutes and 360 minutes).

Table 4: The percentage of the impervious area in each sub-river basin

| Development Condition | Imperviousness (%) | | |
|---|---|---|---|
| | Existing | Intermediate | Ultimate |
| Sub-River Basin 1 | 25 | 50 | 90 |
| Sub-River Basin 2 | 25 | 50 | 90 |
| Sub-River Basin 3 | 65 | 80 | 90 |
| Sub-River Basin 4 | 35 | 70 | 90 |
| Sub-River Basin 5 | 65 | 80 | 90 |

## RESULTS AND DISCUSSION

The hydrological models, such as HEC-HMS, simulate the hydrograph of the generated runoff caused by a rainfall event. Based on this definition of hydrological modelling, the main input for the hydrological model is rainfall event hyetograph. Beside rainfall event hyetograph, some values for various components parameters are required, as discussed in the previous section. To simulate the HEC-HMS for Sungai Kayu Ara basin, input design rainfall hyetograph is required for each scenario. The input hyetograph for each scenario, with a total of 36 rainfall hyetographs, was extracted according to the storm water management manual (DID, 2000). Table 5 shows the results of the HEC-HMS simulation for all 36 scenarios, it is clear that the runoff peak discharge and runoff volume were calculated for each scenario.

Table 5: Results of the HEC-HMS3.1.0 for the 36 scenarios

| Development condition | Duration | ARI20year | | ARI50year | | ARI100year | |
|---|---|---|---|---|---|---|---|
| | | Runoff peak ($m^3/s$) | Runoff volume ($1000m^3$) | Runoff peak ($m^3/s$) | Runoff volume ($1000m^3$) | Runoff peak ($m^3/s$) | Runoff volume ($1000m^3$) |
| Existing | 1 hr | 368.7 | 1856 | 413.1 | 2107 | 460 | 2354 |
| | 2 hr | 319.9 | 2197 | 357.6 | 2480 | 397.6 | 2761 |
| | 6 hr | 246.1 | 2426 | 277 | 2697 | 306.73 | 3052 |
| Intermediate | 1 hr | 396.5 | 2088 | 441.2 | 2254 | 488.1 | 2486 |
| | 2 hr | 347.3 | 2428 | 384.9 | 2696 | 425 | 2980 |
| | 6 hr | 270.8 | 2856 | 301.5 | 3124 | 331.3 | 3472 |
| Ultimate | 1 hr | 427.9 | 2164 | 472.6 | 2417 | 519.5 | 2683 |
| | 2 hr | 378 | 2649 | 416 | 2938 | 456.1 | 3225 |
| | 6 hr | 298.6 | 3280 | 325 | 3692 | 359 | 3960 |

## ROLE OF RAINFALL EVENT DURATION

Duration is one of the most important characteristics of the rainfall event which can significantly affects on the generated runoff hydrograph. In order to investigate on the role and the importance of the rainfall event duration on the river basin hydrological response, three different rainfall event durations were defined, namely, 60 minutes, 120 minutes and 360 minutes. As depicted in Table 5, the increase in the rainfall events duration, i.e. from 60 minutes to 360 minutes in the same rainfall magnitude (ARI) and land-use development condition, reduces the runoff peak discharge and runoff volume.

For instance, the runoff peak discharge for 60 minutes rainfall event with 20 years ARI in the existing land-use development condition is $368.7m^3/s$, and this was $246.1m^3/s$ for 360 minutes' rainfall event. This shows that the increase of the rainfall event duration from 60 minutes to 360 minutes will to 33% reduction in runoff peak discharge in this case. On the other hand, the runoff volume for the above mentioned rainfall events were $1856000m^3$ and $2426000m^3$, respectively, indicating that the increase of the rainfall event, from 60 minutes to 360 minutes, will increase the runoff volume up to 30%. By considering to other values for the runoff peak discharge and the volume, it is obvious that the increase of the rainfall event duration will lead to a decrease in the runoff peak discharge and the increase of the runoff volume. Fig.7 illustrates the generated runoff hydrographs for different durations of the rainfall events (20, 50 and 100 years ARI) in the existing land-use development condition.

As shown in Fig.7, it appears that the rainfall event with shorter duration has a sharper shape compared with those with longer durations. In other words, shorter rainfall event reaches the peak discharge and comes down faster than those with longer rainfall event. As for the longer rainfall duration, the runoff hydrograph has a gentle slope in both rising and falling limbs of the runoff peak discharge. In term of the runoff volume, it was revealed that longer rainfall event contributed more amount of rainfall but it was distributed in a longer time period. Hence, the rainfall event with longer duration has lower peak discharge and higher runoff volume in comparison to those with shorter rainfall events. It also indicates that the rainfall event with

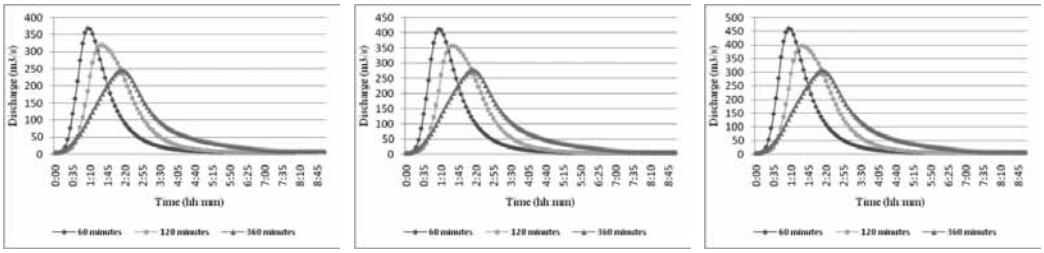


a. 20 years ARI b. 50 years ARI c. 100 years ARI

Fig.7: The runoff hydrographs for the rainfall events with 20, 50 and 100 years ARI in the existing land-use development condition with different durations

longer duration has less intensity in compare with rainfall event with shorter duration in similar ARI and land-use development condition.

Moreover, rainfall event duration has a considerable effect on the time to peak of the runoff hydrograph. For example, for the rainfall event with similar ARI in the existing land-use development condition with 60 minutes, 120 minutes and 360 minutes durations, the times to peak were found to be 1 hour and 5 minutes, 1 hour and thirty five minutes, and two hours and fifteen minutes, respectively. In other words, shorter rainfall event duration causes shorter time to peak, while longer duration leads to a longer time to peak (see Fig.7).

*Role of the Rainfall Event ARI*

The other rainfall event characteristic which was investigated in this research was the rainfall event ARI (magnitude). As depicted in Table 5, the rainfall event ARI apparently plays an important role in the river basin hydrological response. As an example, for a 60 minutes' rainfall event in existing land-use development condition for 20 years, the ARI peak discharge is 368.7$m^3$/s, whereas this value (ARI) is 460 $m^3$/s for 100 years. In other words, the increase in the rainfall event ARI from 20 to 100 years increases the runoff peak discharge up to 25%. In term of the runoff volume, the same trend can be observed. This is because the volume increases from 1856000$m^3$ to 2354000$m^3$ for the above mentioned rainfall events runoff when the rainfall event ARI which is equivalent to 26% increases. Fig.7 demonstrates the generated runoff hydrographs for the different rainfall events ARI with different durations of 60 minutes, 120 minutes and 360 minutes in the existing river basin land-use development condition.

Fig.7 illustrates the effects of the rainfall event ARI on the generated runoff hydrographs for the different rainfall durations in the existing river basin land-use development condition. It is important to note that this particular trend is the same for other land-use development conditions. In addition, Fig.7 also depicts that the rainfall ARI does not have any consequence on the time to peak of the rainfall hydrograph. To sum up, it has been proven that rainfall event ARI has a direct relation with runoff peak and volume. In other words, with the increase in the rainfall event ARI, the runoff peak discharge and volume will increase as well.

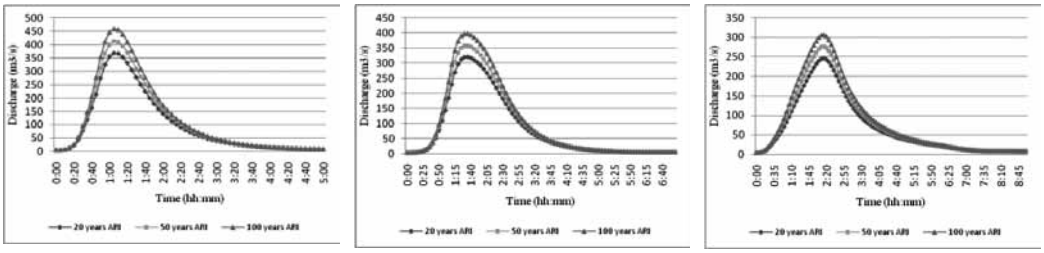


a. 60 minutes b. 120 minutes c. 360 minutes

Fig.8: The runoff hydrographs for different durations of 60 minutes, 120 minutes and 360 minutes in the existing land-use development condition with different ARIs

*Role of River Basin Land-use Development Condition*

In order to study on the responsibility of the river basin land-use development condition on the river basin hydrological response, three types of land-use scenarios were defined; the existing, intermediate and ultimate. These land-use scenarios were differentiated based on the percentages of imperviousness (Table 4). The results presented in Table 5 clarify that the river basin land-use development from the existing to the ultimate condition increases the runoff peak discharge and the runoff volume as well. As evidenced, the runoff peak discharge for the 60-minute duration rainfall event with 20 years ARI in the existing condition is 368.7$m^3$/s, while this value for the same rainfall event in the ultimate condition is higher, i.e. 427.9$m^3$/s, revealing a 16% of increase. Beside this, runoff volume is also influenced by the development changes as well as the runoff peak discharge as the runoff volumes for the above mentioned rainfall events are 1856000$m^3$ and 2164000$m^3$, respectively. In other words, in the case of Sungai Kayu Ara, the increase in development from the exiting to the ultimate condition will lead to 16% increase in the runoff volume. The reason relies on the increase of imperviousness percentage caused by the river basin land-use development. Increasing the imperviousness percentage of the river basin, the percentage of the generated surface runoff by a specific rainfall event is also increased. This also means that more developed river basin contributes to higher amount of runoff in terms of peak discharge and volume. Meanwhile, changes can be observed in the trend of the generated runoff hydrographs, as illustrated in Fig.8-10, which demonstrate the runoff hydrographs for all the twenty seven defined scenarios.

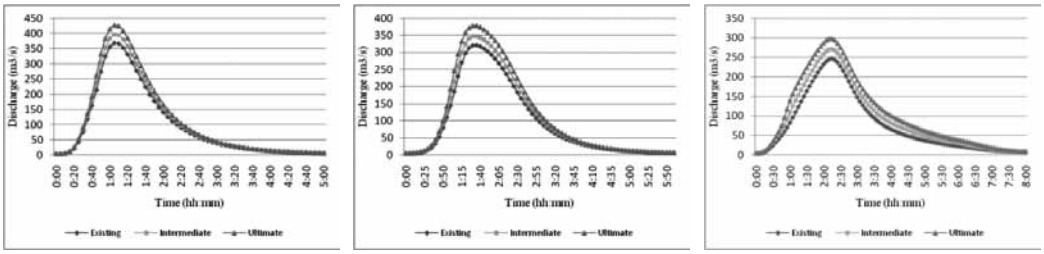


60 minutes b. 120 minutes c. 360 minutes

Fig.9: The runoff hydrographs for the rainfall events with 20 years ARI in different development conditions at Sungai Kayu Ara basin

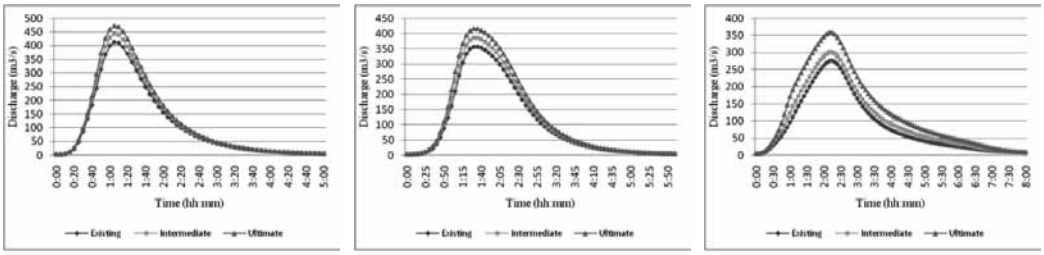


a. 60 minutes b. 120 minutes c. 360 minutes

Fig.10: The runoff hydrographs for the rainfall events with 50 years ARI in different development conditions in Sungai Kayu Ara basin

As depicted in Fig.8-10, changes in land-use development apparently have obvious effects on the river basin hydrological response. In fact, land-use development has a direct relation with both the runoff peak discharge and volume. Hence, for the rainfall events with similar duration and ARI, the runoff peak discharge and volume are higher in the ultimate development condition as compared to the existing condition.

Time to peak is another runoff hydrograph characteristic which is considerable beside runoff peak and volume. Based on the information given in Table 5 and Fig.8-10, it can be approved that land-use development is not responsible for the time to peak changes for the rainfall events with similar duration and ARI. Hence, it must be noted that the quantitative results of the effects of land-use development in this research were investigated based on Sungai Kayu Ara basin or any river basin with similar land-use development condition.

*The Multi-relationship between Rainfall Duration, ARI and Land-use Condition for Sungai Kayu Ara Basin*

The results of this research have given a better understanding of the effects of the rainfall event characteristics and river basin land-use development on river basin hydrological response. According to these results, it is possible to investigate on a multi-relationship between rainfall duration, rainfall ARI, land-use development and runoff peak discharge and volume for Sungai Kayu Ara basin (Fig.11 and Fig.12).

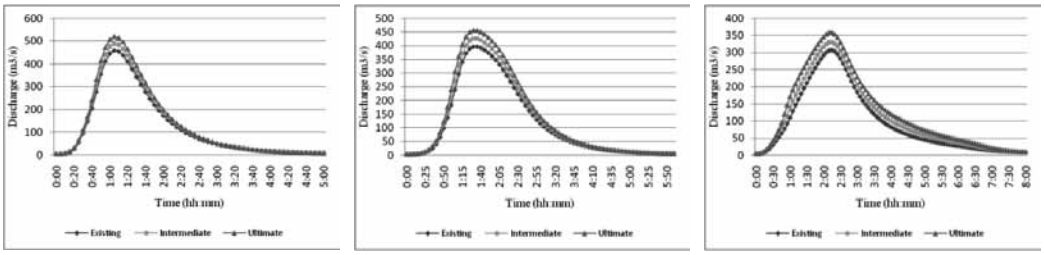


a. 60 minutes b. 120 minutes c. 360 minutes

Fig.11: The runoff hydrographs for the rainfall events with 100 years ARI in different development condition at Sungai Kayu Ara basin

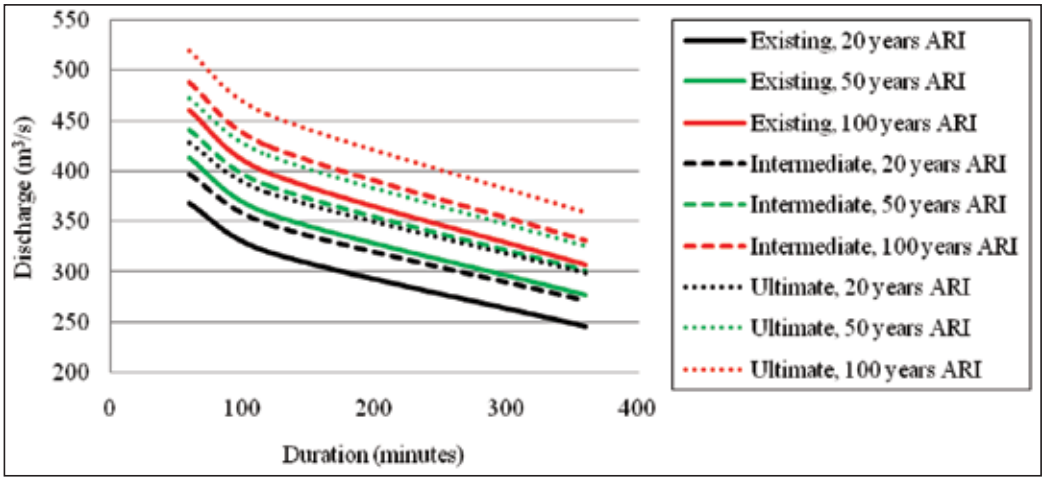


Fig.12: The relationships between rainfall duration, rainfall ARI, land-use development and runoff peak discharge for Sungai Kayu Ara basin

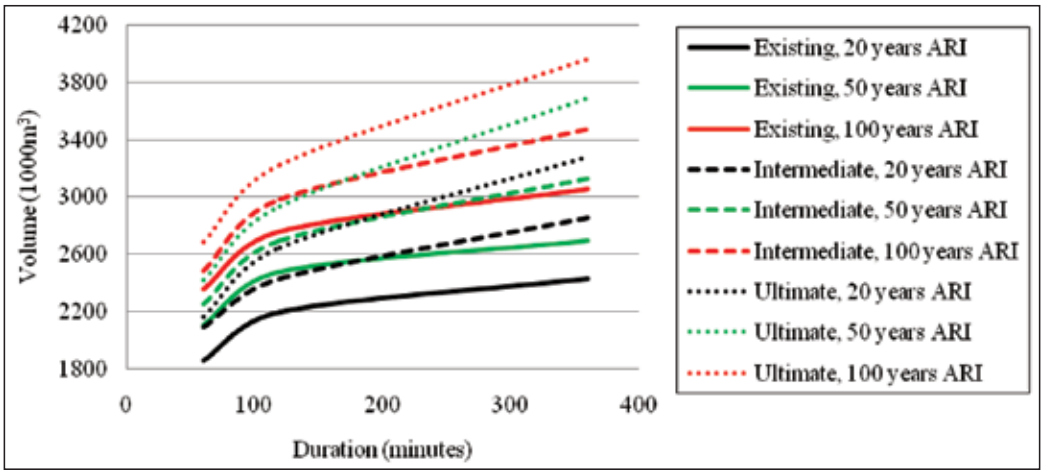


Fig.13: The relationships between rainfall duration, rainfall ARI, land-use development and runoff volume for Sungai Kayu Ara basin

As illustrated in Fig.11 and Fig.12, the results indicated in sub-sections 4.1, 4.2 and 4.3 are approved. Based on the graphs given in Fig.11 and Fig.12, the increase in the rainfall event duration, the runoff peak discharge also increases, but the runoff volume adversely decreases. For similar rainfall event duration, on the other hand, the increases of the rainfall event ARI and river basin land-use development increase the runoff peak discharge and volume. In fact, Fig.11 and Fig.12 can be counted as a local model for Sungai Kayu Ara basin. In other words, these figures are quantified forms of interactions between rainfall event durations, ARIs and river basin land-use development conditions.

## CONCLUSIONS

This research has shown the capability of the HEC-GeoHMS which can be readily employed as a reliable and accurate tool for extraction of input geometric data for the HEC-HMS hydrological model. Beside this, it was found that with increased development (from the existing to the ultimate development condition), the runoff peak discharge and runoff volume also increased, and this can be attributed to the increase in the impervious area in the river basin. Furthermore, the effect of development condition in the river basin's response is more pronounced than the ARI. For example, a comparison made between the runoff peak discharges and the runoff volumes of 20 year ARI and 100 year ARI in the existing development condition shows 19% and 33% increases, respectively, whereas the increase of the development from the existing condition to the ultimate condition, gives an increase of 91% and 45%, respectively. These findings prove that that the runoff peak discharge is more sensitive to development condition changes, but the runoff volume is more sensitive to ARI changes.

## ACKNOWLEDGMENT

This work was funded by Universiti Sains Malaysia under Short-term Research Grant.

## REFERENCES

Cunderlik, J. M., & Simonovic, S. P. (2005). Hydrological extremes in a southwestern Ontario river basin under future climate conditions. *Hydrological Sciences Journal, 50*(4), 631-654.

DID - Department of Irrigation and Drainage, Malaysia. (2000). *Urban Stormwater Management Manual for Malaysia*. Kuala Lumpur: PNMB.

Ellouze, M., Abida, H., & Safi, R. (2009). A triangular model for the generation of synthetic hyetographs. *Hydrological Sciences Journal, 54*(2), 287-299.

U.S. Army Corps of Engineers, Hydrologic Engineering Center. (2006). *HEC Hydrologic Modeling System User's Manual, 2006*. Davis, CA, USA: Institute for Water Resources.

Hoyt, W. G., & Langbein, W. B. (1958). *Floods*. New Jersey: Princeton University Press.

Kingma, N. C. (2002). Flood Hazard Assessment and Zonation, Lecture Note, ITC, Enschede, the Netherlands.

Knight, D. W., & Shiono, K. (1996). River Channel and Floodplain Hydraulics. In Anderson, Walling and Bates (Eds.), *Floodplain Processes* (p. 139). Chichester, USA: John Wiley and Sons Ltd.

Leong, W. C. (2007). *Development of Malaysian Urban Rainfall-Runoff Characteristics: Case Study of Sungai Kayu Ara, Damansara, Selangor* (M.Sc. Thesis dissertation). Universiti Sains Malaysia (USM).

Linsley, R. K., Franzini, J. B., Freyberg, D. L., & Tchbanogolous, G. (1992). *Water Resources Engineering* (p.12-15). Singapore: McGraw-Hill, Inc.

Omen, G. S., Kessler, A. C., Anderson, N. T., Chiu, P. Y., Doull, J., Goldstein, B., Lederberg, J., McGuire, S., Rall, D., & Weldon, V. V. (1997). *Framework for Environmental Health Risk Management, Vol. 1 and 2 (Final Report)*. Washington, USA: The Presidential/Congressional Commission on Risk Assessment and Risk Management.

Smith, K. (1996). *Environmental Hazards: Assessing Risk and Reducing Disaster* (2nd ed). London, U.S.A., Canada: Routledge.

Smith, K., & Ward, R. (1998). *Floods: Physical Processes and Human Impacts*. Chichester, USA: John Wiley and Sons.

Stehr, A., Debels, P., Romero, F., & Alcayaga, H. (2008). Hydrological modelling with SWAT under conditions of limited data availability: evaluation of results from a Chilean case study. *Hydrological Sciences Journal, 53*(3), 588-601.

Walesh, G. S. (1989). *Urban Surface Water Management*. Chichester, USA: John Wiley & Sons Ltd.

Whitehead, P. G., & Robinson, P. G. (1993). Experimental Basin Studies; an International and Historical Perspective of Forest Impacts. *Journal of Hydrology, 145*(3-4), 217-230.

Yawson, D. K., Kongo, V. M., & Kachroo, R. K. (2005). Application of linear and nonlinear techniques in river flow forecasting in the Kilombero River basin, Tanzania. *Hydrological Sciences Journal, 50*(5), 783-796.

Pertanika J. Sci. & Technol. 20 (2): 221 - 241 (2012)

SCIENCE & TECHNOLOGY

Journal homepage: http://www.pertanika.upm.edu.my/

# A Behavior of Reinforced Vibrocompacted Stone Column in Peat

**Arun Prasad[1*], Sina Kazemian[2], Behzad Kalantari[3] and Bujang B. K. Huat[4]**

[1]*Department of Civil Engineering, Indian Institute of Technology (BHU), Varanasi – 221005, India*

[2]*Department of Civil Engineering, Bojnourd Branch, Islamic Azad University, Bojnourd, Iran*

[3]*Department of Civil Engineering, Hormozgan University, Bandar abbas, Iran*

[4]*Department of Civil Engineering, Faculty of Engineering, University Putra Malaysia, 43400 Serdang, Selangor, Malaysia*

## ABSTRACT

In the literature, several methods of ground improvement have been presented including compacted stone columns. The bearing capacity of the granular column is governed mainly by the lateral confining pressure mobilized in the soft soil to restrain or prevent bulging of the granular column. Therefore, the technique becomes unfeasible in peat that does not provide sufficient lateral confinement. This condition can be overcome by encasing the stone column with geogrid. This paper investigates the performance of the geogrid encased vibrocompacted stone column in peat. This study was carried out using PLAXIS software equipped with unit cell concept. The peat was modelled using soft soil model and the stone column using Mohr-Coulomb soil model, respectively. The geogrid was modelled using the geogrid option and could take only tensile force. The results indicate that the geogrid encased stone column can take much higher load in comparison to ordinary stone columns as the stiffness of the column increases. Meanwhile, the length of encasement also varied and it was observed that it was very effective up to about two times the diameter of the column. It also increased the column stiffness, and therefore led to a significant strain reduction. It was also observed that the columns at a spacing of three times the diameter are very effective. The results presented here can be used by the geotechnical engineers to design the geogrid reinforced stone column based on the strength of the soil, diameter of the column, spacing of the columns and stiffness of the geogrid.

**Keywords: Peat, Stabilization, Stone column, Unit cell, Geogrid encasement, Finite element**

*Article History:*
Received: 22 April 2010
Accepted: 2 November 2011

*Email addresses:*
arunprasad64@yahoo.com (Arun Prasad),
sina.kazemian@gmail.com (Sina Kazemian),
behzad996@yahoo.com (Behzad Kalantari),
bujang@eng.upm.edu.my (Bujang B. K. Huat)
*Corresponding Author

ISSN: 0128-7680 

## INTRODUCTION

In Malaysia, the increasing cost of land prices in the urban areas has forced the building industry to look for cheaper land for construction, many a times on poor ground conditions, particularly on peat. Various ground improvement techniques,

such as compacted-stone, have been increasingly used to reinforce soft soils and to increase the bearing capacity of the foundation soil (Aboshi *et al*., 1979; Al-Homud & Degen, 2006; Ambily & Gandhi, 2007; Goughnour & Bayuk, 1979; Chen *et al*., 2008; Christoulas *et al*., 1997; Elshazly *et al*., 2007, 2008; Li & Rowe 2008; Narsimha *et al*., 1992). This ground improvement technique has been successfully applied for foundation of structures like liquid storage tanks, earthen embankments, raft foundations, etc., where a relatively large settlement can be tolerated by the structure. It is preferred among other methods as it gives the advantage of reduced settlements and also accelerated consolidation settlements due to reduction in the drainage paths (Han & Gabr, 2002). The stone columns develop their load carrying capacity through bulging, while near-passive pressure conditions are developed in the surrounding soil. Several papers have been published on the stone column as a ground reinforcing technique. The bearing capacity and settlement response of the reinforced soil depend upon several parameters, the mechanical properties of the granular column, the native soft soil including the replacement factor, as well as the group effect and the loading process and rate, and the radial drainage through the columns. The technique is most effective in soft soils with undrained shear strength ranging from 15-50 kPa (Juran & Guermazi 1988). However, it becomes unfeasible in more compressible soils, such as peat, which do not provide sufficient lateral confinement.

In weak deposits, the lateral support is significantly low and the column fails by bulging. In order to improve the performance of the stone columns when treating weak deposits, it is imperative that the tendency of the columns to bulge should be resisted or prevented effectively. This will facilitate an increase of the load transfer through the stone column and thus enhance the load-carrying capacity. Such a condition can be achieved through encasement of stone columns through geosynthetics over the full or partial height of the column (Alexiew *et al*., 2005; Black *et al*., 2007; de Mello *et al*., 2008; Gniel & Bouazza, 2009; Huang & Han 2009; Kempfert, 2003; Murugesan & Rajagopal, 2006, 2009, 2010; Raithel *et al*., 2002; Yoo & Kim, 2009). The geosynthetic encasement will significantly increase the load carrying capacity of the stone columns due to the additional confinement from the geosynthetic. The geosynthetic encasement will also prevent the lateral squeezing of stones when the stone column is installed in some extremely soft soils, and this will lead to a minimal loss of stones.

Murugesan and Rajagopal (2010) carried out a load test on single and group of geogrid encased columns and concluded that the load capacity and stiffness of the stone column could be increased by all-round encasement by geosynthetic. The performance of the encased stone columns of smaller diameters was found to be superior than that of the larger diameter stone columns for the same encasement because of the mobilization of higher confining stresses in smaller diameter stone columns. Meanwhile, the elastic modulus of the geosynthetic encasement plays an important role in enhancing the capacity and stiffness of the encased columns.

Black *et al*. (2007) examined the performance of stone columns by jacketing them with tubular wire mesh and observed that the bearing capacity of soft soil could be improved using this particular technique.

Ayadat and Hanna (2005) performed an experimental investigation on the load carrying capacity and the settlement of the geogrid encased stone columns and concluded that the

ultimate carrying capacity of a stone column increased with the increase in the stiffness of the geofabric material used to encapsulate the sand column.

A method to estimate the settlement of foundation resting on the infinite grid of stone columns based on the unit cell concept was proposed by Priebe (1995). In this concept, the soil around a stone column for an area that was represented by a single column and dependent upon the column spacing was considered for the analysis. As all the columns in such analyses are simultaneously loaded, it is assumed that the lateral deformations in soil at the boundary of unit cell are zero. The behaviour of all column soil units is the same except near the edges of the loaded area, and thus only one column soil unit needs to be analyzed (Balaam & Booker, 1985). The unit cell concept has also been used (Ambily & Gandhi, 2007; Goughnour, 1983; Yoo & Kim, 2009). The modelling of a group of columns using unit cell concept was carried out by Mitchell and Huber (1985). In this modelling, the group of columns surrounding the central column was replaced by a ring of stone material having an equivalent thickness. The technique can be limited by the relatively large settlements that occur as a result of minimal compaction received during installation and also geotextile strain during loading. As such, the current research work focused on using stiffer geosynthetics such as geogrid for encasement.

In the present study, the effectiveness of geogrid encasement on the vibrocompacted stone columns is investigated through parametric study carried out by commercially available finite element package PLAXIS. The effects of the parameters, such as the stiffness of geogrid encasement, the depth of encasement from ground level, the diameter of stone columns, as well as spacing of the stone columns and shear strength of the surrounding peat, were analyzed. The simulation of the column installation in peat by means of vibro-compaction technique is as per the method described by Guetif *et al*. (2003, 2007). The analyses were carried out assuming a unit cell concept for columns that were arranged in a triangular pattern and the deformations in peat were restrained within the unit cell represented by the equivalent area of each column. The analysis for a group of columns was carried out as the group of columns surrounding the central column replaced by a ring of stone material having equivalent thickness (Mitchell & Huber 1985).

## FINITE ELEMENT ANALYSIS

The parametric analysis was carried out using the finite element package PLAXIS. The package was validated by analyzing the load settlement behaviour with the results of Black *et al*. (2007) which were found to match well, as shown in Fig.1. The index properties of the peat and stone aggregates were evaluated in the laboratory and are shown in Tables 1 and 2, respectively. Meanwhile, the properties of peat, stones and geogrid used in the modelling are shown in Table 3. The parameters required for the peat are modified compression index ($\lambda^*$), modified swelling index ($\kappa^*$), cohesion (c), friction angle ($\varphi$), and dilatancy angle ($\psi$). Similarly, the parameters required for the stone are Elastic modulus (E), Poisson ratio ($\nu$), cohesion (c), friction angle ($\varphi$), and dilatancy angle ($\psi$). The only material property required for the geogrid is material stiffness (EI). An axisymmetric analysis was carried out using Mohr-Coulomb's criterion for soil and stones. The column material justifies its low drained cohesion and reliable friction angle

value as the choice is for well-graded gravel. As recommended in Brinkgreve and Vermeer (1998), the angle of dilatancy is taken null for peat, this being extremely soft. An undrained condition is assumed for peat and drained for columns. This condition is justified in the peat as large consolidation settlement takes place after the application of the load.

The stone columns are usually installed in a triangular plan pattern in the field; for design and analysis purposes, a cylindrical unit cell considered consists of stone column and soil from the affected area. The concept of the composite cell model has been considered by many

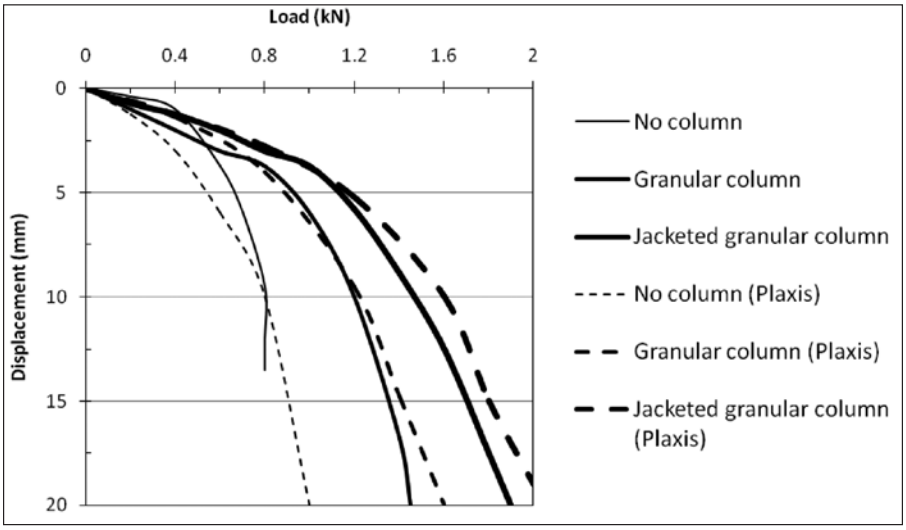


(a) Black *et al*. (2007)

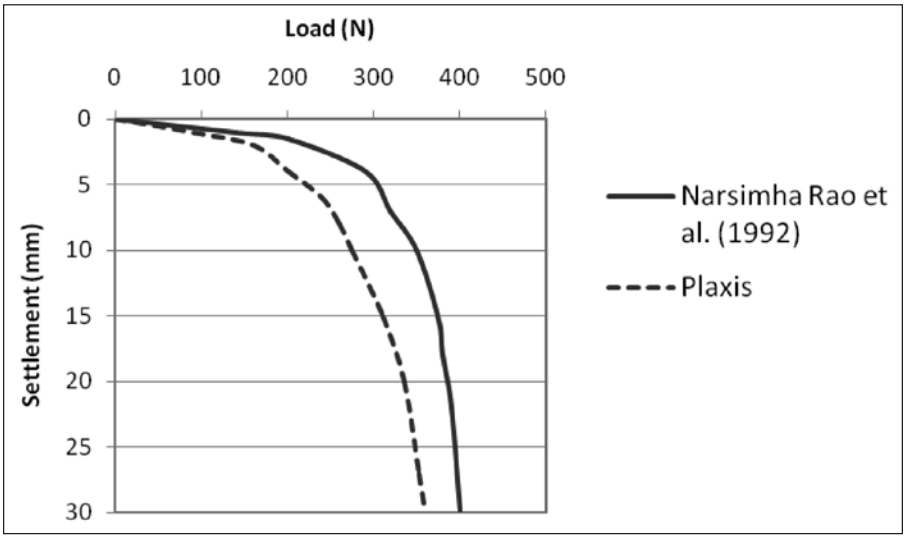


(b) Narasimha Rao *et al*. (1992)

Fig.1: Validation of Plaxis by the results of (a) Black *et al*., 2007, and (b) Narasimha Rao *et al*., 1992.

researchers for investigating several aspects of reinforced soils by columns, such as increase of bearing capacity, prediction of settlement, and reduction of soil consolidation (Bouassida *et al*., 1995; Guetif *et al*., 2003, 2007). The influenced areas for stone columns installed in triangular plan patterns were calculated from that of an equivalent hexagonal area. Barron (1948) suggested a method to calculate the radius of the circular influenced area as 0.525s for the triangular pattern, where 's' is the centre to centre spacing between the stone columns. The cylindrical unit cell has been idealized in the finite element model, using axisymetric model with the radial symmetry around the vertical axis that passes through the centre of the stone column.

Drainage was permitted from the top as in the oedometric test, as the soil profile was assumed to be 5.0 m thick peat underlain by a hard stratum. As the columns are installed by vibro-compaction, the interface between the column and soft clay is assumed to be perfectly rigid. This implies that the shear stresses can occur at the contact between the column and the peat. The contact between the column and the peat is assumed pervious, while the borders of the composite cell model are kept impervious, except for the top level since the stone columns are installed in a short period of time, and the expansion process is considered to occur in undrained conditions. The simulation of the vibrocompacted stone column was carried out following the procedure discussed by Guetif *et al*. (2007). It consisted of modelling the cylindrical hole occupied by the vibroprobe with a radius of 0.25 m by a fictitious purely elastic material having a weakest Young's modulus equivalent to 25 kPa [*see* Fig.2(a)]. Then, along the border of the cylindrical hole, the peat was subjected to the radial displacement that simulated the vibro-compaction installation until the horizontal expansion reached the column radius of 0.3 m or 0.5 m, as shown in Fig.2(b). Finally, the real parameters of the column material (Table 3) were introduced for further calculation using the PLAXIS.

This numerical study was carried out using the PLAXIS software as an axisymmetric model and the results were found to have matched well with the composite cell model. The typical finite element mesh consisted of 1750 nodes and 550 15-node triangular elements. Since the lateral expansion generates large strains in the soft soil in the neighbourhood of column, the updated mesh option provided by the Plaxis software was adopted to take care of this (Guetif *et al*., 2007). In order to incorporate the reinforcing effect during the column installation and the consolidation occurring in peat, a two stage modelling was performed; firstly, the undrained expansion of the column within peat, and secondly, the consolidation of the improved peat till the excess pore water pressure was reduced to the minimum (Debats *et al*., 2003).

Nonetheless, the creep effects of the geogrid were not considered in this study by assuming that the hoop tension force developed in the encasement was much smaller than the tensile capacity of the geogrid (Murugesan & Rajagopal, 2006). The radial deformation was restricted along the periphery of the tank but settlement was allowed, and along the bottom of the tank, both the radial deformation and settlement were also restricted. It is crucial to note that no interface element was used at the interface between the stone column and the peat, as the deformation of the column was mainly by radial bulging and no significant shear was possible (Mitchell & Huber, 1985). The external loading was applied in the form of a displacement equivalent to 20% of the column diameter.

## RESULTS AND DISCUSSION

In order to evaluate the improvement achieved due to the geogrid encasement, two cases were analyzed, namely, the stone columns without geogrid encasement (SC) and the stone columns encased with geogrid (GC). In order to directly assess the influence of the confinement effects due to encasement, the analyses were performed by applying uniform pressure on the stone column portion alone. Meanwhile, the analysis was also performed by applying load on the entire area of the unit cell and finally loading was applied to group of columns having seven columns arranged in a triangular pattern.

As mentioned earlier, the model was validated by analyzing the load settlement's behaviour with the results of Black *et al*. (2007) and Narsimha Rao *et al*. (1992). These results are

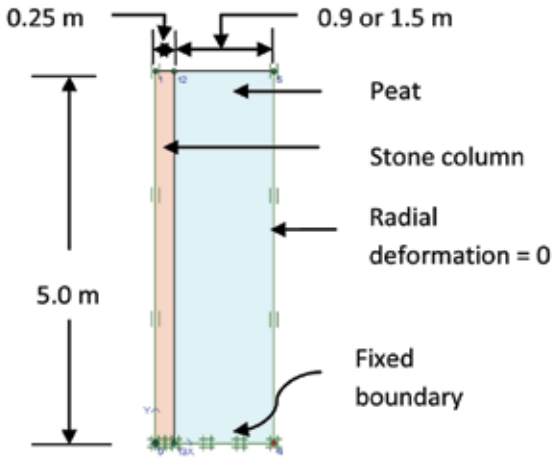


(a) Model of the stone column with a dummy column

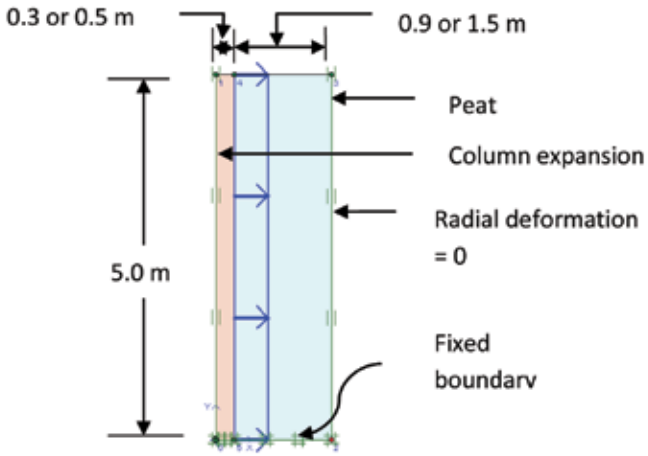


(b) Stone column modelled (column expansion)

Fig.2: Stone column installations by simulating column expansion

presented in Fig.1. Three cases were investigated, namely; no column, granular column, and jacketed granular column. The results of PLAXIS showed some deviations with the results of Black *et al*. (2007) for the case with no column, which was probably due to the fact that the peat used in the present analysis was more compressible as compared with clay used by Black *et al*. (2007). As for all the other cases, a reasonable matching was shown. Similarly, the results of PLAXIS also revealed a very small deviation with the results of Narsimha Rao *et al*. (1992), as shown in Fig.1(b), and this could be attributed to the different nature of soils used in the analyses.

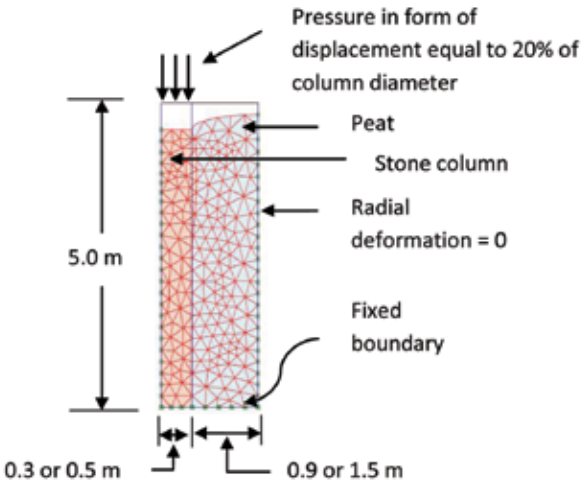


(a) Deformed mesh for column area alone loaded for SC

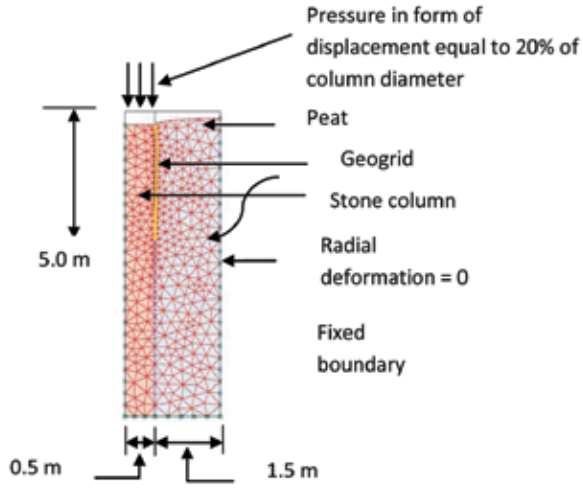


(b) Deformed mesh for column area alone loaded for GC

Fig.3: Deformed mesh for SC and GC, s/d = 3, c = 6 kPa, diameter = 1.0m, geogrid upto 3d

All the analyses for column diameters (0.6 m and 1.0 m) and the group of seven columns were carried out by varying s/d from 2 to 4, geogrid stiffness from 50 to 5000 kN/m, the length of encasement from 1d to 4d from the top (d is the diameter and s is the centre to centre spacing of the columns). Also, three different combinations of shear strength parameters, cohesion and angle of internal friction of the peat were used: 4 kPa & 16°, 6 kPa & 18° and 8 kPa & 20°, respectively. The loading was applied in terms of the prescribed displacement equivalent to 20% of the column diameter. All the cases were idealized through axisymmetric modelling, whereas the improved performance was evaluated based on the reduced settlement and the lateral bulging of the stone column.

Fig.3 show the typical deformed mesh, at a prescribed displacement, for the case of column alone loaded for SC and GC for s/d = 3 and c = 6 kPa. It was observed that failure was caused by the bulging of the column at a depth about 0.5 to 2.0 times the diameter of the column [Fig.3(a)]. The bulging disappeared when the column was encased with geogrid, as illustrated in Fig.3(b).

Fig.4 shows a typical deformed mesh for SC, when the entire area was loaded for s/d = 3 and c = 6 kPa. Nevertheless, no bulging of the column was observed. The analysis was also carried out for a group of seven columns using the axisymmetric model with surrounding six columns that were replaced by a ring of stones having equivalent thickness and material properties of stone, as adopted by Mitchell and Huber (1985).

A typical deformed mesh for the group of seven columns is shown in Fig.5. For this study, s/d was varied from 2 to 4 and c ranged from 4 to 8 kPa.

*Effect of the Shear Strength*

The impact of the strength of the foundation soil was studied by performing some analyses and the pressure-settlement responses observed are shown in Fig.6 for s/d = 3. The pressure

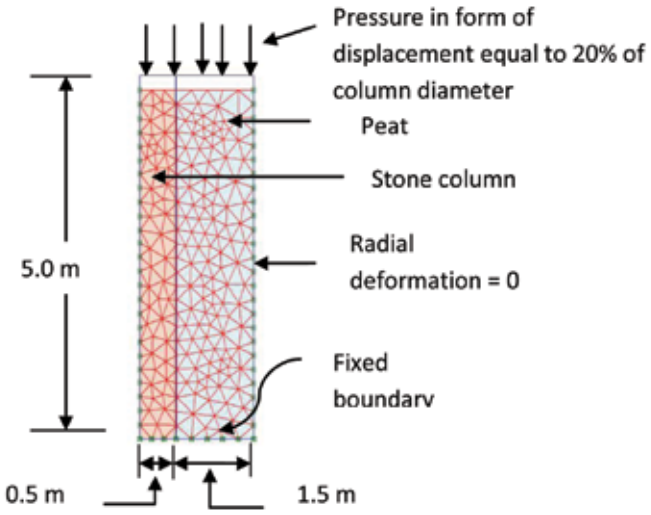


Fig.4: Deformed mesh, entire area loaded, single column ( SC), s/d = 3, c = 6 kPa, diameter = 1.0m

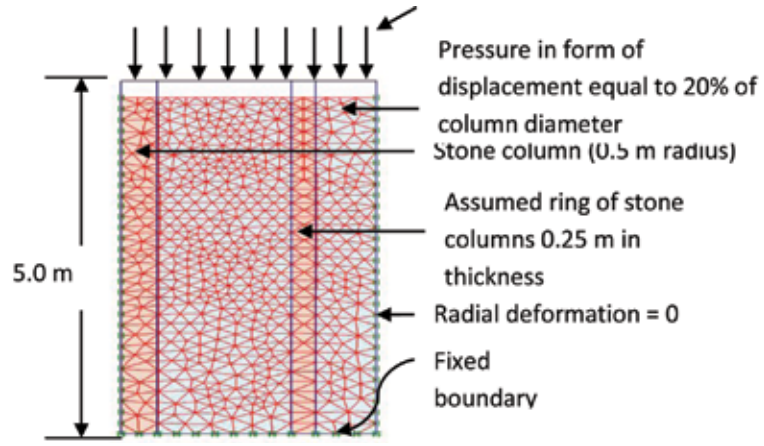


(a)

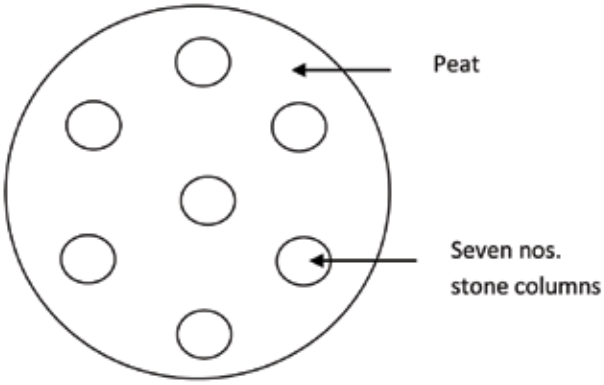


(b)

Fig.5: (a) Deformed mesh, entire area loaded, a group of seven columns (SC), s/d = 3, c = 6 kPa, diameter = 1.0 m; (b) plan view of the group layout

at a displacement equivalent to 20% of the column diameter is 150.6 kPa for the peat with a cohesion equivalent to 4 kN/m$^2$. This increased to 245.4 kPa for the peat with a cohesion equivalent to 8 kN/m$^2$. A similar behaviour was also observed for the other s/d values.

It was observed that the load capacity of the SC was dependent on the cohesive strength of the surrounding clay soil. On the other hand, the effect of the strength of the surrounding soil on the load capacity of the GC gradually decreased as the stiffness of the geogrid was increased. When the encasement stiffness was increased from 50 to 5000 kN/m, the pressure–settlement response of GC was practically independent of the strength of the surrounding clay soil, as shown in Fig.7.

As the stiffness of the encasement increases, the lateral bulging of the stone column reduces, thereby reducing the stresses transferred into the surrounding soil. Hence, it can be said that the contribution of the surrounding soil to the stability of the encased stone column reduces as the stiffness of the encasement increases. This implies that the capacity of the encased

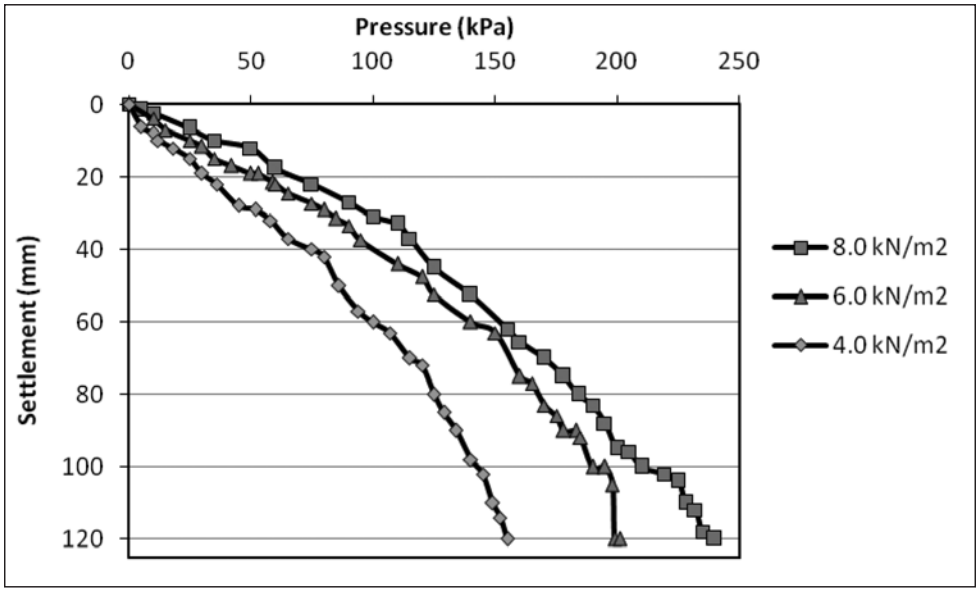


Fig.6: Pressure vs. settlement curves for different shear strengths; s/d = 3, diameter = 0.6 m, encasement up to 2d

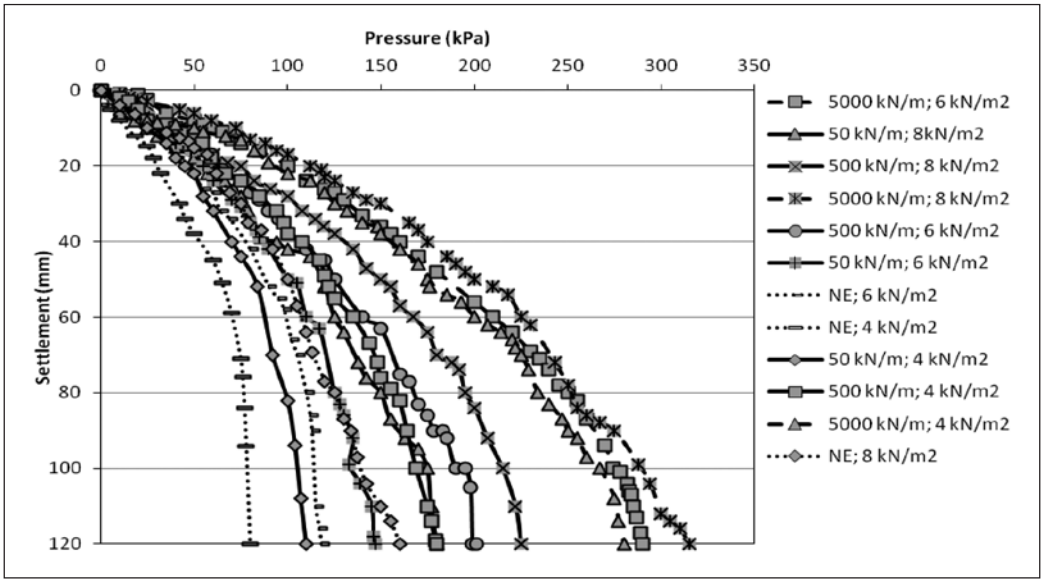


Fig.7: Pressure vs. settlement curves; different shear strengths and different geogrid encasement stiffness; column diameter = 0.5 m, s/d =3 (NE = No encasement)

columns is almost independent of the strength of the surrounding soil for tje extremely stiff geogrid encasement. Murugesan and Rajagopal (2006, 2010) also observed that the stiffness of the encasement plays an important role in reducing the bulging of the columns, and thus leading to a higher bearing capacity of the columns.

*Effect of the s/d Ratio*

Fig.8 shows the effects of s/d ratio on the pressure-settlement response of the SC of 1.0 m diameter and c = 6 kPa. The pressure for the encasement up to 2d was 181.8 kPa and this increased to 228.1 kPa for the encasement up to 4d.

The results were also found to be similar for other soil strengths. It was observed that the pressure on the column decreased as the s/d increased, but the effect was not much pronounced beyond s/d = 3.

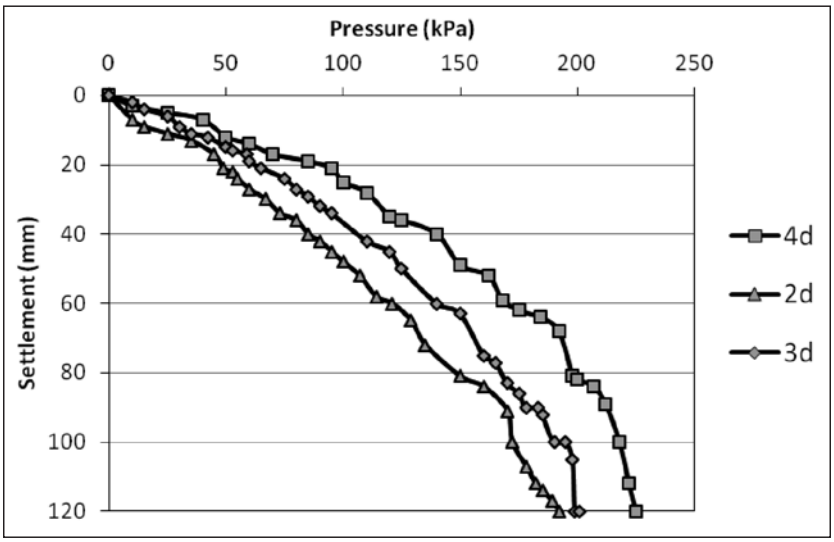


Fig.8: Pressure vs. settlement curves; different s/d ratios; c = 6 kPa, diameter = 1.0 m

*Effect of Encasement Stiffness*

Fig.9 shows the effects of the geogrid encasement (up to 2d) on the settlement of the single column loaded on the column area alone, s/d = 3, c = 6 kPa and diameter =1.0 m. Without encasement, the capacity of the column was 108.6 kPa and this increased up to 302.4 kPa with the encasement of strength 5,000 kN/m. It was seen that the capacity of the GC increased as the stiffness of the encasement increased.

*Effect of the Length of Encasement*

In the current research work, the effect of the length of encasement was also studied. It has been well established that the bulging of stone column due to loading is predominant up to a depth of 1.5–2 times the diameter of the stone column from the ground surface. Hence, only the top portion of the stone column needs lateral confinement so as to improve its performance. For very long stone columns, it may not be necessary to provide encasement over the full height. Hence, the effects of the encasement depth on the response of the stone columns need to be investigated and the encasement was provided up to 4d from the top of the column. Fig.10 shows the pressure-settlement response of 1.0 m diameter stone columns with different depths of encasement.

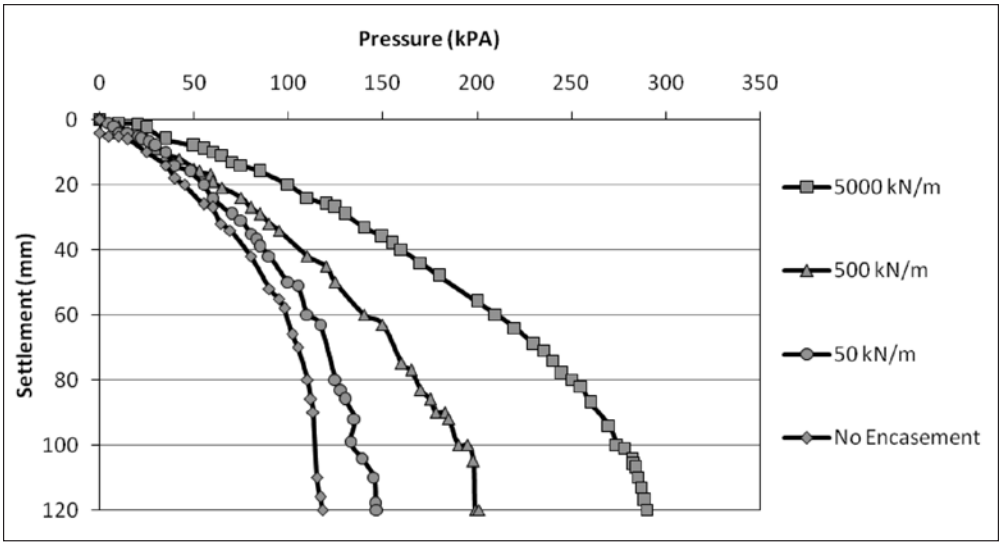


Fig.9: Effect of encasement; s/d = 3, c = 6 kPa, diameter = 1.0 m

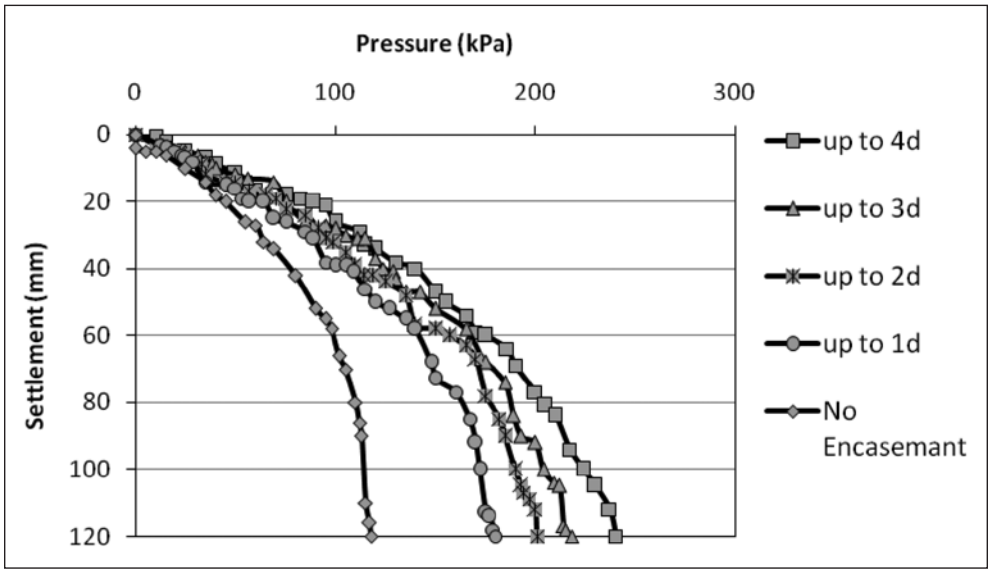


Fig.10: Effect of length of encasement (s/d = 3, c = 6 kPa, diameter = 1.0 m)

It was observed that the encasement beyond a depth equivalent to twice the diameter of the column did not lead to much improvement in the load capacity. It clearly showed that the confinement at the top portion of the stone column was adequate enough to improve the performance of the stone column. Similarly, Bauer and Al-Joulani (1996) also observed a similar behaviour but under uniaxial and triaxial compression tests.

It is also seen from the graph that the encasement is most effective up to 2d from the top even in very soft soil like peat. The lateral bulging along the length of the column is shown in Fig.11 at an applied pressure of 250 kPa for both, 0.6 m and 1.0 m diameter columns.

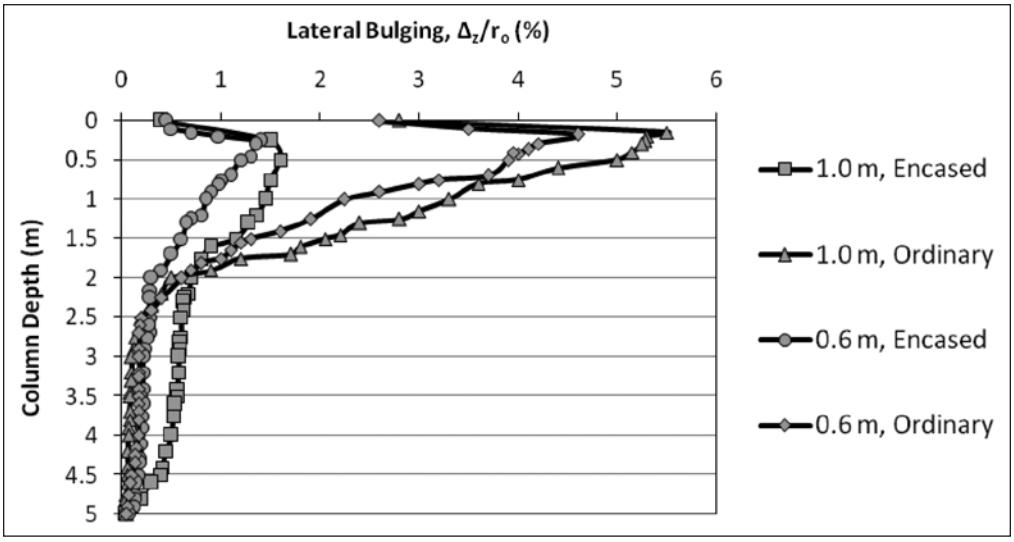


Fig.11: Effect of encasement on lateral bulging at 250 kPa, s/d = 3, c = 6 kPa

*Effect of Encasement on Bulging*

The improvement in the load capacity of the stone column due to geogrid encasement was studied by applying pressure over the stone column area only. By encasing with geogrid, it was observed that the stone columns were confined, and the lateral bulging had significantly reduced. The lateral bulging observed in the stone columns of two sizes (0.6 and 1m diameters), with and without geogrid encasement, is presented for comparison in Fig.12.

In Fig.12, the lateral bulging at different depths is presented in terms of the increase in radius ($\Delta_z$) at different depths and normalized with original radius of the stone column ($r_o$) (Murugesan & Rajagopal, 2006). It was observed that in SCs, there is severe bulging near the ground surface up to a depth equivalent to twice the diameter of the stone column. On the other hand, the encased stone columns underwent much lesser lateral expansion near the ground surface. In particular, the encased columns underwent slightly higher lateral expansions at deeper depths as compared to the SCs. This happened because the applied surface load was transmitted deeper into the column due to the encasement effects.

Fig.13 shows the effects of encasement stiffness on the lateral bulging when the entire area is loaded. The effect of the tensile stiffness of the geogrid used for the encasement on the performance of the stone column was investigated by varying the stiffness of geogrid, i.e. from 50 to 5000 kN/m, while keeping all the other parameters constant. It was observed that the lateral bulging decreased when the stiffness of the geogrid was increased.

*Behaviour of a Group of Columns*

This analysis was carried out to evaluate the improvement of the stiffness of the reinforced soil. The loading of both the stone column and the surrounding area, with confinement at the boundary, represents an actual field condition for the interior columns of a large group of stone columns. Fig.11 shows typical pressure-settlement behaviour for non-reinforced and

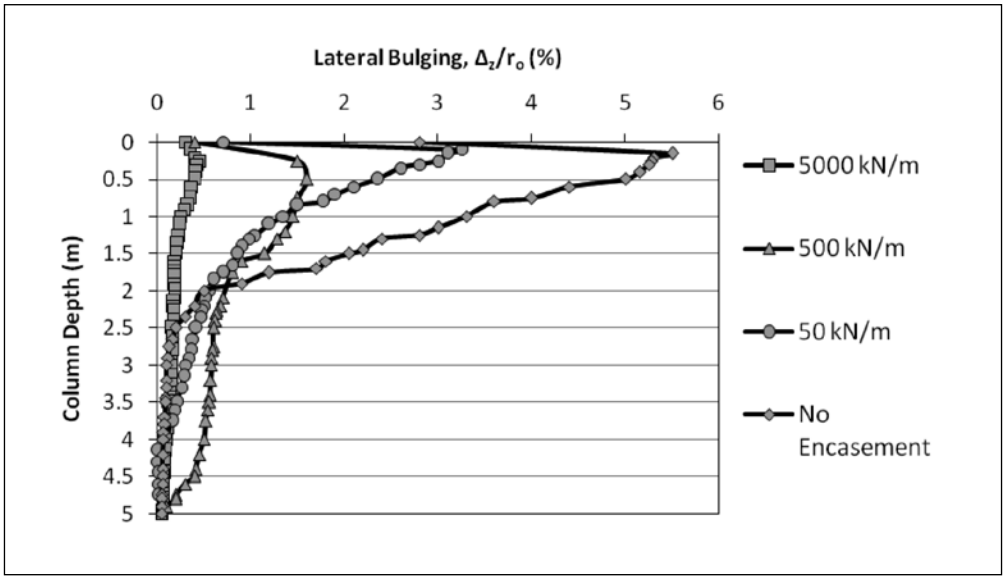


Fig.12: Effect of encasement on lateral bulging; pressure applied corresponding to displacement equivalent to 20% of column diameter; s/d = 3, c = 6 kPa, diameter = 1.0 m

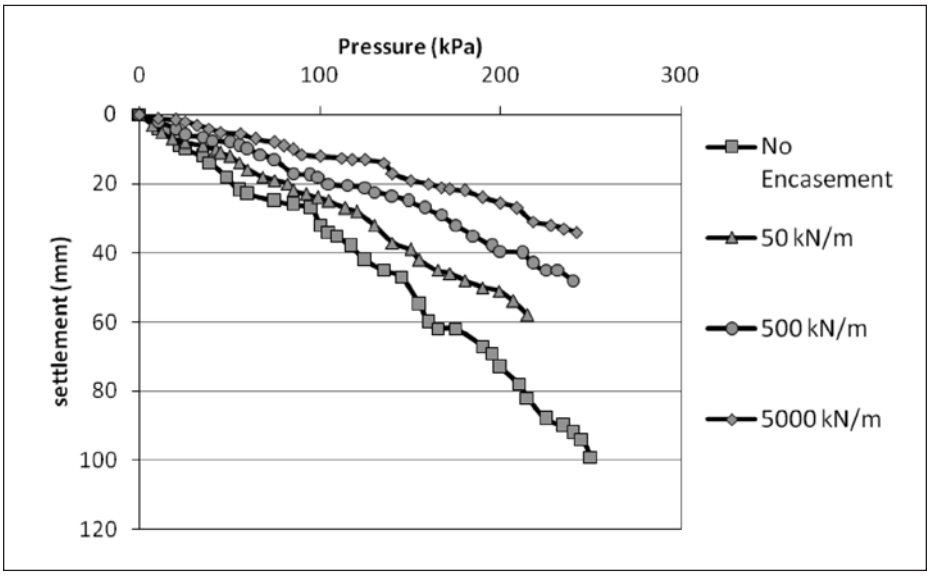


Fig.13: Effect of encasement on settlement, entire area loaded, s/d = 3, c = 6 kPa, diameter = 1.0m

reinforced peats based on the finite-element analysis for s/d of 3. When the entire area was loaded, failure did not take place even for a very large settlement because of the confining effect from the boundary of the unit cell.

Meanwhile, Fig.14 shows a comparison of the axial stress versus the settlement behaviour of a group of seven columns, and of a single column when the entire area was loaded based on

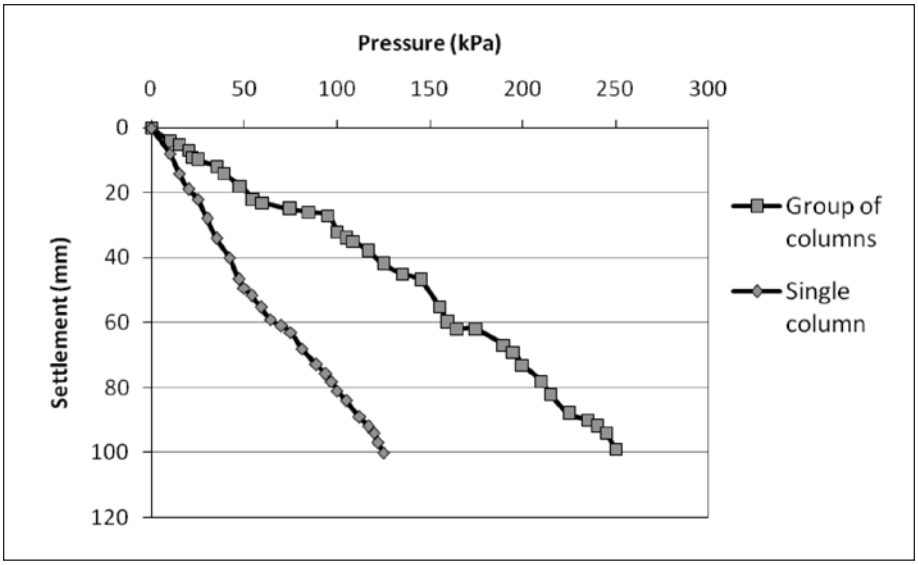


Fig.14: Pressure vs. settlement for single and a group of columns, entire area loaded, s/d = 3

Table 1: Physical properties peat

| Parameters | Value |
|---|---|
| Moisture content (%) | 198.2 |
| Liquid limit (%) | 231.8 |
| Specific gravity | 1.36 |
| Organic content (%) | 77.31 |
| Fibre content (%) | 28.3 |
| Bulk density (Mg/m$^3$) | 1.078 |

Table 2: Physical properties stone aggregates

| **Parameters** | **Value** |
|---|---|
| Size range | 40-80 mm |
| $D_{10}$ | 65 mm |
| Specific gravity | 2.68 |
| Relative density | 70% |
| Angularity number | 7.0 |
| Friction angle | 42° |
| Classification (ASTM D2487 - 10) | GP |

the finite-element analysis for s/d = 3. It could be seen that the behaviour of a single column and a group of columns was almost comparable.

Hence, the field behaviour of an interior column can be simulated with the single column behaviour with a unit cell concept when a large number of columns are simultaneously loaded.

Table 3: Material properties used in modelling

| Materials | Peat | Stone | Geogrid |
|---|---|---|---|
| Material model | Soft soil | Mohr-Coulomb | Elastic |
| Type of behaviour | Undrained | Drained | -- |
| Bulk density ($Mg/m^3$) | -- | 2.0 | -- |
| Elastic modulus, E (kPa) | -- | $3.0x10^4$ | -- |
| Poisson's ratio, ν | -- | 0.3 | -- |
| Modified compression index, λ* | 0.2 | -- | -- |
| Modified swelling index, κ* | 0.01 | -- | -- |
| Cohesion, c (kPa) | 4, 6, 8 | 0.01 | -- |
| Friction angle, φ (°) | 16, 18, 20 | 42 | -- |
| Dilatancy angle, ψ (°) | 0 | 10 | -- |
| Hydraulic conductivity, k (m/day) | -- | 100 | -- |
| Stiffness, EI (kN/m) | -- | -- | 50, 500, 5000 |

A similar behaviour of a group of columns has also been reported by Dhouib and Blondeau (2005), as well as Maurya *et al*. (2005).

Further, the pressure at a prescribed settlement equivalent to 20% of the column diameter was evaluated for all the cases (column area alone loaded) and is presented in Table 4. In addition, the settlement at a specified pressure (group of columns) for the entire area loaded was calculated and the results are presented in Table 5.

## CONCLUSIONS

The performance of the stone columns encased with geogrid reinforcement was studied in this research work. The results from the parametric studies have been presented to show the effects of confinement for improvement in the load capacity of the stone column due to geogrid encasement. The installation of the stone column in peat was simulated by adopting the composite cell model. Meanwhile, the numerical analyses were carried out by using the finite element software PLAXIS. The simulation shows a significant improvement in the characteristics of the peat subjected to vibro-compacted column encased with geogrid.

Based on the results obtained in this study, the following conclusions were made:

- The load carrying capacity and the stiffness of the stone column in peat can be increased by encasing the stone column by geogrid. The lateral bulging is minimized by geogrid encasement as the stone columns are confined.
- The stiffness of the geogrid encasement is very important in increasing the load capacity and the stiffness of the geogrid encased stone columns.
- The performance of the geogrid encased stone columns of smaller diameters (0.6 m) is better than that of stone columns with larger diameter (1.0 m) in peat due to the mobilization of higher confining stresses in a larger stone column.

Table 4: Pressure at 20% settlement (column area alone loaded)

| Column diameter (m) | Shear strength ($kN/m^2$) | Spacing of columns | No encasement | Length of encasement | | | | | | | | | | | |
|---|---|---|---|---|---|---|---|---|---|---|---|---|---|---|---|
| | | | | 1d | | | 2d | | | 3d | | | 4d | | |
| | | | | Geogrid tensile stiffness (kN/m) | | | | | | | | | | | |
| | | | | 50 | 500 | 5000 | 50 | 500 | 5000 | 50 | 500 | 5000 | 50 | 500 | 5000 |
| 0.6 | 4 | 2d | 105 | 85 | 170 | 248 | 140 | 191 | 294 | 147 | 204 | 317 | 154 | 229 | 340 |
| | | 3d | 100 | 112 | 151 | 213 | 117 | 168 | 263 | 120 | 183 | 282 | 124 | 201 | 296 |
| | | 4d | 82 | 104 | 147 | 210 | 110 | 165 | 260 | 115 | 181 | 279 | 115 | 196 | 290 |
| | 6 | 2d | 137 | 155 | 200 | 270 | 173 | 225 | 320 | 182 | 240 | 345 | 191 | 270 | 370 |
| | | 3d | 118 | 140 | 180 | 235 | 147 | 201 | 290 | 151 | 218 | 310 | 151 | 240 | 325 |
| | | 4d | 112 | 132 | 171 | 226 | 140 | 192 | 280 | 146 | 211 | 301 | 146 | 230 | 313 |
| | 8 | 2d | 164 | 176 | 224 | 294 | 197 | 252 | 348 | 207 | 269 | 376 | 206 | 302 | 403 |
| | | 3d | 143 | 161 | 200 | 254 | 169 | 223 | 314 | 173 | 241 | 336 | 178 | 266 | 353 |
| | | 4d | 134 | 152 | 193 | 248 | 161 | 216 | 308 | 168 | 238 | 331 | 168 | 259 | 344 |
| 1.0 | 4 | 2d | 192 | 228 | 192 | 228 | 247 | 357 | 552 | 258 | 387 | 603 | 275 | 413 | 624 |
| | | 3d | 161 | 201 | 161 | 201 | 219 | 338 | 505 | 233 | 340 | 540 | 239 | 365 | 560 |
| | | 4d | 155 | 191 | 155 | 191 | 210 | 330 | 493 | 223 | 335 | 535 | 229 | 358 | 551 |
| | 6 | 2d | 253 | 282 | 370 | 490 | 305 | 420 | 600 | 318 | 455 | 655 | 329 | 486 | 678 |
| | | 3d | 220 | 251 | 338 | 441 | 274 | 397 | 555 | 292 | 405 | 590 | 299 | 430 | 610 |
| | | 4d | 210 | 242 | 329 | 321 | 267 | 388 | 542 | 283 | 394 | 578 | 290 | 420 | 598 |
| | 8 | 2d | 303 | 321 | 303 | 321 | 347 | 470 | 654 | 362 | 510 | 714 | 375 | 544 | 739 |
| | | 3d | 268 | 288 | 268 | 288 | 315 | 441 | 602 | 338 | 450 | 640 | 344 | 477 | 662 |
| | | 4d | 251 | 279 | 251 | 242 | 308 | 431 | 596 | 327 | 444 | 635 | 323 | 468 | 657 |

Table 5: Settlement at the specified pressure (a group of columns)

| Column diameter (m) | Shear strength ($kN/m^2$) | Spacing of columns | No encasement | Length of encasement | | | | | | | | | | | |
|---|---|---|---|---|---|---|---|---|---|---|---|---|---|---|---|
| | | | | 1d | | | 2d | | | 3d | | | 4d | | |
| | | | | Geogrid tensile stiffness (kN/m) | | | | | | | | | | | |
| | | | | 50 | 500 | 5000 | 50 | 500 | 5000 | 50 | 500 | 5000 | 50 | 500 | 5000 |
| 0.6 | 4 | 2d | 50 | 39 | 34 | 27 | 33 | 25 | 19 | 29 | 20 | 14 | 24 | 16 | 12 |
| | | 3d | 65 | 52 | 45 | 35 | 44 | 31 | 26 | 38 | 24 | 22 | 33 | 21 | 19 |
| | | 4d | 80 | 62 | 54 | 44 | 52 | 42 | 33 | 46 | 34 | 32 | 39 | 28 | 26 |
| | 6 | 2d | 42 | 34 | 30 | 24 | 29 | 22 | 17 | 25 | 18 | 13 | 21 | 14 | 11 |
| | | 3d | 53 | 45 | 40 | 32 | 38 | 28 | 24 | 33 | 21 | 20 | 29 | 19 | 17 |
| | | 4d | 67 | 54 | 48 | 40 | 45 | 38 | 30 | 40 | 30 | 29 | 34 | 25 | 24 |
| | 8 | 2d | 32 | 28 | 26 | 22 | 24 | 19 | 15 | 20 | 15 | 11 | 17 | 11 | 10 |
| | | 3d | 39 | 36 | 34 | 28 | 30 | 23 | 21 | 25 | 23 | 18 | 22 | 16 | 15 |
| | | 4d | 49 | 43 | 41 | 36 | 36 | 32 | 27 | 27 | 25 | 32 | 27 | 21 | 21 |
| 1.0 | 4 | 2d | 107 | 82 | 71 | 44 | 74 | 48 | 33 | 63 | 41 | 28 | 54 | 36 | 24 |
| | | 3d | 121 | 92 | 78 | 49 | 81 | 58 | 39 | 71 | 50 | 35 | 59 | 44 | 30 |
| | | 4d | 134 | 103 | 91 | 57 | 92 | 70 | 45 | 79 | 58 | 41 | 66 | 53 | 34 |
| | 6 | 2d | 90 | 72 | 63 | 40 | 65 | 43 | 30 | 55 | 37 | 26 | 48 | 32 | 22 |
| | | 3d | 99 | 80 | 70 | 45 | 71 | 52 | 36 | 62 | 45 | 32 | 52 | 40 | 27 |
| | | 4d | 112 | 89 | 81 | 52 | 80 | 62 | 41 | 69 | 53 | 37 | 58 | 48 | 31 |
| | 8 | 2d | 68 | 58 | 54 | 36 | 53 | 37 | 27 | 44 | 30 | 23 | 38 | 27 | 19 |
| | | 3d | 72 | 64 | 59 | 48 | 56 | 44 | 32 | 49 | 35 | 29 | 41 | 32 | 24 |
| | | 4d | 83 | 70 | 60 | 48 | 63 | 53 | 38 | 55 | 42 | 31 | 46 | 38 | 28 |

- The encasement of the stone column up to a depth equivalent to two times the diameter of the stone column can substantially increase its load carrying capacity as the maximum bulging is at a depth of about 1.5 times of the diameter of the column.
- The load capacity of the stone column decreases as the spacing increases up to s/d of 3, beyond which, there is very small change.
- The field behaviour of an interior column when a large number of columns are simultaneously loaded can be simulated with a single column test using a unit cell concept.

## REFERENCES

Aboshi, H., Ichimoto, E., Harada, K., & Emoki, M. (1979). The composer - A method to improve the characteristics of soft clays by inclusion of large diameter sand columns. *Proc., Int. Conf. on Soil Reinforcement., E.N.P.C., 1, Paris*, 211-216.

Alexiew, D., Brokemper, D., & Lothspeich, S. (2005). Geotextile encased columns (gec): load capacity, geotextile selection and pre-design graphs. *Proceedings of Geo- Frontiers 2005*, Austin, Texas, US, 497-510.

Al-Homud, A., & Degen, W. (2006). Marine stone columns to prevent earthquake induced soil liquefaction. *Geotech. Geol. Eng*., *24*(3), 775-790.

Ambily, A. P., & Gandhi, S. R. (2007). Behavior of stone columns based on experimental and FEM analysis. *Journal of Geotech. and Geoenviron. Engg.*, *133*(4), 405-415.

ASTM D2487-10. (2010). *Standard Practice for Classification of Soils for Engineering Purposes (Unified Soil Classification System)* (p. 1-11). PA, USA: ASTM International, West Conshohocken.

Ayadat, T., & Hanna, A. M. (2005). Encapsulated stone columns as a soil improvement technique for collapsible soil. *Ground Improvement*, *9*(4), 137-147.

Balaam, N. P., & Booker, J. R. (1985). Effect of stone columns yield on settlement of rigid foundations in stabilized clay. *Int. J. Numer. Anal. Meth. Geomech.*, *9*(4), 351-81.

Barron, R. A. (1948). Consolidation of soil using vertical drain wells. *Géotechnique*, *31*, 718-742.

Bauer, G. E., & Al-Joulani, N. (2005). Laboratory and analytical investigation of sleeve reinforced stone columns. *Geosynthetics: Application, Design and Construction*, 463-466.

Black, J. A., Sivakumar, V., Madhav, M. R., & Hamill, G. A. (2007). Reinforced stone columns in weak deposits: Laboratory model study. *J. Geotech. Geoenviron. Eng*., *133*(9), 1154-1161.

Bouassida, M., de Buhan, P., & Dormieux, L. (1995). Bearing capacity of a foundation resting on a soil reinforced by a group of columns. *Géotechnique*, *45*(1), 25-34.

Brinkgreve, R. B., & Vermeer, P. A. (1998). *Plaxis-finite element code for soil and rocks analysis. Version 8*. AA Balkema, Netherlands: Rotterdam Brookfield.

Chen, Y. M., Cao, W. P., & Chen, R. P. (2008). An experimental investigation of soil arching within basal reinforced and unreinforced piled embankments. *Geotextiles and Geomembranes*, *26*(2), 164-174.

Christoulas, S., Giannaros, C., & Tsiambaos, G. (1997). Stabilization of embankment foundations by using stone columns. *Geotechnical and Geological Engineering, 15*(3), 247-258.

de Mello, L. G., Mondolfo, M., Montez, F., Tsukahara, C. N., & Bilfinger, W. (2008). First use of geosynthetic encased sand columns in South America. *Proceedings of 1st Pan-American Geosynthetics Conference*, Cancun, 1332-1341.

Dhouib, A., & Blondeau, F. (2005). *Colonnes Ballastées*. Edition Presses de l'école nationale des ponts et chaussées, Paris.

Elshazly, H. A., Elkasabgy, P., & Elleboudy, A. (2007). Effect of inter-column spacing on soil stresses due to vibro-installed stone columns: interesting findings. *Geotechnical and Geological Engineering*, *26*(2), 225-236.

Elshazly, H. A., Hafez, D. H., & Mossaad, M. E. (2008). Reliability of conventional settlement evaluation for circular foundations on stone columns. *Geotech. Geol. Eng.*, *26*, 323-334.

Gniel, J., & Bouazza, A. (2009). Improvement of soft soils using geogrid encased stone columns. *Geotextiles and Geomembranes*, *27*(3), 167-175.

Goughnour, R. R. (1983). Settlement of vertically loaded stone columns in soft ground. *Proc., 8th European Conf. on Soil Mechanics, and Foundations Engineering,* Helsinki, Finland, 1, 235-240.

Goughnour, R. R., & Bayuk, A. A. (1979). A field study of long-term settlements of loads supported by stone columns in soft ground. *Proc., Int. Conf. on Soil Reinforcement, Paris*, 279-285.

Guetif, Z., Bouassida, M., & Debats, J. M. (2003a). Parametric study of the improvement due to vibrocompacted columns installation in soft soils. *Proceedings, 13th African Regional Conference of Soil Mech. and Geotech. Eng.*, Marrakech (Morocco), December 8–11th, 463-466.

Guetif, Z., Bouassida, M., & Debats, J. M. (2003b). Soft soil improvement due to vibro-compacted columns installation. In Vermeer *et al*. (Eds). *Proceedings of Workshop Geotechnics of Soft Soils. Theory and Practice*. The Netherlands, September 17–19th, 551-557.

Guetif, Z., Bouassida, M., & Debats, J. M. (2007). Improved soft clay characteristics due to stone column installation. *Computers and Geotechnics*, *34*, 104-111.

Han, J., & Gabr, M. A. (2002). Numerical analysis of geosynthetic-reinforced and pile-supported earth platforms over soft soil. *Journal of Geotechnical and Geoenvironmental Engineering*, *128*(1), 44-53.

Huang, J., & Han, J. (2009). 3D coupled mechanical and hydraulic modeling of a geosynthetic-reinforced deep mixed column-supported embankment. *Geotextiles and Geomembranes*, *27*, 272-280.

Juran, I., & Guermazi, A. (1988). Settlement response of soft soils reinforced by compacted sand columns. *J. Geotech. Geoenviron. Eng.*, *114*(8), 903-943.

Kempfert, H. -G. (2003). Ground improvement methods with special emphasis on column-type techniques. Keynote lecture. *Proceedings of the Intern. Workshop on Geotechnics of Soft Soils –Theory and Practice*. Netherlands, Verlag Glückauf, 101 – 112.

Li, A. L., & Rowe, R. K. (2008). Effects of viscous behaviour of geosynthetic reinforcement and foundation soils on embankment performance. *Geotextiles and Geomembranes*, *26*(4), 317-334.

Maurya, R. R., Sharma, B. V. R., & Naresh, D. N. (2005). Footing load tests on single and group of stone columns. *Proceedings of the 16th International Conference on Soil Mechanics and Geotechnical Engineering*, Osaka, Japan, 3, 1385-1388.

Mitchell, J. K., & Huber, T. R. (1985). Performance of a stone column foundation. *J. Geotech. Engrg.*, *111*(2), 205-223.

Murugesan, S., & Rajagopal, K. (2006). Geosynthetic-encased stone columns: Numerical evaluation. *Geotextiles and Geomembranes*, *24*, 349-358.

Murugesan, S., & Rajagopal, K. (2009). Shear load tests on stone columns with and without geosynthetic encasement. *Geotech. Testing Journal*, *32*(1), 35-44.

Murugesan, S., & Rajagopal, K. (2010). Studies on the behavior of single and group of geosynthetic encased stone columns. *J. of Geotech. and Geoenvironmental Eng*., *136*(1), 129-139.

Narasimha Rao, S., Madhiyan, M., & Prasad, Y. V. S. N. (1992). Influence of bearing area on the behavior of stone columns. *Proceedings of Indian Geotechnical Confererence*, Calcutta, India, 235-237.

Priebe, H. J. (1995). The design of vibro replacement. *Ground Eng.*, *28*(12), 31-37.

Raithel, M., & Kempfert, H. G. (2000). Calculation models for dam foundations with geotextile coated sand columns. *Proceedings of the International Conference on Geotechnical & Geological Engineering*, GeoEngg, Melbourne.

Raithel, M., Kempfert, H. G., & Kirchner, A. (2002). Geotextile-encased columns (GEC) for foundation of a dike on very soft soils. *Proceedings of the Seventh International Conference on Geosynthetics*, Nice, France, 1025-1028.

Yoo, C., & Kim, S. B. (2009). Numerical modeling of geosynthetic-encased stone column- reinforced ground. *Geosynthetics International*, *16*(3), 116-126.

Pertanika J. Sci. & Technol. 20 (2): 243 - 255 (2012)

SCIENCE & TECHNOLOGY

Journal homepage: http://www.pertanika.upm.edu.my/

# Turnbull versus Kaplan-Meier Estimators of Cure Rate Estimation Using Interval Censored Data

**Bader Ahmad Aljawadi*, Mohd Rizam Abu Bakar and Noor Akma**

*Institute for Mathematical Research, Universiti Putra Malaysia, 43400 Serdang, Selangor, Malaysia*

## ABSTRACT

This study deals with the analysis of the cure rate estimation based on the Bounded Cumulative Hazard (BCH) model using interval censored data, given that the exact distribution of the data set is unknown. Thus, the non-parametric estimation methods are employed by means of the EM algorithm. The Turnbull and Kaplan Meier estimators were proposed to estimate the survival function, even though the Kaplan Meier estimator faces some restrictions in term of interval survival data. A comparison of the cure rate estimation based on the two estimators was done through a simulation study.

**Keywords: BCH model, interval censored data, cure fraction, EM algorithm, Turnbull estimator, Kaplan Meier estimator**

## INTRODUCTION

Cancer is one of the major chronic diseases which cause a notable amount of health administrative costs. Prognosis and possible cure from cancer are important measures of lifetimes which can be assessed by analyzing the survival of cancer patients. In survival data from cancer studies, the term cure may refer to a substance or procedure that changes the lifestyle, or may refer to the state of being healed or cured. The proportion of the individuals with a disease that is cured by a given treatment is called the cure fraction.

Survival models incorporating the cure fraction in the analysis known as the cure rate models are being widely used in analyzing data from cancer clinical trials (Zeng *et al.,* 2006). These models were basically developed to estimate the proportion of the patients who are cured as well as the odds of survival of the patients not cured up to a certain point of time (Andreas *et al.,* 2006).

The first cure rate model was published by Boag in 1949 and this was later developed by Berkson and Gage in 1952. In this model, the probability of survival at any given time

*Article history:*
Received: 29 January 2010
Accepted: 18 January 2012

*Email addresses:*
Bader_aljawadi@yahoo.com (Bader Ahmad Aljawadi),
mrizam@science.upm.edu.my (Mohd Rizam Abu Bakar),
noorakma@science.upm.edu.my (Noor Akma Ibrahim)
*Corresponding Author

ISSN: 0128-7680 

t equals to the proportion of those who are cured ($\pi$) plus those who are not cured ($1 - \pi$) but have not died. This model is known as the mixture cure rate model which can be defined mathematically, as follows:

$$S(t) = \pi + (1 - \pi)\, S^{*}(t) \tag{1}$$

where $S(t)$ and $S^{*}(t)$ are the survival functions for the entire population and the uncured patients, respectively.

The mixture model plays an important role in reliability and survival analysis, and it is becoming increasingly popular in analyzing data from clinical trials. In fact, the model has been extensively discussed by several authors including Farewell (1986), Gamel *et al.* (1990), Cantor and Shuster (1992), Kuk and Chen (1992), Peng and Dear (2000), Peng and Carreier (2002), Binbing *et al.* (2004), Abu Bakar *et al.* (2009), and in many more recent studies which have been conducted based on this model, as in Kim *et al.* (2009) who proposed a new mixture model via latent cure rate markers for survival data with a cure fraction. Seppa *et al.* (2010) applied a mixture cure fraction model with random effects to cause-specific survival data of female breast cancer patients. The researchers used two sets of random effects to capture the regional variation in the cure fraction and in the survival of the uncured patients, respectively. Furthermore, Castro *et al.* (2010) described an application of the mixture and bounded cumulative hazard models for location, scale, and shape (GAMLSS) framework to the fitting of long-term survival models. On the other hand, Peng and Taylor (2011) considered the mixture cure model with random effects and proposed several estimation methods based on Gaussian quadrature, rejection sampling, and importance sampling to obtain the maximum likelihood estimates of the model for clustered survival data with a cure fraction. Meanwhile, Xiang *et al.* (2011) proposed a mixture cure modelling procedure for analyzing clustered and interval censored survival time data by incorporating random effects in both the logistic regression and PH regression components.

Although this model appears to be attractive and is widely used in survival analysis, Chen *et al.* (1999) stated that it has some drawbacks which include the following:

- When covariates are involved in the analysis, the mixture model does not have a proportional hazard structure.
- The mixture model yields improper posterior distributions for many types of non-informative improper priors when covariates are included through the parameter $\pi$ via a standard regression model.
- This model does not appear to describe the underlying biological process generating the failure time, at least in the context of cancer relapse.

However, Chen *et al.* (1999) proposed the bounded cumulative hazard (BCH) model developed by Yakovlev *et al.* (1993) as a viable alternative to the mixture model. This model can be derived based on the assumption that for a group of cancer patients entering a clinical trial and after the initial treatment, a number of cancer cells left active and may grow rapidly to produce a detectable cancer mass later on (i.e. cancer relapse). The number of cancer cells denoted by $N$ is assumed to follow Bernoulli, negative binomial or Poisson distribution,

whereby considering a Bernoulli distribution is related to the classical mixture model specified in equation (1), where $\pi = P(N = 0)$, while considering a negative binomial distribution with parameters $\alpha$ and $\theta$, at the same time, where $\theta = E(N)$ and $\alpha$ are real numbers. For $\theta > 0$ and $\alpha\theta > -1$, the survival function is defined as follows (Rodrigues *et al*., 2009):

$$S(t) = [1 + \alpha\theta F(t)]^{-1/\alpha}$$

where $F(t)$ is the cumulative distribution function.

When $N$ is assumed to follow Poisson distribution with mean $\theta$ which is considered as the most attractive assumption since it provides more flexible model (Rodrigues *et al*., 2009). Then, the survival function for the BCH model under this assumption can be obtained by:

$$S(t) = \exp(-\theta F(t)) \tag{2}$$

where $F(t)$ is the cumulative distribution function such that $F(t) = 1 - S(t)$. See Chen *et al.* (1999) and Aljawadi *et al*. (2011).

Based on the BCH model defined in (2), the cure fraction ($\pi$) can therefore be obtained using:

$$\pi = \lim_{t\to\infty} S(t) = P(N = 0)$$
$$\lim_{t\to\infty} \exp(-\theta F(t)) = \exp(-\theta)$$

Note that when $\theta \to \infty$, then $\pi \to 0$, whereas $\theta \to 0$ then $\pi \to 1$.

In the survival data analysis, the lifetime $t$ can be considered as an exact or censored lifetime; however, other cases often occur in cancer studies, where the follow-up of the patients is a pre-fixed time period or visited periodically for a fixed number of times. In this article, the lifetime of the individuals is only known to fall in an interval, such that $t_i \in (L_i, R_i], i = 1,\ldots,n$, where $L_i$ and $R_i$ are the left and right endpoints of the observed intervals, respectively.

The cure rate models are said to be a parametric or semi-parametric models. In the parametric models, a standard probability distributions such as exponential, weibull, Gompertz and generalized $F$ can be employed. Nonetheless, the main limitation of the parametric cure models is that it is sometimes hard to find a distribution flexible enough to fit the observed data. Therefore, the non-parametric techniques are considered to be more attractive under the violation of the parametric assumptions.

In the following sections, however, the non-parametric techniques are employed to estimate the survival function, based on Turnbull and Kaplan Meier estimators, and followed on to compare the estimation of the cure fraction via a simulation study considering the two non-parametric estimators.

## MATERIALS AND METHODS

### *Turnbull Estimator*

In case of right censored data, one can use the Kaplan-Meier estimator to obtain the survival function. However, with interval censored data, this particular estimator is not a suitable one, and it is Turnbull who formulated an algorithm that works on the principle of EM algorithm

based on a sample of observed intervals $[L_i, R_i]$, $i = 1, ..., n$, which contains the independent random variables $t_1, ..., t_n$.

For this algorithm, equivalence intervals such as $J_1 = (q_1, p_1]$, $J_2 = (q_2, p_2]$, ..., $J_m = (q_m, p_m]$ must be extracted to determine the jumps $(s_1, s_2, ..., s_m)$ of the cumulative distribution function and hence the survival function. To find the equivalence intervals, consider all the intervals $[L_i, R_i]$ for $i = 1, ..., n$, and order the $2n$ endpoints in ascending order, and each end point "$L$" that is then immediately followed by the end point "$R$" which is an equivalence interval.

Let $\alpha_{ij} = 1_{\{[q_j,p_j]\subseteq[L_i,R_i]\}}$, $i = 1, ..., n, j = 1, ..., m$,be the indicator variable of whether or not $[q_j, p_j]$lies within $[L_i, R_i]$. Then, the probability that $t_i$ falls in the $[q_j, p_j]$ given vector of the jumps $s = (s_1, ..., s_m)^T$ is given by:

$$\mu_{ij}(s) = \frac{\alpha_{ij}s_j}{\sum_{j=1}^{m}\alpha_{ij}s_j}, \qquad i = 1,\ldots,n, \qquad j = 1,\ldots,m$$

Since the survival function is constant outside the intervals $[q_j, p_j]$, the proportion of the observations in $[q_j, p_j]$ is given by:

$$\pi_j(s) = \frac{\sum_{i=1}^{n}\mu_{ij}(s)}{n}, \qquad j = 1,\ldots m$$

The vector $\boldsymbol{s}$ is said to be self consistent if,

$$s_j = \pi_j(s),\ j = 1,\ldots,m$$

**Note:** to find $\mu_{ij}$, we can use an initialization of **s** such that $s^k = \left(\frac{1}{m},\ldots,\frac{1}{m}\right), k = 0$ , and then follow up to find $s_j^{k+1}$ until stopping conditions such as $\sum_{j=1}^{m}(s_j^{k+1} - s_j^k)^2 < \in, \in > 0$.
Thus, the Turnbull estimator of the survival function can be defined as follows:

$$\hat{S}(t) = \begin{cases} 1 & : \ if\ t_i < q_1 \\ 1 - \sum_{k=1}^{j} s_k & : \ if\ p_j \le t_i < q_{j+1}, \qquad j = 1,\ldots,m, \qquad i = 1,\ldots,n \\ 0 & : \ if\ t_i < q_1 \end{cases} \tag{3}$$

See Klein and Moeschberger (2003).

*Estimation of the Entire Survival Function*

Since the survival function is not observed in the equivalence intervals and hence, the survival function amongst the interval $[L_i, R_i]$ which contains at least one of the equivalent classes is unknown if $t_i \in [q_j, p_j]$. Furthermore, the details about the true lifetime are not available, and the only thing that is known is that it belongs to an observed interval. Then, the lifetime $t_i$ can be generated randomly from the interval $[L_i, R_i]$ when both endpoints are observed, while in the case of right censoring where the right endpoint $R_i$ is not observed, it is possible to substitute this endpoint by the last visit time and to do the generation.

In case the generated life times fall in the equivalence intervals, the survival function can then be defined as follows:

- Generating a sufficient number $W$ of sequential values from the equivalence interval $(q_j, p_j)$, such that $T_{jW} = (T_{j1}, ..., T_{jW})$ and $q_j < T_{j1} < T_{j2}$. $1 \leq j \leq m$.
- Generating $W$ sequential values between the corresponding values of the survival function at the endpoints of the equivalence interval $(q_j, p_j)$, such that $S_{jW} = (S_{j1}, ..., S_{jW})$, and $S_{j1} > S_{j2} ... > S_{jW}$, where $S_{ji} = \lim_{t \to qj-} \hat{S}(t)$, and $S_{jw} = \lim_{t \to pj+} \hat{S}(t)$. Note that $S_{j1} = 1$ if $q_j = 0$, and $S_{jW} = 0$ if $p_j = 0$ for all $j = 1, ..., m$.

Then, the survival function can be defined as follows:

$$\hat{S}_j(t) = \begin{cases} \dfrac{(S_{jk}) + (S_{j(k+1)})}{2} & : \ if \ T_{jk} \leq t_{ji} < T_{j(k+1)} \\ \hat{S}(t) & : \ otherwise \end{cases} \tag{4}$$

$$k = 1, ..., W, \qquad i = 1, ..., n \qquad j = 1, ..., m$$

*Kaplan-Meier Estimator*

The standard non-parametric estimator of the survival function is the Kaplan-Meier (KM) estimator, which is also known as the product limit estimator. This estimator is defined as follows:

$$\hat{S}(t) = \prod_{tj \leq t} \left( \frac{n_i - d_i}{n_i} \right) = \prod_{i=1}^{n} \left( 1 - \frac{d_i}{n_i} \right) \tag{5}$$

where ti $t_i \leq t \leq t_{i+1}$, $d_i$ represents the number of failures at time $t$ such that $J_1 = (q_1, p_1]$, $J_2 = (q_2, p_2]$, ... , $J_m = (q_m, p_m]$, and $n_i$ indicates the number of individuals who have not experienced the interested event, and have also not been censored by time $t$. From equation (5), it is seen that $\hat{S}(t) = 1$ when $t$ is less than the first failure time, i.e. $t < t_i$.

The Kaplan-Meier estimator estimates the jumps of the survival function at the observed times. The jumps on the survival curve are dependent upon the number of events observed at each event time, and also on the pattern of the censored observations before the event time.

In the case of interval data, using the midpoint of each interval to represent the exact survival time is a common practice amongst the analysts, and then applying the Kaplan-Meier method will yield the estimated survival function. If the right endpoints of some intervals are not specified, i.e. right censored, it is then possible to use the maximum value of the visit times to represent the right endpoint for that interval. However, this procedure may produce invalid inference. Due to the lack of efficient statistical methodology and available software, the Kaplan Meier estimator can be implemented.

Midpoint imputation is only applicable when the time periods between the consecutive visits are short (Law & Brookmeyer, 1992). Thus, when the width of the interval increases, we may run into problems. Furthermore, the standard error of the estimator is underestimated since the midpoint imputation assumes that the failure times are exactly known when in fact they are not, (Kim, 2003).

## RESULTS AND DISCUSSION

Let the censoring and cure indicators for interval censored data be as follows:

$$\alpha = \begin{cases} 0: censored \\ 1: otherwise \end{cases} \qquad c = \begin{cases} 0: cured \\ 1: otherwise \end{cases}$$

Then, the log likelihood function can be obtained by:

$$L_c = \log \prod_{i=1}^{n} \left[ \{(f_i^*)\}(1 - e^{-\theta})^{c_i} \right]^{\alpha_i} \left[ \{e^{-\theta}\}^{1-c_i} \{(1 - e^{-\theta}) S_i^*\}^{c_i} \right]^{1-\alpha_i} \tag{6}$$

where $S_i^*$ is the survival function of the censored-uncured patients which might be evaluated using the Turnbull or Kaplan Meier estimators, and $f_i^*$ is the probability density function of the uncensored individuals.

One of the most attractive features of the BCH model is that it can be written as a mixture model, where the survival function can be obtained using:

$$\begin{aligned} S(t) &= \exp(-\theta F(t)) \\ &= \exp(-\theta) + [1 - \exp(-\theta)] \left[ \frac{\exp(-\theta F(t)) - \exp(-\theta)}{1 - \exp(-\theta)} \right] \end{aligned}$$

Comparing this formula with the mixture model in Equation (1), the survival function of the uncured patients $S_i^*$ can then be represented by:

$$\begin{aligned} S_i^* &= \frac{\exp(-\theta F(t_i)) - \exp(-\theta)}{1 - \exp(-\theta)} \\ &= \frac{\exp(\theta[1 - F(t_i)]) - 1}{\exp(\theta) - 1} \end{aligned}$$

since $S(t_i) = 1 - F(t_i)$, then

$$S_i^* = \frac{\exp(\theta S(t_i)) - 1}{\exp(\theta) - 1} \tag{7}$$

where $S(t_i)$ is the survival function for the $i^{th}$ censored individual.

Furthermore, the probability density function $f_i^*$ can be estimated using the jumps of the survival function which can be obtained by:

$$f_i^* = M_i = F(R_i) - F(L_i), \qquad i = 1, 2, \ldots, n$$

where $F(R_i)$ and $F(L_i)$ are the cumulative distribution functions at the endpoints of the observed interval. Therefore, the log likelihood function can be re-written as follows:

$$\begin{aligned} L_c &= \log \prod_{i=1}^{n} \left[ \{(M_i)(1 - e^{-\theta})\}^{c_i} \right]^{\alpha_i} \cdot \left[ \{e^{-\theta}\}^{1-c_i} \left\{ (1 - e^{-\theta}) \left( \frac{e^{\theta S(t_i)} - 1}{e^{\theta} - 1} \right) \right\}^{c_i} \right]^{1-\alpha_i} \\ &= \sum_{i=1}^{n} \alpha_i c_i \log(M_i) - \theta \sum_{i=1}^{n} (1 - \alpha_i)(1 - c_i) + \log(1 - e^{-\theta}) \sum_{i=1}^{n} c_i \\ &\quad + \sum_{i=1}^{n} c_i (1 - \alpha_i) \log \left[ \frac{e^{\theta S(t_i)} - 1}{e^{\theta} - 1} \right] \end{aligned} \tag{8}$$

Maximizing $L_c$ is subjected to the condition $\sum_{i=1}^{n} M_i \leq 1$. Let $q$ be a non-negative slack variable i.e. $\sum_{i=1}^{n} M + q = 1$. By adding the Lagrange multiplier λ, the log likelihood function can then be re-written as follows:

$$\begin{aligned} L_c = & \sum_{i=1}^{n} \alpha_i c_i \log(M_i) - \theta \sum_{i=1}^{n} (1-\alpha_i)(1-c_i) + \log(1-e^{-\theta}) \sum_{i=1}^{n} c_i \\ & + \sum_{i=1}^{n} c_i (1-\alpha_i) \log\left[\frac{e^{\theta S(t_i)}-1}{e^{\theta}-1}\right] - \lambda\left[\left(\sum_{i=1}^{n} M_i + q\right) - 1\right] \end{aligned} \tag{9}$$

The solution of the following equations is the desired estimates of the parameters:

$$\frac{\partial L_c}{\partial \theta} = 0, \frac{\partial L_c}{\partial M_i} = 0, \frac{\partial L_c}{\partial \lambda} = 0, \frac{\partial L_c}{\partial q} = 0$$

such that $\frac{\partial L_c}{\partial \theta} = 0$ implies

$$\begin{aligned} \frac{\partial L_c}{\partial \theta} = & \left(\frac{e^{-\theta}}{1-e^{-\theta}}\right) \sum_{i=1}^{n} c_i - \sum_{i=1}^{n} (1-\alpha_i)(1-c_i) \\ & + \sum_{i=1}^{n} c_i (1-\alpha_i) \left[\frac{(e^{\theta}-1)(S(t_i)e^{\theta S(t_i)}) - e^{\theta}(e^{\theta S(t_i)}-1)}{(e^{\theta S(t_i)}-1)(e^{\theta}-1)}\right] \end{aligned} \tag{10}$$

which can be simplified as follows:

$$\begin{aligned} & \sum_{i=1}^{n} c_i - e^{\theta} \sum_{i=1}^{n} (1-\alpha_i) + \sum_{i=1}^{n} (1-\alpha_i)(1-c_i) \\ & + (e^{\theta}-1) \sum_{i=1}^{n} c_i (1-\alpha_i) \left[\frac{(S(t_i))}{(1-e^{-\theta S(t_i)})}\right] = 0 \end{aligned} \tag{11}$$

Similarly, $\frac{\partial L_c}{\partial M_i} = 0, i = 1, \ldots, n$ implies:

$$\sum_{i=1}^{n} \alpha_i c_i \frac{1}{M_i} - n\lambda = 0 \tag{12}$$

$\frac{\partial L_c}{\partial \lambda} = 0$ also implies:

$$\sum_{i=1}^{n} M_i + q - 1 = 0 \tag{13}$$

$\frac{\partial L_c}{\partial q} = 0$ implies:

$$\lambda = 0 \tag{14}$$

The solution of equation (11) is our desired estimate of $\theta$, but $c_i$ is partially missing and so the EM algorithm is necessary.

*The EM Algorithm*

Suppose that the data set is given in the form $([L_i,R_i], \alpha_i)$, $i = 1, 2, ..., n$, where $[L_i,R_i]$ denotes the observed interval that includes the $i^{th}$ patient lifetime, and $\alpha_i$ is the censoring indicator. The cure indicator $c_i$ is partially missing and this will be handled in the EM algorithm.

However, for the $m$ uncensored individuals $\alpha_i$ and $c_i$, $j = 1, ..., m$, are observed and both are equal to 1, while for $i = m + 1$, $\alpha_i$ is observed and equals to 0 but $c_i$ is not observed and it might be 1 or 0. Thus, in the EM algorithm, the E-step calculates the expectation of (8) given the observed data set. The expected value of the log likelihood function can be represented by:

$$E[L_c] = E_1[L_c/a_j, c_j] + E_2[L_c/\alpha_i]$$

The expected value of the log likelihood function basically depends on $E_2[L_c/\alpha_i]$ which can be defined as follows:

$$\begin{aligned} E_2[L_c/\alpha_i] &= -\theta\textstyle\sum_{i=m+1}^{n}(1-c_i) + \log(1-e^{-\theta})\sum_{i=m+1}^{n} c_i + \sum_{i=m+1}^{n} c_i \log\left(\frac{e^{\theta S(t_i)}-1}{e^{\theta}-1}\right) \\ &= -\theta\textstyle\sum_{i=m+1}^{n}(1-c_i) + \sum_{i=m+1}^{n} c_i\left[\log\left(\frac{e^{\theta S(t_i)}-1}{e^{\theta}-1}\right)\right] \end{aligned} \tag{15}$$

Where $\sum_{i=m+1}^{n}(1-c_i)$, $\sum_{i=m+1}^{n} c_i \log\left(\frac{e^{\theta S(t_i)}-1}{e^{\theta}-1}\right)$ and $\sum_{i=m+1}^{n} c_i$ are the sufficient statistics.

Peng and Carriere (2002) defined $g_i$ as the expected value of the $i^{th}$ patient to be uncured conditional on the current estimates of $\alpha_i$ and the survival function of uncured patients $S_i^*$, such that:

$$g_i = \alpha_i + (1-\alpha_i)\left[\frac{[1-e^{-\theta}]S_i^*}{[e^{-\theta}]+[1-e^{-\theta}]S_i^*}\right]$$

For simplicity, let $p_i = E(1-c_i) = 1-g$, $i = m + 1$, which indicates the expected value of the $i^{th}$ patient to be cured such that for censored individuals:

$$p_i = 1-g_i = 1-\left[\frac{[1-e^{-\theta}]S_i^*}{[e^{-\theta}]+[1-e^{-\theta}]S_i^*}\right] = 1-\left\{\frac{[1-e^{-\theta}]\left(\frac{e^{\theta S(t_i)}-1}{e^{\theta}-1}\right)}{[e^{-\theta}]+[1-e^{-\theta}]\left(\frac{e^{\theta S(t_i)}-1}{e^{\theta}-1}\right)}\right\} = -e^{\theta S(t_i)} \tag{16}$$

Using these notations, the sufficient statistics can then be re-written as follows:

$$\begin{aligned} e_1 &= \textstyle\sum_{i=m+1}^{n} E(1-c_i) = \sum_{i=m+1}^{n} p_i = \sum_{i=m+1}^{n} e^{-\theta S(t_i)} \\ e_2 &= \textstyle\sum_{i=m+1}^{n} E(c_i) = \sum_{i=m+1}^{n}(1-p_i) = \sum_{i=m+1}^{n}(1-e^{-\theta S(t_i)}) \\ e_3 &= \textstyle\sum_{i=m+1}^{n} E\left[c_i \log\left(\frac{e^{\theta S(t_i)}-1}{e^{\theta}-1}\right)\right] = \sum_{i=m+1}^{n}(1-p_i)\log\left(\frac{e^{\theta S(t_i)}-1}{e^{\theta}-1}\right) \end{aligned}$$

In the light of this equation (11), it can be re-written as follows:

$$\begin{aligned} &\left[\textstyle\sum_{j=1}^{m} c_j + \sum_{i=m+1}^{n} c_i\right] - e^{\theta}\left[\sum_{j=1}^{m}(1-\alpha_j) + \sum_{i=m+1}^{n}(1-\alpha_i)\right] + \\ &\left[\textstyle\sum_{j=1}^{m}(1-\alpha_j)(1-c_j)\right] + \sum_{i=m+1}^{n}(1-\alpha_i)(1-c_i) + \\ &(e^{\theta}-1)\left[\textstyle\sum_{j=1}^{m} c_j(1-\alpha_j)\left(\frac{S(t_j)}{1-e^{-\theta S(t_j)}}\right) + \sum_{i=m+1}^{n} c_i(1-\alpha_i)\left(\frac{S(t_j)}{1-e^{-\theta S(t_j)}}\right)\right] = 0 \end{aligned} \tag{17}$$

However, for some initial values of ($\theta^t$) solve for $e_1$, $e_2$ and $p_i$ then $\theta^{t+1}$ is the numerical solution of equation (17) with respect to $\theta$. Repeat until stopping condition such as $\theta^{t+1} + \theta^t$, ε is small positive value (e.g. 0.0001).

*Simulation Study*

In simulation studies based on survival analysis, many common distributions can be used to generate the failure time data sets, where the most common distributions that might be employed in such studies are the exponential and Weibull distribution since they fit the data very well. However, in this simulation and to control the data generation process, the exponential distribution with various values of the scale parameter λ has been considered, where λ can be replaced by the values 0.5, 1, 1.5 and 2 respectively which imply various censoring rates for the generated data sets. For each assigned value of λ, a 100 data sets were generated such that each data set comprised 100 observations. The steps used for data generation are as follows (Goulin *et al.,* 2008):

(a) Generate the true survival time $t$ from an exponential distribution using the proposed values of the scale parameter.

(b) Generate a vector V for the clinic visits, assuming that there are 20 clinic visits, in case of exponential distribution, the first visit $v_1$ was generated from $U(0,0.115)$, and then the next visit $v_2$ was generated from $U(v_1, v_1 + 0.115)$. The other visit times were generated in the same manner. A uniform distribution is considered in such case to regulate the times of the clinic visits and hence gain short and equivalent lengths of the intervals.

(c) Generate a 100 × 2 empty matrix named "bound" for each data set. The entries of bound matrix are the intervals endpoints for each individual after comparing the true survival time with the 20 visit times. In case of right censoring the right end point is replaced by "*Inf*". The formula used for end points determination is:

For $i = 1, ..., 100, j = 1, .., 20$

$$bound[i,1] = \begin{cases} 0 : if \;\; t[i] < V[1] \\ V[j] : if \;\; V[j] < t[i] < V[j+1] \\ V[20] : if \;\; t[i] > V[20] \end{cases}$$

$$bound[i,2] = \begin{cases} V[1] : if \;\; t[i] < V[1] \\ V[j+1] : if \;\; V[j] < t[i] < V[j+1] \\ Inf \;\; : t[i] > V[20] \end{cases}$$

(d) Generate a 100 × 2 empty matrix named "status" based on the "bound" matrix and the "status" matrix can then be defined as follows:

$$\text{status}\,[i,1] \equiv \text{censoring indicator } \alpha_i = \begin{cases} 0 \;\; : \;\; if \; bound\,[i,2] = Inf \\ 1 \;\; : \;\; if \;\; otherwise \end{cases}$$

$$\text{status } [i,1] \equiv \text{cured indicator } c_i = \begin{cases} 0 & : \ if \ \alpha_i = 0 \\ 1 & : \ if \ otherwise \end{cases}$$

***Note***: We assumed that all right censored individuals are cured as a special case.

The Turnbull and Kaplan Meier procedures are employed for each generated data set to estimate the survival function, and hence estimate the cure fraction. In this simulation, the bias of the cure fraction and also the relative efficiency (*RE*) based on the two non-parametric estimators are considered in such that:

$$\text{bias} = \pi - E(\hat{\pi}) \tag{18}$$

and

$$RE = \frac{MSE(Turnbull)}{MSE(KM)} \tag{19}$$

Where, $\hat{\pi}$ is the maximum likelihood estimator for $\pi$, and the mean square error $MSE = (biase(\hat{\pi}))^2 + Var(\hat{\pi})$.

A small bias indicates that the estimator is closer to the true value on average and hence more accurate. While *RE* being less than one indicates that the Turnbull estimator is the viable estimator that may be employed to estimate the cure fraction using interval censored data.

Table 1 shows the results of the cure rate estimation based on the two proposed scenarios, where the estimated measures (i.e. Bias, MSE and RE) represent the average of these measures for the whole data sets that have equivalent censoring rate. All the relative efficiency values are less than one, which indicates that the Turnbull estimator in the case of interval censored data and whatever the censoring rate is more efficient than the Kaplan Meier estimator when the midpoint of the observed interval is considered. The bias values obtained from both the

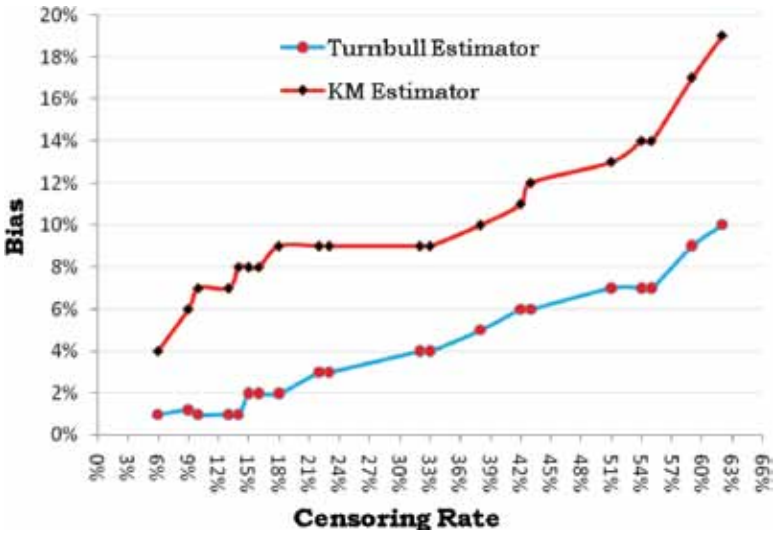


Fig.1: Censoring rates versus bias for Kaplan Meier and Turnbull Estimators

Table 1: Simulation results based on the various values of λ

| Run | Censoring Rate | True Cure Rate (**R**) | Turnbull Estimator | | Kaplan Meier estimator | | Relative Efficiency |
|---|---|---|---|---|---|---|---|
| | | | Estimated Cure Rate (**E**) | Bias (**R-E**) | Estimated Cure Rate (**E**) | Bias (**R-E**) | |
| | | | | λ = 2 | | | |
| 1 | 6% | 6% | 5% | 1% | 2% | 4% | 0.988 |
| 2 | 9% | 9% | 8% | 1% | 3% | 6% | 0.946 |
| 3 | 10% | 10% | 9% | 1% | 3% | 7% | 0.900 |
| 4 | 13% | 13% | 12% | 1% | 6% | 7% | 0.900 |
| 5 | 14% | 14% | 13% | 1% | 6% | 8% | 0.853 |
| | | | | λ = 1.5 | | | |
| 6 | 15% | 15% | 13% | 2% | 7% | 8% | 0.864 |
| 7 | 16% | 16% | 14% | 2% | 8% | 8% | 0.864 |
| 8 | 18% | 18% | 16% | 2% | 9% | 9% | 0.816 |
| 9 | 22% | 22% | 19% | 3% | 13% | 9% | 0.832 |
| 10 | 23% | 23% | 20% | 3% | 14% | 9% | 0.832 |
| | | | | λ = 1 | | | |
| 11 | 32% | 32% | 28% | 4% | 23% | 9% | 0.855 |
| 12 | 33% | 33% | 29% | 4% | 24% | 9% | 0.855 |
| 13 | 38% | 38% | 33% | 5% | 28% | 10% | 0.833 |
| 14 | 42% | 42% | 36% | 6% | 31% | 11% | 0.814 |
| 15 | 43% | 43% | 37% | 6% | 31% | 12% | 0.764 |
| | | | | λ = 0.5 | | | |
| 16 | 51% | 51% | 44% | 7% | 38% | 13% | 0.748 |
| 17 | 54% | 54% | 47% | 7% | 40% | 14% | 0.700 |
| 18 | 55% | 55% | 48% | 7% | 41% | 14% | 0.700 |
| 19 | 59% | 59% | 50% | 9% | 42% | 17% | 0.636 |
| 20 | 62% | 62% | 52% | 10% | 43% | 19% | 0.591 |

estimators yield the same indication, and it is noticed that the efficiency of both the estimators declines when the censoring rate goes up, as shown in Fig.1.

## CONCLUSION

In this research, two non-parametric estimation methods of the cure fraction were investigated based on the bounded cumulative hazard model using interval censored data. Both the Turnbull and Kaplan Meir estimators were considered, whereby in the case of Kaplan Meir estimator, the midpoint of the intervals could be adopted to represent the exact failure time. The estimation methods were combinations of the straightforward maximum likelihood estimation and the EM algorithm. Hence, the estimating equations were solved numerically since no explicit solutions could be found.

Based on the simulation results and the obtained RE values, however, it was concluded that the Turnbull estimator provides more efficient estimates for the cure fraction using interval

censored data compared to the Kaplan Meir estimator. Therefore, based on these results, the analysts who have considered the Kaplan Meier estimator in case of interval censored data should not be too confident with their results. Thus, the Turnbull estimator is recommended to be used for the cure rate estimation rather than the Kaplan Meier estimator.

## REFERENCES

Abu Bakar, M. R., Salah, K. A., Ibrahim, N. A., & Haron, K. (2009). Bayesian Approach for Joint Longitudinal and Time-to-Event Data with Survival Fraction. *Bulletin of the Malaysian Mathematical Sciences Society, 32*(1), 75-100.

Aljawadi, B. A., Abu Bakar, M. R., Ibrahim, N. A., & Midi, H. (2011). Parametric Estimation of the Cure Fraction based on BCH Model and Exponential Distribution using Left Censored Data. *Journal of Applied Sciences, 11*(15), 2861-2865.

Andreas, W., Isabella, L., & Antoli, I. (2006). The Modelling of a Cure Fraction in Bivariate Time-to-Event Data. *Australian Journal of Statistics, 35*(1)*,* 67-76.

Berkson, J., & Gage, R. P. (1952). Survival curves for cancer patients following treatment. *Journal of the American Statistical Association, 47*(259)*,* 501-515.

Boag, J. W. (1949). Maximum likelihood estimates of the proportion of patients cured by cancer therapy. *Journal of the Royal Statistical Society, Series B 11*, 15-44.

Cantor, A. B., & Shuster, J. J. (1992). Parametric versus non-parametric methods for estimating cure rates based on censored survival data. *Statistics in Medicine, 11*, 931-937.

Castro, M. D., Cancho, V. D., & Rodrigues, J. (2010). A hands-on Approach for fitting Long-term Survival Models Under the GSMLSS Framework. *Computer Methods and Programs in Medicine, 97,* 168-177.

Chen, M. H., Ibrahim, J. G., & Sinha, D. (1999). A new Bayesian model for survival data with a surviving fraction. *Journal of the American Statistical Association, 94,* 909-919.

Farewell, V. T. (1986). Mixture models in survival analysis: Are they worth the risk? *The Canadian Journal of Statistic, 14*, 257-262.

Gamel, J. W., McLean, I. W., & Rosenberg, S. H. (1990). Proportion cured and mean log survival time as functions of tumour size. *Statistics in Medicine, 9*, 999-1006.

Hanin, L., Tsodikov, A., & Yakovlev, A. (2001). Optimal Schedules of Cancer Surveillance and Tumor Size at Detection. *Mathematical and Computer Modeling 33*, 1419-1430.

Goulin, Z. (2008). *Nonparametric and Parametric survival analysis of censored data with possible violation of method assumptions* (Master thesis dissertaion). University of North Carolina at Greensboro.

Kim, J. (2003). Maximum likelihood estimation for the proportional hazards model with partly interval-censored data. *Journal of the Royal Statistical Society: Series B, 65*(Part 2), 489-502.

Kim, S., Chen, M. H., & Dey, D. K. (2009). A new threshold regression model for survival data with a cure fraction. *Lifetime Data Analysis, 16*, 478-490.

Klein, J. P., & Moeschberger, M. L. (2003). *Survival Analysis Techniques for Censored and Truncated Data,* (2nd ed.). New York, USA: Springer.

Kuk, A. Y. C., & Chen, C. H. (1992). A mixture model combining logistic regression with proportional hazards regression. *Biometrika, 79*, 531-541.

Law, G., Brookmeyer, R. (1992). Effects of mid-point imputation on the analysis of doubly censored data. *Statistics in Medicine, 11*, 1569-1578.

Peng, Y., & Dear, K. B. G. (2000). *A non-parametric mixture model for cure rate estimation*. *Biometrics, 56*, 237-243.

Peng, Y., & Carriere, K. C. (2002). An Empirical Comparison of Parametric and Semi-parametric Cure Models. *Biometrical, 44*, 1002-1014.

Peng, Y., & Taylor, J. M. G. (2011). Mixture Cure Model with Random Effects for the Analysis of a Multi-center Tonsil Cancer Study. *Statistics in Medicine, 30*, 211-223.

Rodrigues, J., Cancho, V. G., Castro, M. D., & Louzada-Neto, F. (2009). On the unification of long-term survival models. *Statistics and Probability Letters, 79*, 753-759.

Seppa, K., Hakulinen, T., Kim, H. J., & Laara, E. (2010). Cure Fraction Model with Random Effects for Regional Variation in Cancer Survival. *Statistics in Medicine, 29*, 2781-2793.

Xiang, L., Ma, X., & Yau, K. K. (2011). Mixture Cure Model with Random Effects for Clustered Interval Censored Survival Data. *Statistics in Medicine, 30*, 995-1006.

Yakovlev A. Y., Asselain, B., Bardou, V. J., Fourquet, A., Hoang, T., Rochefediere, A., & Tsodikov, A. D. (1993) . A Simple Stochastic Model of Tumor Recurrence and Its Applications to Data on pre-menopausal Breast Cancer. In B. Asselain, M. Boniface, C. Duby, C. Lopez, J. P.Masson, and J.Tranchefort (Eds.), *Biometrie et Analyse de Dormees Spatio – Temporelles 12* (p. 66-82). ENSA Renned, France: Société Francaise de Biométrie.

Yu, B., Tiwari, R. C., Cronin, K. A., & Feuer, E. J. (2004). Cure fraction estimation from the mixture cure models for grouped survival data. *Statistic in Medicine, 23*(11), 1733-1747.

Zeng, D., Yin, G., & Ibrihim, J. G. (2006). Semiparametric transformation models for survival data with a cure fraction. *Journal of the American Statistical Association, 101*, 670-684.

Pertanika J. Sci. & Technol. 20 (2): 257 - 268 (2012)

SCIENCE & TECHNOLOGY

Journal homepage: http://www.pertanika.upm.edu.my/

# Optimization of In-feed Centreless Cylindrical Grinding Process Parameters Using Grey Relational Analysis

**Khan, Z. A.[1], Siddiquee, A. N.[1] and Kamaruddin, S.[2]***

[1]*Mechanical Engineering Department, Jamia Millia Islamia, New Delhi - 110025, India*

[2]*School of Mechanical Engineering, Engineering Campus, Universiti Sains Malaysia, 14300 Nibong Tebal, Pulau Pinang, Malaysia*

## ABSTRACT

This paper presents an effective approach for the optimization of an in-feed centreless cylindrical grinding of EN52 austenitic grade steel (DIN: X45CrSi93) with multiple performance characteristics based on the grey relational analysis. To study the effect of the entire space of the input variables, nine experimental runs, based on the Taguchi method of $L_9$ orthogonal arrays, were performed to determine the best factor level condition. The response table and response graph for each level of the machining parameters were obtained from the grey relational grade. In this study, the in-feed centreless cylindrical grinding process parameters, such as dressing feed, grinding feed, dwell time and cycle time, were optimized by taking into consideration the multiple-performance characteristics like surface roughness and out of cylindricity. By analyzing the grey relational grade, it was observed that dressing feed, grinding feed and cycle time had significant effect on the responses. The optimal multiple performance characteristics were achieved with dressing feed at level 1 (5 mm/min), grinding feed at level 2 (6 mm/min), dwell time at level 2 (2.5 s), and cycle time at level 2 (11 s). It is clearly shown that the above performance characteristics in the in-feed Centreless cylindrical grinding process can be improved effectively through this approach.

**Keywords**: **Centreless cylindrical grinding, surface roughness, out of cylindricity, grey relational analysis, optimization, multi-performance**

*Article history:*
Received: 4 November 2010
Accepted: 12 February 2011

*Email addresses:*
zahid_jmi@yahoo.com (Khan, Z. A.),
arshadnsiddiqui@gmail.com (Siddiquee, A. N.),
meshah@eng.usm.my (Kamaruddin, S.)
*Corresponding Author

## INTRODUCTION

In-feed centreless cylindrical grinding is used to finish parts that have projections, variation in shapes, varying diameters, or shoulders. In the in-feed method, the shape variations are accommodated in the form of grinding wheel (or wheels) truing to form various part diameters and lengths that describe the part

ISSN: 0128-7680 

geometry. In this process, the part is fed to the wheels from above with no lateral movement of the piece while it is being ground. This makes the process well suited for profiles and multi-diameter components. Fig.1 illustrates the schematic diagram of the in-feed cylindrical grinding. Centreless cylindrical grinding process involves a large number of influencing factors that are non-linear, interdependent and difficult to quantify. It is the process of choice for high volume finishing of the surfaces of revolution shaped components. Despite all its merits, it is marked with instability problems.

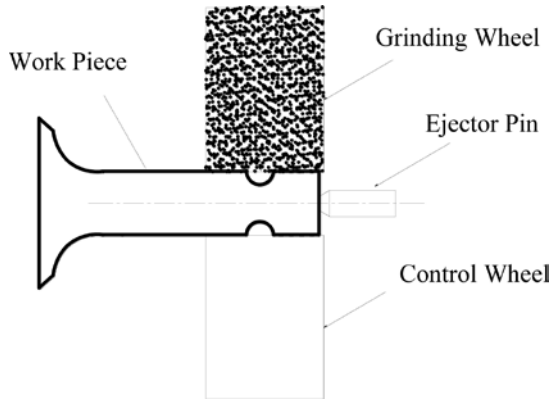


Fig.1: Schematic of In-feed Centreless Grinding Process

Furthermore, the characteristics of the machined surfaces, such as surface finish and roundness, are largely dependent on the machine's attributes, including its condition, dynamics, setup and also process parameters (Bueno *et al*., 1990; Hashimoto & Lahoti, 2004). Available literature also shows that such issues have been extensively studied and analytically addressed (Bueno *et al*., 1990). This has led to remarkable improvements in the technology of accurate machines. Yet, due to complexities related to the machine and its setup, the success of the process is dependent a large extent on the initial setup conditions and process parameters, which in many cases, are done by extensive trial and errors based on the operator's skills (Hashimoto & Lahoti, 2004). Thus, finding the optimum process parameters is still a challenge from the manufacturing process point of view.

In order to control the grinding process, it is necessary to quantify roundness and surface roughness, which are the most critical quality characteristics for the selection of cylindrical grinding process parameters. The roundness of a part is defined by the initial conditions, i.e. blade angle and part height (Hashimoto & Lahoti, 2004). The surface roughness of the finished component depends on the centreless cylindrical grinding gap set-up, the dressing condition and the significant process kinematical factors (Hashimoto & Lahoti, 2004).

It appears from the literature that grey relational analysis has been extensively used by the researchers in determining the optimal parameters for different machining processes. For example, grey relational analysis, coupled with principal component analysis, was used to optimize the process parameter of high-speed end milling of SKD61 tool steel (Lu *et al*., 2008). The grey relational analysis was employed for the optimization of the laser cutting process of

St-37 steel (Çaydaş & Hasçalık, 2008) so as to determine the optimal wire electrical discharge machining (WEDM) parameters for machining $Al_2O_3$ particle reinforced material with multiple-performance characteristics (surface removal rate and maximum surface roughness) (Chiang & Chang, 2006), optimize the drilling process parameters, such as feed rate, cutting speed, drill type and point angles of drill for the workpiece surface roughness and burr height (Tosun, 2006), optimize turning operations with multi-performance characteristics (tool life, cutting forces and surface roughness) (Lin, 2004), determine the cutting parameters for optimizing the side milling process with multi-performance characteristics (Chang & Lu, 2007), and determine the optimal machining parameter setting for the end-milling of high-purity graphite under dry machining condition (Yang, 2006).

A fuzzy based grey relational analysis was used to find the optimal process conditions of an injection-molded thermoplastic part with a thin shell feature (Ko-Ta, 2007). Turning parameters, such as cutting speed, feed rate, depth of cut and machining time, were also optimized based on the multiple-performance characteristics which included material removal rate, tool wear, surface roughness and specific cutting pressure by using grey relational analysis method (Palanikumar *et al*., 2006).

The out-of-roundness of a part is determined mainly by grinding speed. It also depends on the height of job axis above the centerline of the grinding and regulating wheels. The height is set so that the axis of the workpiece is above the centerline of the grinding and regulating wheels. The surface roughness of the finished component, on the other hand, is significantly dependent on the dressing condition and the process kinematical factors (Hashimoto & Lahoti, 2004). Meanwhile, the dimensional deviations of the finished part are established by work rest setting and feed. The feed affects all the quality attributes including out-of-roundness, surface roughness and dimensional accuracy.

The present study was carried out with the purpose to select the optimal in-feed centreless cylindrical grinding process parameters that would optimize the multiple-performance characteristics, namely, work piece surface roughness and out of cylindricity of internal combustion engine valve stems using grey relational analysis. The cylindrical grinding of valve stems was chosen owing to the fact that any error beyond permissible limits would progressively cause growing deposits of combustion residues and increase oil consumption, in addition to disturbed heat transmission and excessive wear. The valve stems were ground finished to very tight tolerances of shape, size and surface finish in order to obtain a consistent in-service performance.

The geometric characteristics of the valve stem (e.g. roundness, surface finish and out of cylindricity) are also important as these affect the specific operating load, noise, faster wear and overall performance of the part in an internal combustion engine. The valve stem is ground finished to the prescribed levels of surface finish as it affects material fatigue strength, corrosion resistance, sealing performance, friction, lubrication, force distribution, etc. The setting of in-feed centreless cylindrical grinding process parameters was accomplished using the Taguchi experimental design method. Moreover, the most effective factor and the order of importance of the controllable factors to the multi-performance characteristics in the in-feed centreless cylindrical grinding process were determined by using the grey relational grade.

## EXPERIMENTAL PROCEDURE

The experiments were conducted on a centreless cylindrical grinding machine (HMT, model GCL-50 TG, CNC centreless grinding machine). A schematic diagram of the In-feed Centreless Cylindrical grinding Process is shown in Fig.1. The process involved a cylindrical grinding of an internal combustion (IC) engine valve stem made of EN52 austenitic grade steel with a 79.6 mm diameter. For this grade of steel and the size of the valve stem to be ground finished, an A80N5V45 grinding wheel rotating at 1440 rpm (giving a surface speed of 45 m/s) and an A80RR control wheel were used based on experience. The cylindrical grinding process was carried out over a length of 98 mm of valve stem (Fig.2) with a job height of 212 mm above the blade. The chemical composition of EN52 is given in Table 1.

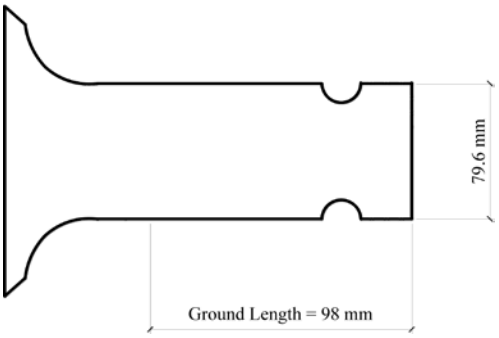


Fig.2: IC Engine Valve

Table 1: Composition of EN52 grade valve steel

| VALVE STEELS Chemical Composition (average values in %) | | | | | | | | | |
|---|---|---|---|---|---|---|---|---|---|
| Grade | C | Si | Mn | P | S | Cr | Mo | Ni | N |
| EN52 | 0.40 – 0.50 | 2.70 – 3.30 | 0.80 max | 0.04 max | 0.03 max | 8.0 – 10.0 | -- | -- | - |

As a large number of independent parameters control the in-feed centreless cylindrical grinding process, some preliminary experiments were conducted to determine the parameters to be taken into consideration for optimization. Four parameters (namely, grinding feed, dressing feed, dwell time and cycle time) were varied to obtain the optimum levels of parameters for acceptable quality. A summary of the experimental conditions is listed in Table 2. In order that the experiments were performed under chatter-free conditions, indirect parameters such as coolant flow rate (50 litre per minute), grinding depth (60 μm), blade angle (32$^o$), control wheel speed (25 rpm), blade height (212 mm), in-feed speed (20 rpm) and control wheel angle (1$^o$) were kept constant during experimentation.

## MEASUREMENT OF THE RESPONSE PARAMETERS

In order to achieve the best cylindrical grinding quality, Taguchi's experimental design was used for conducting the experiments (Roy, 1990). The experimental results after the cylindrical

Table 2: Design factors and their levels

| Trial No | Grinding Parameters | Notation | Units | Levels | | |
|---|---|---|---|---|---|---|
| | | | | Level -1 | Level -2 | Level - 3 |
| 1 | Dressing Feed | A | mm/min | 5 | 8 | 10 |
| 2 | Grinding Feed | B | mm/min | 2 | 6 | 10 |
| 3 | Dwell Time | C | s | 1.5 | 2.5 | 3 |
| 4 | Cycle Time | D | s | 10 | 11 | 12 |

grinding were evaluated in terms of the following measured cylindrical grinding performances: (1) surface roughness ($R_a$) and (2) out of cylindricity. Meanwhile, the surface roughness was measured with a surface roughness measuring instrument (Taylor Hobson, model SurfCom). The sampling length of each measurement was set to 6 mm as per the recommendations of ASME B-46.1-2002. In order to measure out of cylindricity, an indigenously made precision fixture was used, on which the ground valve-stem was held. Three equidistant sampling lengths of 6 mm each were taken on the valve-stem. At each end of the first sampling length, the probe of a dial-micrometer-gauge (Mitutoyo, AGD series 1010SB-11) was touched to the valve-stem. Subsequently, the valve-stem was given one complete rotation, while the minimum and maximum deflections in the pointer were recorded. The difference between the maximum and minimum deflections gave the valve's out of cylindricity over the sampling length. The above steps were repeated on the other sampling lengths and the average was taken as the valve's out of cylindricity for the ground valve-stem.

## DETERMINATION OF THE IN-FEED CENTRELESS CYLINDRICAL GRINDING PROCESS PARAMETERS

In this section, the use of the grey-based Taguchi method to determine the in-feed centreless cylindrical grinding process parameters is reported. The optimal in-feed centreless cylindrical grinding process parameters, with considerations of the multiple performance characteristics are also obtained and verified.

### *Orthogonal Array Experiment*

An $L_9$ orthogonal array, with 4 columns and 9 rows, is used. This array has eight degrees of freedom and it can handle three-level process parameters. Nine experiments are required to study the entire in-feed centreless cylindrical grinding process parameter space when the $L_9$ orthogonal array is used. The experiment layout for the in-feed centreless cylindrical grinding process parameters using the $L_9$ orthogonal array is shown in Table 3.

### *S/N Ratio for the Multiple Performance Characteristics*

In the Taguchi method, the term "signal" represents the desirable value (mean) for the output characteristic and the term "noise" represents the undesirable value for the output. There are three categories of quality characteristics, namely, the-lower-the-better, the-higher-the-better,

Table 3: Experimental layout using an L9 orthogonal array

| Experiment number | Grinding Parameter | | | |
|---|---|---|---|---|
| | Dressing Feed (mm/min) | Grinding Feed (mm/min) | Dwell Time (s) | Cycle Time (s) |
| 1 | 1 | 1 | 1 | 1 |
| 2 | 1 | 2 | 2 | 2 |
| 3 | 1 | 3 | 3 | 3 |
| 4 | 2 | 1 | 2 | 3 |
| 5 | 2 | 2 | 3 | 1 |
| 6 | 2 | 3 | 1 | 2 |
| 7 | 3 | 1 | 3 | 2 |
| 8 | 3 | 2 | 1 | 3 |
| 9 | 3 | 3 | 2 | 1 |

and the-nominal-the better. Surface roughness and out of cylindricity are the lower-the-better performance characteristics, with the loss function can be expressed as (Hsiao *et al*., 2007):

$$L_{ij} = \frac{1}{n}\sum_{k=1}^{n} y^2 ijk \qquad [1]$$

where $L_{ij}$ is the loss function of the *i*th performance characteristic in the *j*th experiment, $y_{ijk}$ is the experimental value of the *i*th performance characteristic in the *j*th experiment at the *k*th trial, and n is the number of trials. The loss function is further transformed into an S/N ratio to determine the deviation of the performance characteristic from the desired value. The S/N ratio $\eta_{ij}$ for the *i*th performance characteristic in the *j*th experiment can be expressed as:

$$\eta_{ij} = -10\log(L_{ij}) \qquad [2]$$

In the next section, the grey relational analysis is used to analyze the complicated inter-relationships among the S/N ratios, as shown in Table 4 and Table 5.

*Grey Relational Analysis for the S/N Ratio*

The grey relational generating (Deng, 1989), i.e. a linear normalization of the S/N ratio, is performed in the range between zero and unity. The normalized S/N ratio $x_{ij}$ for the *i*th performance characteristic in the *j*th experiment can be expressed as:

$$x_{ij} = \frac{\eta_{ij} - \min_j \eta_{ij}}{\max_j \eta_{ij} - \min_j \eta_{ij}} \qquad [3]$$

Table 6 shows the normalized S/N ratio for surface roughness and out of cylindricity. Basically, the larger normalized S/N ratio corresponds to the better performance and the best-normalized S/N ratio is equal to unity. The grey relational coefficient is calculated to express the relationship between the ideal (best) and actual normalized S/N ratio. Meanwhile, the

Table 4: Experimental results for surface roughness and its S/N ratio

| Experiment number | A | B | C | D | Surface roughness (μm) | S/N Ratio (dB) |
|---|---|---|---|---|---|---|
| 1 | 1 | 1 | 1 | 1 | 0.43 | 7.26 |
| 2 | 1 | 2 | 2 | 2 | 0.44 | 7.13 |
| 3 | 1 | 3 | 3 | 3 | 0.43 | 7.40 |
| 4 | 2 | 1 | 2 | 3 | 0.58 | 4.78 |
| 5 | 2 | 2 | 3 | 1 | 0.61 | 4.25 |
| 6 | 2 | 3 | 1 | 2 | 0.76 | 2.35 |
| 7 | 3 | 1 | 3 | 2 | 0.50 | 5.96 |
| 8 | 3 | 2 | 1 | 3 | 0.52 | 5.74 |
| 9 | 3 | 3 | 2 | 1 | 0.55 | 5.14 |

Table 5: Experimental results for out of cylindricity and its S/N ratio

| Experiment number | A | B | C | D | Out of cylindricity (mm) | S/N Ratio (dB) |
|---|---|---|---|---|---|---|
| 1 | 1 | 1 | 1 | 1 | 0.0007 | 63.52 |
| 2 | 1 | 2 | 2 | 2 | 0.0007 | 63.52 |
| 3 | 1 | 3 | 3 | 3 | 0.0010 | 60.00 |
| 4 | 2 | 1 | 2 | 3 | 0.0017 | 55.56 |
| 5 | 2 | 2 | 3 | 1 | 0.0010 | 60.00 |
| 6 | 2 | 3 | 1 | 2 | 0.0013 | 57.50 |
| 7 | 3 | 1 | 3 | 2 | 0.0033 | 49.54 |
| 8 | 3 | 2 | 1 | 3 | 0.0030 | 50.46 |
| 9 | 3 | 3 | 2 | 1 | 0.0037 | 48.71 |

grey relational coefficient $\xi_{ij}$ for the *i*th performance characteristic in the *j*th experiment can be expressed as:

$$\xi_{ij} = \frac{\min_i \min_j \left| x_i^0 - x_{ij} \right| + \xi \max_i \max_j \left| x_i^0 - x_{ij} \right|}{\left| x_i^0 - x_{ij} \right| + \xi \max_i \max_j \left| x_i^0 - x_{ij} \right|} \quad [4]$$

where $x_i^0$ is the ideal normalized S/N ratio for the ith performance characteristic, and $\xi$ distinguishing coefficient which is defined in the range of $0 \leq \xi \leq 1$.

A weighting method is then used to integrate the grey relational coefficients of each experiment into the grey relational grade. The overall evaluation of the multiple performance characteristics is based on the grey relational grade (Hsiao *et al*., 2007), as follows:

$$\gamma_j = \frac{1}{m} \sum_{i=1}^{m} w_i \xi_{ij} \quad [5]$$

Assume $w_1 = w_2 = 0.5$ as it is required to be taken to be equal in grey relational analysis, where $\gamma_j$ is the grey relational grade for the *j*th experiment, $w_i$ is the weighting factor for the *i*th performance characteristic, and m is the number of the performance characteristics.

Table 6: Normalized S/N ratios

| Experiment number | Surface roughness | Out of cylindricity |
|---|---|---|
| Ideal sequence | 1.00 | 1.00 |
| 1 | 0.97 | 1.00 |
| 2 | 0.95 | 1.00 |
| 3 | 1.00 | 0.76 |
| 4 | 0.48 | 0.46 |
| 5 | 0.38 | 0.76 |
| 6 | 0.00 | 0.59 |
| 7 | 0.72 | 0.06 |
| 8 | 0.67 | 0.12 |
| 9 | 0.55 | 0.00 |

Table 7 shows the grey relational grade for each experiment using the $L_9$ orthogonal array. A higher grey relational grade indicates that the corresponding S/N ratio is closer to the ideally normalized S/N ratio. The findings revealed that experiment 1 obtained the best multiple performance characteristics among the nine experiments because it has the highest grey relational grade (*see* Table 7). In other words, the optimization of the complicated multiple performance characteristics can be converted into the optimization of a single grey relational grade.

Table 7: Grey relational grade and its order

| Experiment number | Grey relational grade | Order |
|---|---|---|
| 1 | 0.9745 | 1 |
| 2 | 0.9520 | 2 |
| 3 | 0.8386 | 3 |
| 4 | 0.4865 | 6 |
| 5 | 0.5612 | 4 |
| 6 | 0.4424 | 8 |
| 7 | 0.4918 | 5 |
| 8 | 0.4823 | 7 |
| 9 | 0.4306 | 9 |

The effect of each in-feed centreless cylindrical grinding process parameter on the grey relational grade at different levels can be independent because the experimental design is orthogonal. The grey relational grade for each level of the in-feed centreless cylindrical grinding process parameters is summarized and shown in Table 8.

In addition, the total mean of the grey relational grade for the 9 experiments is also calculated and presented in Table 8. Fig.3 shows the grey relational grade graph, where the dashed line is the value of the total mean of the grey relational grade. Basically, the larger the grey relational grade, the better the multiple performance characteristics will be. However, the relative importance among the in-feed centreless cylindrical grinding process parameters for the multiple performance characteristics still needs to be known, so that the optimal combinations of the in-feed centreless cylindrical grinding process parameter levels can be determined.

Table 8: Response table for the grey relational grade

| Symbol | Process parameter | Grey relational grade | | | |
|---|---|---|---|---|---|
| | | Level 1 | Level 2 | Level 3 | Maximum- minimum |
| A | Dressing feed | 0.92 | 0.50 | 0.47 | 0.45 |
| B | Grinding feed | 0.65 | 0.67 | 0.57 | 0.10 |
| C | Dwell time | 0.63 | 0.62 | 0.63 | 0.01 |
| D | Cycle time | 0.66 | 0.63 | 0.60 | 0.06 |
| Total mean value of the relational grade = 0.63 | | | | | |

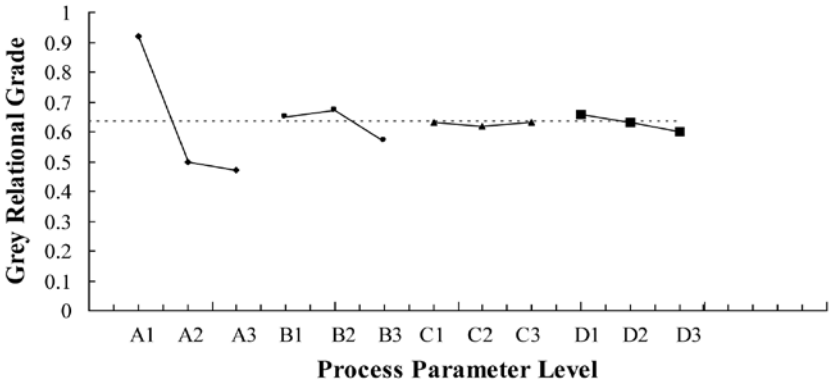


Fig.3: Grey Relational Grade Graph

*Analysis of Variance*

The purpose of the analysis of variance (ANOVA) is to investigate which in-feed centreless cylindrical grinding process parameters significantly affect the performance characteristics. This was accomplished by separating the total variability of the S/N ratios, which was measured by the sum of the squared deviations from the total mean S/N ratio into contributions by each of the design parameters and the error. First, the total sum of the squared deviations $SS_T$ from the mean S/N ratio $\eta_m$ was calculated (Hsiao *et al*., 2007) as follows:

$$SS_T \sum_{i=1}^{n} (\eta_i - \eta_m)^2 \quad [6]$$

where $n$ is number of the experiments in the orthogonal array, and $\eta_i$ is the mean S/N ratio for the $i$ th experiment.

The total sum of the squared deviations $SS_T$ is decomposed into two sources, namely, the sum of the squared deviations $SS_d$ (due to each process parameter), and the sum of the squared error $SS_e$. The percentage contribution by each of the process parameters in the total sum of the squared deviations $SS_T$ is a ratio of the sum of the squared deviations $SS_d$ due to each process parameter to the total sum of the squared deviations $SS_T$.

Statistically, there is a tool called $F$ test to determine which process parameters have significant effect on the quality characteristic. To perform the $F$ test, the mean of squared

deviations $SS_m$ needs to be calculated due to each process parameter. The mean of the squared deviations $SS_m$ is equal to the sum of the squared deviations $SS_d$ divided by the number of degree of freedom associated with the process parameter. Then, the *F* value for each process parameter is simply the ratio of the mean of the squared deviations $SS_m$ to the mean of squared error $SS_e$.

The results of ANOVA (Table 9) indicate that dressing feed, grinding feed and cycle time are the significant in-feed centreless cylindrical grinding process parameters that affect the multiple performance characteristics. Furthermore, the dressing feed is the most significant process parameter due to its highest percentage contribution among the process parameters. Based on the above discussion, the optimal in-feed centreless cylindrical grinding process parameters are dressing feed at level 1 (5 mm/min), grinding feed at level 2 (6 mm/min), dwell time at level 2 (2.5 s) and cycle time at level 2 (11 s).

Table 9: Results of analysis of variance (ANOVA)

| Source of variation | Degree of freedom | Sum of squares | Mean square | Variance Ratio (F) | Contribution (%) | P-value |
|---|---|---|---|---|---|---|
| A, Dressing feed | 2 | 0.387 | 0.194 | 2363 | 95.045 | 0.0004 |
| B, Grinding feed | 2 | 0.016 | 0.008 | 95.4 | 3.799 | 0.0104 |
| C, Dwell time | 2 | (0.00016) | - | - | - | - |
| D, Cycle time | 2 | 0.004 | 0.002 | 25.7 | 0.995 | 0.0375 |
| Residual | 2 | 0.00016 | 0.00008 | | 0.161 | |
| Total | 8 | 0.407 | 0.051 | | 100.000 | |

## CONFIRMATION TESTS

Once the optimal level of the design parameters has been selected, the final step is to predict and verify the improvement of the quality characteristic using the optimum level of the design parameters. The estimated S/N ratio $\hat{\eta}$ using the optimal level of the design parameters can be calculated as follows (Yang & Tarng, 1998):

$$\hat{\eta} = \eta_m + \sum_{i=1}^{0} (\eta_i - \eta_m) \quad [7]$$

where $\eta_m$ is the total mean S/N ratio, $\eta_i$ is the mean S/N ratio at the optimal level, and *o* is the number of the main design parameters that affect the quality characteristic.

The estimated S/N ratio using the optimal level of the process parameters can be calculated from Table 7, considering only the process parameters that significantly affect the multiple performance characteristics. Table 10 shows the comparison of the experimental results using the initial and optimal in-feed centreless cylindrical grinding process parameters. It is important to note that the in-feed centreless cylindrical grinding performance has been greatly improved through this study. As shown in Table 10, the surface roughness is decreased from 0.55 to 0.44 μm, and the out of cylindricity is changed from $37.0 \times 10^{-4}$ to $7.00 \times 10^{-4}$ mm.

Table 10: Results of in-feed centreless grinding performance using the initial and optimal process parameters

| | Initial Process Parameter | Optimal Process Parameters | |
|---|---|---|---|
| | | Prediction | Experiment (Average) |
| Level | $A_3B_3C_2D_1$ | $A_1B_2C_2D_2$ | $A_1B_2C_2D_2$ |
| Surface roughness, μm (Average) | 0.55 | | 0.44 |
| Out of cylindricity, mm (Average) | $37.0 \times 10^{-4}$ | | $7.00 \times 10^{-4}$ |
| Grey relational grade | 0.4306 | 0.958 | 0.952 |
| Improvement of the grey relational grade = 0.5214 | | | |

## CONCLUSION

This study engaged in the testing of the surface roughness and the out of cylindricity of internal combustion engine valve stem that had been ground finished on the in-feed centreless cylindrical grinding machine. The following conclusions are derived at:

- The multiple performance characteristics of the lowest surface roughness and out of cylindricity were obtained from the process parameters and the greatest grey relation value of 0.9745.
- The optimal multiple performance characteristics were achieved with dressing feed at level 1 (5 mm/min), grinding feed at level 2 (6 mm/min), dwell time at level 2 (2.5 s) and cycle time at level 2 (11 s).
- Using ANOVA, the dressing feed, grinding feed and cycle time were found to have significant impacts on the multiple performance characteristics while dwell time have insignificant impact.
- The experimental outcomes indicated that based on the optimal parameter combination level of the multiple performance characteristics, the experimental values of the surface roughness and out of cylindricity have been reduced. The grey relation was improved by 0.5214. Meanwhile, the grey relation value of the optimal parameter level fits the predicted value of the optimal parameter level very well and this serves as a proof of the projection power of this study.

The optimization of the complicated multiple performance characteristics can be greatly simplified through this approach. The performance characteristics of the in-feed centreless cylindrical grinding process, such as the surface roughness and the out of cylindricity, have been found to be reduced together by using the proposed method. In addition, the use of the Taguchi method, through the grey relational analysis, has been shown to have greatly simplified the optimization procedure for determining the optimal process parameters with the multiple performance characteristics in the in-feed centreless cylindrical grinding process.

## REFERENCES

American Society of Mechanical Engineer, ASME. (2003). *Surface Texture (Surface Roughness, Waviness & Lay)*, *ASME B46.1-2002*. American Society of Mechanical Engineer.

Bueno, R., Zatarain, M., & Aguinagalde, J. M. (1990). Geometric and Dynamic Stability in Centerless Grinding, *Annals of the CIRP*, *39*, 395–398.

Çaydaş, U., & Hasçalık, A. (2008). Use of the grey relational analysis to determine optimum laser cutting parameters with multi-performance characteristics. *Optics & Laser Technology, 40*, 987-994.

Chang, C. K., & Lu, H. S. (2007). Design optimization of cutting parameters for side milling operations with multiple performance characteristics. *International Journal of Advance Manufacturing Technology*, *32*, 18–26.

Chiang, K. T., & Chang, F. P. (2006). Optimization of WEDM process of particle reinforced material with multiply performance characteristics using grey relational analysis. *Journal of Material Processing Technology*, *180*, 96–101.

Deng, J. (1989). Introduction to grey system. *Journal of Grey System*, *1,* 1-24.

Hashimoto, F., & Lahoti, G. D. (2004). Optimization of Set-up conditions for stability of the Centerless Grinding Process, *CIRP Annals – Manufacturing Technology, 53*, 271-274.

Hsiao, Y. F., Tarng, Y. S., & Kung, K. Y. (2007). Application of grey-based Taguchi methods on determining process parameter of linear motion guide with multiple performance characteristics. *MATH'07 Proceedings of the 11th WSEAS International Conference on Applied Mathematics*, 72-79.

Ko-Ta, C. (2007). The optimal process conditions of an injection-molded thermoplastic part with a thin shell feature using grey -fuzzy logic: A case study on machining the PC/ABS cell phone shell. *Materials & Design, 28,* 1851-1860.

Lin, C. L. (2004). Use of the Taguchi method and grey relational analysis to optimize turning operations with multiple performance characteristics, *Materials and Manufacturing Processes, 19*, 209–220.

Lu, H. S., Chang, C. K., Hwanga, N. C., & Chung, C. T. (2009). Grey relational analysis coupled with principal component analysis for optimization design of the cutting parameters in high speed end milling. *Journal of Materials Processing Technology*, *209*(8), 3808-3817.

Palanikumar, K., Karunamoorthy, L., & Karthilesyan, R. (2006). Multiple performance optimization of machining parameters on the machining of GFRP composites using carbide (K10) tool, *Materials and Manufacturing Processes, 21*, 846–852.

Roy, R. K. (1990). *A primer on the Taguchi Method*. New York, USA, Competitive Manufacturing Series, Van Nostrand Reinhold.

Tosun, N. (2006). Determination of optimum parameters for multi-performance characteristics in drilling by using grey relational analysis, *International Journal of Advance Manufacturing Technology, 28*, 450–455.

Yang, W. H., & Tarng, Y. S. (1998). Design optimization of cutting parameters for turning operations based on the Taguchi method. *Journal of Materials Processing Technology*, *84*, 122–129.

Yang, Y. Y., Shie, J. R., & Huang, C. H. (2006). Optimization of dry machining parameters for high purity graphite in end-milling process. *Materials and Manufacturing Processes*, *21*, 832–837.

Pertanika J. Sci. & Technol. 20 (2): 269 - 281 (2012)

SCIENCE & TECHNOLOGY

Journal homepage: http://www.pertanika.upm.edu.my/

# Production of Lentivirus Carrying Green Fluorescent Protein with Different Promoters for *in vitro* Gene Transfer

**Siew Ching Ngai[1,a], Rajesh Ramasamy[2, 3] and Syahril Abdullah[1, 3 *]**

[1]*Medical Genetics Laboratory, Faculty of Medicine and Health Sciences, Universiti Putra Malaysia, 43400 Serdang, Selangor, Malaysia.*

[2]*Department of Pathology, Faculty of Medicine and Health Sciences, Universiti Putra Malaysia, 43400 Serdang, Selangor, Malaysia*

[3]*UPM-MAKNA Cancer Research Laboratory, Institute of Bioscience, Universiti Putra Malaysia, 43400 Serdang, Selangor, Malaysia*

## ABSTRACT

Many diseases are potential targets for gene therapy using either non-viral or viral vectors. Unlike non-viral methods, viral vectors, such as lentiviruses, have the ability to integrate into the host chromosome, which can lead to long-term transgene expression. Lentiviruses have advantages over other types of viruses due to their capacity to transduce non-dividing cells. An optimized generation of lentiviruses carrying green fluorescent protein (GFP) reporter gene driven by either UbC (LV/UbC/GFP) or CMV (LV/CMV/GFP) promoter is described in this paper. The lentiviruses were produced by co-transfecting lentiviral expression constructs and packaging mix into 293FT lentivirus producer cell lines. Lipofectamine was highly efficient in transfecting the cells compared to Transfast and Polyethyleneimine (PEI). Following cell transfection, syncytia were clearly visible at day 2. Lentiviruses were harvested at days 1, 2 and 3 post-transfection. The highest transduction efficiency was read from LV/CMV/GFP harvested at day 2 post-transfection and LV/UbC/GFP harvested at day 3 post-transfection. Finally, the GFP expression in COS-7 cells was determined at day 2 and day 14 post-transduction for transient and stable GFP expression. It was found that the GFP expression declined overtime. However, the transduction efficiency and duration of the transgene expression in COS-7 cells transduced with LV/CMV/GFP were higher compared to LV/UbC/GFP. In conclusion, we have successfully produced lentiviruses carrying GFP with different promoters and shown that the viruses were able to infect COS-7 cells at different efficiencies. Meanwhile, the generation of the active lentiviruses will allow us to proceed to the subsequent analysis of the effect of regulatory elements in future study.

**Keywords: GFP, Lentivirus, UbC, CMV, Gene transfer**

*Article history:*
Received: 6 December 2010
Accepted: 18 April 2011

*Email addresses:*
eunice_ngai@yahoo.com (Siew Ching Ngai),
r.rajesh@medic.upm.edu.my (Rajesh Ramasamy),
syahril@medic.upm.edu.my (Syahril Abdullah)
*Corresponding Author

[a]*Present address:*
Division of Human Biology, International Medical University, 57000 Kuala Lumpur, Malaysia

ISSN: 0128-7680 

## INTRODUCTION

Gene therapy is the introduction of a therapeutic gene into target cells to replace, manipulate or supplement non-functional or misfunctioning genes to treat diseases (Yang *et al*., 2006). Unlike non-viral methods, which are limited by their low rate of gene transfer and short duration of transgene expression, retroviral vectors have the ability to integrate into the host genome permanently, and this can further lead to a long-term transgene expression (Malik & Arumugam, 2005). Recombinant retroviruses derived from murine leukemia viruses are widely used as a gene transfer vector in research and clinical settings (Verma & Somia, 1997). However, retroviral vectors can only transduce actively dividing cell (Lewis & Emerman, 1994), and thus limit their application in gene therapy.

Lentiviruses are a genus of slow viruses of Retroviridae family, many of which, produce tumours (Kontaratos *et al*., 2010). They resemble retroviruses in their ability to integrate the transgene into the cell genome, which is in theory, should lead to a permanent transgene expression. Hence, lentivirus vectors have appeared to be an attractive gene therapy vector due to their ability to transduce non-proliferating cells (Bukrinsky *et al*., 1993; Gallay *et al*., 1997; Gallay *et al*., 1995). In 2010, lentiviruses have been applied in about 1.8% of the gene therapy clinical trials for various diseases (http://www.wiley.co.uk/genmed/clinical/[June2010]). Although lentiviruses are created based on human immunodeficiency virus type (HIV)-1, the lentiviruses used for the purpose of gene therapy have been modified to enhance their biosafety features (Dull *et al*., 1998). In the first generation of HIV-derived vectors (Naldini *et al*., 1996), the hybrid viral particles were produced from the expression of HIV-1 core proteins, enzymes, accessory factors and envelope of vesicular stomatitis virus G glycoprotein (VSVG) (Burns *et al*., 1993). In the second version, the component plasmids of the lentivirus have been reduced to *gag*, *pol*, *tat* and *rev* genes (Zufferey *et al*., 1997). In the latest generation of the lentivirus system (the third-generation), only a fractional set of HIV genes were used (*gag*, *pol* and *rev*). A deletion in the 3'LTR of the lentiviral expression construct resulted in a "self-inactivation" of the lentivirus after transduction into the target cells (Zufferey *et al*., 1998), rendering the proviral components to be unable to produce more viruses. The lentivirus was generated by the co-transfection of lentiviral expression plasmid with three lentiviral component plasmids in the transformed embryonal human kidney cells (293FT). These component plasmids supply the structural and replication proteins *in trans* for the generation of a complete virion. The co-transfection process can be performed by using a myriad of transfection agents, such as FuGene, GeneJuice, Lipofectamine, Transfast, Polyethyleneimine and several others. Meanwhile, the lentivirus can be harvested a day or few days post-transfection.

The transduction efficiency of the lentivirus vectors is regulated by many regulatory elements, such as promoters, enhancers, polyadenylation signals, etc. Lentiviral vectors can be designed to carry different types of promoters, depending on the target cell type and the target gene. The commonly used human cytomegalovirus (CMV) immediate-early promoter/enhancer has been shown to generate efficient and high level of gene expression (Andersson *et al*., 1989; Boshart *et al*., 1985; Nelson *et al*., 1987). Meanwhile, increased transduction efficiency and transgene expression were observed with CMV promoter in the presence of central polypurine tract (cPPT) and woodchuck posttranscriptional regulatory element (WPRE) in a lentiviral gene delivery context (Barry *et al.,* 2001). Interestingly, it has been reported

that human ubiquitin C (UbC) promoter generates a higher expression level of transgene in a wider range of tissues as compared to other routinely used promoters, such as H2-K, CMV or Pgk-1 (Schorpp *et al*., 1996). In a non-viral context, Gill *et al*. (2001) reported that UbC promoter directs higher and more durable transgene expression as compared to the CMV promoter in the lung of mouse.

In the present study, two types of lentivirus vectors carrying green fluorescent protein (GFP) reporter gene were produced. One was driven by UbC promoter (LV/UbC/GFP) and the other by CMV promoter (LV/CMV/GFP). Unlike LV/UbC/GFP, LV/CMV/GFP contained cPPT and WPRE. Prior to the production of lentivirus, different types of transfection reagents were tested for their transfection efficiency in order to select the most effective transfection reagent. Lentiviruses were harvested at different days of post-transduction to determine the highest titre of the lentivirus produced. Finally, the transduction efficiency of LV/UbC/GFP and LV/CMV/GFP in African green monkey kidney fibroblast (COS-7) were also checked for the transient and stable GFP expression.

## MATERIALS AND METHODS

### *Cell Cultures*

Transformed embryonal human kidney (293FT) and African green monkey kidney fibroblast (COS-7) cell lines were purchased from Invitrogen (Carlsbad, CA, USA) and American Type Culture Collection (ATCC) (Manassas, VA, USA), respectively. The 293FT cells were cultured in Dulbecco's modified Eagle's medium (DMEM) (Sigma-Aldrich, MO, USA) supplemented with 6 mM L-glutamine (PAA Laboratories GmbH, Austria), 0.1 mM MEM non-essential amino acids (PAA Laboratories GmbH), 1 mM MEM sodium pyruvate (Sigma-Aldrich), 50 µg/ml Geneticin (Gibco BRL, Paisley, UK) and 10% foetal bovine serum (FBS) (Gibco). COS-7 cells were cultured in DMEM supplemented with 10% FBS. The cells were maintained at 37°C in humidified 5% $CO_2$ atmosphere.

### *Construction of the Lentiviral Expression Vectors*

Plasmid phMGFP (Promega, Madison, WI, USA) was transformed into *E. coli* JM109 Competent Cells (Promega), whereas the pENTR™4 (Invitrogen) was transformed into Library Efficiency® *E. Coli* DB3.1™ Competent Cells (Invitrogen). The plasmids were purified using PureLink™ HQ Mini Plasmid Purification kit (Invitrogen). The plasmids were restriction digested and subjected to agarose gel electrophoresis to separate the GFP and pENTR™ backbone from the other digested fragments. Following gel extraction, the GFP was subcloned into the pENTR™4. The resulting pENTR™4/GFP was verified using a restriction enzyme analysis on agarose gel. Next, a recombination reaction was performed between pENTR™4/GFP and pLenti6/UbC/V5-DEST (Lentivirus plasmid destination vector construct) (Invitrogen) using LR Clonase™ II enzyme mix (Invitrogen) to produce pLenti6/UbC/GFP/V5-DEST. The product was transformed into One Shot® Stbl3™ chemically competent *E. coli* (Invitrogen) and verified using the restriction enzyme analysis and DNA sequencing. Meanwhile, pLenti6/CMV/GFP/V5-DEST plasmid was purchased from Invitrogen and used as a control in this study.

*Transfection*

293FT cells were seeded in 24-well tissue culture plate at 5 x $10^4$ cells per well. After 24 hours of culturing, the cells were transfected with 1 μg of phMGFP, pLenti6/UbC/GFP/V5-DEST (pL/UbC/GFP) or pLenti6/CMV/GFP/V5-DEST (pL/CMV/GFP) by using Lipofectamine (Invitrogen), Polyethyleneimine (PEI) (Sigma-Aldrich) or Transfast (Promega), according to the protocol suggested by the manufacturer. The medium containing the transfection mixture was discarded and replaced with fresh DMEM complete medium at day 1 post-transfection. The transfection efficiency was evaluated as a percentage of GFP-expressing cells within the total cells acquired by flow cytometry analysis at day 2 post-transfection.

*Lentivirus Production*

Lentivirus vectors, pseudotyped with vesicular stomatitis virus G glycoprotein (VSV-G), were generated. Briefly, 293FT cells (1 x $10^6$ cells per well in 6-wells tissue culture plate) were co-transfected with packaging mix (plasmids to provide structural and replication proteins *in trans* required to produce the virions) (Invitrogen) and the lentiviral expression plasmid (pL/UbC/GFP or pL/CMV/GFP) in the OptiMEM (Invitrogen) medium. The packaging mix is comprised of three expression plasmids encoding the packaging protein gag-pol (pLP1), rev-expressing construct (pLP2) and VSVG-expressing construct (pLP/VSV-G). Meanwhile, the morphology of the cells was analyzed under inverted brightfield microscopy examination for the presence of syncytia, and virus supernatant was harvested after 24, 48 and 72 hours by centrifugation at 1000 x g for 15 minutes at 4°C. The lentiviruses produced were LV/UbC/GFP (GFP expression controlled by UbC promoter) and LV/CMV/GFP (GFP expression controlled by CMV promoter).

*Transduction Efficiency*

COS-7 cells were seeded at 5 x $10^4$ cells per well in 24-well tissue culture plates . On the following day, the cells were transduced with LV/UbC/GFP or LV/CMV/GFP in a complete DMEM tissue culture medium with polybrene (Sigma) at a final concentration of 6 μg/ml. The medium containing the virus was removed and replaced with fresh complete medium at day 1 post-transduction. At day 2 post-transduction, growth medium was removed and replaced with a dissociation solution. The GFP expression of COS-7 transduced with the viruses was evaluated as a percentage of GFP-expressing cells within the total cells acquired by flow cytometry. The percentage of the GFP expression was used to calculate the titre of lentivirus. Once the titre of the viruses had been determined, the GFP expression was evaluated at day 2 and 14 post-transduction for the transient and stable expression at multiplicity of infection (MOI) of 0.8.

*Flow Cytometry*

The cells were dissociated and centrifuged at 250 x g for 5 minutes to remove residual media components. Next, the cell pellet was resuspended in PBS with 1% foetal bovine serum. The total events of 10,000 were set. The cells were analyzed for green fluorescence by

FACSvantage (Becton Dickinson, San Jose, CA) using CellQuest software. Dead cells were excluded and negative green fluorescence was set at around 1% for the untreated cells.

### *Statistical Analysis*

Numerical data were expressed as mean with standard deviations. ANOVA was applied to compare the means of the experiment samples, followed by a *post-hoc* test to determine the statistical significance in the mean difference. The differences with $P \leq 0.05$ were considered to be statistically significant.

## RESULTS AND DISCUSSION

### *Construction of Lentiviral Expression Vector*

Successful gene delivery into somatic cells relies on the ability of the gene delivery vector to deliver the gene with high efficiency. Lentivirus (LV) was selected for this study because it can transduce non-proliferating cell (Zufferey *et al*., 1997) and integrate into the host genome (He *et al*., 2005). In addition, Dull *et al*. (1998) reported that the LV was highly efficient for *in vivo* gene delivery and exhibited prolonged transgene expression in several tissues. In this study, the production of two types of LV vectors carrying GFP reporter gene, driven by a UbC (LV/UbC/GFP) or CMV (LV/CMV/GFP) promoter, are described. Unlike LV/UbC/GFP, LV/CMV/GFP contains two additional *cis*-acting regulatory sequences, namely, the Woodchuck Post-transcriptional Regulatory Element (WPRE) and the central Polypurine Track (cPPT).

To construct the lentiviral expression vector carrying GFP reporter gene, driven by UbC promoter, a GFP gene from phMGFP was subcloned into a pENTR4 to generate pENTR4/GFP, which is an entry clone for the Gateway Expression System. Subsequently, the LR recombination reaction was performed between pENTR4/GFP and pLenti6/UbC/V5-DEST to generate pLenti/UbC/GFP/V5-DEST (pL/UbC/GFP). The resulting construct was verified by restriction enzyme analysis and sequencing. The lentiviral expression vector construct pLenti/CMV/GFP/V5-DEST (pL/CMV/GFP), which is driven by CMV promoter with extra

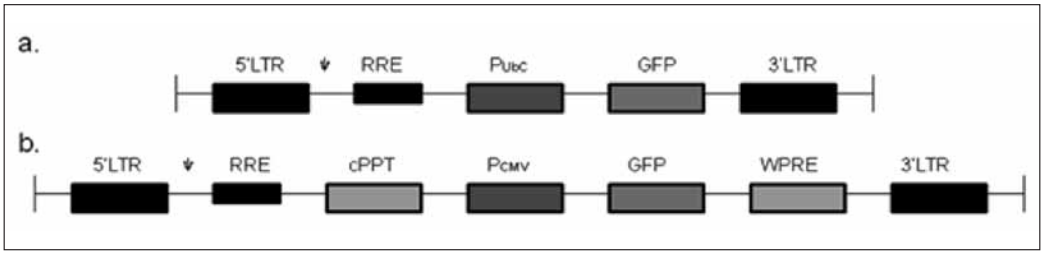


Fig.1: Genomic structure of the lentiviral expression vectors; (a) The LV construct encoding GFP under the control of the UbC promoter, (b) The LV construct encoding GFP under the control of the CMV promoter with cPPT and WPRE. Long terminal repeat (LTR), HIV-1 psi packaging signal (ψ), HIV-1 Rev-response element (RRE), Polypurine Tract from HIV (cPPT), human ubiquitin C promoter ($P_{UbC}$), human cytomegalovirus immediate-early promoter ($P_{CMV}$), Green Fluorescent Protein reporter gene (GFP), Woodchuck Posttranscriptional Regulatory Element (WPRE) are indicated

post-transcriptional regulatory element (WPRE) and transduction enhancer (cPPT), was used as a control. The genomic structure of the lentiviral expression vectors is shown in Figure 1.

### *Transfection Efficiency of Lipofectamine, Polyethyleneimine (PEI) and Transfast on 293FT*

To produce the virus, the 293FT cells were co-transfected with lentiviral expression vector and the packaging mix. Due to the myriad of the transfection agents available, it was pertinent to select the transfection agent that could shuttle the plasmids into the cells efficiently. In this study, the transfection efficiency of Lipofectamine, Transfast and Polyethyleneimine (PEI) was compared. Plasmids pL/UbC/GFP and pL/CMV/GFP were transfected into 293FT cell lines and the cells were subjected for examination under fluorescent microscopy and flow cytometry at day 2 of post-transfection.

GFP expression was observed from the cells transfected with pDNAs by all the transfection agents tested (see Fig. 2). Transfast and Lipofectamine appeared to be more efficient at transfecting cells compared to PEI, based on the number of the cells transfected qualitatively. With Transfast, the transfected cells were evenly spread across the plate, whereas the transfection by Lipofectamine was localized to a few populations of the cells. Meanwhile, the delivery of the naked pDNAs did not show qualitatively significant GFP expression.

The flow cytometry analysis was performed to further verify the qualitative observations. The percentage of 293FT cells transfected with the pDNAs using Lipofectamine and Transfast was found to be significantly higher than PEI and naked pDNA (Figure 3). For Lipofectamine, the percentages of the cells with GFP reading were 72.15, 81.90 and 92.29 for pL/UbC/GFP, pL/CMV/GFP and phMGFP, respectively. Transfast showed GFP readings of 71.00% (pL/UbC/GFP), 86.72% (pL/CMV/GFP) and 67.60% (phMGFP). Although Lipofectamine showed a trend of higher percentage of a number of cells transfected, the values were not significantly different than Transfast. The transfection efficiency of PEI was the lowest among the transfection reagents, with GFP readings of 9.93% (pL/UbC/GFP), 13.92% (pL/CMV/GFP) and 4.30% (phMGFP). Mock transfections without transfection agent showed values that are less than 2% for all the pDNAs.

To produce the virus, the lentiviral expression plasmid construct was co-transfected with 3 other plasmids (pLP1, pLP2 and pLP/VSV-G) in packaging mix, which provide the structural, replication protein and envelope of the virus *in trans*. Prior to the production of the virus, different transfection reagents were tested for their ability to transfect the GFP expression plasmids (pL/UbC/GFP, pL/CMV/GFP and phMGFP) into the 293FT LV producer cell line efficiently. Among the transfection reagents tested, Lipofectamine exhibited the highest transfection efficiency. Therefore, Lipofectamine was used to co-transfect the packaging mix and the GFP expressing LV plasmid (either pL/UbC/GFP or pL/CMV/GFP) into the LV producer cell line to produce the virus.

### *Lentivirus Production and Infectivity*

Lentivirus was generated by the co-transfection of 293FT cells with packaging mix (pLP1, pLP2 and pLP/VSV-G) and a lentiviral expression plasmid construct (either pL/UbC/GFP or

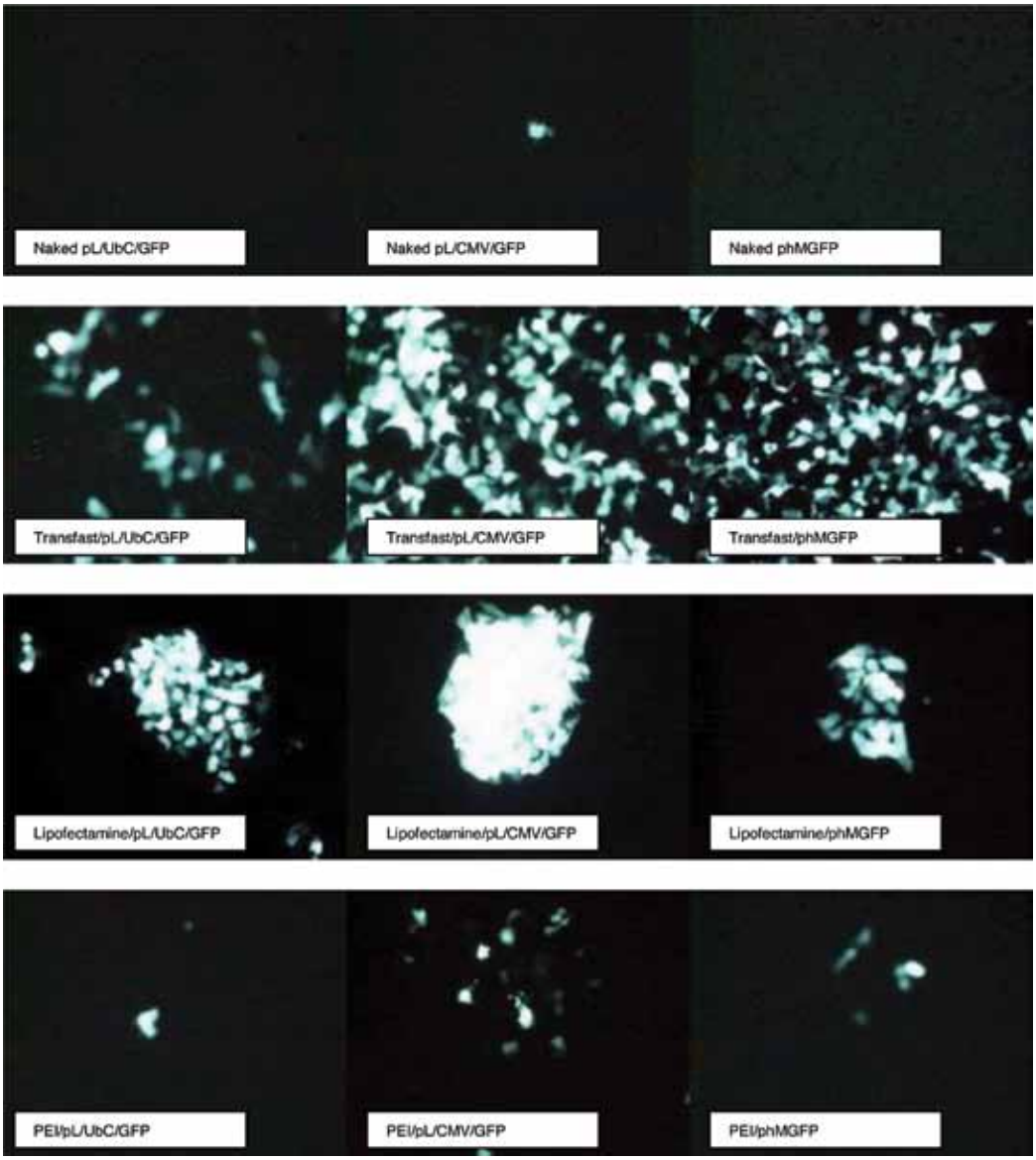


Fig.2: Fluorescent microscopy of the GFP expression in the 293FT cell lines transfected with different plasmids using different transfection reagents; Original magnification x20

pL/CMV/GFP), using Lipofectamine as the transfection reagent. As shown in Fig. 4, syncytia were clearly visible at day 2 post-transfection. The formation of syncytia is a sign for the lentivirus production. Meanwhile, the formation of the multinucleated cells implied that the packaging plasmid had been transfected and expressed successfully in the 293FT cells. The formation of syncytia was due to the expression of VSV-G glycoprotein translated from pL/VSVG, which subsequently caused the fusion of the 293FT cells into large and multinucleated cells. Lentiviruses LV/UbC/GFP and LV/CMV/GFP were harvested at days 1, 2 and 3 post-transfection. To determine the infectivity of the virus, COS-7 cells were transduced with the

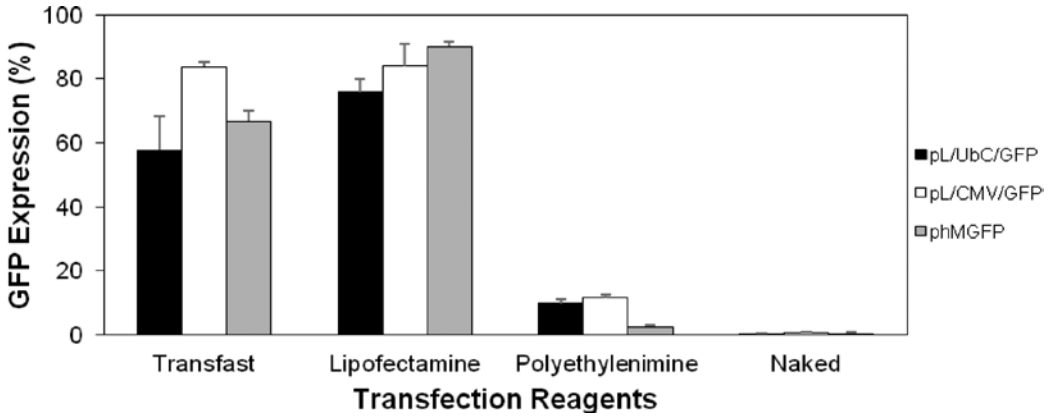


Fig.3: Transfection efficiency using Transfast, Lipofectamine and PEI in the 293FT cell line with plasmid pL/UbC/GFP, pL/CMV/GFP and phMGFP. The GFP expression was measured at 48h post-transfection as the percentage of GFP-expressing cells within the total cells acquired. Data are presented as mean ± SD of experiments conducted in triplicates

harvested viruses and the percentage of GFP expressions was determined by flow cytometry at day 2 of post-transduction.

Based on the information illustrated in Fig. 5, LV/UbC/GFP harvested at day 3 post-transfection showed the highest GFP expression (32.81%) although the reading was not statistically different from the virus harvested at day 2 (19.74%). For LV/CMV/GFP, the lentivirus harvested at day 2 post-transfection showed the highest GFP reading, followed by day 3 and day 1 post-transfection, with GFP expressions of 89.41%, 83.48% and 46.86%. In general, the results also exhibit that the GFP readings from LV/CMV/GFP at all days of post-transfection were significantly higher compared to LV/UbC/GFP. Since there were no significant differences between the values of both the viruses harvested at day 2 and day 3, it was decided that the lentiviruses should be harvested at day 2 post-transfection for the following experiments to avoid the risks of contamination.

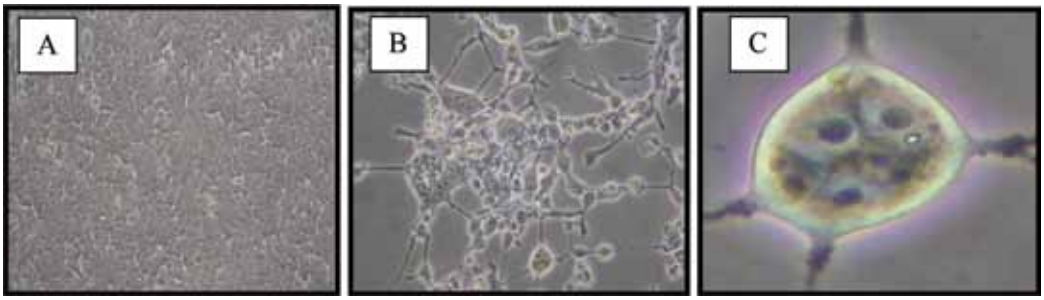


Fig.4: The morphology of the 293FT cell line transfected with lentiviral vector expression plasmid and packaging mix at day 2 of post-transfection; (A) Untreated cells, (B) Transfected cells. 293FT cells were fused together and became multinucleated (syncytia). (C) A single multinucleated cell from the original photo. 293FT cells were examined under inverted brightfield microscope at original magnification x20

The harvested lentivirus was subsequently used to transduce COS-7 cells. Higher transduction efficiency was obtained from the cells transduced with LV/CMV/GFP compared to LV/UbC/GFP harvested at all days post-transfection even though the same parameters had been used to produce both the viruses. It was speculated that the higher GFP expression by LV/CMV/GFP was either caused by the differences in the promoter used or by the incorporation of WPRE and cPPT in LV/CMV/GFP. A previous study reported that the incorporation of WPRE and cPPT into lentiviral vector driven by CMV promoter provided increased transduction

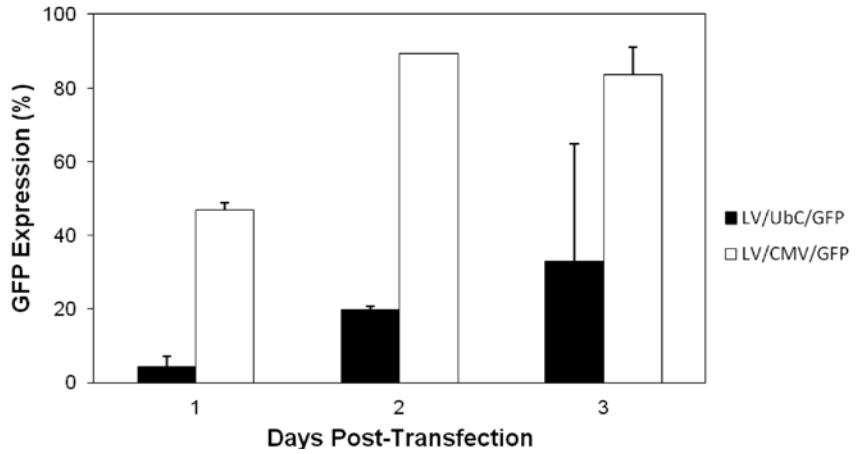


Fig.5: The GFP expression of COS-7 cells transduced with either LV/UbC/GFP or LV/CMV/GFP harvested at days 1, 2 and 3 post-transfection. The GFP expression was measured at day 2 post-transduction as the percentage of the GFP-expressing cells within the total cells acquired. Data are presented as the mean ± SD of experiments conducted in triplicates

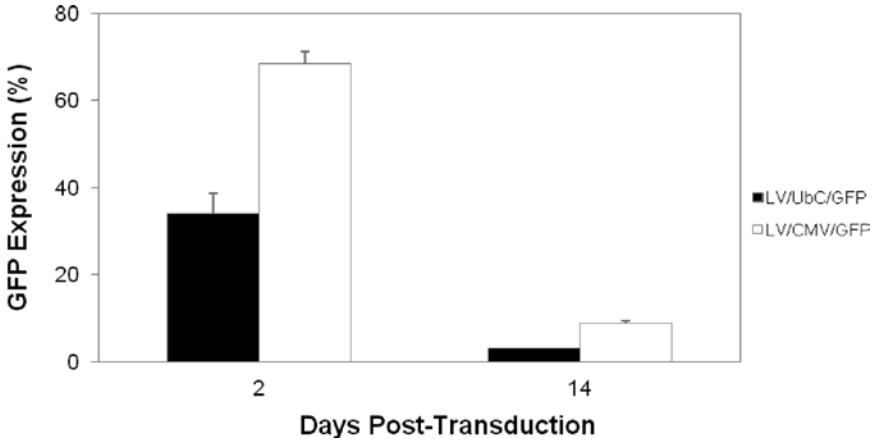


Fig.6: The GFP expression of COS-7 cell lines transduced either with LV/UbC/GFP or LV/CMV/GFP at MOI of 0.8. GFP was measured as the percentage of the GFP-expressing cells within the total cells acquiredat day 2 and day 14 post-transduction. Data are presented as the mean ± SD of the experiments conducted in triplicates

efficiency (Barry *et al*., 2001). However, Gill *et al*. (2001) reported that UbC promoter generated greater transgene expression as compared to CMV promoter in a non-viral gene delivery context. The main reason for the high transgene expression by the LV/CMV/GFP will only be determined when a new LV/UbC/GFP is developed with the presence of WPRE and cPPT in future investigations.

*Transient and Stable Lentivirus Reporter Gene Expression*

GFP activities were also evaluated for the transient and stable expression. Prior to this experiment, the Multiplicity of Infection (MOI) of 0.8 was detected as the most efficient MOI for COS-7 cells transduction (data not shown). Therefore in this study, the cells were transduced with LV/UbC/GFP and LV/CMV/GFP at MOI of 0.8 in the presence of Polybrene. The medium was replaced at day 1 post-transduction and the cells were subjected to flow cytometry analysis at day 2 and day 14 post-transduction. As illustrated in Fig. 6, the GFP expressions for COS-7 transduced with LV/UbC/GFP (33.92%) and LV/CMV/GFP (68.5%) were significantly higher at day 2 post-transduction as compared to day 14 post-transduction (LV/UbC/GFP of 3.1% and LV/CMV/GFP of 8.82%). The results also show that the GFP expression of the cells transduced with LV/CMV/GFP was approximately 2-folds higher than the cells transduced with LV/UbC/GFP at both time points of the study.

The reduction in GFP expression from the cells transduced by both viruses diminished over time, which might be due to transgene silencing or promoter attenuation. Nevertheless, the GFP readings for both LV/CMV/GFP and LV/UbC/GFP at day 14 post-transduction were still significantly high as compared to the untreated control. Similar results were also seen with the GFP expression from murine embryonic carcinoma (EC) P19 cells transduced with the LV (He *et al*., 2005). The authors reported that the decrease in the transgene expression was due to the transcriptional silencing and not by the deletion of the transgene. Meanwhile, DNA methylation and chromatin modification have been reported as the two modes of epigenetic control of genome function (Ou *et al*., 2007). These may lead to the GFP silencing as observed in our study. Based on the results obtained in the current study, the cells transduced by LV/UbC/GFP were probably subjected to the transgene silencing more severely as compared to the cells that were transduced by LV/CMV/GFP. Hence, it was speculated that the transgene silencing was caused by the DNA methylation at the CpGs site in the promoter region. The UbC promoter has more CpGs (88 CpGs) as compared to CMV promoter (30 CpGs), and therefore, it may be prone to the silencing effects compared to the CMV promoter. To further confirm whether methylation at the CpG site was the factor for the transgene silencing, sodium bisulfate sequencing performed to compare the percentage of methylation in the UbC and CMV regions in the upcoming study.

The reporter gene, driven by UbC promoter, has been reported to exhibit higher transgene expression *in vivo* as compared to its CMV counterpart, in a non-viral gene delivery context (Gill *et al*., 2001). However, in the LV gene delivery context study, the LV/CMV/GFP has been shown to exhibit better transduction efficiency and a stable gene expression as compared to LV/UbC/GFP. The superior results exhibited by the LV/CMV/GFP in this study could be due to the presence of cPPT and WPRE in the viral construct. In addition, the LV vector, with

cPPT in its construct, has been shown to have high copy number of provirus integrated into the host genome (Park & Kay, 2001), and thus resulting in the higher reporter gene expression. Sirven *et al*. (2000) also reported that the inefficiency of gene transfer by lentivirus, which was due to the limitation of nuclear translocation, had been overcome by the presence of cPPT. Meanwhile, WPRE, which is purified from woodchuck hepatitis virus, has been exploited as an enhancer of the transgene expression by increasing the nuclear export of mRNA to the cytoplasm and subsequently increased protein synthesis (Mastroyiannopoulos *et al.,* 2005).

## CONCLUSION

The production of two types of lentiviral vectors has been described in the current study. As indicated earlier, the two types of lentiviral vectors are driven differently; one driven by a UbC promoter (LV/UbC/GFP) and the other by CMV promoter with two additional *cis*-acting regulatory sequences (LV/CMV/GFP). Among the transfection reagents tested to deliver the lentiviral construct and structural plasmids into the 293FT cells, Lipofectamine showed the highest transfection efficiency. The higher transduction efficiency and gene expression were exhibited by LV/CMV/GFP as compared to LV/UbC/GFP. The successful production of these lentiviruses will allow the researchers to further analyze the effects of the UbC promoter and the two regulatory sequences in the LV construct in the subsequent study.

## ACKNOWLEDGEMENT

This work was supported by a grant from the Ministry of Science, Technology and Innovation, Malaysia (ScienceFund: 02-01-04-SF0230).

## REFERENCES

Andersson, S., Davis, D. L, Dahlback, H., Jornvall, H., & Russell, D. W. (1989). Cloning, Structure, and expression of the mitochondrial cytochrome P-450 sterol 26-hydroxylase, a bile acid biosynthetic enzyme.*The Journal of Biological Biochemistry, 264*, 8222-8229.

Barry, S. C., Harder, B., Brzezinski, M., Flint, L. Y., Seppen, J., & Osborne, W. R. (2001). Lentivirus vectors encoding both central polypurine tract and posttranscriptional regulatory element provide enhanced transduction and transgene expression. *Human Gene Therapy, 12* (9), 1103-1108.

Boshart, M., Weber, F., Jahn, G., Dorsch-Häsler, K., Fleckenstein, B., & Schaffner, W. (1985). A very strong enhancer is located upstream of an immediate early gene of human cytomegalovirus. *Cell, 41*, 521-530.

Bukrinsky, M. I., Haggerty, S., Demopsey, M. P., Sharova, N., Adzhubel, A., Spitz, L., Lewis, P., Goldfarb, D., Emerman, M., & Stevenson, M. (1993). A nuclear localization signal within HIV-1 matrix protein that governs infection of non-dividing cells. *Nature,* 365, 666-669.

Burns, J. C., Friedmann, T., Driever, W., Burrascano, M., & Yee, J. K. (1993). Vesicular stomatitis virus G glycoprotein pseudotyped retroviral vectors: concentration to very high titer and efficient gene transfer into mammalian and non-mammalian cells. *Proceedings of the National Academy of Sciences of the United States of America*, *90*, 8033-8037.

Dull, T., Zufferey, R., Kelly, M., Mandel, R. J., Nguyen, M., Trono, D., & Naldini, L. (1998). A third-generation lentivirus vector with a conditional packaging system. *Journal of Virology, 72*(11), 8463-8471.

Gallay, P., Chin, D., Hope, T. J., & Trono, D. (1997). HIV-1 infection of nondividing cells mediated through the recognition of integrase by the import/karyopherin pathway. *Proceedings of the National Academy of Sciences of the United States of America*, *94*, 9825-9830.

Gallay, P., Swingler, S., Aiken, C., & Trono, D. (1995). HIV-1 infection of nondividing cells: C-terminal tyrosine phosphorylation of the viral matrix protein is a key regulator. *Cell, 80*, 379-388.

Gill, D. R., Smyth, S. E., Goddard, C. A., Pringle, I. A, Higgins, C. F., Colledge, W. H., & Hyde, S. C. (2001). Increased persistence of lung gene expression using plasmids containing the ubiquitin C or elongation factor 1α promoter. *Gene Therapy, 8*, 1539-1546.

He, J., Yang, Q., & Chang, L. J. (2005). Dynamic DNA methylation and histone modifications contribute to lentiviral transgene silencing in murine embryonic carcinoma cells. *Journal of Virology, 79*(21), 13497-13508.

Kontaratos, N., Sourvinos, G., & Spandidos, D. A. (2010). Examining the discovery of the human retrovirus. *Journal of BUON*, *15*, 174-181

Lewis, P. F., & Emerman, M. I. (1994). Passage through mitosis is required for oncoretroviruses but not for the human immunodeficiency virus. *Journal of Virology*, *68*, 510-516.

Malik, P., & Arumugam, P. I. (2005). Gene Therapy for beta-thalassemia. *Hematology Am Soc Hematol Educ Program*, 45-50.

Mastroyiannopoulos, N. P., Feldman, M. L., Uney, J. B., Mahadevan, M. S., & Phulactou, L. A. (2005). Woodchuck post-transcriptional element induces nuclear export of myotonic dystrophy 30 untranslated region transcripts. *The EMBO Journal, 6*(5), 458-463.

Naldini, I., Blomer, U., Gallay, P., Ory, D., Mulligan, R., Gage, F. H., Verma, I. M., & Trono, D. (1996). *In vivo*gene delivery and stable transduction of nondividing cells by a lentiviral vector. *Science*, *272*, 263-267.

Nelson, J. A., Reynolds-Kohler, C., & Smith, B. A. (1987). Negative and positive regulation by a short segment in the 5′-flanking region of the human cytomegalovirus major immediate-early gene. *Molecular and Cellular Biology, 7*, 4125-4129.

Ou, J. N., Torrisani, J., Unterberger, A., Provencal, N., Shikimi, K., Karimi, M., Ekstrom, T. J., & Szyf, M. (2007).Histone deacetylase inhibitor Trichostatin A induces global and gene-specific DNA demethylation in human cancer cell lines. *Biochemical Pharmacology*, *73*, 1297-1307.

Park, F., & Kay, M. A. (2001). Modified HIV-1 based lentiviral vectors have an effect on viral transduction and gene expression *in vitro* and *in vivo*. *Molecular Therapy*, *4*(3), 164-174.

Schorpp, M., Jager, R., Schellander, K., Schenkel, J., Wagner, E. F., Weiher, H., & Angel, P. (1996). The human ubiquitin C promoter directs high ubiquitous expression of transgenes in mice. *Nucleic Acids Research*, *24*(9), 1787-1788.

Sirven, A., Pflumio, F., Zennou, V., Titeux, M., Vainchenker, W., Coulombel, L., Dubart-Kupperschmitt, A., & Charneau, P. (2000). The human immunodeficiency virus type-1 central DNA flap is a crucial determinant for lentiviral vector nuclear import and gene transduction of human hematopoietic stem cells. *Blood, 96*(13), 4103-4110.

Verma, I. M., & Somia, N. (1997). Gene therapy -- promises, problems and prospects. *Nature, 389*(6648), 239-242.

Zufferey, R., Dull, T., Mandel, R. J., Bukovsky, A., Quiroz, D., Naldini, L., & Trono, D. (1998). Self-inactivating lentivirus vector for safe and efficient in vivo gene delivery. *J Virol, 72*(12), 9873-9880.

Zufferey, R., Nagy, D., Mandel, R. J., Naldini, L., & Trono, D. (1997). Multiply attenuated lentiviral vector achieves efficient gene delivery in vivo. *Nat Biotechnol, 15*(9), 871-875.

Pertanika J. Sci. & Technol. 20 (2): 283 - 298 (2012)

SCIENCE & TECHNOLOGY

Journal homepage: http://www.pertanika.upm.edu.my/

# Numerical Simulation on the Reflection Characterisation and Performance of a Solar Collector - A Case Study of UPM Solar Bowl

**Ng, K. M.[1, 3]*, Adam, N. M.[2] and Azmi, B. Z.[1]**

[1]*Alternative and Renewable Energy Laboratory, Institute of Advanced Technology, Universiti Putra Malaysia, 43400 Serdang, Selangor, Malaysia*

[2]*Department of Mechanical and Manufacturing Engineering, Faculty of Engineering, Universiti Putra Malaysia, 43400 Serdang, Selangor, Malaysia*

[3]*Department of Mechanical and Automotive Engineering, School of Engineering and Technology Infrastructure, Kuala Lumpur Infrastructure University College, 43000 Kajang, Selangor, Malaysia*

## ABSTRACT

A numerical simulation of UPM Solar Bowl is presented in this paper. The numerical analysis considered a general model of solar bowl, which was divided into three modules: (a) reflection characterisation of the bowl, (b) solar flux density along the receiver, and (c) radiation contour mapping of the receiver. The governing equations are resolved in a segregated manner using Matlab programming environment. The influence of the tropical clear sky irradiance on the collector was numerically studied, whereas the collector performance in time domain was also quantified. Single reflection is a major element in thermal concentration. It was observed that solar flux density of collector substantially deteriorated during off solar noon hour, in which during 08:00 and 16:00 under clear sky of tropics, the percentage reduction of flux density is over 82% at all points of the receiver. The simulated radiation contour mapping of the receiver supports the finding. Other results of the UPM Solar Bowl simulation model are also shown and discussed.

**Keywords: numerical simulation, reflection characterisation, collector performance, time domain, UPM Solar Bowl**

*Article history:*
Received: 6 December 2010
Accepted: 30 May 2011

*Email addresses:*
mun_311@hotmail.com (Ng, K. M.),
mariah@eng.upm.edu.my (Adam, N. M.),
azmizak@fsas.upm.edu.my (Azmi, B. Z.)
*Corresponding Author

## INTRODUCTION

UPM Solar Bowl is a kind of fixed mirror distributed focus (FMDF) solar collector, which was designed to collect solar energy for power generation purposes. It was constructed at Universiti Putra Malaysia in 1997 as a pioneer solar bowl in Malaysia

ISSN: 0128-7680 

(Sulaiman *et al*., 1997). This system consists of a large and stationary spherical bowl that serves to reflect and focus incident sunrays on a sun tracking linear solar receiver. In addition, a similar solar concentrator was also developed and has been operated since 1980s at Crosbyton, Texas as a research and test facility to investigate its operation components (O'Hair & Green, 1990, 1992). It was a solar thermal power plant employing a steam driven turbine generator as a solar power conversion system (Bethea *et al*., 1981).

Several studies have been conducted to investigate solar bowl technology. Kreider (1975) presented the thermal performance evaluation of the collector by incorporating the effects of mirror reflectance, concentration ratio, insolation level, fluid flow rate, envelope evacuation and incidence angle in the analysis. Clausing (1976) presented an analytical study for the FMDF collector to evaluate the collector system efficiency. Gandhe *et al*. (1989) fabricated a spherical reflecting bowl to analyse the heat transfer feature of the absorber and the results agreed well with the prediction from mathematical models. Variations of optical concentration for oblique incident rays striking the reflector had also been investigated in another study of Gandhe *et al*. (1986a) who showed that the optical concentration and the surface temperature of absorber decreased with the increment of solar zenith angle. The researchers also presented an optical analysis of a cylindrical absorber and showed the effect of optical concentration on absorber with and without glass cover (Gandhe *et al*., 1986b). El-Refaie (1989) studied a mathematical model to determine the concentration profiles along the receiver under different conditions. The effects of the reflector rim angle, absorber-to-reflector diameter ratio and multi-reflection zones on the collector are discussed.

Sulaiman *et al*. (1997) have presented a conceptual design of hybrid thermal and photovoltaic receiver for FMDF solar concentrator to harvest solar energy. A solar tracking mechanism of UPM Solar Bowl was designed and demonstrated in both active and passive means (Sulaiman *et al*., 2008). Similarly, O'Hair and Green (1992) discussed and compared the component efficiencies developed by Battelle laboratory with the actual efficiency factors of solar bowl. Their analysis generated a good agreement between these efficiencies. Dirks *et al*. (1992) presented the performance and cost analysis of a FMDF device to study its reliability in solar energy application. In particular, they studied the efficiency factors that could influence the performance of the collector. The factors involved are cosine losses, shadowing, blocking, reflectivity, atmosphere attenuation, and spillage.

From the previous literature, there are numerous studies presented on the collector performance. However, there is very little investigation conducted on the performance of solar bowl on specific local point of receiver in daytime basis, which is essential to allow utilisation of solar energy collection. Meanwhile, several studies have shown the analysis of reflection and performance characteristics of collector that is limited to solar noon (El-Refaie, 1989; Sulaiman *et al*., 1997). Although some authors have presented the investigation of collector beyond solar noon (Gandhe *et al*., 1989; Dicks *et al*., 1992), there is a need to highlight the information for UPM Solar Bowl that is situated under tropical zone.

In this paper, a detailed numerical simulation of the UPM Solar Bowl is presented on daytime basis. The reflection behaviour, interception of solar irradiation, solar power concentration performance and solar contour mapping of the receiver are resolved iteratively by segregated method on Matlab platform. An average local concentration equation and its

respective boundary condition in accordance with different solar hour are introduced in the model. Then, a simulated clear sky solar irradiance at UPM Solar Bowl is associated in the numerical model to predict its overall solar flux concentration along the receiver in time domain. The simulated results are presented and discussed in the present work.

## MODEL DESCRIPTION AND MATHEMATICAL FORMULATION

The simulation model was developed following the features of UPM Solar Bowl which is located at 2° 59' N 101° 42' E and an elevation of 59 m. Fig.1 displays the plant. Meanwhile, the parameters of the collector layout are listed in Table 1.

Table 1: The basic physical parameters of UPM Solar Bowl

| Parameter | Value |
|---|---|
| Rim angle (degree) | 60 |
| Radius of curvature of solar reflector (m) | 27.9 |
| Aperture diameter (m) | 48 |
| Receiver-to-collector diameter ratio, R (dimensionless) | 0.015 |

In this study, a mathematical model was developed to simulate the system. Nonetheless, the theoretical approach is not able to consider all reality aspects, and thus, simplification and assumption were done to achieve an approximate solution from the theoretical derivation. The assumptions are: (i) mirror surfaces have ideal spherical curvature, (ii) surface of the reflector is reflecting specularly, (iii) shape of the collector surface is constant, and (iv) tracking error of the receiver within an acceptable range that can be ignored (Garcia-Valladares & Velazquez, 2009).


(a) (b)

Fig. 1: (a) UPM Solar Bowl at Universiti Putra Malaysia; (b) Spherical curvature of the UPM Solar Bowl

*Reflection Characterisation of the Reflector Model*

Optical characteristics of a spherical reflector are characterised by the reflector rim angle and the angle of incoming sunrays on the reflector. The degree of reflection zone for a range of incident position angles can be determined by the number of reflection as given in the following equation (El-Refaie, 1989):

$$n^{th} = \left[(\theta - \sin^{-1}R)/(\pi - 2\theta)\right] + 1 \quad (1)$$

where $n^{th} \geq 1$ and $\sin^{-1} R$ is shadow angle, $\lambda$. The consideration of shadow angle due to the shading of receiver can improve the accuracy of the reflection characterisation of the system. Some previous studies have neglected the effect of receiver thickness in estimating the performance of the solar bowl system (Gandhe *et al*., 1986a; 1986b; 1989). Fig. 2 illustrates the reflection behaviour of the spherical reflector.

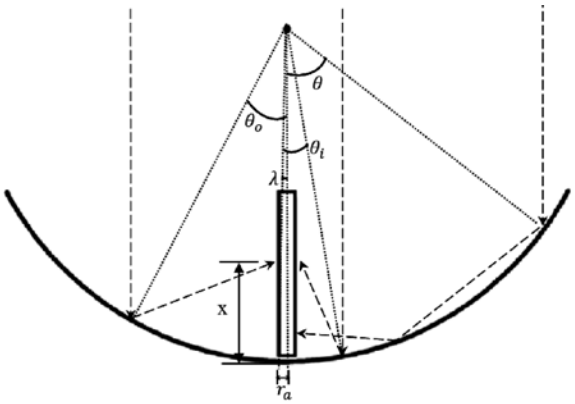


Fig. 2: The optical characteristics of the solar reflector

*Solar Receiver Model*

Solar receiver is an important component of a solar collector. The incident radiation is reflected and concentrated by a stationary spherical reflector on a certain point along the receiver. The receiver, with a cylindrical shape, is applied in the system. To achieve a more detailed analysis of the receiver, i.e. the term normalised distance, X, was introduced to represent a coordinate along the receiver. X is the ratio of the distance of the reflected rays on the receiver measured from the reflector surface (x) to the radius of reflector ($r_s$). By referring to the geometry and reflection characteristics of the collector, the normalised distance can be formulated in the form (El-Refaie, 1989):

$$X = \sqrt{(1 - R^2)} + (-1)^n \sin\theta / \sin(2n\theta) - R\cot(2n\theta) \quad (2)$$

The normalised distance is influenced by the diameter ratio of the receiver to reflector and the number of reflection shaped on the reflector. After analysing the range of incident angle for each reflection zone, the corresponding incident angles are substituted in equation (2) to

find the exact point of the reflected radiation on the receiver. The size of the receiver should be appropriate to prevent miss interception of the incoming solar radiation. The minimum diameter ratio that is required to intercept the rays at a particular position angle can be determined using the following equation (El-Refaie, 1989):

$$R \geq \frac{4.65 \times 10^{-3} \sin(2n\theta)\left[(n-1)\dfrac{\sin(2\theta)}{\sin\theta} + \dfrac{\sin(2n-1)\theta}{\sin(2n\theta)}\right]}{\sin(2n\theta) - (-1)^n \times 4.65 \times 10^{-3}} \tag{3}$$

*Solar Bowl Performance Model*

The performance of the UPM Solar Bowl can be predicted by simulating its concentration ratio profile at any particular point, x, along the receiver. Meanwhile, the local concentration ratio can be formulated as follows (El-Refaie, 1989):

$$C_L = \frac{1}{2R}\left\{\sum_{n=1}^{j} \rho^n \left[S(\theta_i, n) - S(\theta_0, n)\right]\right\} \tag{4}$$

where,

$$S(\theta, n) = \frac{\sin 2\theta \sin^2(2n\theta)}{(-1)^n\left[\sin(2n\theta)\cos\theta - 2n\sin\theta\cos(2n\theta)\right] + 2nR} \tag{5}$$

Equation (4) was derived for the condition in which the outer incident angle of the corresponding number of reflection zone, $j$ is less than the rim angle of reflector. This equation was applied to analyse the power concentration ratio when the incident radiation is normal to the aperture of the reflector. Hence, the derivation is merely valid for solar noon. To investigate the system performance in time domain, a theoretical model of the incident solar radiation for the off solar noon hour should be developed. A portion of the stationary solar bowl surface would be shaded for zenith angle, $\xi > 90° - \psi$. According to El-Refaie (1989), a full circumferentially uniform distribution of solar radiation can be reflected on the receiver in the limiting incident angle, $\bar{\theta} = \psi - \xi$. For the incident angle higher than $\bar{\theta}$, there is only a portion of the incident radiation that may be reflected to the receiver. Fig.3 illustrates this particular feature of the bowl during oblique incident case. The sector angle in which no reflection is produced at a particular incident angle is termed as the angle of non-irradiated region, $2\phi$. The section with an included angle of radiation ($2\pi - 2\phi$) will reflect the incident radiation to the receiver. Since the angle of the non-irradiated region for each respective incident angle varies from time to time as the zenith angle changes, the portion of the reflected radiation arriving on the receiver should be identified to determine the average local concentration ratio for the inclined incident radiation. Thus, a mathematical model could be developed to find the angle $\phi$, considering the relationship of the functions of elliptical formation, Cartesian coordinates, rim angle, zenith angle and incident angle. After solving the function, the half angle of the non-irradiated region can be written as follows (El-Refaie, 1989):

$$\phi = \tan^{-1}\left\{\left[(\sin\psi\sin\xi)^2 - (\cos\theta - \cos\psi\cos\xi)^2\right]^{1/2} / \left[\cos\xi\cos\theta - \cos\psi\right]\right\} \tag{6}$$

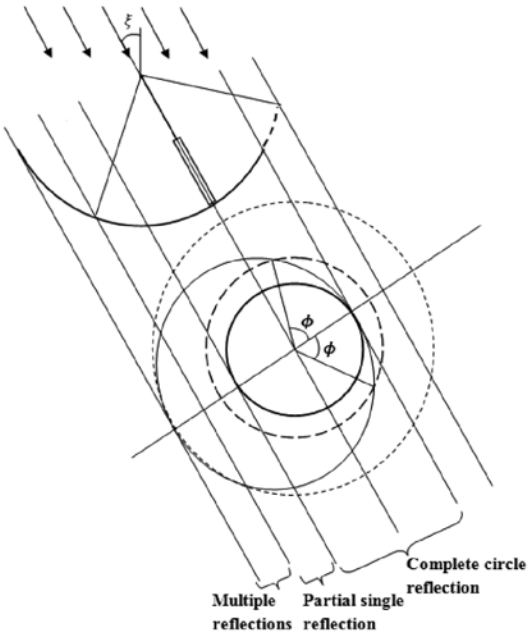


Fig. 3: A projected view on plane normal to incident sunrays for oblique incident investigation (Gandhe *et al*., 1986a; El-Refaie, 1989; Sulaiman *et al*., 1997)

A fraction of the incident radiation reflected on the receiver for a particular incident angle can be determined after solving the angle of non-irradiated region of the solar bowl. The fraction of reflected solar flux on the receiver can be defined as:

$$\alpha = 1 - \phi/\pi \tag{7}$$

In the performance analysis of solar bowl during the oblique incident radiation, the analytical model indicated in equation (4) can be applied with modification. Since the mathematical model is derived merely for a complete circle reflection, improvement of the existing model can be introduced considering the partial radiation reflected on the receiver that can provide solution for the off solar noon period. The understanding of the incident angle in affecting solar intensity is important to model the system analysis. The local concentration ratio at a specific location on the receiver with complete circle reflection can be carried out without amending the equation. For the remaining portion of the single reflection (partial single reflection shown in Fig.3), the local power concentration ratio was evaluated separately. The third region of reflection, namely multiple reflections zone, was not taken into consideration in the present work because the multi reflected irradiation might not illuminate the receiver for the absence of lower order of radiation on that point (El-Refaie, 1989; Sulaiman *et al*., 1997). At the same time, the concentrated energy was assumed to be uniformly absorbed by the receiver circumference on its respective normalised distance. Then, the total concentrated energy for the partial reflection of radiation at a particular location on the receiver could be determined. The average local concentration ratio,

$C_{L'}$, could be calculated using equation (7), together with equation (5), to predict the local concentration in daytime basis. A proposed equation is introduced as follows:

$$C_{L'} = \frac{1}{2R}\left\{\sum_{N=1}^{J} \rho^{n}\left[\alpha_i S(\theta_i, n) - \alpha_0, n\right]\right\} \tag{8}$$

The model presented above was based on the elementary analysis of the incident radiation reflected on reflector surface for all ranges of single reflection (*see* Fig.3). As illustrated in Fig.2, two beam radiations with different incident angles (known as the inner and outer radiations) may arrive at the same normalised distance, x. Thus, the local concentration at a specific coordinate of receiver can be determined by taking into account the different fractions of the reflected solar flux from both the beams on the receiver. The fraction for a particular incident angle, at different zenith angles, can be simulated according to equations (6) and (7). To predict the power concentration, the boundary conditions of the incident angle for complete and partial radiations at different zenith angles should be clearly defined. The boundary conditions of the complete and partial radiation are defined as follows:

(i) Limit of complete radiation, $\bar{\theta}$: $\lambda < \bar{\theta} \leq \psi - \xi$

(ii) Limit of partial radiation, $\theta_\alpha$: $\psi - \xi < \theta_\alpha \leq \psi$ (9)

Table 2 presents the proposed boundary conditions for both the complete and partial radiations on the receiver.

Table 2: Boundary conditions for complete and partial radiations at different solar time

| Solar time | Zenith angle, $\xi$ | Range of complete radiation, $\bar{\theta}$ | Range of partial radiation, $\theta_\alpha$ |
|---|---|---|---|
| 08:00 | 60 | 0 | $\lambda < \theta_\alpha \leq 60$ |
| 09:00 | 45 | $\lambda < \bar{\theta} \leq 15$ | $15 < \theta_\alpha \leq 60$ |
| 10:00 | 30 | $\lambda < \bar{\theta} \leq 30$ | $30 < \theta_\alpha \leq 60$ |
| 11:00 | 15 | $\lambda < \bar{\theta} \leq 45$ | $45 < \theta_\alpha \leq 60$ |
| 12:00 | 0 | $\lambda < \bar{\theta} \leq 60$ | 0 |
| 13:00 | 15 | $\lambda < \bar{\theta} \leq 45$ | $45 < \theta_\alpha \leq 60$ |
| 14:00 | 30 | $\lambda < \bar{\theta} \leq 30$ | $30 < \theta_\alpha \leq 60$ |
| 15:00 | 45 | $\lambda < \bar{\theta} \leq 15$ | $15 < \theta_\alpha \leq 60$ |
| 16:00 | 60 | 0 | $\lambda < \theta_\alpha \leq 60$ |

*Solar Irradiance Model*

In the solar collector analysis, accurate climatic data are needed to obtain a realistic prediction. The actual weather database at the site of UPM Solar Bowl is not available for the present study. Therefore, the estimation of the solar radiation variations at that place during a particular time with tolerable quality was required in the numerical model. Only direct radiation was taken

into account when evaluating the collector performance. Meanwhile, the direct solar radiation intensity on the bowl was assumed to be uniform under a clear sky condition. According to Hottel (1976), the clear day atmospheric transmittance, $\tau_b$, for the beam radiation can be predicted using the following equation:

$$\tau_b = a_0 + a_1 e^{(-k/\cos\xi)} \tag{11}$$

where $a_0$, $a_1$ and $k$ are constants and defined as:

$$\begin{aligned} a_0 &= r_0\{0.4237 - 0.00821(6 - A)^2\} \\ a_1 &= r_1\{0.5055 - 0.00595(6.5 - A)^2\} \\ k &= r_k\{0.2711 - 0.01858(2.5 - A)^2\} \end{aligned} \tag{12}$$

where $r_0$, $r_1$ and $r_k$ are the recommended correction factors for different climate zone. From the literature (Hottel, 1976), the values of $r_0$, $r_1$ and $r_k$ for the tropical sky are 0.95, 0.98 and 1.02, respectively. The estimation of the clear sky horizontal direct solar radiation, $G_{cb}$, can be determined by (Duffie & Beckman, 2006):

$$G_{cb} = G_{on}\tau_b \cos\xi \tag{13}$$

Then, the simulated $G_{cb}$ is associated in the collector simulation model to predict the performance of the solar bowl for a typical day.

## NUMERICAL SIMULATION

The simulation of the numerical model was divided into three modules: (i) reflection characterisation of the bowl, (ii) solar flux density along the receiver, and (iii) radiation contours mapping of the receiver. Matlab version R2008a, *v*7.6.0, was used as a platform to perform the iterative simulation of the UPM Solar Bowl. All the outputs generated by the simulation model are presented in GUI interface. 24-hour notation was used in the function of time. In the study, the incident sunray was assumed normal to the surface of collector at 12:00 solar time and the operating duration of the model system is 8 hours starting from 08:00 to 16:00. The UPM Solar Bowl was modelled under cloudless circumstance in one daytime under the tropical zone. The simulation was conducted on 1st July that is a typical day of clear sky to better estimate its performance (Assilzadeh *et al*., 2005).

## RESULTS AND DISCUSSION

Fig.4 shows the relationship between the number of reflections and the incident angle of radiation. In the UPM Solar Bowl, due to the 60° rim angle, only single reflection was generated when the incoming radiation is normal to the bowl surface. A higher number of reflection was formed as the apparent position of the sun was deviated from the normal axis of the bowl. To quantify the results, Table 3 is tabulated to present the reflection distribution of the bowl up to tenth order of reflection zone. The first order of reflection represents a shadow angle of the model system that the bowl surface forms no reflection within the indicated range (1.01%)

due to the blocking of incident rays by the receiver. The second order of the reflection zone represents a single reflection, whereas the third zone is for double reflection and so forth. The simulated result shows that the single reflection covers the largest range of incident angle up to 69.66%. Meanwhile, the multiple reflections appear for a relatively small range and keep reducing at the higher order of reflection zone.

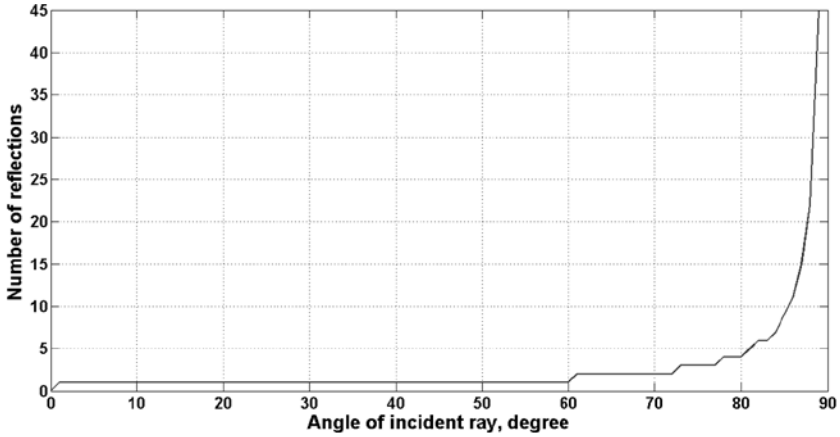


Fig. 4: Multiple reflection characteristics in various angles of the incident rays

Table 3: Reflection distribution of the solar bowl

| Order of reflection zone ($n^{th}$) | Number of reflection (n) | Range of incident angle (degree) | Percentage of the range of incident angle (%) |
|---|---|---|---|
| First | Non (λ) | $0 \leq \theta < 0.859$ | 1.01 |
| Second | 1 | $0.859 \leq \theta < 60.286$ | 69.66 |
| Third | 2 | $60.286 \leq \theta < 72.172$ | 13.93 |
| Fourth | 3 | $72.172 \leq \theta < 77.266$ | 5.97 |
| Fifth | 4 | $77.266 \leq \theta < 80.095$ | 3.32 |
| Sixth | 5 | $80.095 \leq \theta < 81.896$ | 2.11 |
| Seventh | 6 | $81.896 \leq \theta < 83.143$ | 1.46 |
| Eight | 7 | $83.143 \leq \theta < 84.057$ | 1.07 |
| Ninth | 8 | $84.057 \leq \theta < 84.756$ | 0.82 |
| Tenth | 9 | $84.756 \leq \theta < 85.308$ | 0.65 |

The range of incident ray varies throughout the daytime due to the apparent movement of the sun position relative to the earth surface. Fig.5 indicates the maximum incident angles and their respective number of reflections in the function of time. The maximum angle of the incident on the reflector is $90^{o}$ at 08:00. After two hours, the maximum incident angle begins to decrease linearly until $60^{o}$ at solar noon. The plots of the results are symmetrical at the daytime axis at 12:00 because of the assumed symmetry property of spherical reflector and the consistent apparent motion of the sun passing through the bowl centre.

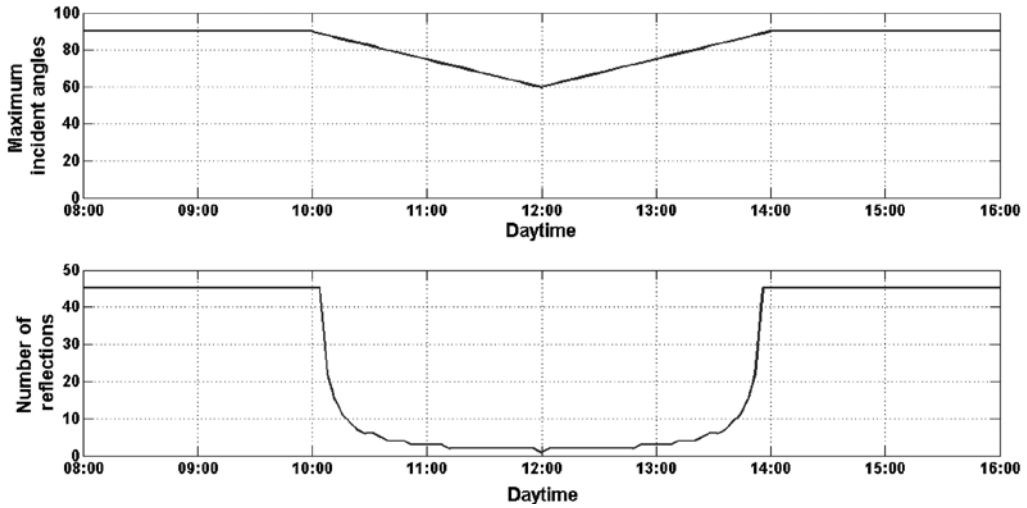


Fig. 5: The maximum incident angles and the number of reflections on the UPM Solar Bowl reflector in one daytime

The reflected solar radiation on a specific coordinate of the cylindrical receiver is shown in Fig.6. The normalised distance result shows a similar shape of plot as compared to the published data that used different quantities of geometry size (El-Refair, 1989; Sulaiman *et al*., 1997). As presented in the figure, the single reflection intercepts the receiver from normalised distances 0 to 0.456 which is equivalent to the actual distance extending from the bowl surface to 12.72 m above it. Nevertheless, there is no incident radiation striking the receiver at normalised distance more than 0.456. Thus, the length of the receiver may not need be extended beyond that point. Fig.7 shows the distance coverage of the receiver which is illuminated by the different numbers of reflection. The coverage region of the reflected ray on the receiver is relatively small for higher reflection zone. This result is important in defining the appropriate length of receiver in the system.

From the information presented in Fig.6 and Fig.7, the multiple reflections may not contribute to the solar energy concentration on the receiver with a normalised distance more than 0.0798 or 2.23 m from the bowl surface. In the model, the length of the receiver was designed to have normalised distance from 0.10 to 0.45. This means the receiver is illuminated by the single radiation only. Thus, the performance evaluation of the UPM Solar Bowl, based on the single reflection zone, is tolerable in determining the collector performance due to the dimension constraint of the receiver. In addition, the optical property of the multiple reflections is uncontrollable and suffering successive losses in efficiency. Fig.8 presents the required minimum diameter of the receiver for a complete interception of the reflected radiation. From this result, it was found that the size of the receiver model is able to intercept all the incoming solar radiations up to the tenth order of the reflection zone. This information is useful to optimise the size of the receiver for the UPM Solar Bowl.

Fig.9 shows the concentration ratio on different normalised distances for incident radiation normal to the reflector's aperture. The simulation result reports that the concentrated solar

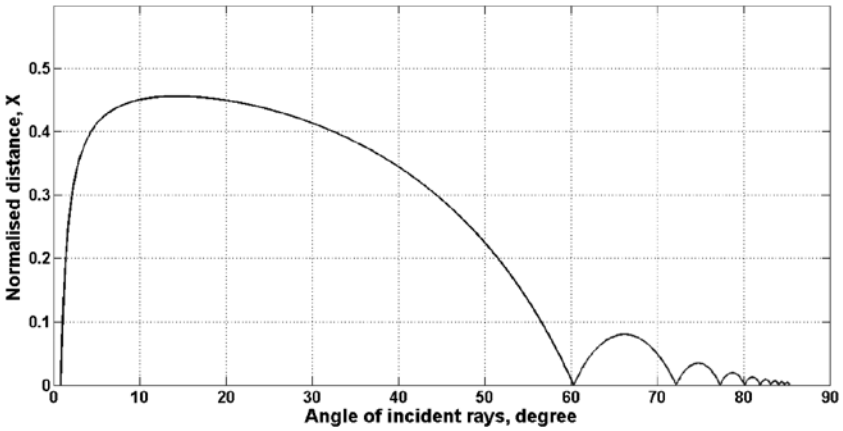


Fig. 6: Normalised distance X against position angle for R= 0.015

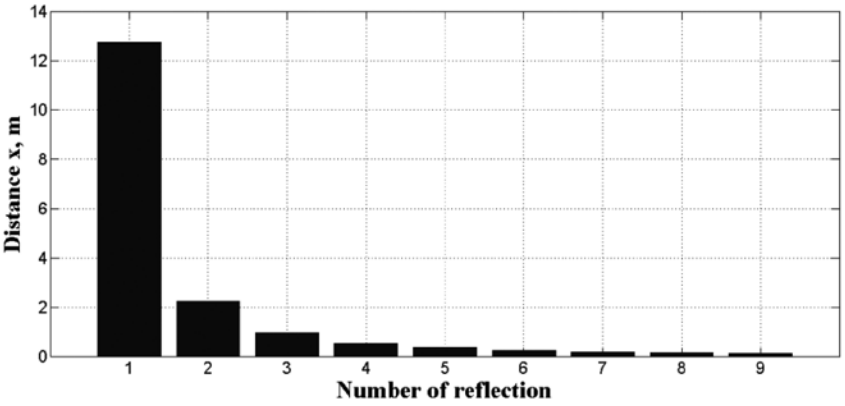


Fig. 7: The range of the distance x on receiver that can receive incident radiation for the different numbers of reflection

irradiation is the highest at the upper part of the receiver and it gradually decreases towards the lower portion of the receiver.

The effect of the angular deviation of incident radiation on the solar bowl due to the apparent motion of the sun is presented in this paper. The fractions of the reflected solar radiation, with continuous incident angles for different zenith angles, are shown in Fig.10. It is obvious that a high zenith angle induces to a relatively low level proportion of the reflected solar flux on the receiver due to the larger cosine loss. As an example, the incident angle of 45$^o$, 100% of the reflected solar flux at this incident angle can reach the receiver at 10$^o$ zenith angle, 73.8% at 20$^o$ zenith angle, 60.3% at 30$^o$ zenith angle, 52.9% at 40$^o$ zenith angle, 47.3% at 50$^o$ zenith angle and 42.3% at 60$^o$ zenith angle.

Fig.11 reports the overall concentration ratio along the receiver in the time domain. The collector concentration ratio varies with the functions of time and normalised distances of the receiver. A higher normalised distance is competent to collect more thermal energy for longer

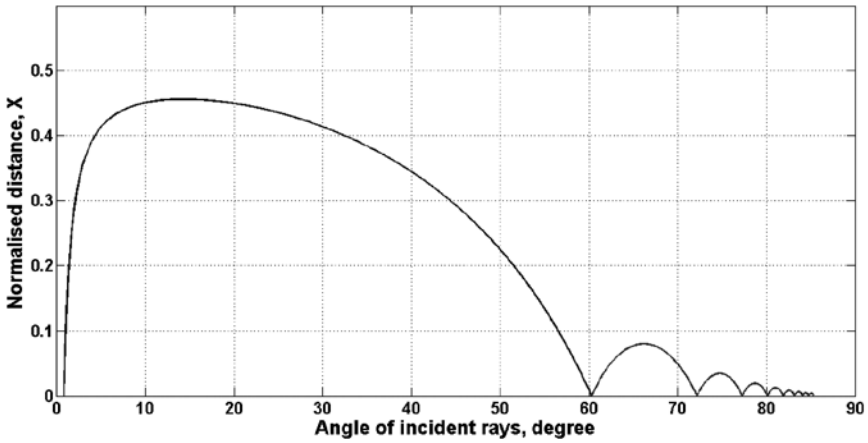


Fig. 8: The minimum size of the receiver for radiation interception

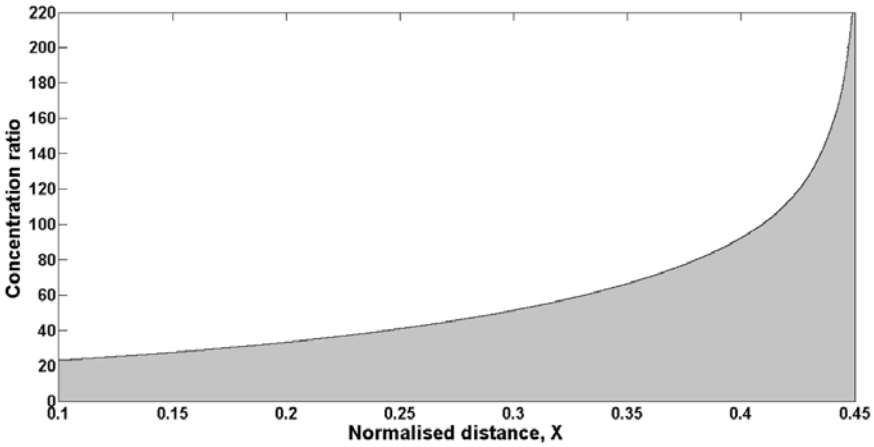


Fig. 9: Concentration ratio along the receiver for normal incident case

period. At 0.44 normalised distance, the concentration ratio is 73 at 08:00 and it increases to 156 after two hours (113.7% increment). The power concentration is then constant for four hours until 14:00 and reducing to 73 at 16:00. On the contrary, the concentration ratio deteriorates substantially during the off solar noon hour. Similar trend profiles were also observed at the lower normalised distances of the receiver.

Fig.12 shows the simulated profile of the solar flux density of the bowl at different normalised distances on 1st July 2010 under the assumed clear sky of tropic. This simulation result was compared to the experimental data from the literature, as in Gandhe *et al*. (1989) and Dirks *et al*. (1992) who had presented thermal performance and collector efficiency respectively in daytime. These comparisons indicated a fair similar shape of curve. According to the result, the maximum solar flux density is 119.1 kW/m$^2$, as can be seen at 0.44 normalised distance during 12:00. At 08:00 and 16:00, the flux concentration at the same coordinate is only 20.95 kW/m$^2$, which is equivalent to the 82.4% reduction of solar flux energy. Table 4

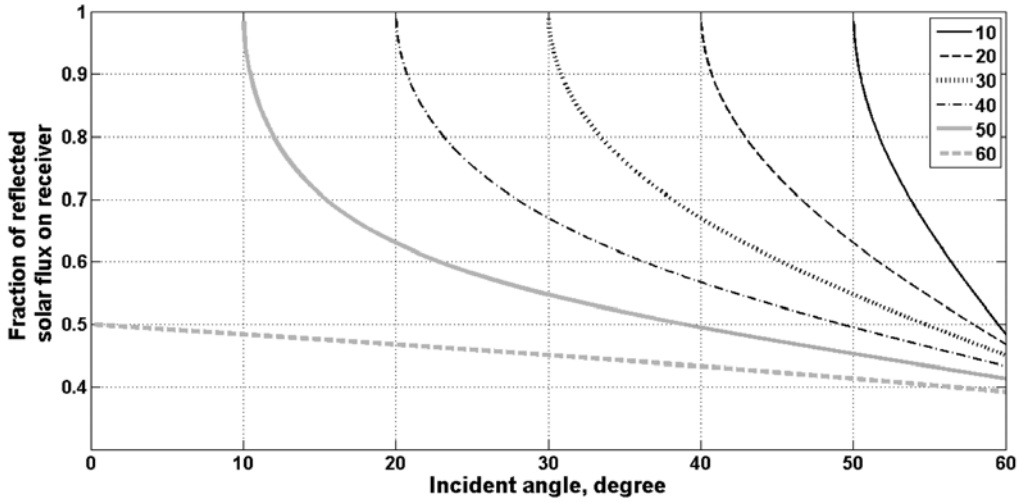


Fig. 10: Fractions of the available reflected solar radiation with respective incident angles for different zenith angles

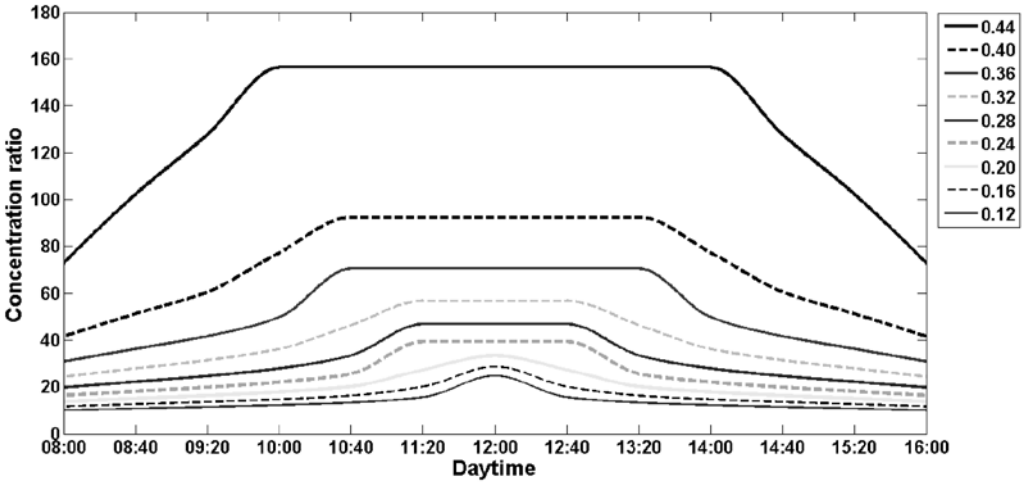


Fig. 11: Estimated concentration ratio at different normalised distances on the receiver in daytime

reports the calculated percentage of reduction of flux density with respect to each individual maximum flux concentration, at different normalised distances along the receiver for the off solar noon hour. This table shows the performance deterioration of the solar bowl. Based on the information presented in Table 4, at the higher region of receiver (normalised distances of 0.44, 0.40 and 0.36), the available solar flux density drops to less than 7.8% within 80 minutes from the solar noon in cloudless sky. It can be noted that the concentrated solar energy at the lower region decreases in a relatively higher rate. The performance of the bowl at a high zenith angle appears to be very undesirable in which the percentage reduction of the flux density is more than 82% at all points of the receiver during 08:00 and 16:00.

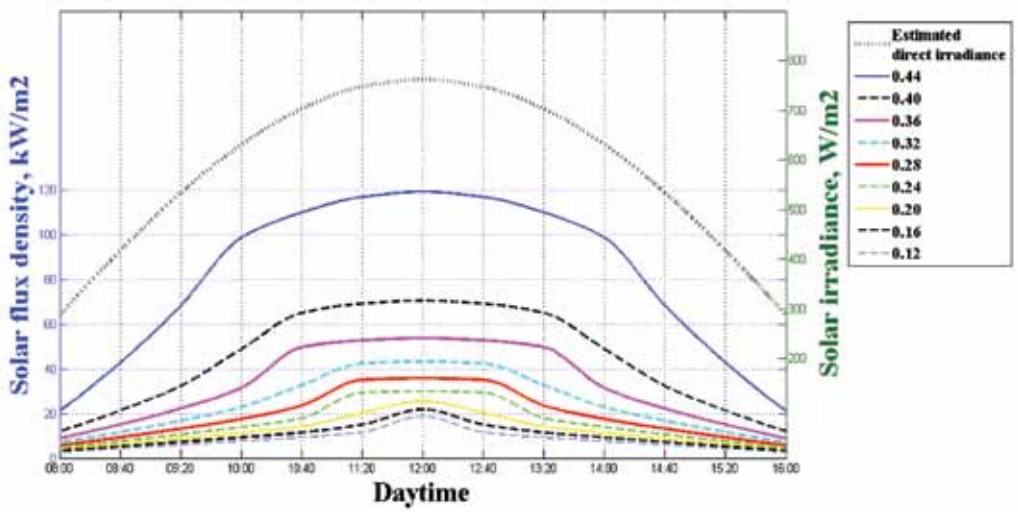


Fig. 12: Solar flux density of the UPM Solar Bowl at different normalised distances on 1st July 2010 under the tropical clear sky condition

Table 4: The percentage of reduction (%) of the solar flux density on the receiver

| Solar time | Normalised distance | | | | | | | | |
|---|---|---|---|---|---|---|---|---|---|
| | 0.12 | 0.16 | 0.20 | 0.24 | 0.28 | 0.32 | 0.36 | 0.40 | 0.44 |
| 08:00/ 16:00 | 84.8 | 84.6 | 84.5 | 84.3 | 84.1 | 83.8 | 83.5 | 83.0 | 82.4 |
| 08:40/ 15:20 | 76.4 | 75.9 | 75.4 | 74.8 | 74.1 | 73.2 | 71.9 | 69.8 | 64.2 |
| 09:20/ 14:40 | 67.7 | 66.9 | 65.8 | 64.6 | 63.2 | 61.3 | 58.6 | 54.2 | 42.8 |
| 10:00/ 14:00 | 59.2 | 57.7 | 55.8 | 53.6 | 50.9 | 47.2 | 41.7 | 30.9 | 17.3 |
| 10:40/ 13:20 | 50.6 | 47.7 | 44.3 | 40.6 | 34.2 | 24.9 | 7.8 | 7.8 | 7.8 |
| 11:20/ 12:40 | 38.3 | 31.1 | 20.2 | 1.9 | 2.0 | 2.0 | 2.0 | 2.0 | 2.0 |

The radiation contour mapping of the receiver is essential to identify the illumination characterisation. There are three types of illumination regions on the receiver, and these are known as completely irradiated region, partially irradiated region and non-irradiated region. Fig.13 presents the receiver contour mapping of UPM Solar Bowl. It shows a similar trend of radiation contour mapping to that of El-Refaie (1989) and Sulaiman *et al*. (1997) which have been analysed at different sizes of collector. At the angular deviation $0^o$, the entire surface area of receiver is completely irradiated. The partially irradiated region, which is also known as the faintly-irradiated region, starts to grow gradually for non-normal incident radiation as can be seen in the angular deviations of $10^o$, $20^o$, $30^o$, $40^o$, $50^o$ and $52^o$. For the angular deviation greater than $50^o$, the partially irradiated region occupies more than 50% of the surface area of the receiver. From this simulation result, it can be observed that in a higher angular deviation, non-irradiated region begins to emerge and expand progressively as shown at the angular deviation of $54^o$, $56^o$, $58^o$ and $60^o$. It is crucial to note that about half of the receiver region is unirradiated at angular deviation $60^o$. This result agrees to the finding discussed by Bar-Lev *et al*. (1983), in which for their solar bowl system, there was only about 50% of the illuminated

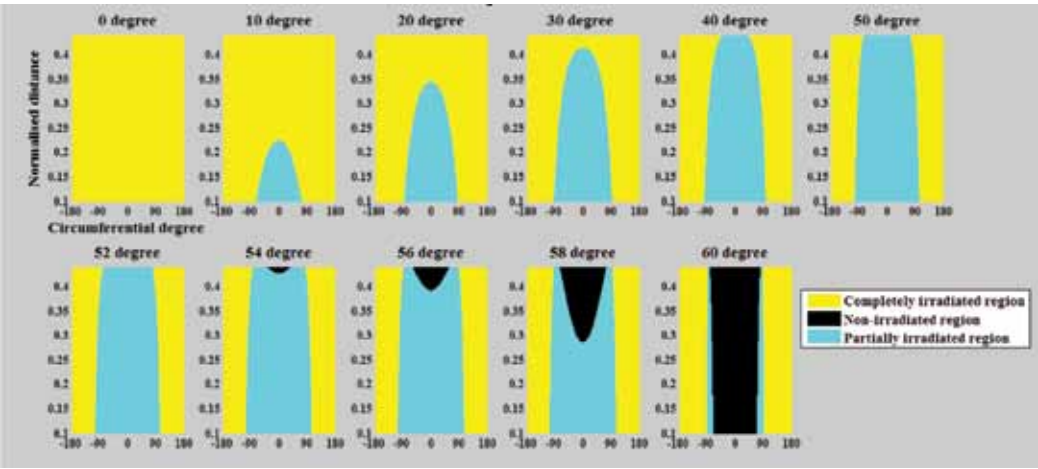


Fig. 13: The contour of completely, partially and non-irradiated region on receiver

receiver area covered with solar cells considering the worst case at 08:00 and 16:00. This contour mapping explains the reason for the substantial low solar concentration power during high solar zenith angle.

## CONCLUSIONS

A numerical simulation model of the UPM Solar Bowl was developed in this study. Reflection characterisation and performance models of the bowl in tropics were successfully assessed in the Matlab simulation platform, which can predict and quantify the results in time domain. The present work can advance the understanding of the fundamental aspects of the solar bowl and be used to achieve useful information on the plant performance. Any further investigation may focus on the experimental study of the solar collector under the real meteorological environment in the tropical area. Thus, a reliable solar harnessing technology and innovative collector design to improve the collector performance should be developed to assess the possibilities of solar bowl power system in the future.

## REFERENCES

Assilzadeh, F., Kalogirou, S. A., Ali, Y., & Sopian, K. (2005). Simulation and optimization of a LiBr solar absorption cooling system with evacuated tube collectors. *Renewable Energy, 30*(8), 1143-1159.

Bar-Lev, A., Waks, S., & Grossman, G. (1983). Analysis of a Combined Thermal-Photovoltaic Solar System Based on the Spherical Reflector/Tracking Absorber Concentrator. *Journal of Solar Energy Engineering, 105*(3), 322-328.

Bethea, R. M., Barriger, M. T., Williams, P. F., & Chin, S. (1981). Environmental effects on solar concentrator mirrors. *Solar Energy, 27*(6), 497-511.

Clausing, A. M. (1976). The performance of a stationary reflector/ tracking absorber solar concentrator. In K. W. Boer (Ed.), *Sharing the Sun - Solar Technology in the Seventies* (Vol. 2): The American Section of the International Solar Energy Society.

Dirks, J. A., Williams, T. A., & Brown, D. R. (1992). Performance and Cost Implications of the Fixed Mirror, Distributed Focus (FMDF) Collector. *Journal of Solar Energy Engineering, 114*(4), 254-259.

Duffie, J. A., & Beckman, W. A. (2006). *Solar Engineering of Thermal Processes* (3rd ed.). United States of America: John Wiley & Sons, Inc.

El-Refaie, M. F. (1989). Performance analysis of the stationary-reflector/tracking-absorber solar collector. *Energy Conversion and Management, 29*(2), 111-127.

Gandhe, V. B., Venkatesh, A., & Sriramulu, V. (1986a). Analysis of a fixed spherical reflector exposed to oblique incident rays. *Energy Conversion and Management, 26*(3-4), 363-368.

Gandhe, V. B., Venkatesh, A., & Sriramulu, V. (1986b). Optical analysis of a cylindrical absorber in a fixed spherical reflector. *Energy, 11*(10), 969-976.

Gandhe, V. B., Venkatesh, A., & Sriramulu, V. (1989). Thermal analysis of an FMDF solar concentrator. *Solar & Wind Technology, 6*(3), 197-202.

Garcia-Valladares, O., & Velazquez, N. (2009). Numerical simulation of parabolic trough solar collector: Improvement using counter flow concentric circular heat exchangers. *International Journal of Heat and Mass Transfer, 52*(3-4), 597-609.

Hottel, H. C. (1976). A simple model for estimating the transmittance of direct solar radiation through clear atmospheres. *Solar Energy, 18*(2), 129-134.

Kreider, J. F. (1975). Thermal Performance Analysis of the Stationary Reflector/Tracking Absorber (SRTA) Solar Concentrator. *Journal of Heat Transfer, 97*(3), 451-456.

O'Hair, E. A., & Green, B. L. (1990). *Component Efficiencies From The Operation Of The Crosbyton Solar Bowl.* Paper presented at the Energy Conversion Engineering Conference, 1990. IECEC-90. Proceedings of the 25th Intersociety.

O'Hair, E. A., & Green, B. L. (1992). Solar Bowl Component Efficiencies. *Journal of Solar Energy Engineering, 114*(4), 272-274.

Sulaiman, M. Y., Bashria, A. Y., Ali, M., & Adam, N. M. (2008). *Design of tracking system for UPM solar bowl.* Paper presented at the Proceeding of Seminar on Progress of Solar Energy Research and Development.

Sulaiman, M. Y., Hlaing Oo, W. M., Wahab, M. A., Sulaiman, Z. A., & Khouzam, K. Y. (1997). Conceptual design of a hybrid thermal and photovoltaic receiver of an FMDF collector. *Renewable Energy, 12*(1), 91-98.

Pertanika J. Sci. & Technol. 20 (2): 299 - 311 (2012)

SCIENCE & TECHNOLOGY

Journal homepage: http://www.pertanika.upm.edu.my/

# Impact Assessment of Climate Change in Iran using LARS-WG Model

**Raheleh Farzanmanesh[1], Ahmad Makmom Abdullah[1*], Alireza Shakiba[2] and Jamil Amanollahi[1]**

*[1]Department of Environmental Sciences, Faculty of Environmental Studies, Universiti Putra Malaysia, 43400 Serdang, Selangor, Malaysia*

*[2]Department of Earth Science, Faculty of Remote Sensing and GIS, Shahid Beheshti University, Iran*

## ABSTRACT

Iran is situated in a very diverse environmental area. The climate of the region is varied and influenced by different patterns. In order to best describe the expected climate change impacts for the region, climate change scenarios and climate variables must be developed on a regional, or even site-specific, scale. The weather generator is one of the valid downscaling methods. In the current study, LARS-WG (a weather generator) and the outputs from ECHO-G for present climate, as well as future time slice of 2010-2039 based on A1 scenario, were used to evaluate LARS-WG as a tool at 13 synoptic stations located in the north and northeast parts of Iran. The results obtained in this study illustrate that LARS-WG has a reasonable capability of simulating the minimum and maximum temperatures and precipitation. In addition, the results showed that the mean precipitation decreased in Semnan, the south of Khorasan and Golestan. Meanwhile, the mean temperature during 2010-2039 would increase by 0.5°C, especially in the cold season.

**Keywords: Climate change, weather generator, LARS-WG, GCM**

*Article history:*
Received: 17 January 2011
Accepted: 27 April 2011

*Email addresses:*
rahil_farzan@yahoo.com (Raheleh Farzanmanesh),
amakmom@env.upm.edu.my (Ahmad Makmom Abdullah),
mypauk@yahoo.com (Alireza Shakiba),
j_aman2005@yahoo.com (Jamil Amanollahi)
*Corresponding Author

## INTRODUCTION

Excessive use of fossil fuels, change of land use, increase in human activities and rise in the world population, especially after the industrial revolution, affect climate change. The summary of the Fourth Assessment Report (AR4) released in February of 2007 by the Intergovernmental Panel on Climate Change (IPCC) confirmed that the warming of the climate system is unequivocal, as is now

ISSN: 0128-7680 

evident from observations of increases in global average air and ocean temperatures, widespread melting of snow and ice, and rising global average sea level (IPCC, 2007; Stathopoulou & Cartalis, 2009). Based on the IPCC report, the earth's average surface temperature has risen by 0.76°C since 1850. Most of the warming over the past 50 years is very likely to have been caused by emissions of carbon dioxide ($CO_2$) and other 'greenhouse gases' as a result of human activities (IPCC, 2007; Ragab & Prudhomme, 2002; Freiwan & Kadioglub, 2008).

In order for policymakers and resource managers to understand the magnitude and timing of the impacts of the climate change and their effects on the local and regional resources, they must be able to study the climate scenarios of key climate variables for future periods. There are three main classes of climate change scenarios which are used to develop climate scenarios: synthetic scenarios, analogue scenarios, and scenarios, based on the outputs from general circulation models that are also known as global climate models (GCMs) (Wilby & Dawson, 2002; Dibike & Coulibaly, 2005; Solomon *et al.,* 2007; Koenig, 2008). The complex computer models of GCMs describe the climatological conditions of the earth at a finite number of grid points (a grid point model) or by a finite number of mathematical functions (a spectral model). In this study, the output from two GCM experiments was combined with a stochastic weather generator, LARS-WG (Long Ashton Research Station Weather Generator), to produce a climate change scenario.

The objectives were to access the performance of the model in simulating climate of specific site and suitability of model application.

## MATERIALS AND METHODS

### *Description of LARS-WG Stochastic Weather Generator*

LARS-WG (Long Ashton Research Station Weather Generator) is a stochastic weather generator which can be used for the simulation of weather data at a single site (Racsko *et al.,* 1991; Semenov *et al.,* 1998; Semenov & Brooks, 1999; Semenov & Barrow, 2002) under both current and future climate conditions. LARS-WG produces synthetic daily time series of maximum and minimum temperatures, precipitation and solar radiation (Semenov & Stratonovitch, 2010). The weather generator distinguishes dry and wet days, depending on whether the precipitation is greater than zero. Precipitation is modelled using semi-empirical probability distributions for the lengths of wet and dry series and for the amount of precipitation on a wet day. A semi-empirical distribution is a histogram with a fixed number of intervals (10 in the case of LARS-WG).

$$Emp = \{a0, ai ; hi \text{ , } i=1,\ldots,10\}$$

A semi-empirical distribution is sufficiently flexible and allows for the accurate simulation of various weather statistics (Semenov *et al.,* 1998). Minimum temperature, maximum temperature and radiation are related to the amount of cloud cover; therefore, LARS-WG uses separate distributions for wet and dry days for each of these variables. Meanwhile, the pattern of the daily temperature distributions is approximated by the normal distribution, with the values of mean and standard deviation changing daily and calculated by a Fourier series.

Time auto-correlations for the minimum and maximum temperatures are site specific, but constant throughout the year (Semenov *et al.,* 1998; Hansen, 1999; Parlange & Katz, 2000).

Two important reasons for using LARS-WG model include the provision of a means of simulating synthetic weather time-series with certain statistical properties which are long enough to be used in an assessment of risk in hydrological or agricultural applications and providing the means of extending the simulation of weather time-series to unobserved locations.

In fact, LARS-WG has been used in various studies, including the assessment of the impacts of climate change (Barrow & Semenov, 1995; Semenov & Barrow, 1996; Weiss *et al.,* 2003; Lawless & Semenov, 2005; Khan *et al.,* 2006; Scibek & Allen, 2006; Semenov, 2007; Semenov & Doblas, 2007; Dubrovsky, 1996). The process of generating synthetic weather data can be divided into three distinct steps; Model Calibration, Model Validation, and Generation of Synthetic Weather Data (Zhang & Garbrecht, 2003; Nakicenovic & Swart, 2000).

*Study Area*

The study area encompasses the north, northeast and a part of central Iran (defined as 38°N to 30°N and 48°E to 59°E), as shown in Fig.1. These areas were selected to enable the researchers to collect data from a variety of climatic zones. In the north of Iran (Near the Caspian Sea), there are two provinces called Gilan and Mazandaran which are covered by forest. The North of Iran has the best type of weather in Iran with a moderate and humid climate that is known as the moderate Caspian climate. The effective factors behind such a climate include the Alborz mountain range, direction of the mountains, the height of the area, and the Caspian Sea, vegetation surface, local winds, as well as the altitude and weather fronts. As a result of the above factors, three different climates exist in the region:

1. Plain moderate climate with an average annual rainfall amounts to 1200 or 1300 mm, decreasing to the east.
2. Mountainous climate which covers the high mountains and northern parts of the Alborz range. In the heights, the weather is cold mountainous and most of the precipitation is in the form of snow.
3. Semi-arid climate with the average annual rainfall stands at 500 mm and the average annual temperature is 18.2°C.

Semnan is in the north of the country and the southeast of Mazandaran. The Semnan province covers an area of 96.816 $Km^2$, stretches along the Alborz mountain range and borders the Dasht-e Kavir desert in its southern parts. The average annual rainfall in this area is 140 mm and the average annual temperature is 11.4°C.

Golestan is located in the north-east of the country, and the south of the Caspian Sea. Most of the year, Golestan enjoys mild weather and a temperate climate. The centre of this area has a semi-arid climate because of its especial topography. The average annual rainfall stands at 500 mm and the average annual temperature is 18.2°C. Khorasan is a region in the north-east of Iran. With a surface area of 313.335 $Km^2$, it is the largest province of the country. Khorasan is bounded on the north by Turkmenistan and on the east by Afghanistan.

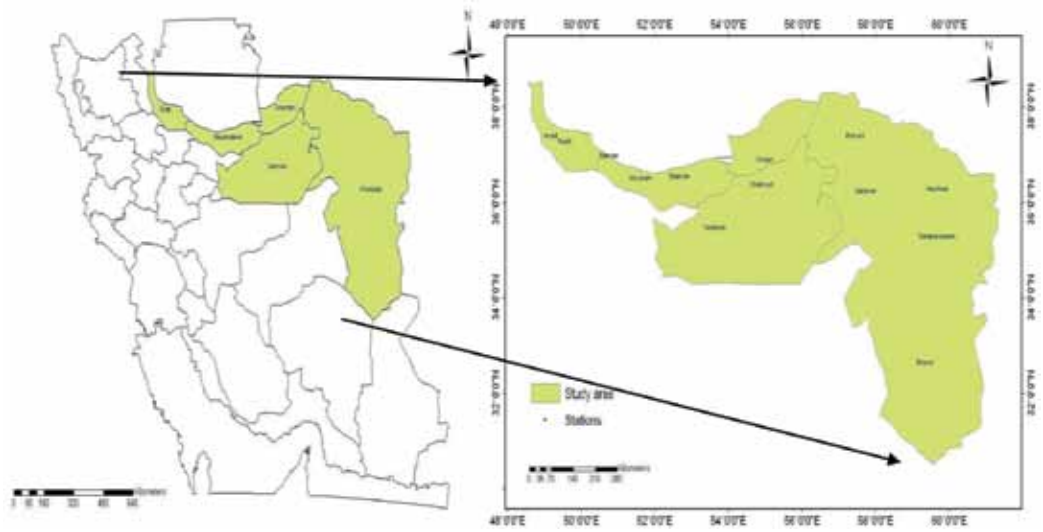


Fig.1: Study area

The climate of this part of Iran varies from semi-dry and locally humid in the north to dry in the south. The annual rainfall in the north of Khorasan Province is about 250 mm and this is 110 mm in the south. The annual mean temperature in the north of the province is about 13°C and this is 18°C in the southern part. In the recent years, some natural disasters have happened in the Khorasan province. During the last decade, there was a severe drought in this location, especially in the central and southern parts. Drought is the most common type of disaster that occurs in this part of country. Following this drought, two heavy floods occurred in the north of Khorasan in 2001 and 2002.

The observed data, GCM output in the same period with observed data, GCM output for the future period and a WG scenario are necessary to generating synthetic data and evaluating the model. A WG scenario can be produced using the GCM outputs in the observed and synthetic period. A scenario, which is needed in WG, consists of relative changes of mean temperature, standard deviation of temperature. Meanwhile, changes in precipitation and mean temperature are at the monthly time scale. The processes that are needed for generating synthetic data using LARS-WG model consist of three main steps, namely, model calibration, performance of the model and generating synthetic data.

In this study, the performance of the LARS-WG stochastic weather generator model was statistically evaluated by comparing the synthesized data with climatology period at 13 selected synoptic stations, based on ECHO-G and A1 scenario. Name, latitude and longitude coordinates, as well as the elevation of the synoptic stations are shown in Table 1.

The period of base data covered a period expanding from 1976 to 2005. Historical daily data contained precipitation, minimum and maximum temperatures. Such site parameters, which are also known as baseline, are commonly employed by LARS-WG in order to create a synthetic and local scale of weather time series on a daily basis. These time periods have arbitrary lengths and are statistically equal to the data collected for 1976-2005. Achieved

Table 1: Location and synoptic stations utilized in the study

| Stations | Latitude (˚N) | Longitude (˚E) | Elevation (m) | Annual total rain (mm) | Annual mean temperature (˚C) |
|---|---|---|---|---|---|
| Anzali | 37.28 | 49.28 | -26.2 | 1773 | 6.0 |
| Babolsar | 36.43 | 52.39 | -21 | 943.1 | 7.5 |
| Birjand | 32.52 | 59.12 | 1491 | 169.8 | 16.2 |
| Bojnurd | 37.46 | 57.31 | 1091 | 269.3 | 12.9 |
| Gorgan | 36.51 | 54.16 | 13.3 | 546.1 | 10.1 |
| Mashhad | 36.28 | 59.6 | 999.2 | 254.7 | 13.0 |
| Noushahr | 36.39 | 51.3 | -20.9 | 1293.5 | 6.8 |
| Ramsar | 36.54 | 50.4 | -20 | 1216.3 | 6.5 |
| Rasht | 37.15 | 49.36 | -6.9 | 1363.3 | 8.5 |
| Sabzevar | 36.2 | 57.66 | 977.6 | 188.6 | 17.4 |
| Semnan | 35.35 | 53.33 | 1130.8 | 142.8 | 11.4 |
| Shahroud | 36.25 | 54.57 | 1345.3 | 162.6 | 12.6 |
| TorbatHeydarieh | 35.27 | 59.22 | 1450.8 | 277.5 | 13.7 |

from a climate model, the predicted variations in the mean and variability of climate were applied to cause perturbation in the site parameters for the baseline climate. This section aims at examining the performance of LARS-WG for the ECHO-G dataset through a comparison of the observed and simulated weather time series on a daily basis. To this end, students' *t*-test was used to compare the means of climatic changes.

## RESULTS AND DISCUSSION

Model validation is one of the most important steps of the entire process. The objective was to assess the performance of the model in simulating climate at the chosen site to determinate whether or not it is suitable for use.

Firstly, LARS-WG model was performed based on the historical climate data obtained from 1976-2005 for verification of the model. For this purpose, a large number of years of simulated daily weather data were generated and the probability distribution for synthetic and the observed data were carried out using the Chi-square goodness-of-fit test and the means and standard deviations using the t test, respectively. In addition, population properties, correlation, RMS and relative errors were computed as well. The skill of the model for generating synthetic data is graphically shown in Fig.2, Fig.3, and Fig.4, which typically represents the comparison between synthetic and observed data. For this aim, the climate stations in the north of Iran, northeast and central of study area were combined. The model shows a better performance for the maximum and minimum temperatures than rainfall. The mean monthly correlation of the precipitation, minimum and maximum temperature is 0.95, which is acceptable in 0.05 level of confidence. The results show that the skill of the model in synthesizing the standard deviation of precipitation is different from that of the observed, except for dry months with lower rain.

At this stage, the precipitation levels, as well as the minimum and maximum temperatures in the period of 2010-2039, were produced for the 13 selected ground-based synoptic stations based on the ECHO-G data. The results showed that except for June, the monthly precipitations

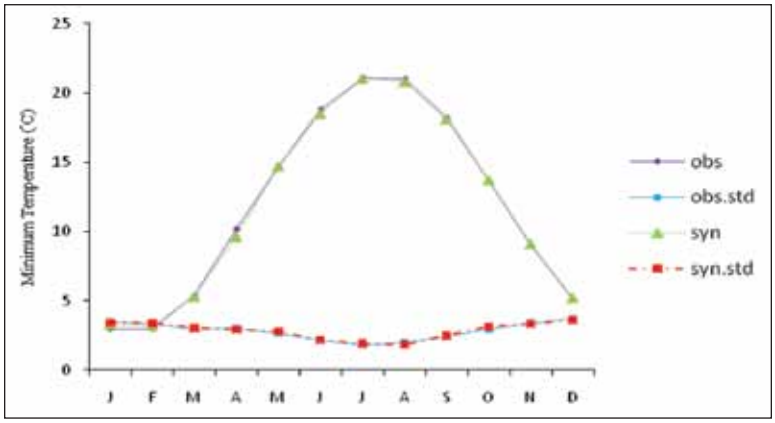


(a)

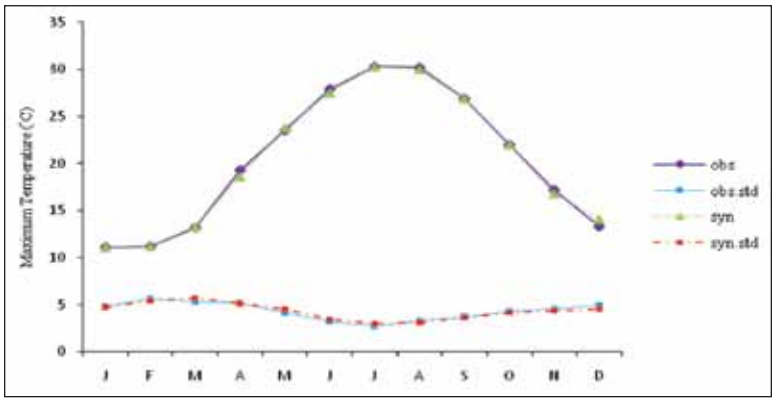


(b)

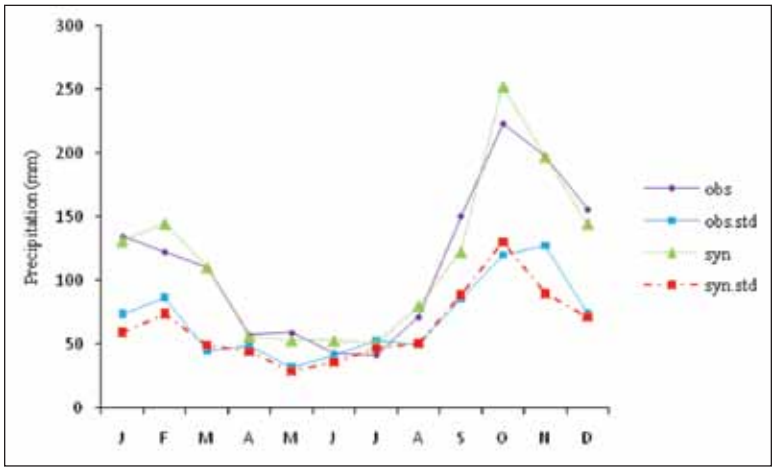


(c)

Fig.2: Comparision of the observed and synthetic data during 1976-2005 in the north of Iran; (a) Minimum temperature; (b) Maximum temperature, and (c) Precipitation

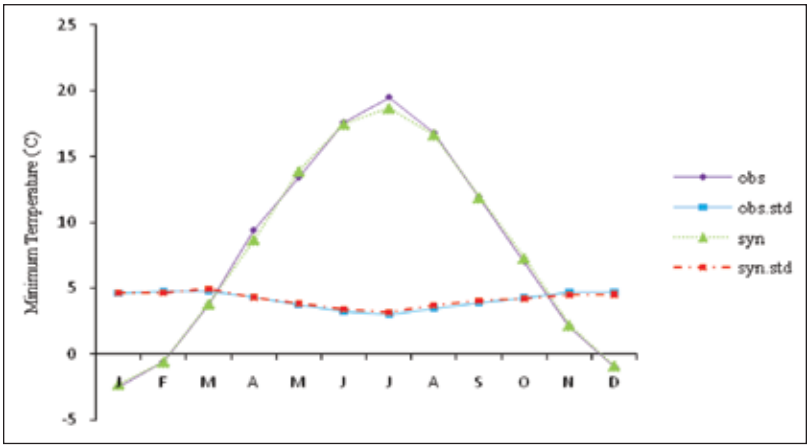


(a)

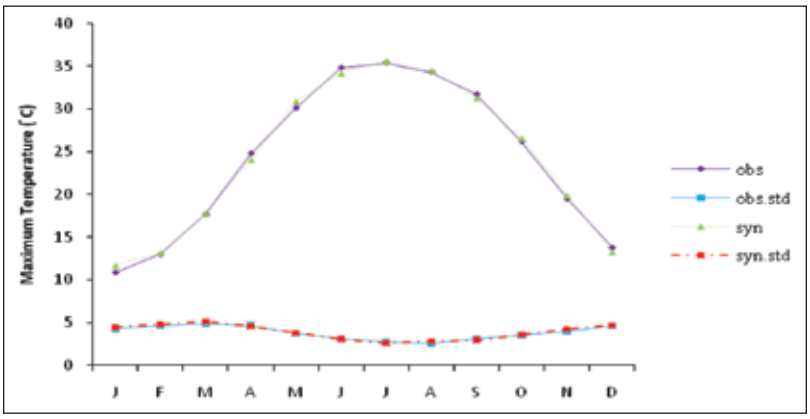


(b)

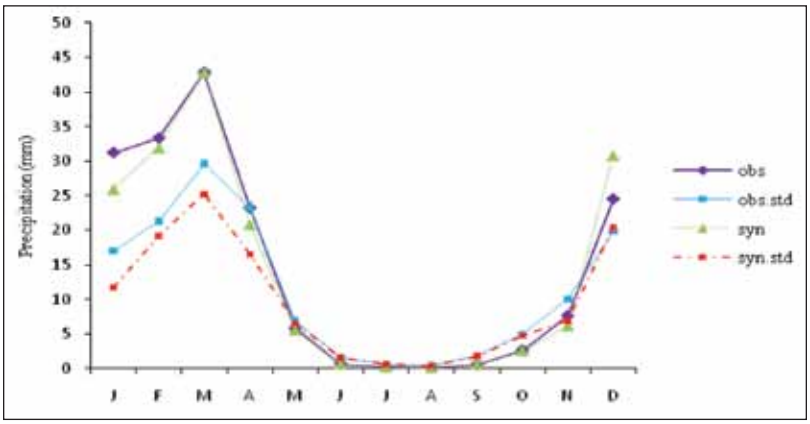


(c)

Fig.3: Comparision of the observed and synthetic data during 1976-2005 in the northeast of Iran; (a) Minimum temperature; (b) Maximum temperature, and (c) Precipitation.

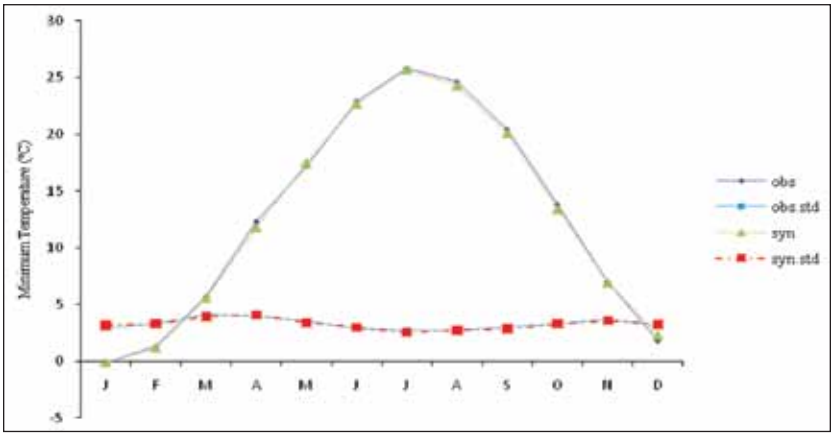


(a)

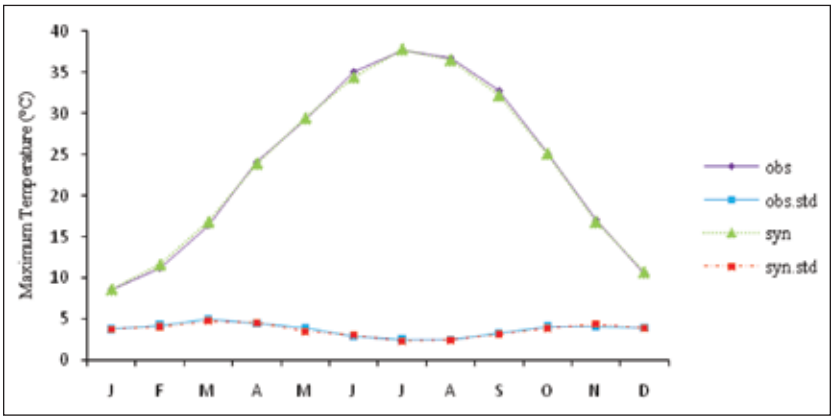


(b)

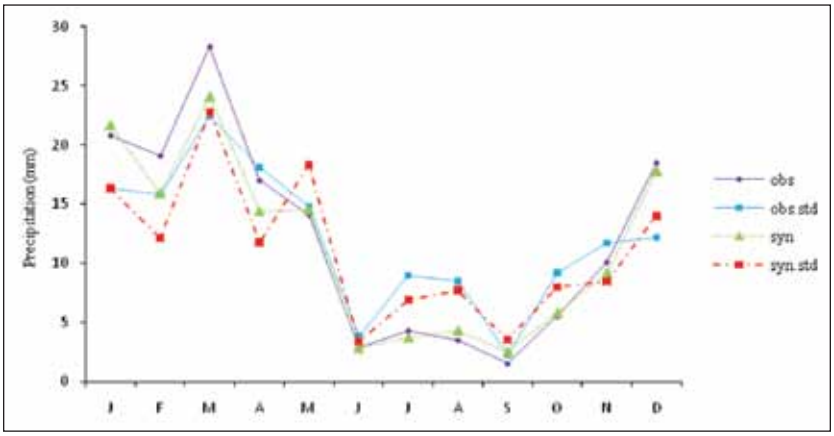


(c)

Fig.4: Comparision of the observed and synthetic data during 1976-2005 in the central Iran; (a) Minimum temperature; (b) Maximum temperature and (c) Precipitation.

would decrease in other months. The decrease in the rainfall during warm season is lower than during cold season. Statistical analysis indicates a decrease of rainfall in Yazd, Golestan and the south of Khorasan, but an increase of rainfall in Gilan and the north of Khorasan. The analysis showed that except for August and June, the mean monthly temperature would increase by 0.5°C in the cold season. The mean monthly increase in temperature was detected to be 1.7°C and 1.4°C in Rasht and Bojnurd, respectively. A stochastic weather generator was used in this study as a computationally cost-effective tool to construct site-specific climate change scenarios which incorporated changes in the climate means and

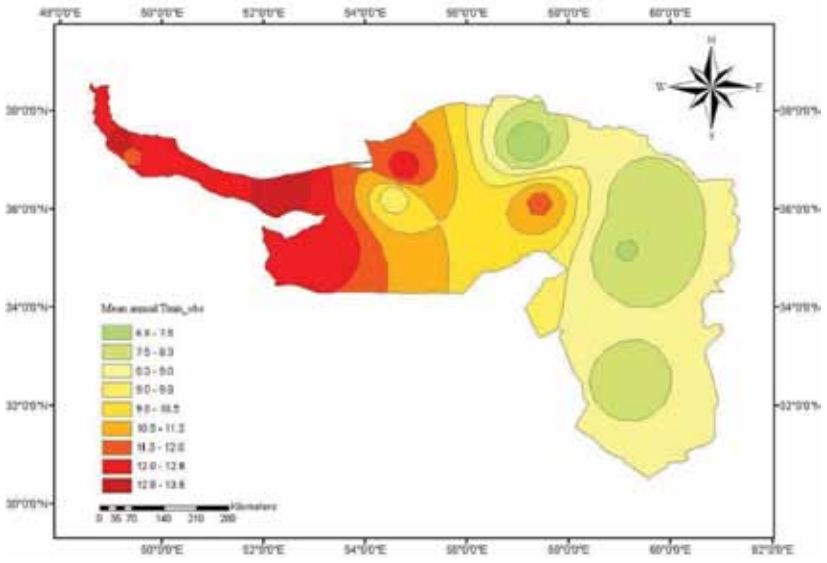

(a)

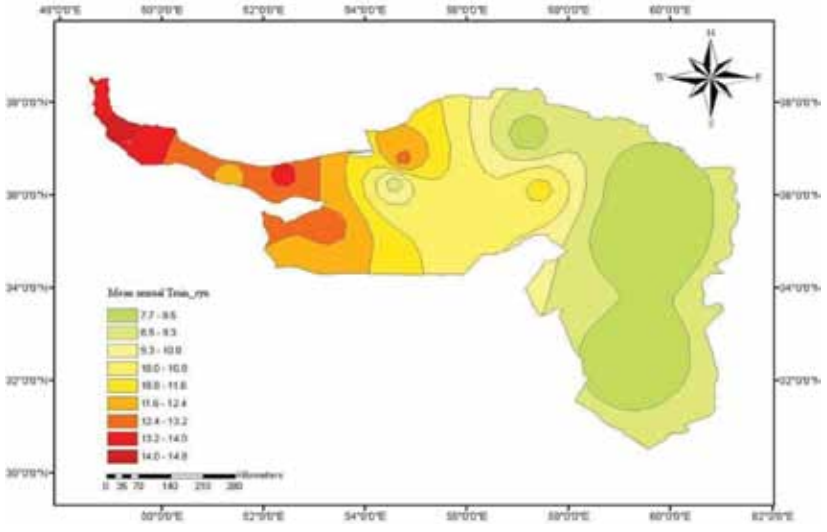

(b)

Fig.5: The mean annual minimum temperature; (a) 1976-2005 and (b) 2010-2039

climate variability. As the first step, the capability of the LARS-WG model was investigated. To obtain this aim, the base data were expanded from 1976 to 2005. The climate parameters contained precipitation, as well as the minimum and maximum temperatures. After validation of the LARS-WG model, this model was based on ECHO-G data for 2010-2039 for the selected stations. The results revealed that the mean precipitation would decrease in Yazd, and the south of Khorasan and Golestan. On the contrary, the mean temperature during 2010-2039 would increase by 0.5°C, especially in the cold season. Fig.5, Fig.6 and Fig.7 indicate the

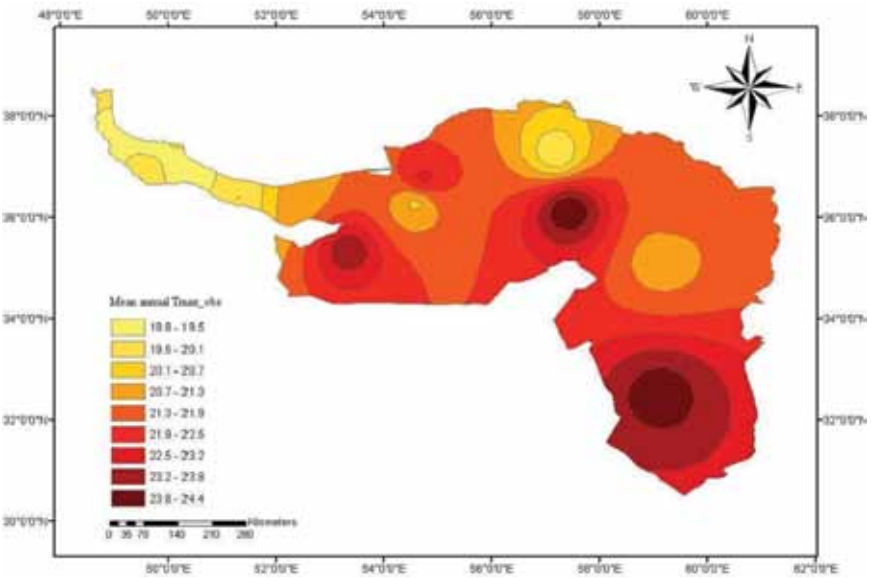


(a)

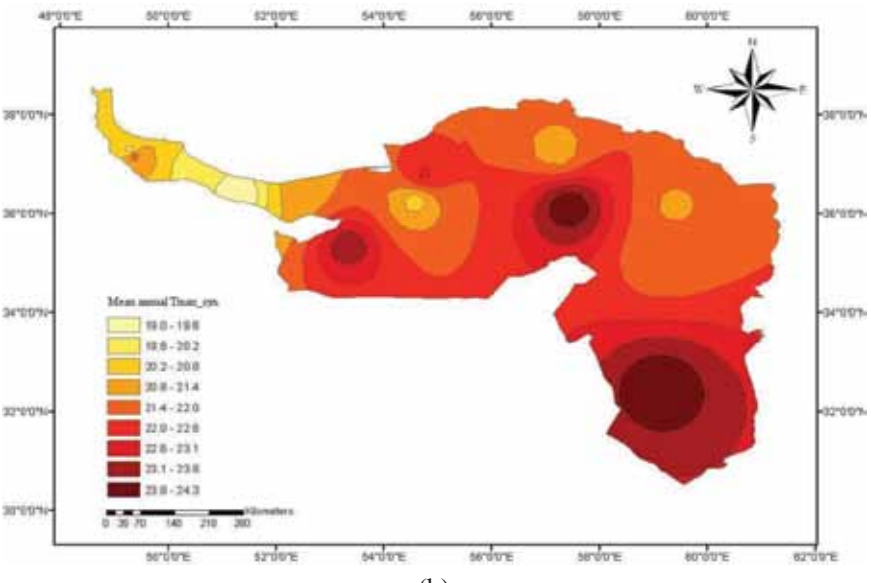


(b)

Fig.6: The mean annual maximum temperature; (a) 1976-2005 and (b) 2010-2039

annual mean minimum and maximum temperatures, as well as the precipitation of the past and future, respectively.

## CONCLUSION

The performance of the weather generator model LARS-WG was examined at 13 synoptic stations in the study area. The results of the current study indicated that the model has

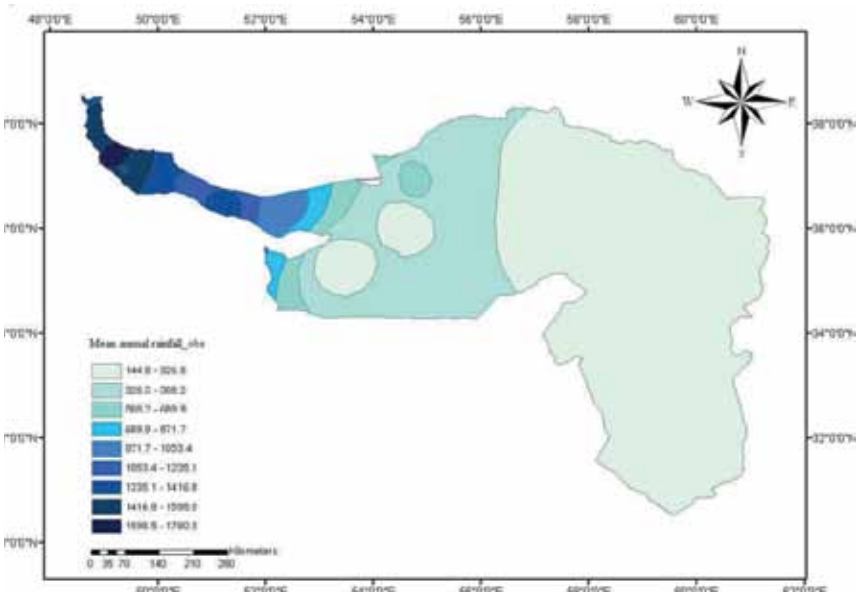

(a)

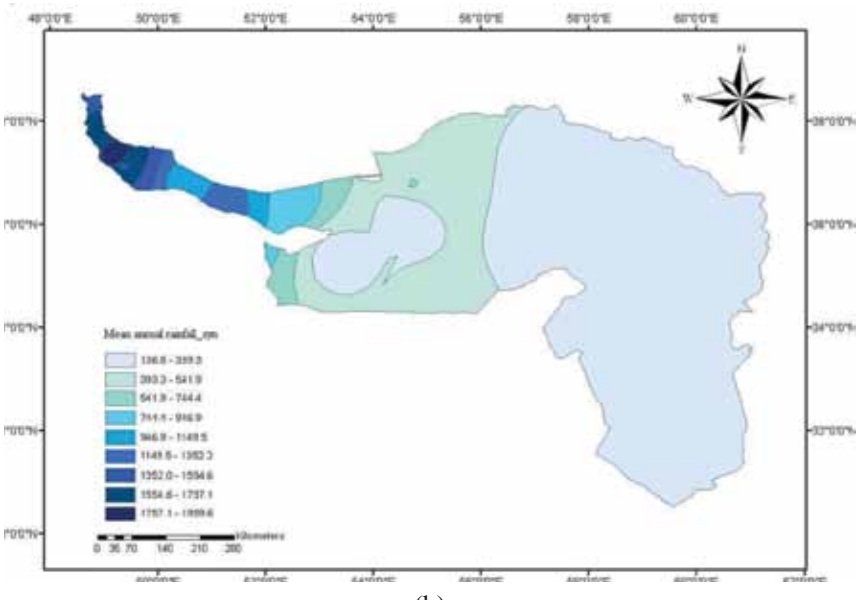

(b)

Fig.7: The mean annual precipitation; (a) 1976-2005 and (b) 2010-2039

different performances in diverse climates and also at different stations in a similar climate. Nonetheless, the model has a better performance in the monthly minimum temperature and also the monthly maximum temperature in comparison with the mean monthly precipitation. This study has demonstrated that the mean monthly precipitation will decrease in the south of the study area (semi-arid regions) and Golestan, whereas it will increase in the northwest of Iran. Meanwhile, the mean temperature will increase by 0.5°C during 2010-2039 in all the climate regions. Hence, it can be strongly recommended that the model be evaluated for each station in which the model is utilized.

## ACKNOWLEDGEMENTS

The authors are grateful to the National Climatology Research Institute (CRI) for the data given, and appreciates Dr. Babaeian, Dr. Nokhandan, Mr. Hosseini Asl and Ms. Malbousi for their helpful comments and beneficial suggestions.

## REFERENCES

Barrow, E. M., & Semenov, M. A. (1995). Climate change scenarios with high spatial and temporal resolution for agricultural applications. *Forestry, 68*, 349-360.

Barrow, E. M., & Semenov, M. A. (1996). Effect of using different methods in the construction of climate change scenarios, Examples from Europe. *Climate Research, 7*, 195-211.

Dibike, Y. B., & Coulibaly, P. (2005). Hydrologic impact of climate change in the Saguenay watershed: comparison of downscaling methods and hydrologic models. *Hydrology, 307*, 145-163.

Dubrovsky, M. (1996). The stochastic generator of daily weather series for the crop growth model. *Meteorology, 49,* 97-105.

Freiwan, M., & Kadioglub, M. (2008).Climate variability in Jordan. *International journal of Climatology, 28*, 69–89.

Hansen, J. W. (1999). Stochastic daily solar irradiance for biological modeling applications. *Agricultural and Forest Meteorology, 94*, 53–63.

IPCC, Climate Change. (2007). *The Physical Science Basis. Contribution of Working Group I to the Fourth Assessment Report of the Intergovernmental Panel on Climate Change*. Cambridge, United Kingdom: Cambridge University Press.

Khan, M. S., Coulibaly, P., & Dibike, Y. (2006). Uncertainty analysis of statistical downscaling methods using Canadian Global Climate Model predictors. *Hydrology Processes, 20*, 3085–3104.

Koenig, K. A. (2008). *An Evaluation of Statistical Downscaling Methods in Central Canada for Climate Change Impact Studies* (Ms. thesis dissertation).University of Manitoba.

Lawless, C., & Semenov, M. A. (2005). Assessing lead time for predicting wheat growth using a crop simulation model. *Agricultural and Forest Meteorology, 135*, 302-313.

Nakicenovic, N, & Swart, R. (2000). *Emissions Scenarios. Special Report of the Intergovernmental Panel on Climate Change*. Cambridge, Uk: Cambridge University Press.

Parlange, M. B, & Katz, R. W. (2000). An extended version of the Richardson model for simulating daily

weather variables. *Journal of Applied Meteorology and Climatology, 39*, 610-622.

Racsko, P., Szeidl, L., & Semenov, M. A. (1991). Serial approach to local stochastic weather models. *Ecological Modeling, 57*, 27-41.

Ragab, R., & Prudhomme, C. (2002). Climate change and water resources management in arid and semi-arid regions: prospective and challenges of the 21st century. *Biosystem Engineering, 81*, 3–34.

Scibek, J., & Allen, D. M. (2006). Modelled impacts of predicted climate change on recharge and groundwater levels. *Water Resource Research, 42*, W11405.

Semenov, M. A., Brooks, R. J., Barrow, E. M., & Richardson, C. W. (1998). Comparison of the WGEN and LARS- WG stochastic weather generators in diverse climates. *Climate Research, 10*, 95–107.

Semenov, M. A, & Brooks, R. J. (1999). Spatial interpolation of the LARS-WG stochastic weather generator in Great Britain. *Climate Research, 11*, 137–148.

Semenov, M. A, & Barrow, E. (2002). *LARS-WG a stochastic weather generator for use in climate impact studies*. *User's manual*. United Kingdom: Rothamsted Research, Harpenden, Hertfordshire.

Semenov, M. A. (2007a). Development of high-resolution UKCIP02-based climate change scenarios in the UK. *Agricultural and Forest Meteorology, 144*, 127-138.

Semenov, M. A., & Doblas, R. F. J. (2007b). Utility of dynamical seasonal forecasts in predicting crop yield. *Climate Research, 34*, 71–81.

Semenov, M. A., & Stratonovitch, P. (2010). The use of multi-model ensembles from global climate models for impact assessments of climate change. *Climate Research, 41*, 1–14.

Solomon, S. D., Manning, Q. M., Marquis, M., Averyt, K., Tignor, M. M. B., & Chen, Z. (2007). *The Physical Science Basis. Contribution of Working Group I to the Fourth Assessment Report of the Intergovernmental Panel on Climate Change*. NY: Cambridge University Press.

Stathopoulou, M., & Cartalis, C. (2009). Downscaling AVHRR land surface temperatures for improved surface urban heat island intensity estimation. *Remote Sensing Of Environment, 113,* 2592–2605.

Weiss, A., Hays, C. J., & Won, J. (2003). Assessing winter wheat responses to climate change scenarios: a simulation study in the U.S. Great Plains. *Climate Change, 58*, 119–147.

Wilby, R. L., & Dawson, C. W. (2002). SDSM-a decision support tool for the assessment of regional climate change impacts. *Environmental Modeling & Software, 17*, 145-157.

Zhang, X. C., & Garbrecht, J. D. (2003). Evaluation of CLIGEN precipitation parameters and their implication on WEPP runoff and erosion prediction. *Trans. ASAE, 46*, 311–320.

Pertanika J. Sci. & Technol. 20 (2): 313 - 325 (2012)

SCIENCE & TECHNOLOGY

Journal homepage: http://www.pertanika.upm.edu.my/

# The Performance of Classical and Robust Logistic Regression Estimators in the Presence of Outliers

**Habshah, M.[1] and Syaiba, B. A.[2*]**

[1]*Laboratory of Applied and Computational Statistics, Institute for Mathematical Research, Universiti Putra Malaysia, 43400 Serdang, Selangor, Malaysia*

[2]*Department of Mathematics, Faculty of Science, Universiti Putra Malaysia, 43400 Serdang, Selangor, Malaysia*

## ABSTRACT

It is now evident that the estimation of logistic regression parameters, using Maximum Likelihood Estimator (MLE), suffers a huge drawback in the presence of outliers. An alternative approach is to use robust logistic regression estimators, such as Mallows type leverage dependent weights estimator (MALLOWS), Conditionally Unbiased Bounded Influence Function estimator (CUBIF), Bianco and Yohai estimator (BY), and Weighted Bianco and Yohai estimator (WBY). This paper investigates the robustness of the preceding robust estimators by using real data sets and Monte Carlo simulations. The results indicate that the MLE behaves poorly in the presence of outliers. On the other hand, the WBY estimator is more efficient than the other existing robust estimators. Thus, it is suggested that the WBY estimator be employed when outliers are present in the data to obtain a reliable estimate.

**Keywords: Maximum Likelihood Estimator, Robust Estimators, Outliers, Goodness of Fit, Monte Carlo Simulation**

## INTRODUCTION

Logistic regression model is used for prediction of the probability of an occurrence $Y = 0$ or a non occurrence $Y = 1$ of an event with predictor variables $X$(s) that may be either numerical, categorical or both. From its original acceptance in epidemiology, the application of this model is now widely used in many research fields. In practice, the Maximum Likelihood Estimator (MLE) is used to estimate the coefficients, standard errors and to compute the goodness of fit test. The MLE is known as the most efficient estimator with good optimality properties for estimating the parameters in the logistic

*Article history:*
Received: 17 January 2011
Accepted: 15 April 2011

*Email addresses:*
habshahmidi@gmail.com (Habshah, M.),
syaibabalqish@gmail.com (Syaiba, B. A.)
*Corresponding Author

ISSN: 0128-7680 

regression model. Unfortunately, the MLE is not robust toward outliers. It is now evident that the MLE estimates are known to be severely sensitive to outliers (Croux *et al*., 2002; Victoria-Feser, 2002; Croux & Haesbroeck, 2003; Imon & Hadi, 2008; Nurunnabi *et al*., 2009; Syaiba & Habshah, 2010; Sarkar *et al*., 2011). Even a single outlier is good enough to cause the estimates to suffer, and thus, resulting in a completely erroneous estimation. In a logistic regression problem, outlying observations which are corresponding to excessively large fitted values and highly influential to the model fit are treated as outliers (Hao, 1992; Croux & Haesbroeck, 2003). Nurunnabi *et al*. (2009) defined outliers as influential observations that need not to be outlined in the sense of having large fitted values. As an alternative, robust estimators which are much less affected by outliers are considered (Künsch *et al*., 1989; Carroll & Pederson, 1993; Bianco & Yohai, 1996; Croux & Haesbroeck, 2003).

In the next section, a brief background of the classical MLE, robust estimators and goodness of fit tests is reviewed. This is followed by an evaluation of the performance of MLE and robust estimators in the real examples and the Monte Carlo simulation study (see sub-section 3). Finally, the conclusion is given in sub-section 4.

## MATERIALS AND METHODS

### *Maximum Likelihood Estimator*

Consider a multiple logistic regression model:

$$Y = \pi(X) + \varepsilon \tag{1}$$

where, with $\eta = \beta_0 + \beta_1 X_1 + \beta_2 X_2 + \ldots + \beta_p X_p = X\beta$. Here, $Y$ is an $n \times 1$ vector of response. Let $y_i = 0$ if the $i^{\text{th}}$ unit does not have the characteristic and $y_i = 1$ if the $i^{\text{th}}$ unit does possess that characteristic. $X$ is an $n \times k$ matrix of explanatory variables with $k = p + 1$. $\beta^T = (\beta_0, \beta_1, \beta_2, \ldots \beta_p)$ is the vector of the regression parameters and ε is an n × 1 vector of the unobserved random errors. The quantity $\pi_i$ is known as probability or fitted value for the $i^{\text{th}}$ covariate. The model given in Eq.(2) satisfies $0 \leq \pi_i \leq 1$. The fitted values in logistic regression model are calculated for each covariate pattern which is dependent on the estimated probability for the covariate pattern, denoted as $y_i = \hat{\pi}_i$. Thus, the $i^{\text{th}}$ residual is defined as:

$$\hat{\varepsilon} = y_i - \hat{\pi}_i \qquad i = 1, 2, ..., n \tag{3}$$

A logit transformation of the logistic regression model which is linear in its parameter is defined in terms of $\pi = (X)$ as follows:

$$g(X) = \log\left(\frac{\pi}{1-\pi}\right) = X\beta \tag{4}$$

Here, "log" shall designate the base *e* logarithm. The conditional distribution of response variable follows a Bernoulli distribution with a probability given by the conditional mean,

$\pi(X)$. Since $Y_i = 0$ for $i = 1, 2, ..., n$ are assumed to be independent with $n$ corresponding to the random variables of $(Y_1, Y_2, ..., Y_n)$, the joint probability density function is written as:

$$\begin{aligned} g(Y_1, Y_2, \ldots, Y_n) &= \prod_{i=1}^{n} f_i(Y_i) \\ &= \prod_{i=1}^{n} \pi_i^{Y_i} (1 - \pi_i)^{(1-Y_i)} \end{aligned} \tag{5}$$

Then, the MLE is obtained by maximizing the logarithm of the likelihood function produces, as follows:

$$\begin{aligned} \log(g(Y_1, Y_2, \ldots, Y_n)) &= \sum_{i=1}^{n} Y_i \log\left(\frac{\pi_i}{1 - \pi_i}\right) + \sum_{i=1}^{n} \log(1 - \pi_i) \\ &= \sum_{i=1}^{n} Y_i (X\beta) - \sum_{i=1}^{n} \log[1 + \exp(X\beta)] \end{aligned} \tag{6}$$

By differenting Eq. (6) with respect to $\beta_0$, produces $\sum_{i=1}^{n} [Y_i - \pi(X_i)] = 0$ and $\sum_{i=1}^{n} X_i [Y_i - \pi(X_i)] = 0$ for $\beta_1, \beta_2, ..., \beta_p$. The iterative estimates of $\beta$ (s) are then obtained as follows:

$$\begin{aligned} \hat{\beta}^{(k+1)} &= (X^T W X)^{-1} X^T W (X\hat{\beta}^k + W^{-1} e) \\ &= \hat{\beta}^{(k)} + (X^T W X)^{-1} X^T e \end{aligned} \tag{7}$$

where $W$ is a diagonal matrix with an element of $\pi_i(1 - \pi_i)$, $e = Y - \hat{\pi}$ and $k$ is number of iterations.

It is important to point out that when a complete separation is found in the data, the parameters of the logistic regression model cannot be estimated by the MLE. The complete separation of data (means no overlapping cases) is when the $X$ values, that correspond to $Y = 1$, exceed all of the $X$ values that correspond to $Y = 0$ (Albert & Anderson, 1984; Santner & Duffy, 1986).

Recently, there are many robust estimators available in the literature due to the sensitivity of the MLE in the presence of outliers. In this section, several selected robust estimators are utilized to compare their performances with the classical MLE in the presence of outliers. These robust estimators are briefly discussed in the subsequent sections.

### *The Mallows Type Leverage Dependent Weights Estimator (MALLOWS)*

Künsch *et al*. (1989) introduced the Mallow-type estimator by minimizing the weighted log-likelihood function where the weights are dependent on covariates. Carrol and Pederson (1993) investigated more on the Mallow-type estimator and proposed to turn the MLE into an estimate with bounded influence by down-weighting the outliers in the $X$-space. The MALLOWS estimator was obtained by minimizing the log-likelihood on a particular weight function.

$$\sum_{i=1}^{n} w_i [y_i \log(\pi_i(\beta)) + (1 - y_i) \log(1 - \pi_i(\beta))] \tag{8}$$

where $w_i = W(h_n(x_i))$. $W$ is a non-increasing function such that $W(u)u$ is bounded which is dependent on a parameter $c > 0$, and $W(u) = \left(1 - \frac{u^2}{c^2}\right)\Big|(|u| \le c)$. $W$ is computed by Robust Mahalanobis Distance (RMD) based on the robust estimation of the centre and scatter matrix of the covariates.

*The Conditionally Unbiased Bounded Influence Function estimator (CUBIF)*

The CUBIF estimator minimizes a measure of efficiency based on the asymptotic covariance matrix under the model subject to a bound on a measure of infinitesimal sensitivity that is similar to the gross error sensitivity (Künsch *et al*., 1989). It is a consistent M-estimator in the form of $\sum_{i=1}^{n} \psi(y_i, x_i, \beta) = 0$ such that $E\left(\psi(y, x, \beta) \,|\, x_i\right) = 0$. The optimal function of $\psi$ is written as follows:

$$\psi(y, x, \beta, B) = W(\beta, y, x, b, B)\left\{y - g(\beta^T x) - c\left(\beta^T x, \frac{b}{h(x, B)}\right)\right\}x \tag{9}$$

where $b$ is bounded on the measure of infinitesimal sensitivity, $B$ is a dispersion matrix, and $h(x, B) = (x^T B^{-1} x)^{1/2}$ is a leverage measure. The function $c\left(\beta^T x, b \big/ h(x, B)\right)$ is a corrected bias with corrected residual as shown below:

$$r(y, x, \beta, b, B) = y_i - g(\beta^T x) - c\left(\beta^T x, \frac{b}{h(x, B)}\right) \tag{10}$$

The weights are in the form of $W(\beta, y, x, b, B) = W_b(r(y, x, \beta)h(x, B))$, where $W_b$ is the Huber weight given by $W_b(x) = \min\left\{1, \frac{b}{|x|}\right\}$. The function $W$ downweights the observation with a large corrected residual and a large leverage making the M-estimator to have a bounded influence.

The MALLOWS and the CUBIF estimators are available in the Robust Packages of SPLUS and R under the command of glmRob.

*The Bianco and Yohai Estimator (BY)*

Pregibon (1981) proposed robust M-estimates to replace the total deviance function based on minimizing the weighted total deviance.

$$M(\beta) = \sum_{i=1}^{n} \rho(d^2(\pi_i(\beta), y_i)) \tag{11}$$

where $\rho(u)$ is an increasing Huber loss function. Meanwhile, deviance residuals measure the discrepancies between the probabilities fitted using the regression coefficients $\beta$ and the observed values. Later, Bianco and Yohai (1996) found that this estimator does not downweight the high leverage points and is not consistent as well. They improved this estimator by minimizing it, as follows:

$$M(\beta) = \sum_{i=1}^{n} [\rho(d^2(\pi_i(\beta), y_i)) + q(\pi_i(\beta))] \tag{12}$$

where $\rho(u)$ is a bounded, differentiable and non-decreasing function, which is defined by:

$$\rho(u) = \begin{cases} u - \left(x^2 \big/ 2k\right), & x \le k \\ k \big/ 2, & \text{otherwise} \end{cases} \tag{13}$$

with $k$ is a positive number. The researchers defined $q(u) = v(u) + v(1-u)$ with $v(u) = 2\int_0^u \psi(-2\log t)dt$ and $\psi = \rho^T$.

*The Weighted Bianco and Yohai Estimator (WBY)*

Croux and Haesbroeck (2003) noticed that when working with Huber loss function, $\rho(u)$ which was suggested by Bianco and Yohai (1996) previously, occurred frequently that the BY estimator did not exist even for uncontaminated data. Thus, Croux and Haesbroeck (2003) accomplished the BY estimator and proposed an extra weights to downweight the high leverage points, $\psi_c^{CH}(u) = \exp\left(-\sqrt{\max(u,c)}\right)$. The WBY estimator minimizes:

$$\sum_{i=1}^{n} w(x_i)\left[\psi(d_i^2(\beta))(y_i - \pi_i(\beta)) - E_\beta\left(\psi(d_i^2(\beta))(y_i - \pi_i(\beta)) \,\middle|\, x_i\right)\right] \tag{14}$$

The weight is to be a decreasing function of RMD with distance is computed using the Minimum Covariance Determinant (MCD) (Rousseuw & Leroy, 1987) that is taken as:

$$w(x_i) = \begin{cases} 1 & \text{if} \quad RMD_i^2 \le \chi^2_{(p,0.975)} \\ 0 & \text{else} \end{cases} \tag{15}$$

The WBY estimator consists a loss-function to guarantee the existence of the BY estimator and to provide a stable and fast algorithm to compute the BY estimator.

$\chi_1 \arcsin 2$ *Goodness of Fit Test*

There are several measurements used to test the goodness of fit for logistic regression model. Nonetheless, Cox and Wermuth (1992) warned not to use $R^2$ when $Y$ only has two possible values; this shows that frequently $R^2 = 0.1$ when good models are used. Meanwhile, Collett (2003) has shown that the deviance, which is dependent on the fitted success probabilities $\pi_i$, can only be used to summarise the goodness of fit test for a group binary data and unreliable for binary data or when data are sparse. The Pearson's $\chi^2$ statistics is the most popular alternative instead the deviance. Both the deviance and this Pearson's $\chi^2$ statistics have the same asymptotic $\chi^2$ distribution when the fitted model is correct. Even if Pearson's $\chi^2$ statistics can be computed to access the goodness of fit test for logistic regression model in the presence of outliers, one cannot solely rely on this statistics. Kordzakhia *et al*. (2001) suggested an alternative measure by using the chi-square statistics based on the arcsin transformation, $\chi^2_{arc}$. Later, this statistic was applied to compute the goodness of fit test and to evaluate the performance of robust estimators (Künsch *et al*., 1989; Croux & Haesbroeck, 2003). The $\chi^2_{arc}$ are defined as follows:

$$\chi^2_{arc} = \sum_{i=1}^{n} 4\left[\arcsin\sqrt{y_i} - \arcsin\sqrt{\pi_i}\right]^2; \quad i = 1,2,\ldots n \tag{16}$$

The arcsin transformation converts a Bernoulli random variable into one that is nearly normal and whose variance is slightly dependent on the parameter $\pi_i$. The arcsin is used to normalize the data in percentages or proportions whose distribution fits the Bernoulli distribution.

## RESULTS AND DISCUSSIONS

In this study, the investigation was focused on the usefulness of the robust estimators on several well-known real data and simulation study.

### *The Prostate Cancer Data*

First, the Prostate Cancer (PC) data given by Brown (1980) were taken into consideration. The data contain the values for two continuous variables, which are an elevated level of acid phosphates (AP) in the blood serum and the age of patients (AGE) that would be of value so as to predict whether or not PC patients also had lymph node involvement (LNI). The original data consisted of 53 patients and this was modified by adding two more outliers, namely, cases 54 ($y$, $x_1$, $x_2$) = (0, 200, 67) and 55 ($y$, $x_1$, $x_2$) = (0, 200, 68). The character plot of the PC data is presented in Figure 1 where AGE is plotted against AP and the character corresponding to occurrence $Y = 1$ and non-occurrence $Y = 0$ is denoted by symbols triangle and circle, respectively.

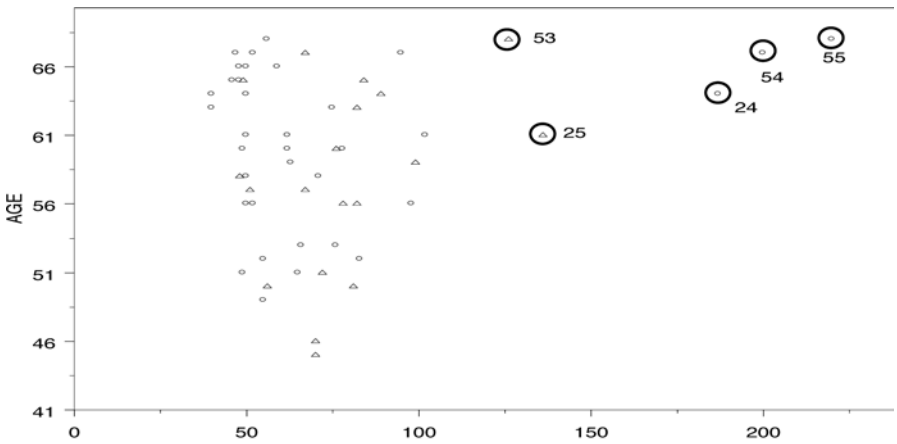


Fig.1: Scatter Plot of AGE vs AP with Outliers (Cases 24, 25, 53, 54, 55) for PC Data

It has been reported by Imon (2006) that the original data on the 53 patients may contain three outliers (cases 24, 25 and 53). Nonetheless, five outliers (*see* Fig. 1) were omitted from 55 observations to perform uncontaminated data.

### *The Neuralgia Data*

Next, other data given by Piergorsch (1992) were considered. The data contain the values for two continuous variables, namely, the age of patients in completed years (AGE) and the

pre-treatment duration of symptoms in month (DUR). There were 18 patients involved in this study and the outcome was whether the patients experienced any pain relief after the treatment. The character plot of the Neuralgia data is presented (*see* Fig.2) where DUR is plotted against AGE and the character corresponding to occurrence $Y = 1$ and non-occurrence $Y = 0$ is denoted by the triangle and circle, respectively.

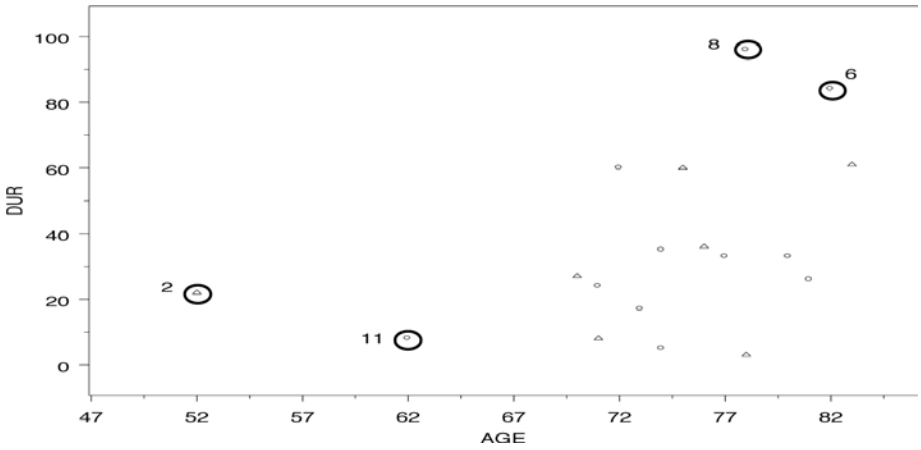


Fig. 2: Scatter Plot of DUR vs AGE with Outliers (Cases 2, 6, 8, 11) for Neuralgia Data

It is crucial to highlight that no identification of outliers for the Neuralgia data can be found in the literature. From the scatter plot (*see* Fig. 2), it pinpoints cases 2, 6, 8 and 11, as the outlying points. Therefore, the four suspected outliers should be removed to perform uncontaminated data.

*The Erythrocyte Sedimentation Rate Data*

The final data in the current study were the Erythrocyte Sedimentation Rate (ESR) data. In this case, the main objective was to see whether the levels of two plasma proteins (namely, Fibrinogen and γ.Globulin) in the blood plasma would be the factor increasing the ESR for healthy individuals. The study was carried out by the Institute of Medical Research, in Kuala Lumpur, Malaysia, involving 32 patients and the original data were collected by Collett and Jemain (1985). The responses of zero signify a healthy individual while the responses of unity refer to an unhealthy individual. Here, the continuous variables are (FIB and γ.GLO) versus the binary response of ESR. The character plot of the ESR data is presented in Fig.3 where γ.GLO is plotted against FIB and the character corresponding to occurrence $Y = 1$ and non-occurrence $Y = 0$ is denoted by the triangle and circle, respectively.

Syaiba and Habshah (2010) identified two outliers (namely, cases 13 and 29) in $X$-space for the original ESR data. As illustrated in Fig 3, it was observed that cases 14 and 15 are influential observations. Therefore, deleting cases 14 and 15 would create non-overlapping cases. In order to perform uncontaminated data, one more overlapping case was added by modifying case 13 with $(y, x_1, x_2) = (3.06, 37)$. From the uncontaminated data, the ESR data were contaminated where the occurrences ($Y = 1$) and non-occurrences ($Y = 0$) were replaced

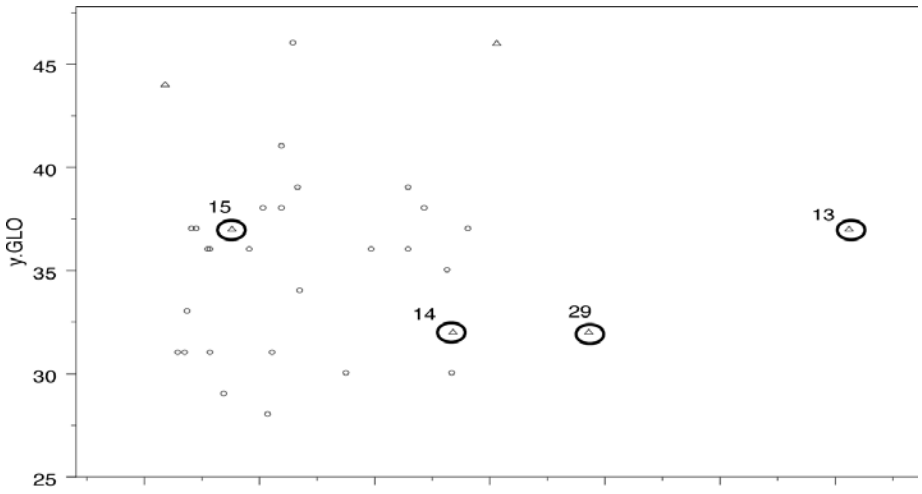


Fig.3: Scatter Plot of γ.GLO vs FIB with Outliers (Cases 13, 14, 15 and 29) for ESR Data

with each other for cases 14 and 15, and this might only leave one out of the three overlapping cases for the ESR data.

*Monte Carlo Simulation Study*

A simulation study was conducted to further assess the performance of the MLE and robust estimators. The evaluations focused on the severity of the outliers and also the number of observations by adding the outliers to the uncontaminated data. Following the work by Croux and Haesbroeck (2003), three different types of data were considered, and these are uncontaminated (Type 1), 5% moderate contaminated (Type 2), and 5% extreme contaminated (Type 3). The explanatory variables for the uncontaminated data (Type 1) were generated according to a standard normal distribution, $x_1 \sim N(0,1)$ and $x_2 \sim N(0,1)$, with four different numbers of observations, $n$ = (100, 200, 300, 400). The choice of a larger sample size was to ensure the existence of the overlapping cases in each replication. As pointed out by Victoria-Feser (2002), small data may lead to unidentifiable parameter estimates for no overlapping cases even without contamination. According to Victoria-Feser (2002), in practice, the number of observations with n = 50 is considered to be small. Thus, setting the true parameters as $\beta = (\beta_0, \beta_1, \beta_2)^T = (0.5, 1, -1)^T$ and the responses are defined as the following model equations:

$$y_i = \begin{cases} 0 & \text{if} \quad \beta_0 + \beta_1 x_1 + \beta_2 x_2 + \varepsilon_i < 0 \\ 1 & \text{if} \quad \beta_0 + \beta_1 x_1 + \beta_2 x_2 + \varepsilon_i \geq 0 \end{cases} \tag{17}$$

where the error terms were generated according to a logistic distribution, $\varepsilon_i \sim \Lambda(0,1)$. The explanatory variables for the contaminated data were generated according to the standard normal distributions, $z_1 \sim N(0,1)$ and $z_2 \sim N(0,1)$. In addition, the percentage of contamination denoted as $s$ was also considered, as such that $s$ = (5%) with magnitude of outlying shift distance in $X$-space for Type 2 and Type 3 taken as $\delta = 5$ and $\delta = 10$ respectively. The new $x$

values are defined as $x_1^* = z_1 + \delta$ and $x_2^* = z_2 - \delta$ and the responses are defined as they are in the following model equations:

$$y_i^* = \begin{cases} 0 & \text{if} \quad \beta_0 + \beta_1 x_1^* + \beta_2 x_2^* + \varepsilon_i \geq 0 \\ 1 & \text{if} \quad \beta_0 + \beta_1 x_1^* + \beta_2 x_2^* + \varepsilon_i < 0 \end{cases} \tag{18}$$

The performance of the estimators of MLE, CUBIF, MALLOWS, BY and WBY was evaluated based on the summary measures combining the individual estimated coefficients over $M = 1000$ replications. Therefore, BIAS and Root Mean Squared Error (RMSE) measures are computed as follows:

$$BIAS = \left\| \frac{1}{M} \sum_{i=1}^{M} \hat{\beta}_i^{(k)} - \beta_i^t \right\| \quad \text{and} \quad RMSE = \sqrt{\frac{1}{M} \sum_{i=1}^{M} \left\| \hat{\beta}_i^{(k)} - \beta_i^t \right\|^2}$$

for $k = 1, 2, ..., M$ and $i = 1, 2, ..., p$, where $\| \cdot \|$ indicates the Euclidean norm.

## RESULTS AND DISCUSSION

A "good" estimator is the one that has parameter estimates fairly close to the MLE estimates of the uncontaminated data. The second criterion is based on the goodness of fit test for the estimator which has the smallest value of $\chi^2_{arc}$. Nevertheless, the complete tables of estimated coefficients, standard errors, and goodness of fit test could not be attached for the uncontaminated data of each real example due to space limitation in this paper. In general, the estimates and $\chi^2_{arc}$ values for the MLE, MALLOWS and CUBIF estimators are reasonably closer for the uncontaminated data. It was observed that for uncontaminated PC and Neuralgia data, the BY and WBY estimators gave different results for the parameter estimates when the outliers were omitted from the data. On deleting the outliers, the remaining data may have few overlapping cases, and thus, leaving the data in situation of quasi-complete separation. This is the reason why the BY and WBY estimators that downweight the outliers have larger estimated coefficients and standard errors compared to the MLE estimator. For the uncontaminated ESR data, the estimated coefficients of the BY and WBY estimators are slightly smaller compared to the MLE when the number of overlapping cases was increased.

Table 1: Estimated coefficients, standard errors, and the goodness of fit for PC (contaminated data)

| | | MLE$^{uc}$ | MLE | MALLOWS | CUBIF | BY | WBY |
|---|---|---|---|---|---|---|---|
| Int. | $\beta_0$ | -0.980 | 11.492 | 7.141 | 7.121 | -1.912 | -4.795 |
| | $se(\beta_0)$ | 13.538 | 10.940 | 11.020 | 11.061 | 10.822 | 11.844 |
| AP | $\beta_1$ | 3.031 | 1.141 | 1.663 | 1.749 | 1.112 | 2.913 |
| | $se(\beta_1)$ | 1.376 | 0.781 | 0.817 | 0.826 | 0.770 | 1.030 |
| | $\beta_2$ | -3.004 | -4.145 | -3.607 | -3.687 | -0.817 | -1.951 |
| AGE | $se(\beta_2)$ | 2.936 | 2.735 | 2.744 | 2.751 | 2.653 | 2.805 |
| | $\chi^2_{arc}$ | 100.516 | 120.013 | 119.514 | 119.651 | 112.512 | 103.003 |

MLE$^{uc}$ indicates the results for the uncontaminated PC data

Table 1 presents the comparison of the five estimators based on parameter estimates, standard errors and goodness-of-fit test for the contaminated PC data. Under the contaminated data, $\beta_0$ of all estimators is mostly affected by the outliers compared to other coefficients. The standard errors were found to be smaller but the $\chi^2_{arc}$ values increased compared to the uncontaminated data. The results presented in Table 1 indicate that the MLE is mostly influenced by the outliers. Among the robust estimators, the WBY is the most efficient estimator because it produces the lowest $\chi^2_{arc}$ value and its estimates are closer to the MLE of uncontaminated data.

Table 2: Estimated coefficients, standard errors, and the goodness of fit for Neuralgia (contaminated data)

| | | MLE$^{uc}$ | MLE | MALLOWS | CUBIF | BY | WBY |
|---|---|---|---|---|---|---|---|
| Int. | $\beta_0$ | -6.507 | 14.449 | 3.109 | 10.784 | 14.558 | 30.921 |
| | $se(\beta_0)$ | 46.406 | 20.390 | 19.688 | 19.794 | 20.373 | 25.749 |
| AGE | $\beta_1$ | 1.581 | -3.312 | -0.710 | -2.492 | -3.411 | -7.480 |
| | $se(\beta_1)$ | 10.798 | 4.836 | 4.674 | 4.698 | 4.836 | 6.133 |
| | $\beta_2$ | -0.196 | -0.213 | -0.200 | -0.185 | -0.123 | 0.209 |
| DUR | $se(\beta_2)$ | 0.612 | 0.542 | 0.541 | 0.541 | 0.544 | 0.604 |
| | $\chi^2_{arc}$ | 33.687 | 41.680 | 40.371 | 40.816 | 40.750 | 38.338 |

MLE$^{uc}$ indicates the results for the uncontaminated Neuralgia data

For the Neuralgia data with outliers (*see* Fig. 2), it is difficult to judge which estimator is the best by inspecting their parameter estimates. However, it is evident that the WBY is the best estimator as it has the smallest $\chi^2_{arc}$ value.

Table 3: Estimated coefficients, standard errors, and the goodness of fit for ESR (contaminated data)

| | | MLE$^{uc}$ | MLE | MALLOWS | CUBIF | BY | WBY |
|---|---|---|---|---|---|---|---|
| Int. | $\beta_0$ | 12.263 | 19.882 | 20.449 | 20.579 | 14.231 | 20.441 |
| | $se(\beta_0)$ | 5.839 | 9.417 | 9.809 | 10.031 | 7.099 | 10.381 |
| FIB | $\beta_1$ | 1.830 | 2.597 | 2.648 | 3.053 | 1.791 | 2.572 |
| | $se(\beta_1)$ | 1.062 | 1.543 | 1.611 | 1.681 | 1.308 | 1.877 |
| | $\beta_2$ | 0.153 | 0.278 | 0.286 | 0.256 | 0.189 | 0.271 |
| γ.GLO | $se(\beta_2)$ | 0.116 | 0.165 | 0.170 | 0.170 | 0.135 | 0.178 |
| | $\chi^2_{arc}$ | 42.237 | 27.050 | 26.628 | 26.047 | 27.805 | 25.724 |

MLE$^{uc}$ indicates the results for the uncontaminated ESR data

Under the contaminated of the ESR data, $\beta_0$ and $se(\beta_0)$ of all the estimators are mostly affected by the outliers as compared to the other parameters (see Table 3). The results shown in Table 3 also indicate that the MLE is mostly influenced by the outliers. On modifying the contaminated data, there is only one overlapping observation, case 13 remains. This is the reason why the WBY that downweight this observation has large coefficients and standard errors. Even though the WBY has the smallest $\chi^2_{arc}$ value, the BY estimator should also be taken

into consideration. The results illustrated in Tables 3 signify that the BY is a good estimator for the ESR data as its estimates are fairly closer to the MLE for the uncontaminated data.

Tables for the results of the summary measures consist BIAS and RMSE, whereby the first row indicates that the computation does not include the intercept term and second row indicates the computation including the intercept term. A "good" estimator is the one that has BIAS and RMSE, which are relatively small or closest to zero.

For the uncontaminated data shown in Table 4, the estimators of MLE, MALLOWS, CUBIF, BY and WBY behave not too differently. It can be seen that the BIAS and RMSE will reduce when the number of observations is increased. Under 5% of the intermediate contamination (*see* Table 5), the WBY estimator performs best in term of BIAS and RMSE. Meanwhile, the weighting step in the WBY estimator becomes more advantageous in the extreme contamination (*see* Table 6). However, the MLE estimator behaves very poorly in

Table 4: BIAS and RMSE of the estimators (Type 1)

| | $n = 100$ | | $n = 200$ | | $n = 300$ | | $n = 400$ | |
|---|---|---|---|---|---|---|---|---|
| | BIAS | RMSE | BIAS | RMSE | BIAS | RMSE | BIAS | RMSE |
| MLE | 0.085 | 0.451 | 0.040 | 0.293 | 0.025 | 0.235 | 0.020 | 0.203 |
| | 0.086 | 0.522 | 0.040 | 0.340 | 0.026 | 0.273 | 0.021 | 0.238 |
| MALLOWS | 0.082 | 0.451 | 0.038 | 0.293 | 0.023 | 0.235 | 0.018 | 0.203 |
| | 0.082 | 0.522 | 0.038 | 0.341 | 0.024 | 0.274 | 0.018 | 0.238 |
| CUBIF | 0.083 | 0.452 | 0.040 | 0.294 | 0.025 | 0.235 | 0.020 | 0.203 |
| | 0.084 | 0.522 | 0.041 | 0.341 | 0.026 | 0.274 | 0.020 | 0.238 |
| BY | 0.094 | 0.472 | 0.045 | 0.304 | 0.026 | 0.240 | 0.022 | 0.207 |
| | 0.095 | 0.544 | 0.045 | 0.352 | 0.027 | 0.279 | 0.023 | 0.242 |
| WBY | 0.096 | 0.498 | 0.046 | 0.315 | 0.028 | 0.249 | 0.022 | 0.215 |
| | 0.097 | 0.569 | 0.047 | 0.363 | 0.289 | 0.287 | 0.023 | 0.249 |

Table 5: Bias and RMSE of the estimators (Type 2)

| | $n = 100$ | | $n = 200$ | | $n = 300$ | | $n = 400$ | |
|---|---|---|---|---|---|---|---|---|
| | BIAS | RMSE | BIAS | RMSE | BIAS | RMSE | BIAS | RMSE |
| MLE | 0.684 | 0.747 | 0.698 | 0.723 | 0.706 | 0.724 | 0.704 | 0.719 |
| | 0.741 | 0.824 | 0.754 | 0.792 | 0.759 | 0.784 | 0.758 | 0.777 |
| MALLOWS | 0.615 | 0.684 | 0.636 | 0.668 | 0.645 | 0.664 | 0.645 | 0.661 |
| | 0.666 | 0.758 | 0.687 | 0.728 | 0.693 | 0.720 | 0.694 | 0.715 |
| CUBIF | 0.586 | 0.660 | 0.605 | 0.639 | 0.613 | 0.634 | 0.614 | 0.630 |
| | 0.639 | 0.736 | 0.658 | 0.702 | 0.663 | 0.691 | 0.664 | 0.686 |
| BY | 0.492 | 0.604 | 0.512 | 0.562 | 0.521 | 0.553 | 0.521 | 0.546 |
| | 0.537 | 0.675 | 0.556 | 0.619 | 0.563 | 0.603 | 0.563 | 0.595 |
| WBY | 0.281 | 0.504 | 0.319 | 0.417 | 0.336 | 0.401 | 0.342 | 0.389 |
| | 0.318 | 0.576 | 0.354 | 0.472 | 0.368 | 0.446 | 0.375 | 0.434 |

the contamination data. There are some losses in the precision (increased RMSE when BIAS is small) for the estimator based on weighting step**.** The intercept coefficient is more affected in the contaminated data, and consequently, the BIAS is larger compared to slope coefficients.

Table 6: BIAS and RMSE of the estimators (Type 3)

| | $n = 100$ | | $n = 200$ | | $n = 300$ | | $n = 400$ | |
|---|---|---|---|---|---|---|---|---|
| | BIAS | RMSE | BIAS | RMSE | BIAS | RMSE | BIAS | RMSE |
| MLE | 1.352 | 1.369 | 1.352 | 1.361 | 1.354 | 1.359 | 1.353 | 1.357 |
| | 1.378 | 1.410 | 1.379 | 1.395 | 1.380 | 1.390 | 1.379 | 1.387 |
| MALLOWS | 0.386 | 0.548 | 0.475 | 0.537 | 0.501 | 0.541 | 0.516 | 0.544 |
| | 0.398 | 0.600 | 0.488 | 0.569 | 0.513 | 0.566 | 0.529 | 0.566 |
| CUBIF | 0.733 | 0.784 | 0.746 | 0.770 | 0.753 | 0.769 | 0.753 | 0.764 |
| | 0.752 | 0.826 | 0.765 | 0.800 | 0.771 | 0.794 | 0.771 | 0.788 |
| BY | 0.852 | 1.050 | 0.904 | 1.029 | 0.921 | 1.018 | 0.916 | 1.005 |
| | 0.872 | 1.090 | 0.926 | 1.061 | 0.943 | 1.046 | 0.939 | 1.032 |
| WBY | 0.096 | 0.492 | 0.046 | 0.313 | 0.028 | 0.247 | 0.021 | 0.213 |
| | 0.097 | 0.563 | 0.047 | 0.360 | 0.029 | 0.286 | 0.022 | 0.248 |

## CONCLUSIONS

The purpose of this analysis was to compare the performance of the MLE and four robust estimators under contaminated and uncontaminated data. The results showed that the MLE estimator is severely affected by the presence of outliers. Among the robust estimators, the WBY estimator produced the smallest BIAS and RMSE in the contaminated data and their estimates are closer to the MLE for the uncontaminated data, followed by MALLOWS, BY and CUBIF. Therefore, it can be concluded that the WBY estimators perform better compared to the MLE estimator and the rest of the robust estimators in the presence of outliers. The results from the real data indicate that the WBY estimator produced the smallest $\chi^2_{arc}$ in the presence of outliers even though its estimates are slightly difference from the MLE estimator in the uncontaminated data due to quasi-complete separation. To protect against the outliers, weighting the covariates is effective. The weighting step can be seen as a way of the uncontaminated in the data before the estimation procedure.

## REFERENCES

Albert, A., & Anderson, J. A. (1984). On the existence of maximum likelihood estimates in logistic regression. *Biometrika, 71*, 1-10.

Bianco, A. M., & Yohai, V. J. (1996). Robust estimation in the logistic regression model. Robust statistics, data analysis and computer intensive methods. *Proceedings of the Workshop in Honor of Huber, P.J. and Rieder, H. Lecturer notes in statistics.* Springer, New York, *109*, 17-34.

Brown, B. W. (1980). Prediction analysis for binary data. In R. G. Miller, B. Efron, B. W. Brown, and L. E. Moses (Eds.). *Biostatistics Casebook* (p. 3-18). New York: John Wiley and Sons, Inc.

Carroll, R. J., & Pederson, S. (1993). On robustness in the logistic regression model. *Journal of Royal Statistics Society B, 55*, 693-706.

Collett, D. (2003). *Modelling binary data* (2nd ed). London: Chapman & Hall.

Collett, D., & Jemain, A. A. (1985). Residuals, outliers and influential observations in regression analysis. *Sains Malaysiana, 14*, 493-511.

Cox, D. R., & Wermuth, N. (1992). A comment on the coefficient of determination for binary response. *American Statisticians, 46,* 1-4.

Croux, C., Flandre, C., & Haesbroeck, G. (2002). The breakdown behaviour of the maximum likelihood estimator in the logistic regression model. *Statistics and Probability Letters, 60,* 377-386.

Croux, C., & Haesbroeck, G. (2003). Implementing the bianco and yohai estimator for logistic regression. *Computational Statistics and Data Analysis, 44,* 273-295.

Hao, Y. (1992). *Maximum median likelihood and maximum trimmed likelihood estimations*. Published Doctoral Dissertation, University of Toronto, Canada.

Imon, A. H. M. R. (2006). Identification of high leverage points in logistic regression. *Pakistan Journal of Statistics, 22,* 147-156.

Imon, A. H. M. R., & Hadi, A. S. (2008). Identification of multiple outliers in logistic regression. *Communication in Statistics – Theory and Methods, 37,* 1697-1709.

Kordzakhia, N., Mishra, G. D., & Reiersølmoen, L. (2001). Robust estimation in logistic regression model. *Journal of Statistical Planning and Inference*, *98,* 211-223.

Künsch, H. R., Stefanski, L. A., & Carroll, R. J. (1989). Conditionally unbiased bounded influence estimation in general regression models with applications to generalized linear models. *Journal of the American Statistical Association, 84*, 460-466.

Nurunnabi, A. A. M., Imon, A. H. M. R., & Nasser, M. (2009). *Identification of multiple influential observations in logistic regression*. Philadelphia: Taylor and Francis, Inc.

Piegorsch, W. W. (1992). Complementary log regression for generalized linear models. *American Statisticians*, *46*, 94-99.

Pregibon, D. (1981). Logistic regression diagnostics. *Annals of Statistics, 9*, 705-724.

Rousseeuw P. J., & Leroy, M. (1987). *Robust regression and outlier detection* (p. 216-247). New York: John Wiley and Sons, Inc.

Santner, T. J., & Duffy, D. E. (1986). A note on A. Albert's and J.A. Anderson's conditions for the existence of maximum likelihood estimates in logistic regression models. *Biometrika, 73,* 755-758.

Sarkar, S. K., Midi, H., & Rana, S. (2011). Detection of outliers and influential observations in binary logistic regression: An empirical study. *Journal of Applied Sciences, 11,* 26-35.

Syaiba, B. A., & Habshah, H. (2010). Robust logistic diagnostic for the identification of high leverage points in logistic regression model. *Journal of Applied Sciences*, *10,* 3042-3050.

Victoria-Feser, M-P. (2002). Robust inference with binary data. *Psychometrika, 67*, 21-32.

Pertanika J. Sci. & Technol. 20 (2): 327 - 330 (2012)

SCIENCE & TECHNOLOGY

Journal homepage: http://www.pertanika.upm.edu.my/

*Case Report*

# Combined Ultrasound and IVU for the Management of Childhood Urolithiasis: A Case Report

**Fathinul Fikri A. S. and Abdul Jalil Nordin**

*Centre for Diagnostic Nuclear Imaging, Universiti Putra Malaysia, 43400 Serdang, Selangor, Malaysia*

## ABSTRACT

The incidence of ureteric calculus as a cause for severe abdominal pain in children is mounting, especially in the tropical country. The course of illness may be non-specific but a swift detection via non-invasive imaging modalities singly or in combination may avert unnecessary radiation hazard and futile surgery in a young child. In this paper, we discussed a case of an 11 year-old boy who was presented with a sudden onset of the right side severe abdominal colic whose a bedside ultrasound was positive for hydronephrosis for which localisation of stone was further confirmed via a low dose limited intravenous urography (IVU). It is important to note that data available on the value of a combined ultrasound and the limited IVU in an emergency setting when urolithiais is being suspected in children with abdominal pain are particularly scarce. Hence, this case documented the potential value of a combined ultrasound and a limited IVU study as a unique combined armamentarium used in a suspected childhood urolithiasis in the tropics.

**Keywords: Child, abdominal colic, ureteric calculus, limited IVU**

## INTRODUCTION

Prevalence of urolithiasis in children is largely attributable to the change in socio-economic conditions and climatological phenomena. Its incidence in the tropical countries is on the rise (Robertson, 2003). Traditionally in children, upper tract stones are associated with urinary tract anomalies and infection rather than metabolic disturbances. Suspicion of stones in a child with acute severe abdominal pain is crucial when there is no other associated symptom confounding the renal colic, especially in children living in the tropics. Robertson further stressed the problem of increasing renal stone in the tropics, where the risk of stone formation is confounded by low urine volume (Robertson,

*Article history:*
Received: 20 June 2011
Accepted: 22 September 2011

*Email addresses:*
ainurff@gmail.com (Fathinul Fikri A. S.),
drimaging@yahoo.com (Abdul Jalil Nordin)
*Corresponding Author

ISSN: 0128-7680 

2003). Immediate suspicion of the renal stone manifestation may avert excessive and time consuming investigation for other non-specific causes of pain in children.

There are varieties of diagnostic tools employed in evaluating childhood abdominal pain, and these include KUB, IVU, ultrasound (US) or computed tomography (CT). In our experience, the use of a combined bedside ultrasound and a limited series IVU is essential in excluding ureterolithiasis in children with acute or severe abdominal pain. CT examination, though it may produce more accurate results as compared to IVU and ultrasound, it imposes escalating radiation dose to the radio-sensitive tissue in the child bearing age. Meanwhile, IVU has a sensitivity of 64% to 97% as compared to ultrasound (74%) when hydronephrosis is added as a positive sign for a ureteric stone (Miler *et al.*, 1998). The accuracy of US/KUB was found to be 71% lower than the accuracy of IVU alone. As for a combination of US/KUB, it has a sensitivity of 79% compared to CT (93%) (Ripolles *et al.*, 2004). Although computerized tomography is more sensitive in detecting urolithiasis than ultrasound, the difference in the usefulness between the 2 radiological tests may not be clinically significant (Carlo *et al.*, 2009). Nonetheless, data on the value of a combined USG and a limited IVU are scarce. This report highlights its potential value when the ultrasound is positive for hydronephrosis whilst optimising the radiation dose to the young patient.

## CASE STUDY

This case study involved an 11 year-old boy who presented with severe intermittent right abdominal pain 2 hours prior to hospital admission. He was fretful without pallor or jaundice. The abdomen was generally soft without guarding or rebound tenderness. Intramuscular morphine (2.0mg) was given but was inadequate as the child continued to be restless despite the sedative effects. Intravenous access and urinary catheterisation were performed. An emergency bedside abdominal ultrasound was ordered and this revealed mild separation of the right renal pelvis without recognisable stones within (*see* Fig.1). A control anterior-posterior (AP) abdominal radiograph and an immediate 15-minute IVU filming were also performed after the intravenous administration of low osmolar contrast medium. The pyelographic IVU phase revealed a small filling defect in the right upper ureter causing mild right hydronephrosis

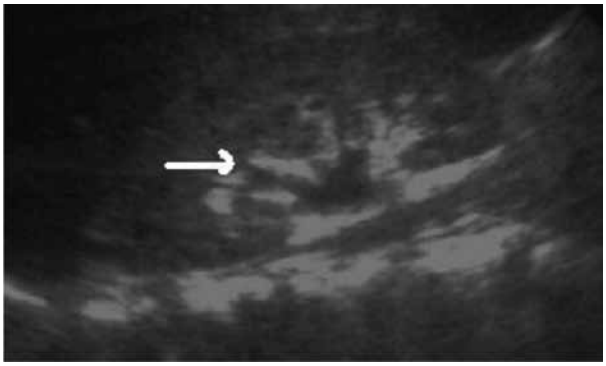

Fig.1: Transaxial ultrasound image shows a mild separation of the right central renal echo-complex (arrowed)


Fig.2: There is a small faint opacity seen in the course of the right upper ureter representing a stone (arrowed)


Fig.3: IVU – 15-minute AP film; there is mild right sided hydronephrosis and proximal right hydroureter with a filling defect seen in the right upper ureter (arrowed)

favouring partial right upper ureteric stone obstruction, as shown in Fig.2 and Fig.3. The stone was removed following a flexible ureteroscopic procedure. This report highlights the value of a combined US and a limited series of IVU in children with acute abdominal pain for which the incidence of urolithiaisis is escalating among those who reside in the tropics.

## DISCUSSION

Abdominal pain is a common problem in children. Although most children with acute abdominal pain have self-limited conditions, the pain may herald a surgical or medical emergency. The most difficult challenge is making a timely diagnosis so that treatment can be initiated and morbidity prevented. Most children with urolithiasis present symptomatically, usually with flank or abdominal pain. Approximately 15 to 20 percent are asymptomatic, primarily young children who are diagnosed with stone detection when abdominal imaging is performed for other purposes (Coward *t al.*, 2005). Traditionally, upper urinary tract stones in children are associated more frequently with metabolic disturbances rather than with urinary tract anomalies and infection (Coward *et al.*, 2005).

The current study documents the value of a combined ultrasound abdomen and a limited IVU series in diagnosing a ureteric stone in a young boy presented with severe acute right abdominal pain. In the tropics, the prevalence of the ureteric stone in children has gained a considerable attention from the treating physicians for which the attributing factor is largely due to the patient's concentrated urine volume. The use of ultrasound in investigating abdominal pain in children is feasible as it provides a quick revelation of solid organ abnormality in question. In a prospective study, fifty-eight patients with renal colic, while fifty-eight of the

104 patients enrolled in the study were diagnosed with renal colic, and the overall sensitivity and specificity of bedside ultrasonography for the detection of hydronephrosis were found to be 86.8% and 82.4%, respectively (Romolo *et al.*, 2005). In the report of the current work, the use of a limited series IVU technique after a positive ultrasound abdomen for hydronephrosis has led to as a swift localisation of a ureteric stone. There are hardly any data on the value of the combined US and the limited IVU technique when compared to other armamentariums in the evaluation of childhood abdominal pain when urolithiasis is being suspected as a cause. The low dose limited IVU technique has not been given a focus in evaluating childhood urolithiasis as most of the concerns related to the reduced radiation dose are limited to renal trauma (Smith *et al.*, 2003). A concern on the absorbed skin dose has been much debated when CT is used as a standard tool on younger children Liu Wesler *et al*., 2000). Of late, a new digital technique known as digital tomosynthesis was found to have a diagnostic quality in 95.5% with the mean of 56% of dose reduction when used for IVU (Wells IT *et al*, 2011).

## CONCLUSION

Urolithiasis in the pediatric population has evolved from a mere clinical curiosity to a disease process worthy of thoughtful and rigorous scientific study when investigating children with severe abdominal pain especially in tropical countries. This report has documented the potential value of a combined ultrasound and a limited series of IVU as a first line investigation method in an emergency setting involving a child with severe abdominal pain in the tropics.

## REFERENCES

Robertson, W. G. (2003). Renal stones in the tropics. *Semin. nephrol., 23*, 77-87.

Miler, O. F., Rineer, S. K., & Reichard, S. R. (1998). Prospective comparison of unenhanced spiral computed tomography and intravenous urogram in the evaluation of acute flank pain. *Urology*, *52*, 982-987.

Ripolles, T., Agramunt, M., Errando, J., Martinez, M. J., & Coronel B. (2004). Suspected ureteric colic, plain film and sonography versus unenhanced helical CT: A prospective study of 66 patients. *Eur. Radiol., 14*(1), 129-136.

Carlo, P., Jeanne, S. C., Andres, S., Cynthia, L. S., & Ilina, R. (2009). Ultrasound Versus Computerized Tomography for Evaluating Urolithiasis. *The Journal of Urology, 182*(4)*, 1*.

Coward, R. J., Peters, C. J., Duffy, P. G., Corry, D., & Kellet, M. J. (2003). Epidemiology of paediatric renal stone disease in the UK. *Arch Dis. Child*, *88*, 962-5.

Romolo, J. G. & Kurt, H. (2005). Emergency ultrasound and urinalysis in the evaluation of flank pain. *Academic Emergency Medicine*, *12*(12), 1180-1184.

Liu Wesler, S. J., Kenny, B. J., Rainbow, A. J., & Stevenson, G. W. (2000). Low dose non-enhanced helical CT of renal colic: Assessment of ureteric stone detection and measurement of effective dose equivalent. *Radiology, 215*, 51-54.

Wells, I. T., Raju, V. M., & Rowberry, B. K. (2011). Digital tomosynthesis- a new lease of life for the intravenous urogram? *Br. J. Radiol*., *84*(1001), 464-8.

Smith, J. K., & Kenney, P. J. (2003). Imaging of renal trauma. *Radiol. Clin. North Am., 41*(5), 1019-1035.

Pertanika J. Sci. & Technol. 20 (2): 331 - 337 (2012)

SCIENCE & TECHNOLOGY

Journal homepage: http://www.pertanika.upm.edu.my/

# Synthesis of Epoxidized Palm Oil-Based Trimethylolpropane Ester by *In Situ* Epoxidation Method

**Ferra Naidir[1], Robiah Yunus[1,3*], Tinia Idaty Mohd. Ghazi[1] and Irmawati Ramli[2]**

[1]*Department of Chemical and Environmental Engineering, Faculty of Engineering, Universiti Putra Malaysia, 43400 Serdang, Selangor, Malaysia*

[2]*Department of Chemistry, Faculty of Science, Universiti Putra Malaysia, 43400 Serdang, Selangor, Malaysia*

[3]*Institute of Advanced Technology, Universiti Putra Malaysia, 43400 Serdang, Selangor, Malaysia*

## ABSTRACT

Palm oil-based Trimethylolpropane ester (TMP ester), with an iodine value of 66.4 g/100g, was epoxidized to produce epoxidized TMP esters. *In situ* epoxidation method was used with peracetic acid to eliminate fatty acid double bonds in palm oil-based TMP ester and change it into oxirane ring. This was done to improve the oxidative stability of trimethylolpropane ester which is a key concern limiting the useful service life in lubricants. The epoxidation was performed by reacting acetic acid as active oxygen carrier with concentrated hydrogen peroxide as oxygen donor and a small amount of homogeneous catalyst (sulphuric acid). The effects of various parameters on the rate of epoxidation (such as the ratio of mole acetic acid to ethylenic unsaturation, hydrogen peroxide to ethylenic unsaturation and acetic acid mole ratio, and amount of catalyst) were studied. The rate of oxidation was investigated by the percentage of oxirane oxygen analysis and iodine value.

**Keywords: *In situ* epoxidation, peracetic acid, percentage of oxirane oxyen, sulphuric acid**

## INTRODUCTION

Vegetable oil based lubricant has superior tribological properties and is rapidly biodegradable, and these make it suitable to be used as a base fluid in environmental acceptable lubricants (EAL). Vegetable oils contain fatty acids esters with unsaturated fractions such as oleic acid (C18:1), linoleic acid (C18:2) and linolenic acid (C18:3), as well as saturated fractions, namely palmitic acid (C16:0) and stearic acid (C18:0). The structures of the fatty acids, i.e. the chain length and degree of unsaturation, directly affect the operational stabilities and lubricating properties of the oil. The oxidative stability of

*Article history:*
Received: 28 March 2011
Accepted: 15 April 2011

*Email addresses:*
robiah@eng.upm.edu.my (Robiah Yunus),
tinia@eng.upm.edu.my (Tinia Idaty Mohd. Ghazi),
irmawati@science.upm.edu.my (Irmawati Ramli)
*Corresponding Author

ISSN: 0128-7680 

vegetable oils increases with the decrease in the amount of polyunsaturated acids (Schneider, 2006). Oxidation is a major concern that limits the use of vegetable oil as lubricating fluid. Oxidation leads to polymerization and degradation whereby polymerization will increase viscosity and reduce lubrication functionality. Meanwhile, degradation leads to break down to products that are volatile, corrosive and diminish the structure and properties of the lubricants (Kodali, 2002). It is important to note that oxidative stability can be improved by either genetic or chemical modification of unsaturated acids. The unsaturated fatty acid structure of trimethylolpropane esters was modified through epoxidation reaction to produce epoxidized trimethylolpropane esters. Epoxidation is a reaction in which the double bond in unsaturated fraction is directly converted into oxirane (epoxide) groups by reaction with organic peracids, either preformed or generated *in situ*. The *in situ* synthesis takes place by reacting carboxylic acid with concentrated hydrogen peroxide to make percarboxylic acid. An oxygen atom from hydrogen peroxide through percarboxylic acid attaches itself to the double bonds of the fatty acid carbon chain of the oil, as shown in Fig.1 (Campanella & Baltanas, 2005).

Epoxidation reaction involves the opening of the double bond, followed by the formation of the oxirane ring on the opened bond. Peracetic acid was used as the epoxidizing agent and was prepared *in situ* using hydrogen peroxide ($H_2O_2$) as the primary source of oxygen and aqueous acetic acid ($CH_3COOH$) and as the oxygen carrier between the aqueous and the oil phases. A small amount of homogeneous catalyst ($H_2SO_4$) was applied and heptane was employed as an inert solvent to minimize the formation side product, such as the opening of the epoxy ring on oxirane, especially at higher temperatures (Gan *et al*., 1992). This paper focuses on the effects of the ratio of mole acetic acid and hydrogen peroxide on the epoxidation reaction of palm oil based synthetic lubricant (TMPester) to reduce the double bond and to change it into oxirane ring. The effect of catalyst was also studied, where the progress of reaction was assessed based on the presence of double bond by measuring the IV value of the sample and the presence of oxirane oxygen.

## MATERIALS AND METHODS

### *Materials*

The palm oil based synthetic lubricant used in the experiment was trimethylolpropane ester (TMPester) derived from palm oil. TMPester was synthesized in our laboratory using palm oil methyl ester (POME) and trimethylolpropane as starting materials and sodium methoxide solution in methanol (30 w/w%) as a catalyst. The chemicals used in the epoxidation reaction were glacial acetic acid 99.7% (Rankem, India), heptane (Merck, Germany), sulphuric acid 96.5% (Rdh, Germany) and hydrogen peroxide 35% (Merck, Germany).

### *Experimental Procedure of Epoxidized TMP Ester*

TMP ester was used as a starting material in the epoxidation reaction and the reaction was carried out based on the procedures described in the Encyclopedia of Chemical Technology (Kirk & Othmer, 1994). The required amount of TMPester and heptane as a solvent was added into the three-necked reaction flask connected to a reflux condenser. Peracetic acid, which

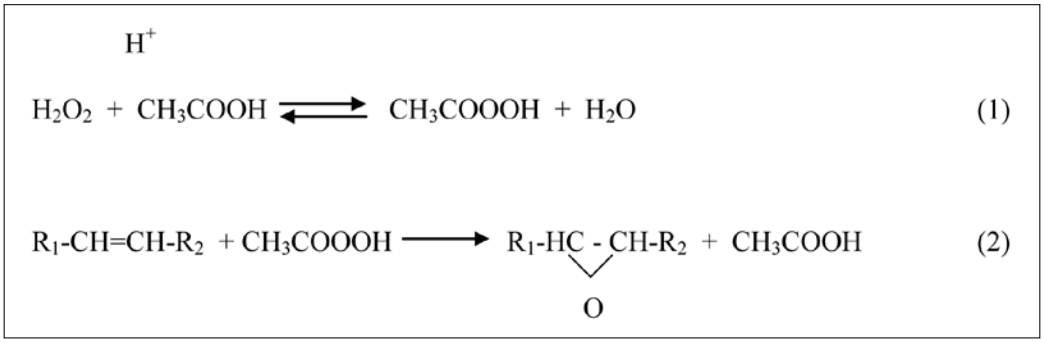


Fig.1: The Epoxidation of the Double Bonds of Vegetable Oils (Unsaturated Triacylglycerides) in the Conventional Acetic Acid-Hydrogen Peroxide Process

had been prepared *in situ* by reacting various mixtures of acetic acid and hydrogen peroxide in the presence of small amounts of concentrated sulphuric acid, was poured into a mixture of TMPester and heptane. Then, the mixture was heated to a desired temperature by using a hotplate with a magnetic stirrer and a thermometer. After the reaction was completed, the mixture was poured into a separatory funnel and the aqueous layer was drawn off. The oil layer was washed with successive portions of warm water (± 40°C) and sodium hydroxide was added into the oil phase to neutralize the sulphuric acid, before it then was stripped off under a low vacuum pressure at 80°C. The mixture was cooled down and the epoxidized TMPester product was filtered. The product was analyzed for the iodine value based on the Porim Test Method (1985), and the percentage of oxirane oxygen was determined using the direct method as obtained in method Cd 9-57 by *American Oil Chemists' Society* (AOCS) (1984).

## RESULTS AND DISCUSSION

### *The Effect of the Ratio of Mole Acetic Acid on Ethylenic Unsaturation*

In the epoxidation reaction, acetic acid functions as an oxygen carrier for hydrogen peroxide to form peracetic acid, which then reacts with ethylenic unsaturation group in TMP ester to form oxirane groups. The reactions were performed at the ratios of 0.5, 0.8, 1 and 1.5 moles of acetic acid per mole of ethylenic unsaturation of TMP esters. The effect of acetic acid and the time of reaction on the epoxidation reaction of TMP esters are shown in Fig.2. The effect was determined based on the formation of oxirane ring oxygen. The yield of oxirane oxygen (%OO) is almost independent of acetic acid concentration. However, the figure shows that for a 20-hour reaction, the percentage of oxirane oxygen (%OO) increases with the concentration of acetic acid until it reaches the optimum value of 0.8 moles of acetic acid per mole of ethylenic unsaturation of TMP esters at which the %OO is 3.84%.

Meanwhile, Fig.3 shows that the lowest iodine value is 0.94 at mole ratio of glacial acetic acid 1.5 at 13 hours of reaction time. To achieve the minimum iodine value and the maximum percentage of oxirane oxygen, the optimum level of the acetic acid should be applied where both effects are balanced. The lower iodine value means a lower level of unsaturation in the epoxidized TMPesters. The opening of the double bonds allows for the formation of oxirane

in the epoxidized TMPester. Acetic acid takes part in the overall reaction as a catalyst in the formation of oxirane ring and as a reactant in the hydrolysis of the oxirane ring (Goud *et al*., 2006). In this study, the optimum mole ratio of glacial acetic acid to ethylenic unsaturation is 0.8 mole/mole, where the percentage oxirane is 3.84% and the iodine value is 1.3.

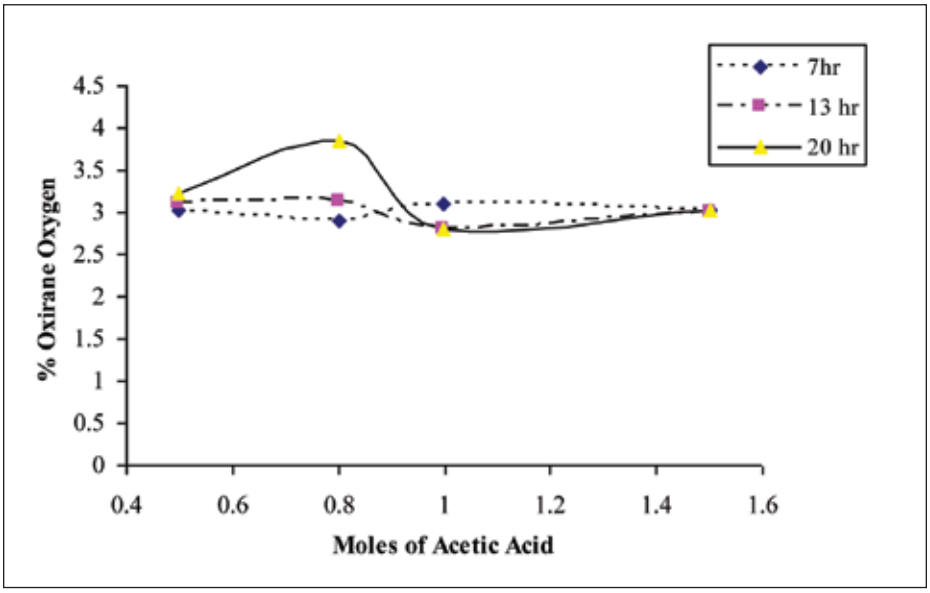


Fig.2: The Effect of Glacial Acetic Acid on the Percentage Oxirane Oxygen Forming an Epoxidized TMPester

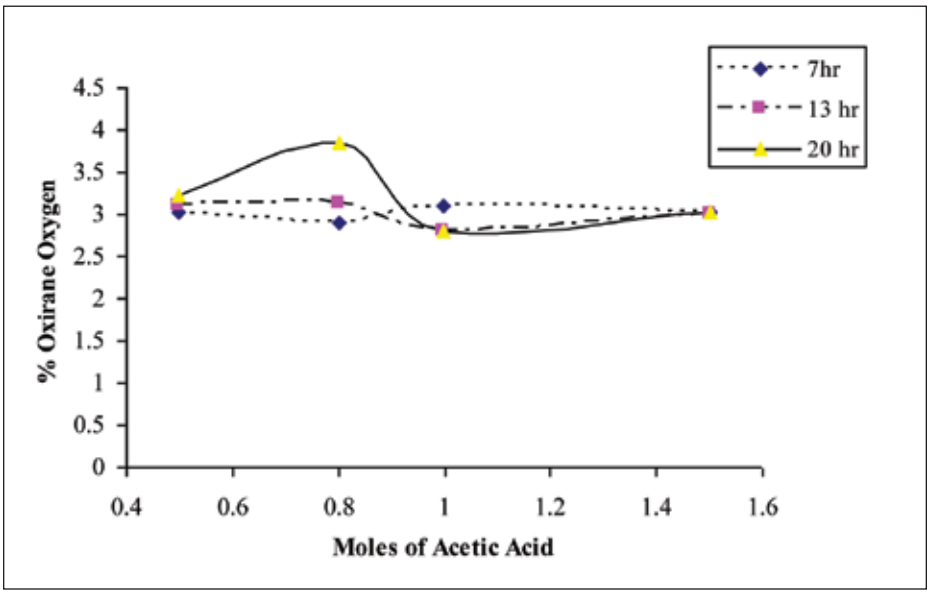


Fig.3: The Effect of Glacial Acetic Acid on the Iodine Value of Epoxidized TMP Esters

### *The Effect of Hydrogen Peroxide on the Ethylenic Unsaturation and Acetic Acid Mole Ratio*

Hydrogen peroxide is the most important source of active oxygen in *in situ* epoxidation and in preformed peracid acid oxidations (Swern, 1971). As a source of oxygen, hydrogen peroxide should be in the stoichiometric quantity based on the number of ethylenic linkage that is present in the product to be epoxidized. In general, a slight excessive amount of hydrogen peroxide is employed (Niederhauser & Koroly, 1949). In this study, the reactions were applied with 3.5, 5, and 7.5 moles of hydrogen peroxide per mole of ethylenic unsaturation, with the aim of investigating the effect of hydrogen peroxide on the conversion of ethylenic unsaturation to oxirane ring. Fig.4 shows that the maximum percentages of oxirane oxygen are at 3.90%, 3.75%, 3.68% and 3.02% which have been obtained using 7.5:1 mole of hydrogen peroxide per mole of ethylenic unsaturation 0.5, 0.8, 1, and 1.5 mole of acetic acid, respectively. However, the minimum iodine value is at 1.75, 1.26, 1.26, and 0.94, which was obtained using 5:1 mole of hydrogen peroxide per mole ethylenic unsaturation to 0.5, 0.8, 1, and 1.5 mole of acetic acid (*see* Fig.5). These experiments show that both the percentages of oxirane oxygen and iodine value are affected by the amount of hydrogen peroxide used in the epoxidation of TMPester.

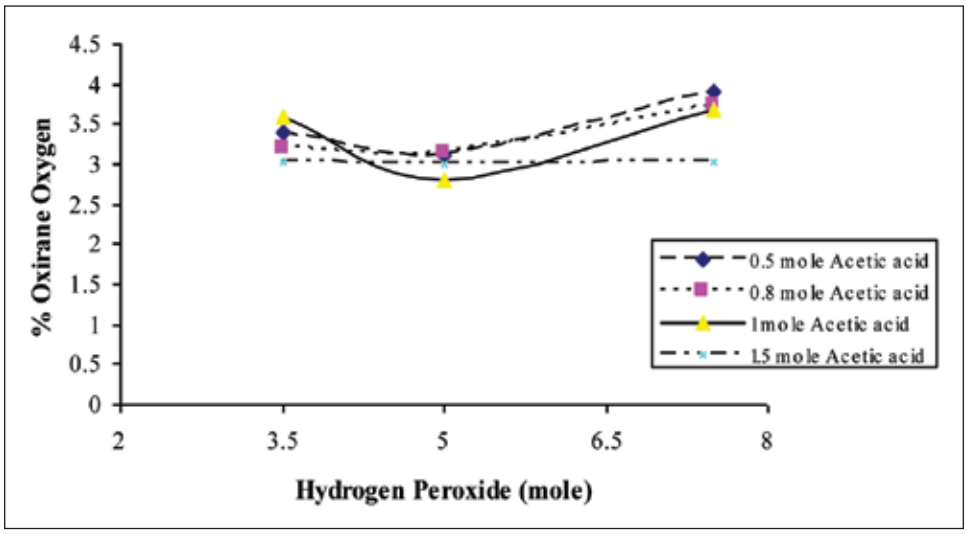


Fig.4: The Effect of Hydrogen Peroxide on the Percentage of Oxirane Oxygen

### *The Effect of Catalyst*

The presence of catalyst in the reaction media is very important to obtain a high conversion of the ethylenic unsaturation in TMP esters to oxirane oxygen. In this study, sulphuric acid was used as a catalyst and the amount was based on the combined weight of acetic acid and aqueous hydrogen peroxide. The effect of catalyst concentration on ethylenic unsaturation TMP ester was studied at various catalyst concentrations of 1%, 2%, 3%, 4%, and 5%. Fig.6 illustrates the effect of sulphuric acid concentration in the epoxidation process to convert ethylenic unsaturation in the TMP esters to oxirane ring.

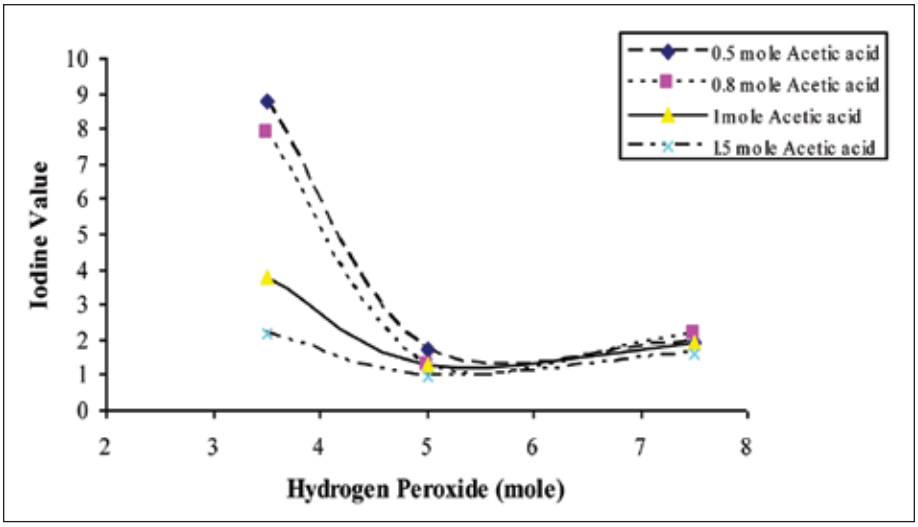


Fig.5: The Effect of Hydrogen Peroxide on Iodine Value

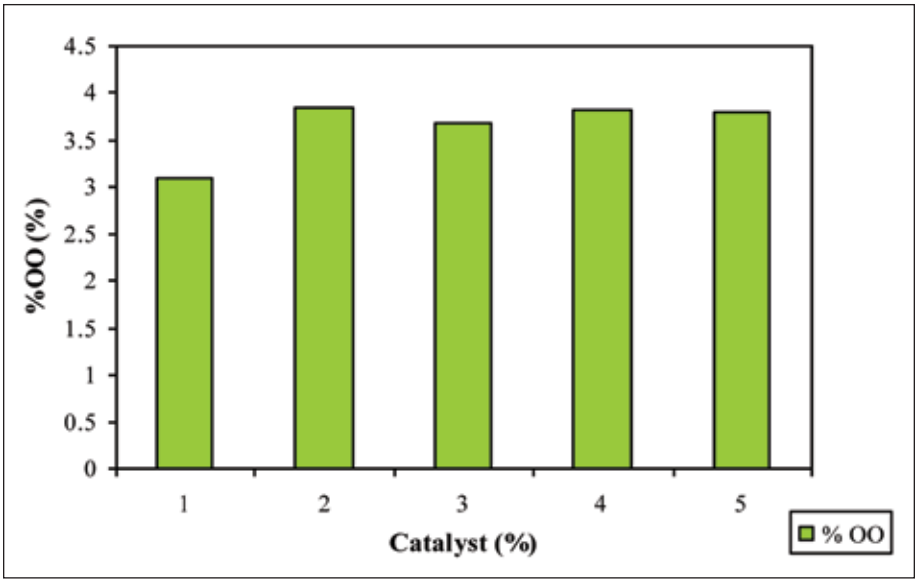


Fig.6: The Effect of Catalyst on Epoxidation Trimrthylolpropane Esters, T= 50°C, 8 Hours, 0.5/ 8/ 1 Ratio of Acetic Acid/ Hydrogen Peroxide/ Ethylenic Unsaturation

The experiment was carried out at 50°C, 8 hours of reaction, and 20% of solvent with 0.5/ 8/ 1 mole ratio of acetic acid/ hydrogen peroxide/ ethylenic unsaturation TMP ester. The optimum oxirane product was achieved at 2% of the catalyst at which the percentage of oxirane oxygen was 3.85%. The maximum percentage of oxirane oxygen that can be obtained from the experiment is 4.02% if 100% ethylenic unsaturated in TMP esters is converted into oxirane oxygen.

## CONCLUSIONS

Based on the results gathered from the experiments on the epoxidized TMP esters, a suitable operation condition for the TMP esters epoxidation reaction was determined. The results show that the maximum yield of percentage oxirane oxygen is 3.9 % with the corresponding iodine value of 1.9, at which as much as 96% of the ethylenic unsaturation converted into oxirane ring. The optimum operation conditions for the epoxidation of TMP esters were 0.5 mole of acetic acid, 7.5 mole of hydrogen peroxide, 2% catalyst, 20% solvent, a temperature of 50$^{o}$C, and 13 hours of reaction time.

## ACKNOWLEDGEMENT

This research was supported by Department of Chemical and Environmental Engineering Faculty of Engineering, Universiti Putra Malaysia and FRGS grant no. 5523430.

## REFERENCES

American Oil Chemists' Society. (1984). Official Methods and Recommended Practices of the American Oil Chemists' Society. Method Cd 9-57.

Campanella, A., & Baltanas, M. A. (2005). Degradation of the Oxirane Ring of Epoxidized Vegetable Oils in Liquid-Liquid Systems: I. Hydrolysis and Attack by $H_2O_2$. *Latin American Applied Research, 35*, 205-210.

Gan, L. H., S. H. Goh, & K. S. Ooi. (1992). Kinetics Study of Epoxidation and Oxirane Cleavage of Palm Olein Methyl Esters. *Journal American Oil Chemical Society, 69*, 347-351.

Goud, V. V., Pradhan, N. C., & Patwardhan, A. V. (2006). Epoxidation of Karanja (*Pongamia glabra*) Oil by $H_2O_2$. *Journal American Oil Chemical Society, 83*(7), 635-640.

Kirk, R. E., & Othmer, D. F. (1984). *Encyclopedia of Chemical Technology* (3rd ed.). 9 Interscience Publisher.

Kodali, D. R. (2002). High Performance Ester Lubricants from Natural Oils. *Industrial lubrication and tribology, 54*, 165-170.

Niederhauser, W. D., & Koroly. J. E. (1949). Process for the Epoxidation of Esters of Oleic and Linoleic Acids. United States Patent No. 2,485,160

Schneider, M. P. (2006). Plant-Oil-Based Lubricants and Hydraulic Fluids. *Journal of the Science of Food and Agriculture*, *86*, 1769-1780.

Swern, D. (1971). *Organic peroxides.* New York,: Wiley-Interscience.

Pertanika J. Sci. & Technol. 20 (2): 339 - 346 (2012)

SCIENCE & TECHNOLOGY

Journal homepage: http://www.pertanika.upm.edu.my/

# Cadmium (Cd) Removal from Aqueous Solution Using Microwave Incinerated Rice Husk Ash (MIRHA)

**Mohamed Hasnain Isa*, Shamsul Rahman Mohamed Kutty, Sri Rahayu Mohd Hussin, Nurhidayati Mat Daud and Amirhossein Malakahmad**

*Civil Engineering Department, Universiti Teknologi PETRONAS, 31750 Tronoh, Perak, Malaysia.*

## ABSTRACT

The presence of heavy metals in aquatic systems has become a serious problem. Heavy metals can have adverse effects on the environment as well as on human health. As a result, much attention has been given to new technologies for removal of heavy metal ions from contaminated waters. In this study, Microwave Incinerated Rice Husk Ash (MIRHA), a locally available agricultural waste, was used for the removal of Cd (as a representative heavy metal) from synthetic wastewater by batch adsorption process. The effects of pH, initial metal concentration, and contact time on Cd removal efficiency were studied. pH 4 was found to be the optimum. The removal efficiency was found to be correlated with the initial metal concentration and contact time between adsorbent and adsorbate. Cd adsorption kinetics followed the pseudo-second-order model and implied chemisorption. The adsorption equilibrium of Cd can be well described by the Freundlich isotherm model.

**Keywords: Adsorption, Cadmium (Cd), kinetic, isotherm, microwave incinerated rice husk ash (MIRHA)**

## INTRODUCTION

Environmental contamination with heavy metals arises mainly as a result of industrial activities, although other sources, such as agriculture and waste disposal, are also contributors. These heavy metals are discharged into the atmosphere, water and land-based environments and may reach high concentrations, mainly near discharge sites. Metals can be distinguished from other toxic pollutants as they are non-biodegradable and cannot be converted to a simpler form than the elemental.

Various treatment techniques have been employed for the removal of heavy metals from water; these include precipitation,

*Article history:*
Received: 13 April 2011
Accepted: 21 April 2011

*Email addresses:*
hasnain_isa@petronas.com.my (Mohamed Hasnain Isa), shamsulrahman@petronas.com.my (Shamsul Rahman Mohamed Kutty), amirhossein@petronas.com.my (Amirhossein Malakahmad)
*Corresponding Author

ISSN: 0128-7680 

adsorption, ion exchange and reverse osmosis (Fu & Wang, 2011). However, most of the techniques were found to be less effective and possess many drawbacks when applied in the field. Moreover, it is very difficult to select an efficient method for heavy metals removal. Some are effective but economically not feasible and vice versa. Some are not user friendly, not technologically sound, are energy dependent, require post-treatment, need skill manpower, etc. Studies on the treatment of heavy metals bearing effluents have revealed adsorption to be a highly effective technique (Chand *et al*., 1994). Research in recent years has focused on the use of some natural biomaterials including agricultural products and by-products for heavy metals removal. This has been a result of the demand for low-cost treatment technology for heavy metal laden wastewaters. Some agricultural materials can be effectively used as low-cost adsorbents and can accumulate high concentration of heavy metals. Meanwhile, modification of agricultural by-products could enhance their natural capacity and improve their efficiency. Adsorbents generated from these biomass are cost effective and efficient (Kumar, 2006). Previous studies have reported successful removal of heavy metals with many agricultural by-products including oil palm fibre, rice husk, maize cobs, and sawdust (Isa *et al*., 2008; Ghani *et al*., 2007; Chuah *et al*., 2005).

Cadmium (Cd) is a toxic and potentially carcinogenic heavy metal from industry (e.g. battery, electroplating and paints). Exposure to its high concentrations can result in respiratory illness (Mugica *et al*., 2002). "Itai-Itai" is a disease that occurred in Japan due to cadmium toxicity. It affected the bones and joints of old women and resulted in a number of deaths. This study explored the possibility of using microwave incinerated rice husk ash (MIRHA) as an adsorbent for the removal of heavy metals such as Cd. Meanwhile, the influences of various factors, such as pH, contact time and initial Cd concentration on adsorption efficiency, were also studied. Adsorption kinetics and isotherm studies were also included.

## MATERIALS AND METHODS

### *Adsorbent*

Rice husk was obtained from BERNAS factory in Kg. Gajah. The husk was thoroughly washed with distilled water to remove dirt and dried at 105 °C for 2 hours until constant weight. Then, it was incinerated at 800 °C for 2 hour in a microwave furnace. Finally, the microwave incinerated rice husk ash (MIRHA) was powdered and stored in desiccators before use. The MIRHA components were determined by X-ray fluorescence (XRF) test. The results obtained are shown in Table 1. MIRHA was found to have high silicon oxide ($SiO_2$) content (75.8%).

### *Adsorbate*

Cd stock solution of 1000 mg/L was prepared from cadmium chloride ($CdCl_2$). Suitable dilutions were made with distilled water to prepare solutions of pre-decided concentrations for the adsorption study. 1N Hydrochloric acid (HCl) and 1.5N sodium hydroxide (NaOH) solutions were used for pH adjustment.

Table 1: MIRHA characteristics

| Item | Percentage | Item | Percentage |
|---|---|---|---|
| O | 45.6 | | |
| Si | 35.4 | SiO2 | 75.8 |
| P | 0.849 | P2O5 | 1.94 |
| K | 7.98 | K2O | 9.62 |
| Ca | 1.66 | CaO | 2.33 |
| Fe | 1.22 | Fe2O3 | 1.75 |
| Re | 3.71 | Re | 3.71 |
| Mg | - | MgO | - |
| Al | - | Al2O3 | - |
| S | - | SO3 | - |
| Cl | - | Cl | - |
| Mn | - | MnO | - |
| Compton | 0.61 | Compton | 0.61 |
| Rayleigh | 1.07 | Rayleigh | 1.07 |
| Norm. | 100 | Norm. | 100 |

*Experimental Procedures*

Batch experiments were conducted by agitating MIRHA in 100 ml synthetic wastewater samples of desired strength and pH at room temperature (27 ± 1 °C) using an orbital shaker operating at 150 rpm. The samples were allowed to settle and filtered through 0.45 µm cellulose acetate membrane filters (Whatman filter) before Cd measurement using an atomic absorption spectrophotometer was carried out. The effect of pH was studied by adjusting the pH (1 to 5) of the test using HCl or NaOH solutions. Two hundred milligram of MIRHA was added into each flask. The flasks were agitated at 150 rpm for 60 minutes on an orbital shaker. The pH was measured using a pH meter. The effect of initial Cd concentration was determined by shaking 100 ml of synthetic wastewater samples of desired concentrations (5, 10, 22, 35, and 50 mg/L) with 200 mg MIRHA at 150 rpm. All samples were adjusted to the optimum pH prior to addition of the adsorbent. The samples were withdrawn from the shaker at pre-determined time intervals (20, 40, 60, 90, 120, 150, 180, 240, and 360 minutes) for analysis.

## RESULTS AND DISCUSSION

*Effect of Initial pH*

pH is an important parameter for adsorption of metal ions from aqueous solution because it affects the solubility of the metal ions, concentration of the counter ions on the functional groups of the adsorbent and the degree of ionization of the adsorbate during reaction (Nomanbhay & Palanisamy, 2005). Fig.1 shows the effect of pH on Cd removal. As pH rises, the percentage of Cd removed increases considerably from 30% at pH 1 to about 70% at initial pH 4 (optimum). Perez-Marin *et al*. (2007) also reported a similar pH effect on Cd removal using orange waste adsorbent, and found enhanced Cd removal at pH 4 to 6. According to Low *et al*. (1995), at low pH values, the surface of the adsorbent would be closely associated with hydronium ions

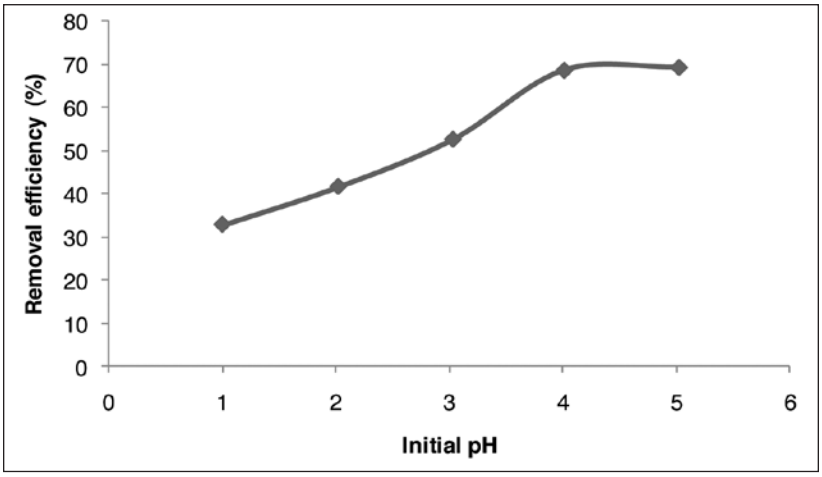


Fig.1: The effect of pH on Cd removal [Cd = 10 mg/L; volume, 100 ml; contact time, 1hr; mixing speed, 150 rpm; temperature 27±1 °C; adsorbent dosage, 2g/L]

($H_3O^+$) which hinders the access of metal ions by repulsive forces to the surface functional groups, and this consequently decreases the percentage of metal removal.

*Effects of Initial Cd Concentration and Contact Time*

Fig.2 shows the effects of initial Cd concentration and agitation time on its removal at pH 4 (as determined above to be the optimum). Cd removal increased with the increase in agitation time due to greater contact between adsorbent and adsorbate; equilibrium was reached in about 4 hours for all the samples (note that lower initial concentrations reached equilibrium sooner).

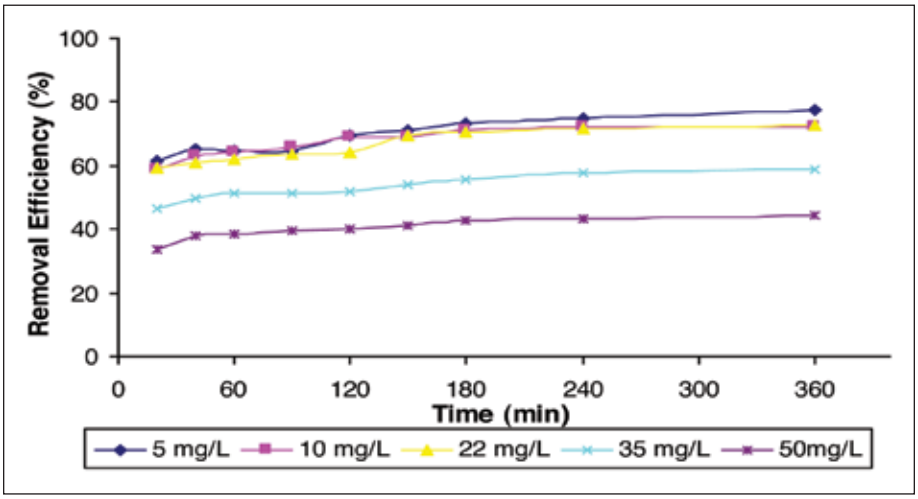


Fig.2: The effects of initial Cd concentration and contact time on Cd removal [pH 4, volume, 100 ml; mixing speed, 150 rpm; temperature 27±1 °C; adsorbent dosage, 2g/L]

This is quicker than the 6 to 7 hours of equilibrium time obtained by Izanloo and Nasseri (2005) using ground pine cone as an adsorbent for Cd removal. It is also seen that the higher the initial Cd concentration of the sample, the lower its percentage removal will be. A simple mass balance, however, shows that the actual amount of Cd removed increases with the increase in the initial Cd concentration. A higher Cd concentration resulted in a higher concentration gradient which accelerated the diffusion of the adsorbate from the solution into the adsorbent.

*Adsorption Kinetics*

Pseudo first- and pseudo second-order kinetic models were studied to determine the adsorption mechanism responsible for Cd removal. The models and their linear forms are as follows (Ho & McKay, 1998; Isa *et al*., 2007):

Pseudo-first order kinetic model,

$$\frac{dq}{dt} = k_1'(q_e - q) \tag{1}$$

$$\log(q_e - q) = \log q_e - \frac{k_1'}{2.303}t \tag{2}$$

Pseudo second-order kinetic model,

$$\frac{dq}{dt} = k_2'(q_e - q)^2 \tag{3}$$

$$\frac{t}{q} = \frac{1}{k_2' q_e^2} + \frac{t}{q_e} \tag{4}$$

where,

$q_e$ = the amount of solute adsorbed at equilibrium per unit weight of adsorbent (mg/g)

q = the amount of solute adsorbed at time t per unit weight of adsorbent (mg/g)

$k'_1$ and $k'_2$ = constants

Fig.3 and Fig.4 show the linear plots of the pseudo first- and pseudo second-order models, respectively. The values of the model constants calculated from these plots are shown in Tables 2 and 3. High the $R^2$ values (> 0.99) obtained show that Cd removal follows the pseudo second-order kinetic model; implying chemisorption between the adsorbent and adsorbate. Izanloo and Nasseri (2005) also found the pseudo second-order kinetic model to be suitable for describing Cd removal.

*Adsorption Isotherms*

Adsorption isotherms are important in the modelling procedure for the analysis and design of an adsorption system. Therefore, to correlate the isotherm with the adsorption of Cd, the sorption data were tested against the most commonly used isotherm models, namely, the Langmuir and Freundlich equations.

The Langmuir equation, derived based on the equilibrium between condensation and

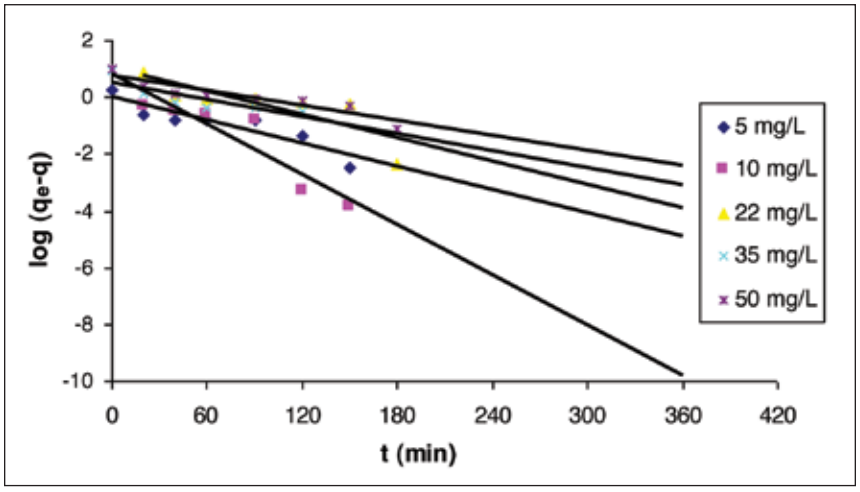


Fig.3: Pseudo first-order kinetic plot for Cd adsorption at different initial concentrations [pH 4; volume, 100 ml; mixing speed, 150 rpm; temperature 27±1 °C; adsorbent dosage, 2g/L]

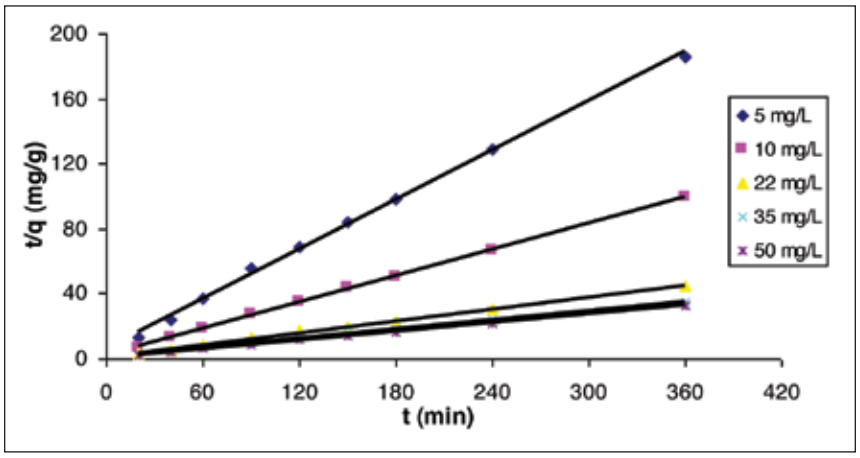


Fig.4: Pseudo second-order kinetic plot for Cd adsorption at different initial concentrations [pH 4; volume, 100 ml; mixing speed, 150 rpm; temperature 27±1 °C; adsorbent dosage, 2g/L]

Table 2: Pseudo first-order reaction rate constant for Cd adsorption

| Cd Concentration (mg/L) | $k'_1$ ($min^{-1}$) | $R^2$ | Equation |
|---|---|---|---|
| 5 | 0.0316 | 0.8242 | y = -0.0137x + 0.0008 |
| 10 | 0.0656 | 0.88 | y = -0.0285x + 0.7032 |
| 22 | 0.0318 | 0.6663 | y = -0.0138x + 1.0255 |
| 35 | 0.0230 | 0.6925 | y = -0.01x + 0.5107 |
| 50 | 0.0200 | 0.8356 | y = -0.0087x + 0.7281 |

Table 3: Pseudo second-order reaction rate constant for Cd adsorption

| Cd Concentration (mg/L) | $k'_2$ (min$^{-1}$) | $R^2$ | Equation |
|---|---|---|---|
| 5 | 0.0389 | 0.9981 | y = 0.5063x + 6.5858 |
| 10 | 0.0334 | 0.9997 | y = 0.2704x + 2.1862 |
| 22 | 0.0109 | 0.9985 | y = 0.122x + 1.3708 |
| 35 | 0.0075 | 0.9979 | y = 0.0946x + 1.1969 |
| 50 | 0.0028 | 0.9958 | y = 0.0896x + 2.9193 |

Table 4: Isotherm constants and correlation coefficients

| Langmuir isotherm coefficients | | | Freundlich isotherm coefficients | | |
|---|---|---|---|---|---|
| a | b | $R^2$ | $K_f$ | n | $R^2$ |
| 15.48 | 2.94 | 0.3267 | 1.08 | 1.29 | 0.7951 |

evaporation of adsorbed molecules, considers a monomolecular adsorption layer (Isa *et al*., 2008) and is represented as:

$$\frac{x}{m} = \frac{abC_e}{1 + bC_e} \tag{5}$$

where,
x/m = amount of adsorbate adsorbed per unit mass of adsorbent (mg/g)
$C_e$= equilibrium concentration of adsorbate in solution after adsorption (mg/L)
n, a and b are constants

Equation 6 shows the straight line form of the Langmuir model.

$$\left(\frac{C_e}{x/m}\right) = \frac{1}{ab} + \frac{1}{a}C_e \tag{6}$$

Meanwhile, Freundlich isotherm model and its straight line forms are given below:

$$\frac{x}{m} = K_f C_e^{1/n} \tag{7}$$

$$\log\left(\frac{x}{m}\right) = \log K_f + \frac{1}{n}\log C_e \tag{8}$$

where $K_f$ is a constant.

The Langmuir and Freundlich isotherm constants (obtained graphically) for Cd are shown in Table 4. A higher $R^2$ value obtained with Freundlich isotherm shows that the adsorption of Cd is better fitted with the Freundlich rather than Langmuir model. The maximum adsorption capacity for Cd was 15.48 mg/g. Mahvi *et al*. (2007) also obtained higher $R^2$ values for Freundlich isotherm when removing Cd.

## CONCLUSIONS

The present study showed that MIRHA was capable of removing Cd from aqueous solution. The adsorption of Cd on MIRHA is pH dependent, and with the optimum pH being 4. Meanwhile, the equilibrium time was adopted as 4 h though it varied with the initial concentration of the adsorbate. The adsorption kinetics of Cd followed the pseudo second-order model and implied chemisorption. The adsorption equilibrium of Cd can be well described by Freundlich isotherm model.

## REFERENCES

Chand, S., Aggarwal V. K., & Kumar P. (1994) Removal of hexavalent chromium from the wastewater by Adsorption. Indian J Environ. *Health, 36*(3), 151-158.

Chuah, T. G., Jumasiah, A., Azni, I., Katayon, S., & Thomas Choong, S. Y. (2005) Rice husk as a potentially low-cost biosorbent for heavy metal and dye removal. *Desalination, 175*(3), 305-316.

Fu, F., & Wang, Q. (2011) Removal of heavy metal ions from wastewaters: A review. *Journal of Environmental Management, 92*(3), 407-418.

Ghani, N. T. A., Hefny, M., & El-Chaghaby, G. A. F. (2007) Removal of lead from aqueous solution using low cost abundantly available adsorbents. *Int. J. Environ. Sci. Tech., 4*(1), 67-73.

Ho, Y. S., & McKay, G. (1998) Sorption of dye from aqueous solution by peat. *Chemical Engineering Journal*, *70*, 115–124.

Isa, M. H., Ibrahim, N., Aziz, H. A., Adlan, M. N., Sabiani, N. H. M., Zinatizadeh, A. A. L., & Kutty, S. R. M. (2008) Removal of chromium (VI) from aqueous solution using treated oil palm fibre. *Journal of Hazardous Materials, 152*, 662-668.

Isa, M. H., Lee, S. L., Asaari, F. A. H., Aziz, H. A., Ramli, N. A., & Dhas, J. P. A. (2007) Low cost removal of disperse dyes from aqueous solution using palm ash. *Dyes and Pigments, 74*(2), 446-453.

Izanloo, H., & Nasseri, S. (2005) Cadmium removal from aqueous solutions by ground pine cone. *Iranian J. Env. Health Sci. Eng., 2*(1), 33-42.

Kumar, U. (2006) Agricultural products and by-products as a low cost adsorbent for heavy metal removal from water and wastewater. *Scientific Research and Essay, 1*(2), 33-37.

Low, K. S., Lee, C. K., & Leo, A. C. (1995) Removal of metals from electroplating wastes using banana pith. *Bioresource Technology, 51*, 227-231.

Mahvi, A. H., Nouri, J., Omrani, G. A., & Gholami, F. (2007). Application of platanusorientalis leaves in removal of cadmium from aqueous solution. *World Applied Sciences Journal, 2*(1), 40-44.

Mugica, V., Maubert, M., Torres, M., Munoz, J., & Rico, E. (2002). Temporal and spatial variations of metal content in TSP and PM10 in Mexico City during 1996–1998. *Journal of Aerosol Science*, 33, 91–102.

Nomanbhay, S. M., & Palanisamy, K. (2005) Removal of heavy metal from industrial wastewater using chitosan coated oil palm shell charcoal. *Electronic Journal of Biotechnology, 8*(1), 43-53.

Perez-Marın, A. B., Zapata, V. M., Ortuno, J. F., Aguilar, M., Saez, J., & Llorens, M. (2007) Removal of cadmium from aqueous solutions by adsorption onto orange waste. *Journal of Hazardous Materials, B139,* 122–131.

Pertanika J. Sci. & Technol. 20 (2): 347 - 353 (2012)

SCIENCE & TECHNOLOGY

Journal homepage: http://www.pertanika.upm.edu.my/

# Pressure Reduction on Blood Flow in Aorta Coronary Sinus Conduit

**Siti Aslina Hussain[1*], Tan Hong Tat[1], Mohd Ismail Abdul Hamid[2], Norhafizah Abdullah[1] and Azni Idris[1]**

*[1]Department of Chemical and Environmental Engineering, Faculty of Engineering, Universiti Putra Malaysia, 43400 Serdang, Selangor, Malaysia*

*[2]Middlesex Hospital, London*

## ABSTRACT

Numerical studies of blood flow system of aorta coronary sinus conduit were carried out using ANSYS™ CFD simulation. A different model of conduit, which differs in the inlet diameter, was investigated. The investigated inlet diameters are 3 mm, 4 mm and 5 mm. Pressure drop from 80 mmHg to 15 mmHg was achieved for all the models. The comparison chart was produced to compare the pattern of pressure reduction as well as velocity distribution in each model. From the analysis of coronary sinus conduit, it was found that a narrow tube needs to be incorporated into the conduit produced. This is to induce a venturi effect to reduce the pressure drop of blood within a specific throat length. As conclusion, a model of 3 mm inlet and a throat diameter of 1.13 mm show satisfactory result for pressure reduction from 80 mmHg to 15 mmHg. This particular model also has a lower peak velocity at the inlet zone of the throat section, which is more preferable in terms of Reynolds number.

**Keywords: Aorta coronary sinus conduit, blood flow, computational fluid dynamics, simulation, velocity**

*Article history:*
Received: 12 April 2011
Accepted: 21 April 2011

*Email addresses:*
aslina@eng.upm.edu.my (Siti Aslina Hussain),
fizah@eng.upm.edu.my (Norhafizah Abdullah),
azni@eng.upm.edu.my (Azni Idris)
*Corresponding Author

## INTRODUCTION

Fluid plays an important task in our daily life. The main fluid in human body is called blood. This particular fluid plays an important role in the human body as an oxygen delivery medium as well as a heat transfer agent. The oxygen that the blood carries is supplied to the muscles or cells in the body in order for it to function properly.

ISSN: 0128-7608 

Each year, over a million people in the U.S. have a heart attack (World Health Organization, 2007). This symptom is also known as Acute Myocardial Infarction in the medical term. It is a medical condition that occurs when the blood supply to a part of the heart's muscles is interrupted. The result of ischemia or oxygen shortage will lead to damage and potential death of heart tissue. A classical treatment to heart attack is usually done by undergoing a bypass surgery, whereby the bypass grafts are frequently harvested from internal thoracic arteries, radial arteries or saphenous veins (Lee, 2006).

Nonetheless, the artificial conduits used in bypass surgery are subjected to analysis. The prime focus is particularly on the coronary sinus conduit. Coronary sinus is a collection of veins joined together to form a large vessel that collects blood from the myocardium of the heart. This sinus receives most of the venous blood from the heart and empties into the right atrium. It is located between the left atrium and ventricle on the posterior surface of the heart. It runs transversely in the groove between the left atrium and ventricle on the posterior surface of the heart (Syoten, 1980). An illustration of the exact location of the coronary sinus is shown in Fig.1.

A simulation was carried out in order to simulate the blood flow condition in the aorta coronary sinus. The main interest of the simulation was to observe the pressure distribution in the conduits, as well as the flow pattern. It is preferable to obtain a pressure drop from 80 mmHg at the inlet of the conduits to 15 mmHg at the outlet of the conduits. Besides that, the flow pattern must be laminar according to the specification.

## MATERIALS AND METHODS

Computational fluid dynamics (CFD) technique was chosen in the simulation of blood flow. It is important to note that computational fluid dynamics is one of the branches of fluid mechanics

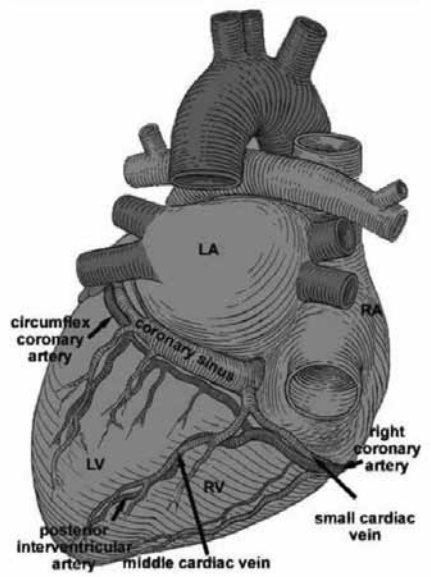


Fig.1: A posterior view of the heart

that uses numerical methods and algorithms to solve and analyze problems that involve fluid flows. Computers are used to perform the millions of calculations required to simulate the interaction of fluids with the complex surfaces used in engineering (Cengel & Cimbala, 2010).

The computational fluid dynamics software used in the simulation of blood flow in the aorta coronary sinus is ANSYS™ CFX. This software used finite element method in the analysis of the flow model. The delivery of the results of the analysis is by numerical method. The fundamental equation lies behind this software is the Navier-Stokes equations.

The purpose of using CFD to simulate the blood flow in the artificial coronary sinus model is because it helps to reduce the time and effort needed to run a real experiment which may not be cost effective. In addition, the actual size of the model will be too difficult to be analyzed directly using the present equipment. Moreover, certain part of the model is too narrow to be physically tested with the normal pressure devices and flow devices. In contrast, several variables and data can be extracted from the result using computational modelling. If there is any amendment to the physical model, the analysis process can be repeated quickly to reflect the result.

The project was carried out in 3 basic phases, namely pre-modelling, modelling and simulation. All the models produced will undergo these 3 phases and their outcome will be summarized. In the process of producing the simulation, the model will undergo each section of the programme in ANSYS™ CFD, such as Design Modeller, Meshing, Pre-Processing, Solver and Post-Processing. In pre-modelling, the dimension and specification of the model were determined. The minimum diameter of a tube was determined for a given pressure drop, length of tube, viscosity of fluid and volumetric flow rate of the fluid. In modelling, the 3-dimensional tube model was created with the ANSYS™ Design Modeller (DM). After the solid model of the flow domain has been created, the next stage is to process the solid flow domain in the ANSYS™ Meshing. In this stage, the domain is divided into small cells. Meshing is an essential processing stage as it provides a surface representation for a complex geometry with a few basic geometry primitives. During the meshing stage, the physical domain of the fluid flow is split into pieces of smaller 3D domains. The smaller domains are termed as sub-domains composing of the elements of simplices such as tetrahedrons. The model that has been meshed will be brought into the processing stage for further analysis. The whole process in this stage is under ANSYS™ Advance CFD. The inlet, outlet and wall condition for the model are specified in detailed. Then, the result is obtained from the conditions specified, and illustrated in a comprehensible graphical manner. The processing stage comprises of pre-processing stage, solver stage and post-processing stage.

The flow chart of the simulation of the coronary sinus conduit is shown in Fig.2. It comprises of a step-by-step procedure that is needed to generate the simulation. Meanwhile, the parameters of the CFD simulation for the models are summarized in Table 1.

## RESULTS AND DISCUSSION

From all the results of the 3 models obtained, an overall analysis was been made. The graphs of the 3 models were combined to see their difference. For the pressure distribution comparison, the graph in Fig.3 was produced.

Table 1: Details of the models constructed

| Parameter | Model 1 | Model 2 | Model 3 |
|---|---|---|---|
| Fluid properties | | | |
| Equation | Power Law for Non-Newtonian Viscosity of Blood [5] $\eta = k\gamma^{n-1}e^{\circ T/T}$ | | |
| Power Law Index, n | 0.4851 | 0.4851 | 0.4851 |
| Consistency index, k ($kg.s^{n-2}/m$) | 0.2073 | 0.2073 | 0.2073 |
| Reference temperature (°T) | 37 | 37 | 37 |
| Maximum viscosity limit, $\mu_{max}$ (kg/m.s) | 0.00125 | 0.00125 | 0.00125 |
| Minimum viscosity limit, $\mu_{min}$ (kg/m.s) | 0.003 | 0.003 | 0.003 |
| Reference pressure (atm) | 1 | 1 | 1 |
| Fluid temperature (T) | 37 | 37 | 37 |
| Turbulance | Laminar | Laminar | Laminar |
| Density ($kg.m^{-3}$) | 1050 | 1050 | 1050 |
| Model properties | | | |
| Minor diameter, $D_n$ (mm) | 3 | 4 | 5 |
| Major diameter, $D_m$ (mm) | 15 | 15 | 15 |
| Tube length, *l* (cm) | 11 | 11 | 11 |
| Bending degree, α (°) | 30 | 30 | 30 |
| Part number, N | 10 | 10 | 10 |
| Throat diameter, $D_T$ (mm) | 1.13 | 1.15 | 1.17 |
| Throat length, $l_T$ (cm) | 4 | 4 | 4 |
| Mesh properties | | | |
| Total number of nodes | 77704 | 77926 | 78297 |
| Total number of tetrahedra | 415245 | 416515 | 418579 |
| Total number of elements | 415245 | 416515 | 418579 |
| Maximum spacing (mm) | 0.5 | 0.5 | 0.5 |
| Angle resolution (degree) | 30 | 30 | 30 |
| Minimum Edge Length (mm) | 0.01 | 0.01 | 0.01 |
| Maximum Edge Length (mm) | 0.8 | 0.8 | 0.8 |
| Simulation properties | | | |
| Inlet | | | |
| Mass flow rate ($kg.s^{-1}$) | - | - | - |
| Pressure (mmHg) | 80 | 80 | 80 |
| Outlet | | | |
| Mass flow rate ($kg.s^{-1}$) | 0.004375 | 0.004375 | 0.004375 |
| Pressure (mmHg) | - | - | - |
| Wall | Free Slip | Free Slip | Free Slip |
| No. Iteration | 100 | 100 | 100 |

Through analytical analysis, Model 1 seems to be smoother than the other models. This proves that Model 1 experiences a steady decrease in pressure along the throat section. In addition, Model 1 gives an outlet pressure of 15 mmHg, which is most in accordance to the specification. Models 2 and Model 3 show a steep drop at the conduit length between 0.095 m to 0.085 m, which is not favorable due to the sudden contraction at the throat entrance zone.

Hence, details of model 1 will be discussed further. Based on the information illustrated in Fig.4, it is noticed that the entrance fluid pressure is about 80 mmHg. The pressure of fluid then decreases along the throat and the maximum reduction of the pressure can be observed to

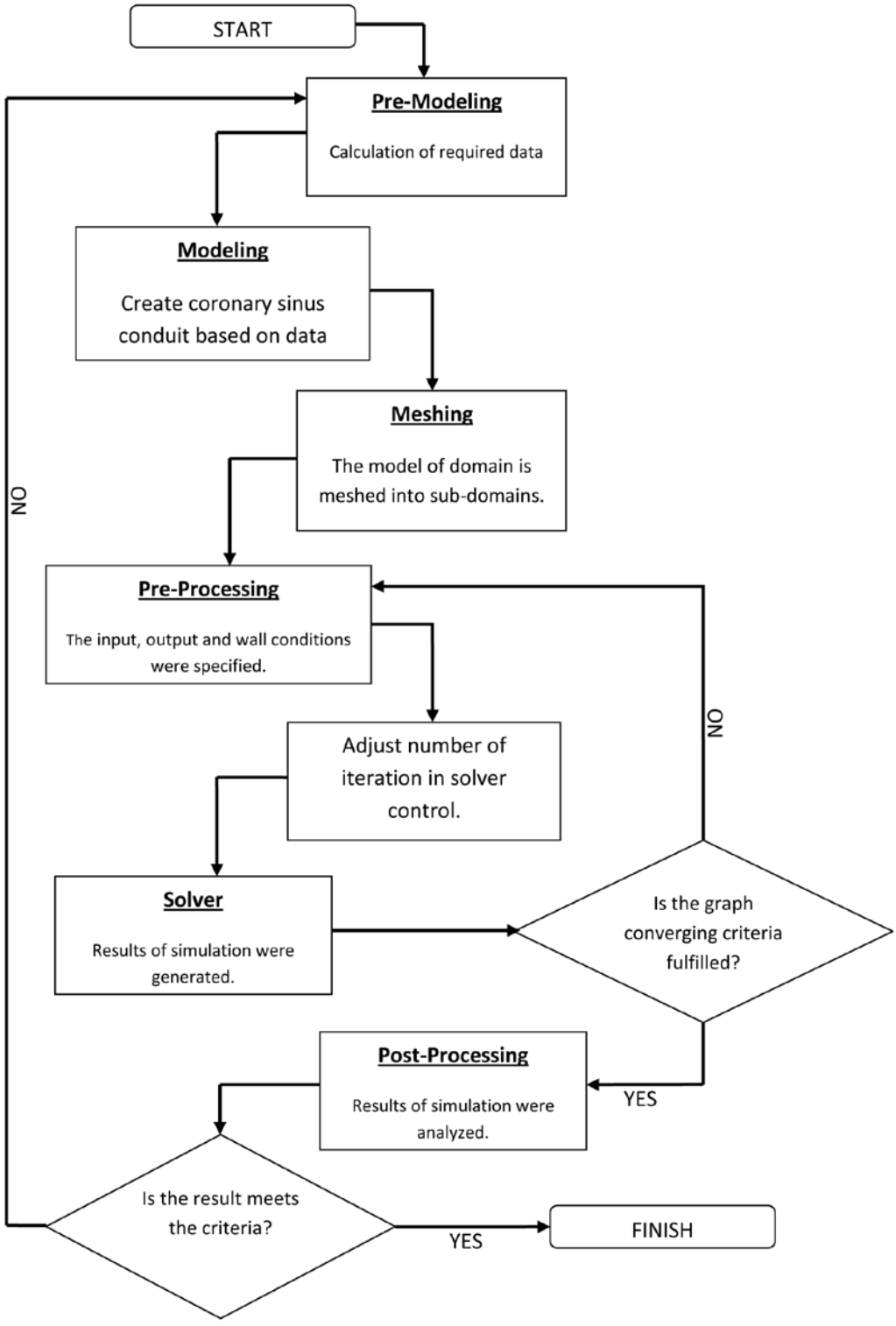


Fig.2: A flow chart of the simulation procedures using ANSYS™ CFX

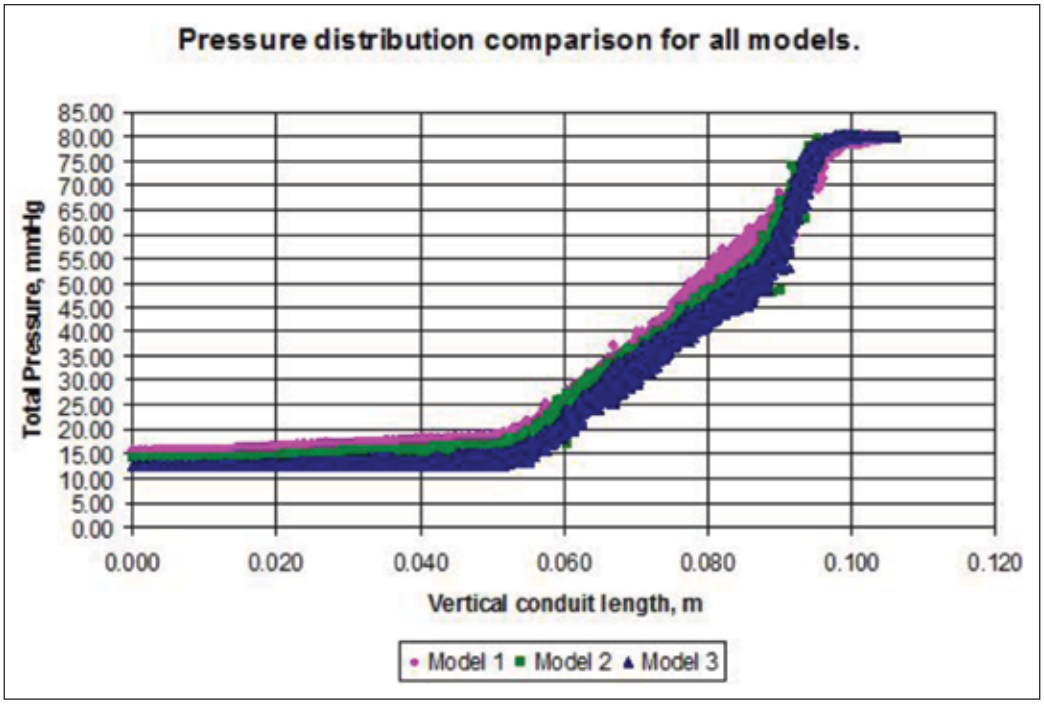


Fig.3: Pressure distribution comparison for all the models

happen at the inlet section of the throat. Towards the outlet of the throat, the pressure of the fluid increases back to a pressure of about 15 mmHg. This is due to the venturi effect, but it is to note that the conduit is not straight and the diameters of the inlet and outlet of the conduit are not uniform. A throat diameter of 1.13 mm can assure that it will not block the flow of blood. The maximum size of a red blood cell is about 8μm; by doing a simple calculation, a diameter of 1.13 mm can actually allow about 141 red blood cells to flow parallel in the throat section.

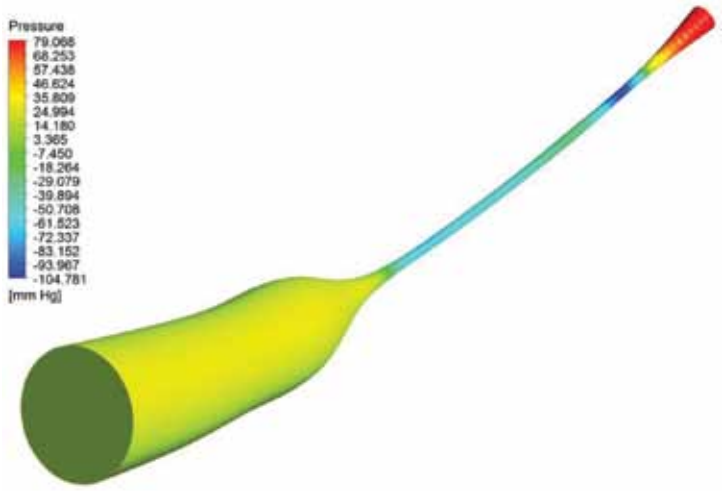


Fig.4: A contour plot on the external of conduit in Model 1

## CONCLUSIONS

As a conclusion, Model 1 was found to be the best model. This is due to the characteristic of its stable pressure reduction along the throat and low peak velocity. In addition, Model 1 also provides a more uniform outlet pressure of 15 mmHg, which is in accordance with the required specification.

The objective of the current study was to investigate the pressure distribution of coronary sinus from the inlet pressure of 80 mmHg to the outlet pressure of 15 mmHg. With the utilization concept of the throat in the design, all the models successfully reduce the pressure from 80 mmHg at the inlet to merely 15 mmHg at the outlet. This pressure reduction effective zone is mainly on the throat section. It is crucial to note that this section was specifically designed to undergone venturi effect on the fluid flow passing through it. However, Model 1 with a 3mm inlet diameter and a 1.13 mm throat diameter was chosen as the best model because of the uniformity of the pressure reduced along the throat section.

Generally, the models provide a more flexible solution for blood flow in coronary sinus conduit. This is because in reality, the veins will undergo certain degree of contraction to push the fluid to move forward. In order to mimic this particular effect of contraction, the throat section was incorporated into the conduit.

## ACKNOWLEDGEMENTS

First and foremost, the authors would like to express their deepest gratitude, appreciation and support to all the research team members, and also to En. Ismail A. Hamid, FRCS, for his advice and knowledge related to this project. This research filed for its patent by Innovation & Commercialisation Centre of Universiti Putra Malaysia on 16 November 2009, with the application number, PI20097028.

## REFERENCES

Cengel, Y. A., & Cimbala J. M. (2007). *Fluid Mechanics: Fundamentals and Applications.* New York: McGraw-Hill Companies, Inc.

Lee, W. (2006). *Biofluid Mechanics in Cardiovascular Systems*. United States of America: McGraw-Hill Companies, Inc.

Petkova, S., Hossain, A., Naser, J., & Palombo, E. (2003). *CFD Modeling Of Blood in Portal Vein Hypertension with And without Thrombosis*. 3rd International Conference on CFD in the Minerals and Process Industries. Australia.

Syoten, O. (1980). Cardiovascular Hemorheology. Cambridge University Press. United Kingdom.World Health Organization - The world health report, 2007. Retrieved on January 27, 2010 from *www.who.int/whr/2007/whr07_en.pdf*.

Pertanika J. Sci. & Technol. 20 (2): 355 - 369 (2012)

SCIENCE & TECHNOLOGY

Journal homepage: http://www.pertanika.upm.edu.my/

# A New Heuristic Method to Solve Straight Assembly Line Balancing Problem

**Mohd Khairol Anuar Mohd Ariffin, Masood Fathi* and Napsiah Ismail**

*Department of Mechanical and Manufacturing Engineering, Faculty of Engineering, Universiti Putra Malaysia, 43400 Serdang, Selangor, Malaysia*

## ABSTRACT

Assembly line balancing is well-known in mass production system but this problem is non-deterministic polynomial-time(NP)-hard, even for a simple straight line. Although several heuristic methods have been introduced and used by researchers, knowing and using an effective method in solving these types of problems in less computational time have a considerable place in the area of line balancing problem. In this research, a new heuristic approach, known as critical node method (CNM), was introduced and tested by solving several test problems available in the literature so as to solve straight assembly lines. Finally, the obtained results are compared with 9 other heuristic rules in some performance measures. Thus, it is concluded that the proposed CNM is better than the rest in all the measures.

**Keywords: Assembly line balancing, heuristic, critical node method, straight line**

## INTRODUCTION

An assembly line consists of several workstations which are generally arranged along a material-handling system, specifically conveyor belt in which parts sequentially move along the line from station to station. A particular amount of assembly works are done in each workstation and the products are completed as they reach the end of the assembly line. Nowadays, most of the industries that are dealing with mass production system have been using a type of assembly lines due to the high-volume production, and complexity of products. Though, assembly line balancing problem has been under study for 50 years and a number of studies on different types of assembly line balancing problems are done based on the fact that the line balancing problem falls into non-deterministic polynomial-time (NP)-hard category (Gutjahr & Nemhauser, 1964; Ajenblit & Wainwright, 1998), exact methods

*Article history:*
Received: 12 April 2011
Accepted: 21 April 2011

*Email addresses:*
khairol@eng.upm.edu.my (Mohd Khairol Anuar Mohd Ariffin),
fathi.masood@gmail.com (Masood Fathi),
napsiah@eng.upm.edu.my (Napsiah Ismail)
*Corresponding Author

ISSN: 0128-7680 

such as integer programming, dynamic programming cannot be used effectually to balance the assembly line problems. Thus, finding a new effective method is necessary.

According to the classification proposed by Ghosh and Gagnon (1989), different types of assembly line balancing problems were grouped into different categories, namely, Single and Multi/Mixed Model Deterministic, and Single and Multi/Mixed Model Stochastic. Most research carried out on assembly line is related to the Single Model Deterministic category, where the cycle time is deterministic and the aim is the optimization of efficiency. It consists of two assembly line balancing forms; one of the two is the original and the simplest type of the assembly line balancing problem known as the simple assembly line balancing (SALB) and the other is the added restriction or factors (e.g. parallel stations, zoning restrictions) which become the General Assembly Line Balancing Problem (GALB). In addition, it should be noted that SALBP can be categorized into two main parts (SALBP-1 and SALBP-2) so that their main objective can be considered as minimizing the number of workstations while cycle time is constant and minimizing the cycle time for a given number of workstations, respectively. Moreover, the other types of simple assembly line balancing belong to the GALB problems.

Balancing the assembly line needs some constraints, as follows:

- Precedence constraint should be satisfied.
- The cycle time is greater than or equal to the time of any work element.
- The workstation time should not exceed the cycle time.

Recently, one of the most important SALBP subdivisions, i.e. SALBP-1, has been studied precisely by many researchers (Bautista & Pereira, 2009). Consequently, as in the previous research by Scholl & Becker (2006), the present study focused on SALBP-1. Although several exact and heuristic approaches in the area of SALBP have been introduced by the researchers and a comprehensive survey can be found in Erel and Sarin (1998) and Scholl and Becker (2006), a number of methods have been suggested and developed by the researchers in the recent decades to find the optimum methods to overcome the complexity of assembly line balancing problem (ALBP). According to Rekiek and Delchambre (2005), all the available methods used in solving line balancing problems can be divided into two main categories, namely, the exact and approximated methods. In addition, in the case of SALBP-1, dynamic programming has been used to determine lower bounds on the number of workstations using the exact approaches several methods such as integer programming, branch and bound, and dynamic programming have been vastly applied to date. According to Baybars (1986) and Scholl and Klein (1999), however, most effective techniques are based on the Dynamic Programming (DP) as well as Branch and Bound (B&B) methods.

Furthermore, Rekiek and Delchambre (2005) state that the approximated methods are divided into two main groups, namely, the heuristic and metaheuristic methods. One of the first proposed heuristics used to solve assembly line balancing problems was the Ranked Positional Weight or RPW (Helgeson *et al*., 1961), but the rules may sometimes be mistakenly utilised as Kilbridge and Wester's heuristic (1996), Moodie and Young's (1965) method and so on. Additionally, Metaheuristics includes several methods, such as Ant Colony Optimization, Tabu search, Genetic Algorithms and simulated annealing, which are used to solve different line

balancing problems like straight and U-shaped line (Hwang *et al*., 2008; Baykasoglu, 2006), two-sided (Özcan & Toklu, 2008), etc.

Since assembly line balancing problems are categorized as NP-hard problems, all the proposed computational methods face difficulties when solving large size problems. Therefore, the heuristic and metaheuristic methods are applied to overcome the difficulties and to obtain the optimal or near the optimal solution in a reasonable amount of time. Furthermore, Scholl and Becker (2006) asserted that most of effective procedures have been proposed in the area of simple assembly line balancing type-1 (SALBP-1) are based on the priority heuristic rules. Recently, several articles have been published on the metaheuristic methods so they are using priority heuristic rules as a foundation (Fathi *et al*., 2010). For example, Sabuncuoglu *et al*. (2000) and Ponnambalam *et al*. (2000) developed the genetic algorithm-based heuristic for SALBP. Meanwhile, Baykasoglo (2006) introduced a simulated annealing (SA) algorithm using several heuristic rules to solve U-shape and straight line.

## METHODOLOGY OF THE PROPOSED HEURISTIC METHOD

Since using the heuristic method has a significant rule to solve assembly line balancing problems, research on this particular method is a hot topic for researchers. More recently, Yeh and Kao (2009) proposed a new heuristic method based on the Critical Path Method (CPM) for solving bidirectional assembly line balancing problem. In this study, a more effective heuristic method called the Critical Node Method (CNM) was introduced based on combining the main concepts of the assembly line balancing problem and project management issues. The main concept of the proposed CNM is based on the well-known rank positional weight (RPW) technique introduced by Helgeson and Birnie (1961) and the proposed method based on CPM by Yeh and Kao (2009).

According to the RPW technique, the task that needs to be assigned is the one that has followers' largest total time. In the RPW, the task with the highest positional weight is selected and assigned to the earlier station. Meanwhile, the weight of each task is computed by summing all the followers' time and each task has its own weight, the tasks with greater weight have more priority to be assigned to the appropriate workstation with respect to all constraints, such as precedence relationship. Moreover, the CPM is a technique used for managing and scheduling the projects during the implementation and it can be defined as the longest path (according to the time duration) from the first (the source) node to the last (the sink) node. In this method, the CPM calculates the longest path of the planned activities to the end of the project, and it computes the earliest and the latest time of every single task that can start and finish without making the project longer. In accordance with the above mentioned explanation about CPM and RPW, the proposed CNM computes the task weight, as follows:

The sequence of the tasks makes the critical path to start with the first task in the project and follows through to the last task in the project. In the first step, CPM is applied to compute the critical path for the assembly network. In this process, the algorithm starts from the first task of the critical path by summing all the critical tasks time to calculate the weight for the considered task. In the next step, the most critical task with the highest weight is removed from the assembly network and a new computation to determine the current critical path is done

using the same procedure. This process is continued until all the tasks have gained their own weights. The tasks are assigned in a descending order of the weight in which as it satisfies the precedence relationship and does not exceed the station's remaining cycle time. Using this particular point of view, the critical nodes also play a pivotal role in assembly line balancing whereby any impediment in assigning the critical nodes may conduce to increase the number of the workstations which are directly associated with higher labour cost and inefficient human resource management.

The proposed CNM can be used to solve almost all types of assembly line problems such as straight and U shaped lines. However, the current study focused on solving the straight assembly line balancing problem. In this method, another criterion is introduced and used instead of the cycle time named OCT.

The parameters used in the proposed method as well as the calculation of introduced OTC are as follows:

| | |
|---|---|
| $T(s_i)$ | total time of each station |
| T(x) | time of each task |
| CT | cycle time |
| N | number of workstation |
| SCT | smallest feasible cycle time |
| $S_t$ | set of all tasks |
| $S_a$ | set of assigned tasks |
| $S_u$ | set of unassigned tasks |
| MS | minimum number of stations |
| OCT | optimum cycle time |

The new introduced cycle time is calculated as bellow:

$$MS = \sum_{i=0}^{n} T(x_i)/CT \quad \text{If MS is not an integer, it will then be rounded up.} \tag{1}$$

$$\text{SCT} = \sum_{i=0}^{n} T(x_i)/\text{MS} \tag{2}$$

$$\text{OCT} = [(\text{SCT} + \text{CT})/2] \tag{3}$$

Note that OCT is selected between SCT and CT. Although CT can be replaced by each value between CT and SCT, based on the researchers' experience, OCT will offer better results. To obtain the desired conditions, the following equations should be maintained in the solving process:

$$\text{T}(s_i) = \sum_{X \in S_i} T(x) \leq \text{CT} \qquad \text{i} = 1, ..., M \tag{4}$$

$$\text{If } (x,y) \in P, \ x \in S_i \text{ and } y \in S_j \text{ then } i \leq j \text{ for all x.} \tag{5}$$

Equation (4) expresses that the sum of the times for all the assigned tasks to one station should not exceed the predetermined cycle time. Equation (5) ensures that the precedence constraints during the assigning process are satisfied.

In order to assign tasks to the current workstation, the critical tasks are determined by the proposed CNM. In relation to this fact, i.e. the higher weight of each task represents a

higher degree of criticality, a high priority to assign is therefore gained. In other words, the task with a higher weight will be assigned sooner, and some tasks with lower weight (lower priority to assign) may be assigned to the current work station due to two reasons. The two reasons are as follows:

- To satisfy the precedence constraints means that a task with a lower priority can be assigned sooner to preserve the precedence relationship.
- The capacity of workstation is not fully completed means that a task with a higher weight is available to be assigned but the current workstation does not have enough time, but the remaining time is enough to assign some other tasks with lower weight (i.e. a lower priority to assign).

This process is continued until no task is left within the assembly network to be assigned. Here, it should be noted that in the situation with an equal weight for some of the tasks in the candidate list, there is no difference to select the tasks, so a task is selected by random chance.

The heuristic CNM based described above involves determining the criticality of each node within the assembly network and assigning the priority based on the obtained weight using the precedence relationship diagram. The assembly network is used to compute the weight of each task and those tasks with higher weight gain more priority for assigning. Task assignment process is continued until all the tasks have been assigned to any station, as shown by $S_t = Ø$. The proposed method should be done in the following steps:

1. Computing the value of OCT for the corresponding problem and replacing the existent cycle time by this value.
2. The set of all tasks within the assembly network is shown by $S_t$ which represents the set of all the available tasks for assignment. The initial value of $S_u$ is equivalent to $S_t$.
3. Weighing each single task and computing it using the CNM method; they are assigned to the stations based on the priority of tasks. In the entire task assignment procedure, precedence constraints should be satisfied even though the higher priority tasks are available. This particular process is continued until no task can be assigned to any workstation anymore. The set of the unassigned tasks is $S_u = S_t - S_a$.
4. $S_t \neq Ø$ expresses the task availability in the assembly network and this procedure goes to step 3. $S_t = Ø$ shows that all the tasks have been assigned to any station and the task assignment operation is ended.

## SOLVING PROCESS OF THE PROPOSED CNM

In this sub-section, an example available in literature taken from Jackson (1956) is graphically shown to describe the proposed CNM.

Note that the assumption is CT = 21 sec. Then, MS, SCT and finally OCT are calculated using Equations 1, 2 and 3.

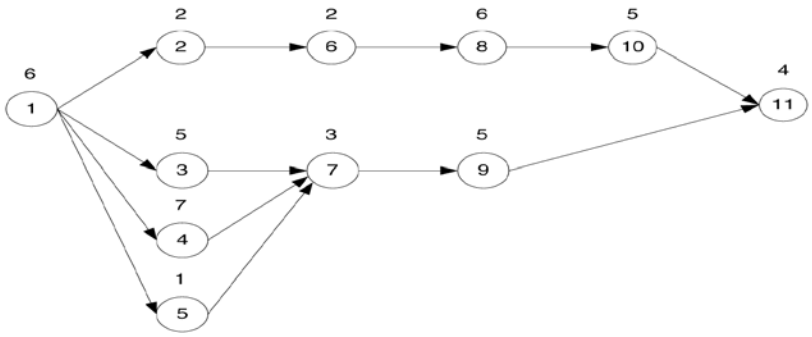


Fig.1: The network of Jackson's problem

Table 1: Weight computation using the CNM method

| Task no. | 1 | 2 | 3 | 4 | 5 | 6 | 7 | 8 | 9 | 10 | 11 |
|---|---|---|---|---|---|---|---|---|---|---|---|
| Weight | 25 | 19 | 17 | 19 | 13 | 17 | 12 | 15 | 9 | 9 | 4 |

The following is a description of the assigning process to clarify the proposed CNM.

1. Calculating MS = 46/21 = 2.19 and after rounding up, it is 3 and SCT = 46/3 = 15.33; therefore, OCT = [(21+15.33)/2]=18.16, so 15.33<18.16< 21, and since all the task times are integer, it should be rounded and set to 18.
2. Creating workstation 1 and calculating the weight for each task. This phase is shown in Table 1; the first candidate task to assign according to the proposed heuristic is task 1, and because it has a higher weight among the other tasks, so task 1 is assigned according to the CNM rule to the first workstation. In the second step according to the task weight, there are two different choices, namely, tasks 2 and 4. In this situation, a task is selected by random chance, and it is assumed that it is task 4 and then task 2 with higher weight is selected to be assigned. This is continued by tasks 3 and 6 with the same weight which can be assigned to the current station; however, according to the remaining cycle time, task 6 should be assigned to the current station. In accordance with the remaining cycle time for the current station, only task 5 can be assigned to this particular station. Although it does not have a higher weight but it can be assigned accorrding to the predefined assigning procedure. Finally, station time is $T = (s_1) = 6+7+2+2+1=18$.
3. Creating workstation 2 according to the tasks weight, task 3 should be assigned to the second station. After that, tasks 8 and 7 are assigned to the current station, respectively. According to the remaining cycle time, there is no other task to be assigned. Total station time equals $T = (s_2) = 5+6+3=14$.
4. Creating workstation 3, tasks 9 and 10 have the same weight, so one of them is selected by random so tasks 10 and 9 are assigned to the current work station, respectively. Then, only task 11 is available to be assigned, so task 11 is assigned to this station. The total process time for this station is $T = (s_3) = 5 + 5 +4= 14$.

A summary of the whole assigning process described above is shown in Table 2.

Table 2: A summary of the assigning process using the proposed CNM

| Iteration | Candidate list | Assigned task | Remaining station time |
|---|---|---|---|
| 1 | 1 | 1 | 12 |
| 2 | 2,4 | 4 | 5 |
| 3 | 2 | 2 | 3 |
| 4 | 6 | 6 | 1 |
| 5 | 5 | 5 | 0 |
| 6 | 3 | 3 | 13 |
| 7 | 8 | 8 | 7 |
| 8 | 7 | 7 | 4 |
| 9 | 9,10 | 10 | 13 |
| 10 | 9 | 9 | 8 |
| 11 | 11 | 11 | 4 |

## HEURISTIC METHODS AND PERFORMANCE INDEXES

In this section, 9 heuristic rules recently used by the researchers are introduced and several benchmark problems are also solved for all the considered heuristics and the suggested CNM to compare and evaluate the CNM. The heuristic rules and their sign and parameters are given in Table 3. The definitions of the parameters used in the heuristic rules are listed in the following table:

Table 3: List of the heuristic rules

| Rule No. | Rule Name | Symbol | Definition |
|---|---|---|---|
| 1 | Maximum positional weight of follower task | Max $\|S_i\|$ | $\sum_{j \in s_i} t_j$ |
| 2 | Maximum task time of immediate follower task | Max $\|IS_i\|$ | $\|IS_i\|$ |
| 3 | Minimum total number of predecessor tasks | $NPS_i$ | $\|P_i\|$ |
| 4 | Minimum total number of successor tasks | MiTNST | $\|S_i\|$ |
| 5 | Maximum total time of successor tasks | MaTTST | $T\|S_i\|$ |
| 6 | Minimum total time of successor tasks | MiTTST | $T\|P_i\|$ |
| 7 | Maximum total number of predecessor tasks | MaTNPT | $\|P_i\|$ |
| 8 | Maximum total number of successor tasks | MaTNST | $\|S_i\|$ |
| 9 | Maximum total time of predecessor tasks | MaTTPT | $T\|P_i\|$ |
| $t_i$ | Assembly time required to complete task i | | |
| i, j | Task index | | |
| $IS_i$ | Set of immediate successors of task i | | |
| N | The number of tasks to be balanced into stations | | |
| $IP_i$ | Set of immediate predecessors of task i | | |
| $S_i$ | Set of all successors of task i | | |
| $P_i$ | Set of all predecessors of task i | | |

## PERFORMANCE INDEXES

As stated above, the main objective of the assembly line balancing problem in the area of type-1 is to minimize the number of stations. To the researchers' best knowledge, most of the methods obtained the same results for the number of stations, and thus, evaluating the different heuristic methods using some other performance measures seems to be necessary. Although several indexes are available in the literature, two indexes (SI and LE) were selected and calculated in the current study. A brief definition of the indexes is given below:

1. Number of Work Station (NWS): The minimum index value shows a decrease in the required number of stations for assembly and better task distribution.
2. Smoothness Index (SI): The smoothness index is an index for the relative smoothness of a given assembly line. A smaller SI results in a smoother line, thereby, reducing the in-process inventory (Baykasoglu, 2006).

$$SI = \sqrt{\frac{\sum_{i=1}^{n} \left(T(s_{\max}) - T(s_i)\right)^2}{N}} \tag{6}$$

3. Line Efficiency (LE): Line efficiency is a ratio between total station time to the product of cycle time and the number of workstations, which is represented as a percentage. The greatest LE results in an efficient line, which is expressed as follows (Ponnambalam *et al*., 2000):

$$LE = \frac{\sum_{i=1}^{n} T(s_i)}{N \times CT} \times 100 \tag{7}$$

It should be noted here that in the above equations $T(S_i)$, is the time of the i-th station, $T(S_{\max})$ is the maximum workstation time, N is the number of workstations and CT is the given cycle time.

## RESULTS OF SOLVING TEST PROBLEMS

In this section, several test problems available in the literature, which can be downloaded from Scholl *et al*. (2010), are solved using the proposed CNM and 9 other mentioned heuristic rules. The results obtained for all the performance measures are given in Table 4. Morover, the optimal results in all the indexes obtained from the heuristic methods are bolted and presented in Table 4.

Meanwhile, a summary of the results obtained by the new method and 9 other methods is shown in Table 5. It is important to note that the comparison results of the new method and the other 9 methods in Table 5 are with respect to the assigned activities to the workstations with multi objectives. In other words, each method will get the first place if all their performance indexes are better than those of the others.

As shown in Table 5, all the indexes show the superiority of the proposd heuristic method in balancing the stright assembly line to 9 other methods. Based on the final results, it is clearly found that the proposed method (CNM) has a better situation than the rest of the methods taken into consideration.

Table 4: The results for the SALBP problems using the task assignment rules given in the order defined in Table 3

| sample name | CT | | CNM | 1 | 2 | 3 | 4 | 5 | 6 | 7 | 8 | 9 |
|---|---|---|---|---|---|---|---|---|---|---|---|---|
| Arcus 83 | 6842 | NS | 12.000 | **12.000** | 12.000 | 13.000 | 13.000 | 12.000 | 13.000 | 13.000 | 13.000 | 13.000 |
| | | SI | 1010.00 | **706.52** | 768.32 | 1482.6 | 1448.7 | 727.70 | 1448.7 | 1482.2 | 1482.6 | 1482.6 |
| | | LE | 92.209 | **92.209** | 92.209 | 85.116 | 85.116 | 92.209 | 85.116 | 85.116 | 85.116 | 85.116 |
| | 4732 | NS | **17.000** | 18.000 | 18.000 | 18.000 | 18.000 | 18.000 | 18.000 | 18.000 | 18.000 | 18.000 |
| | | SI | **421.312** | 924.23 | 925.88 | 954.300 | 856.22 | 924.17 | 856.22 | 622.27 | 954.30 | 954.30 |
| | | LE | **94.111** | 88.883 | 88.883 | 88.883 | 88.883 | 88.883 | 88.883 | 88.883 | 88.883 | 88.883 |
| | 4454 | NS | **18.000** | 19.000 | 20.000 | 19.000 | 19.000 | 19.000 | 19.000 | 19.000 | 19.000 | 19.000 |
| | | SI | **515.253** | 828.383 | 855.38 | 644.35 | 733.53 | 817.66 | 733.53 | 697.01 | 644.35 | 836.23 |
| | | LE | **94.431** | 89.461 | 84.988 | 89.461 | 89.461 | 89.461 | 89.461 | 89.461 | 89.461 | 89.461 |
| | 4206 | NS | **19.000** | 20.000 | 20.000 | 21.000 | 22.000 | 20.000 | 22.000 | 20.000 | 21.000 | 20.000 |
| | | SI | **402.903** | 725.53 | 506.02 | 929.18 | 983.41 | 728.65 | 983.41 | 713.16 | 929.18 | 755.83 |
| | | LE | **94.736** | 89.999 | 89.999 | 85.713 | 81.817 | 89.999 | 81.817 | 89.999 | 85.713 | 89.999 |
| | 3985 | NS | 21.000 | 21.000 | 21.000 | 22.000 | 23.000 | **21.000** | 23.000 | 22.000 | 22.000 | 22.000 |
| | | SI | 737.081 | 675.814 | 590.97 | 757.28 | 909.34 | **414.63** | 909.34 | 672.13 | 757.28 | 786.93 |
| | | LE | 90.467 | 90.467 | 90.467 | 86.355 | 82.600 | **90.467** | 82.600 | 86.355 | 86.355 | 86.355 |

Table 4 (Cont.)

| | | | | | | | | | | | | |
|---|---|---|---|---|---|---|---|---|---|---|---|---|
| Mitchell | 39 | NS | **3.000** | 3.000 | 3.000 | 3.000 | 3.000 | 3.000 | 3.000 | 3.000 | 3.000 | 3.000 |
| | | SI | **2.377** | 5.477 | 3.697 | 3.464 | 3.464 | 6.377 | 3.464 | 5.196 | 3.464 | 3.464 |
| | | LE | **89.744** | 89.744 | 89.744 | 89.744 | 89.744 | 89.744 | 89.744 | 89.744 | 89.744 | 89.744 |
| | 26 | NS | **5.000** | 5.000 | 5.000 | 5.000 | 5.000 | 5.000 | 5.000 | 5.000 | 5.000 | 5.000 |
| | | SI | **3.236** | 6.957 | 6.943 | 6.213 | 5.020 | 7.987 | 5.020 | 6.213 | 6.213 | 6.213 |
| | | LE | **80.769** | 80.769 | 80.769 | 80.769 | 80.769 | 80.769 | 80.769 | 80.769 | 80.769 | 80.769 |
| | 21 | NS | **6.000** | 6.000 | 6.000 | 6.000 | 6.000 | 6.000 | 6.000 | 6.000 | 6.000 | 6.000 |
| | | SI | **4.767** | 6.096 | 6.096 | 6.671 | 5.115 | 7.382 | 5.115 | 6.646 | 6.671 | 6.671 |
| | | LE | **83.333** | 83.333 | 83.333 | 83.333 | 83.333 | 83.333 | 83.333 | 83.333 | 83.333 | 83.333 |
| | 15 | NS | **8.000** | 8.000 | 9.000 | 9.000 | 10.000 | 8.000 | 10.000 | 8.000 | 9.000 | 9.000 |
| | | SI | **1.674** | 2.318 | 4.447 | 4.738 | 4.970 | 2.318 | 4.970 | 2.318 | 4.738 | 4.738 |
| | | LE | **87.500** | 87.500 | 77.778 | 77.778 | 70.000 | 93.750 | 70.000 | 87.500 | 77.778 | 77.778 |
| | 14 | NS | **8.000** | 8.000 | 9.000 | 10.000 | 10.000 | 8.000 | 10.000 | 9.000 | 10.000 | 10.000 |
| | | SI | **1.061** | 1.173 | 3.215 | 4.848 | 4.970 | 1.173 | 4.970 | 4.069 | 4.848 | 4.848 |
| | | LE | **93.750** | 93.750 | 83.333 | 75.000 | 75.000 | 93.750 | 75.000 | 83.333 | 75.000 | 75.000 |
| Mertens | 18 | NS | **2.000** | 2.000 | 2.000 | 2.000 | 2.000 | 2.000 | 2.000 | 2.000 | 2.000 | 2.000 |
| | | SI | **0.707** | 4.950 | 4.950 | 4.950 | 4.950 | 4.950 | 4.950 | 4.950 | 4.950 | 4.950 |
| | | LE | **80.556** | 80.556 | 80.556 | 80.556 | 80.556 | 80.556 | 80.556 | 80.556 | 80.556 | 80.556 |
| | 15 | NS | 3.000 | **2.000** | 3.000 | **2.000** | **2.000** | 2.000 | 2.000 | 2.000 | 2.000 | 2.000 |
| | | SI | 6.028 | **0.707** | 4.761 | **0.707** | **0.707** | 0.707 | 0.707 | 0.707 | 0.707 | 0.707 |
| | | LE | 64.444 | **96.667** | 64.444 | **96.667** | **96.667** | 96.667 | 96.667 | 96.667 | 96.667 | 96.667 |
| | 10 | NS | 4.000 | 4.000 | 4.000 | **3.000** | 4.000 | 3.000 | 4.000 | **3.000** | **3.000** | 3.000 |
| | | SI | 2.500 | 2.500 | 3.354 | **0.577** | 2.500 | 0.577 | 2.500 | **0.577** | 0.577 | 0.577 |
| | | LE | 72.500 | 72.500 | 72.500 | **96.667** | 72.500 | 69.667 | 72.500 | **96.667** | 96.667 | 96.667 |
| | 8 | NS | **5.000** | 5.000 | 5.000 | 6.000 | 6.000 | 5.000 | 6.000 | 6.000 | 6.000 | 6.000 |
| | | SI | **1.414** | 2.569 | 1.414 | 1.354 | 1.354 | 2.569 | 1.354 | 1.354 | 1.354 | 1.354 |
| | | LE | **72.500** | 72.500 | 72.500 | 60.417 | 60.417 | 72.500 | 60.417 | 60.417 | 60.417 | 60.417 |
| | 6 | NS | 6.000 | 6.000 | 6.000 | **6.000** | **6.000** | 6.000 | **6.000** | **6.000** | **6.000** | **6.000** |
| | | SI | 1.581 | 1.581 | 1.581 | **1.354** | **1.354** | 1.581 | **1.354** | **1.354** | **1.354** | **1.354** |
| | | LE | 80.556 | 80.556 | 80.556 | **80.556** | **80.556** | 80.556 | **80.556** | **80.556** | **80.556** | **80.556** |

Table 4 (Cont.)

| | | | | | | | | | | | | |
|---|---|---|---|---|---|---|---|---|---|---|---|---|
| Lutz1 | 2828 | NS | **6.000** | 6.000 | 6.000 | 6.000 | 6.000 | 6.000 | 6.000 | 6.000 | 6.000 | 6.000 |
| | | SI | **770.10** | 970.10 | 974.04 | 974.04 | 974.04 | 862.53 | 862.96 | 884.13 | 974.04 | 974.04 |
| | | LE | **83.333** | 83.333 | 83.333 | 83.333 | 83.333 | 83.333 | 83.333 | 83.333 | 83.333 | 83.333 |
| | 2357 | NS | 7.000 | **7.000** | 8.000 | 7.000 | 7.000 | 7.000 | 7.000 | 7.000 | 7.000 | 7.000 |
| | | SI | 543.55 | **367.05** | 716.92 | 408.58 | 484.67 | 540.17 | 484.55 | 484.80 | 408.58 | 408.58 |
| | | LE | 85.702 | **85.702** | 74.989 | 85.702 | 85.702 | 85.702 | 85.702 | 85.702 | 85.702 | 85.702 |
| | 2020 | NS | 8.000 | 8.000 | 8.000 | 8.000 | 8.000 | **8.000** | 8.000 | 8.000 | 8.000 | 8.000 |
| | | SI | 405.35 | 296.55 | 366.80 | 324.49 | 324.49 | **290.31** | 303.74 | 352.83 | 324.49 | 324.49 |
| | | LE | 87.500 | 87.500 | 87.500 | 87.500 | 87.500 | **87.500** | 87.500 | 87.500 | 87.500 | 87.500 |
| | 1768 | NS | 9.000 | 9.000 | 9.000 | 9.000 | 9.000 | 9.000 | **9.000** | 9.000 | 9.000 | 9.000 |
| | | SI | 226.09 | 225.42 | 230.72 | 235.03 | 248.48 | 260.32 | **203.313** | 225.88 | 235.03 | 235.03 |
| | | LE | 88.864 | 88.864 | 88.864 | 88.864 | 88.864 | 88.864 | **88.864** | 88.864 | 88.864 | 88.864 |
| | 1572 | NS | **11.000** | 11.000 | 11.000 | 11.000 | 11.000 | 11.000 | 11.000 | 11.000 | 11.000 | 11.000 |
| | | SI | **237.23** | 365.79 | 397.41 | 396.59 | 396.59 | 289.11 | 398.97 | 369.29 | 396.59 | 396.59 |
| | | LE | **81.772** | 81.772 | 81.772 | 81.772 | 81.772 | 81.772 | 81.772 | 81.772 | 81.772 | 81.772 |
| Roszieg | 32 | NS | 5.000 | **4.000** | 5.000 | 5.000 | 5.000 | **4.000** | 5.000 | 5.000 | 5.000 | 5.000 |
| | | SI | 12.657 | **1.118** | 12.116 | 12.689 | 11.713 | **1.118** | 11.713 | 12.149 | 12.689 | 12.689 |
| | | LE | 78.125 | **97.656** | 78.125 | 78.125 | 78.125 | **97.656** | 78.125 | 78.125 | 78.125 | 78.125 |
| | 25 | NS | 6.000 | 6.000 | **6.000** | 6.000 | 6.000 | 6.000 | 6.000 | 6.000 | 6.000 | 6.000 |
| | | SI | 8.727 | 7.246 | **5.148** | 6.843 | 7.200 | 7.246 | 7.200 | 7.583 | 6.843 | 6.843 |
| | | LE | 83.333 | 83.333 | **83.333** | 83.333 | 83.333 | 83.333 | 83.333 | 83.333 | 83.333 | 83.333 |
| | 18 | NS | 8.000 | 8.000 | 8.000 | **8.000** | 8.000 | 8.000 | 8.000 | 8.000 | **8.000** | 8.000 |
| | | SI | 5.062 | 5.062 | 5.062 | **1.768** | 2.894 | 4.730 | 2.894 | 4.228 | **1.768** | 2.806 |
| | | LE | 86.806 | 86.806 | 86.806 | **86.806** | 86.806 | 86.806 | 86.806 | 86.806 | **86.806** | 86.806 |
| | 16 | NS | 9.000 | 9.000 | 9.000 | **9.000** | **9.000** | 9.000 | **9.000** | 9.000 | **9.000** | **9.000** |
| | | SI | 4.203 | 3.283 | 4.203 | **3.073** | **3.073** | 3.283 | **3.073** | 3.416 | **3.073** | **3.073** |
| | | LE | 86.806 | 86.806 | 86.806 | **86.806** | **86.806** | 86.806 | **86.806** | 86.806 | **86.806** | **86.806** |
| | 14 | NS | 11.000 | 10.000 | **10.000** | 10.000 | 10.000 | 10.000 | 10.000 | 10.000 | 10.000 | 10.000 |
| | | SI | 2.860 | 2.627 | **2.470** | 2.510 | 2.550 | 2.627 | 2.550 | 3.826 | 2.510 | 2.510 |
| | | LE | 81.169 | 89.286 | **89.286** | 89.286 | 89.286 | 89.286 | 89.286 | 81.169 | 89.286 | 89.286 |

Table 4 (Cont.)

| | | | | | | | | | | | | |
|---|---|---|---|---|---|---|---|---|---|---|---|---|
| Gunther | 81 | NS | 7.000 | 7.000 | 7.000 | **7.000** | 7.000 | 7.000 | 7.000 | 7.000 | **7.000** | **7.000** |
| | | SI | 29.155 | 29.135 | 20.410 | **16.912** | 20.452 | 29.135 | 20.452 | 20.494 | **16.912** | **16.912** |
| | | LE | 85.185 | 85.185 | 85.185 | **85.185** | 85.185 | 85.185 | 85.185 | 85.185 | **85.185** | **85.185** |
| | 69 | NS | **8.000** | 8.000 | 8.000 | 8.000 | 9.000 | 8.000 | 9.000 | 9.000 | 8.000 | 8.000 |
| | | SI | **8.870** | 13.120 | 13.262 | 12.515 | 18.421 | 13.120 | 18.421 | 17.648 | 12.515 | 13.290 |
| | | LE | **87.500** | 87.500 | 87.500 | 87.500 | 77.778 | 87.500 | 77.778 | 77.778 | 87.500 | 87.500 |
| | 61 | NS | 9.000 | 9.000 | 9.000 | 10.000 | 10.000 | 9.000 | 10.000 | 10.000 | 10.000 | 10.000 |
| | | SI | 11.470 | 10.520 | 9.510 | 16.097 | 15.852 | 10.520 | 15.852 | 17.009 | 16.097 | 16.047 |
| | | LE | 87.978 | 87.978 | 87.978 | 79.180 | 79.180 | 87.978 | 79.180 | 79.180 | 79.180 | 79.180 |
| | 54 | NS | **10.000** | 10.000 | 10.000 | 10.000 | 10.000 | 10.000 | 10.000 | 10.000 | 10.000 | 10.000 |
| | | SI | **6.156** | 7.880 | 7.176 | 7.342 | 6.834 | 7.880 | 6.834 | 9.160 | 7.342 | 7.218 |
| | | LE | **89.444** | 89.444 | 89.444 | 89.444 | 89.444 | 89.444 | 89.444 | 89.444 | 89.444 | 89.444 |
| | 49 | NS | 12.000 | 12.000 | 12.000 | 12.000 | **11.000** | 12.000 | **11.000** | 12.000 | 12.000 | 12.000 |
| | | SI | 12.480 | 11.836 | 13.817 | 10.634 | **7.224** | 11.836 | **7.224** | 10.712 | 10.634 | 10.642 |
| | | LE | 82.143 | 82.143 | 82.143 | 82.143 | **89.610** | 82.143 | **89.610** | 82.143 | 82.143 | 82.143 |
| | 41 | NS | **15.000** | 16.000 | 17.000 | 16.000 | 18.000 | 16.000 | 18.000 | 18.000 | 16.000 | 16.000 |
| | | SI | **12.694** | 14.506 | 17.222 | 16.491 | 18.118 | 14.506 | 18.118 | 19.019 | 16.491 | 16.342 |
| | | LE | **78.537** | 73.628 | 69.297 | 73.628 | 65.447 | 73.628 | 65.447 | 65.447 | 73.628 | 73.628 |
| Mansoor | 94 | NS | 3.000 | 2.000 | 3.000 | 3.000 | 3.000 | 3.000 | 3.000 | **2.000** | 3.000 | 3.000 |
| | | SI | 33.357 | 2.121 | 33.357 | 33.357 | 33.357 | 32.378 | 33.357 | **0.707** | 33.357 | 33.357 |
| | | LE | 65.603 | 98.404 | 65.603 | 65.603 | 65.603 | 65.603 | 65.603 | **98.404** | 65.603 | 65.603 |
| | 62 | NS | 4.000 | 4.000 | 4.000 | 4.000 | 4.000 | 4.000 | 4.000 | **4.000** | 4.000 | 4.000 |
| | | SI | 20.561 | 18.688 | 20.106 | 18.954 | 18.954 | 18.688 | 18.954 | **14.603** | 18.954 | 16.741 |
| | | LE | 74.597 | 74.597 | 74.597 | 74.597 | 74.597 | 74.597 | 74.597 | **74.597** | 74.597 | 74.597 |
| | 48 | NS | 5.000 | 5.000 | 5.000 | 5.000 | 5.000 | 5.000 | 5.000 | **4.000** | 5.000 | 5.000 |
| | | SI | 10.918 | 12.296 | 12.296 | 12.296 | 12.296 | 12.296 | 12.296 | **2.500** | 12.296 | 12.296 |
| | | LE | 77.083 | 77.083 | 77.083 | 77.083 | 77.083 | 77.083 | 77.083 | **96.354** | 77.083 | 77.083 |
| Bowman | 20 | NS | 5.000 | 5.000 | 5.000 | **5.000** | **5.000** | 5.000 | **5.000** | **5.000** | **5.000** | 5.000 |
| | | SI | 5.916 | 5.916 | 5.916 | **3.873** | **3.873** | 5.916 | **3.873** | **3.873** | **3.873** | 5.916 |
| | | LE | 75.000 | 75.000 | 75.000 | **75.000** | **75.000** | 75.000 | **75.000** | **75.000** | **75.000** | 75.000 |

Table 5: A summary of the results comparing the proposed method and 9 other methods

| Rules Number | CNM | 1 | 2 | 3 | 4 | 5 | 6 | 7 | 8 | 9 |
|---|---|---|---|---|---|---|---|---|---|---|
| Total optimal answer | 15 | 4 | 3 | 6 | 5 | 4 | 6 | 7 | 5 | 4 |
| Total problems | 35 | 35 | 35 | 35 | 35 | 35 | 35 | 35 | 35 | 35 |
| Percentage | 42.85% | 11.42% | 8.57% | 17.14% | 14.28% | 11.42% | 17.14% | 20% | 14.28% | 11.42% |

Finally, Fig.2 demonstrates the number of times every method obtained the first place in comparison to the other methods. According to this graph, it can be asserted that the proposed CNM achieved the optimal number of stations in 15 test problems out of 35 and thus took the first place among all the methods. In addition, the second place goes to the heuristic rule 7 (i.e. the maximum total number of the predecessor tasks), whereas rule 6 (the minimum total time of successor tasks) and rule 3 (the minimum total number of predecessor tasks) are both in the third place by achieving the best results for 17.14% of the solved problems.

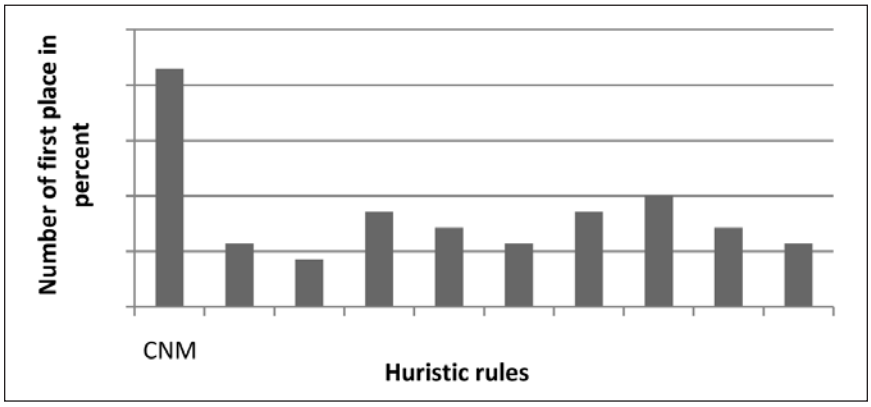


Fig.2: The number of times the best solution is obtained by each method in comparison to the other methods

## CONCLUSION

Based on the results obtained for the performance measures, it can easily be concluded that the proposed heuristic method (CNM) has given better results in assigning tasks and in minimizing the number of workstations. Although some other methods have obtained good results for a number of the workstations, they do not give considerable results for other indexes like smoothness index. Another advantage of the proposed CNM can be considered in achieving good results in a reasonable of time. Since the heuristic methods are the foundation of the metaheuristic methods, the proposed method can be used as the main base for most of the metaheuristic methods like simulated annealing, genetic algorithm and ant colony optimization. Furthermore, although the proposed method are introduced and solved for stight line in the area of type-1, it can be efficiently applied for other kind of assembly lines such as parallel, U-shaped, and other types of assembly line balancing problem such as type-2 in future research.

## REFERENCES

Ajenblit, D. A., & Wainwright, R. L. (1998) *Applying genetic algorithms to the U-shaped assembly line balancing problem.* Paper presented at the Proceedings of the IEEE Conference on Evolutionary Computation, ICEC, Anchorage, AK, USA.

Bautista, J., & Pereira, J. (2009). A dynamic programming based heuristic for the assembly line balancing problem. *European Journal of Operational Research, 194*(3), 787-794.

Baybars, I. (1986). Efficient heuristic method for the simple assembly line balance problem. *International Journal of Production Research, 24*(1), 149-166.

Baykasoglu, A. (2006). Multi-rule multi-objective simulated annealing algorithm for straight and U type assembly line balancing problems. *Journal of Intelligent Manufacturing, 17*(2), 217-232.

Erel, E., & Sarin, S. C. (1998). *A survey of the assembly line balancing procedures. Production Planning and Control, 9*(5), 414-434.

Erel, E., Sabuncuoglu, I., & Aksu, B. A. (2001). *Balancing of U-type assembly systems using simulated annealing*. International Journal of Production Research. 39(13): 3003-3015.

Erel, E., & Sarin, S. C. (1998). A survey of the assembly line balancing procedures. *Production Planning and Control, 9*(5), 414-434.

Ghosh, S., & Gagnon, R. J. (1989). A comprehensive literature review and analysis of the design, balancing and scheduling of assembly systems. *International Journal of Production Research, 27*(4), 637 - 670.

Gutjahr, A. L., & Nemhauser, G. L. (1964). An algorithm for the line balancing problem. *Management Science, 11*(2), 308-315.

Helgeson, W. B., & Birnie, D. P. (1961). Assembly line balancing using the ranked positional weight technique. *Journal of Industrial Engineering, 12*(6), 394-398.

Hwang, R. K., Katayama, H., & Gen, M. (2008). U-shaped assembly line balancing problem with genetic algorithm. *International Journal of Production Research, 46*(16), 4637-4649.

Jackson, J. R. (1956). A computing procedure for a line balancing problem. *Management Science, 2*(3), 261-271.

Kim, Y. K., Song, W. S., & Kim, J. H. (2009). A mathematical model and a genetic algorithm for two-sided assembly line balancing. *Computers and Operations Research, 36*(3), 853-865.

Kilbridge, M. D., & Wester, L. (1996). A heuristic method of assembly line balancing. *Journal of Industrial Engineering, 12*, 394-398.

Kao, E. P. C., & Queyranne, M. (1982). *On dynamic programming methods for assembly line balancing*. Paper presented at the Operations Research.

Masood Fathi, M. K. A. Ariffin, & Napsiah Ismail (2010). A note on "A multi-objective genetic algorithm for solving assembly line balancing problem. *The International Journal of Advanced Manufacturing Technology, 50*(5-8), 771-773.

Moodie, C. L., & Young, H. H. (1965). A heuristic method of assembly line balancing for assumptions of constant/variable work element times. *Journal of Industrial Engineering, 16*, 456-467.

Nicosia, G., Pacciarelli, D., & Pacifici, A. (2002). Optimally balancing assembly lines with different workstations. *Discrete Applied Mathematics, 118*(1-2), 99-113.

Özcan, U., & Toklu, B. (2008). A tabu search algorithm for two-sided assembly line balancing. *International Journal of Advanced Manufacturing Technology*, 1-8.

Ponnambalam, S. G., Aravindan, P., & Mogileeswar Naidu, G. (2000). Multi-objective genetic algorithm for solving assembly line balancing problem. *International Journal of Advanced Manufacturing Technology, 16*(5), 341-352.

Rekiek, B., & Delchambre, A. (2005). Assembly Line Design: *The Balancing of Mixed-Model Hybrid Assembly Lines with Genetic Algorithms*. Springer Series in Advanced Manufacturing.

Sabuncuoglu, I., Erel, E., & Alp, A. (2000). Ant colony optimization for the single model U-type assembly line balancing problem. *International Journal of Production Economics*.

Scholl, A., & Becker, C. (2006). State-of-the-art exact and heuristic solution procedures for simple assembly line balancing. *European Journal of Operational Research, 168*(3), 666-693.

Scholl, A., & Klein, R. (1999). ULINO: Optimally balancing U-shaped JIT assembly lines. *International Journal of Production Research, 37*(4), 721-736.

Scholl, A., Boysen, N., Fliedner, M., & Klein R. (n.d.). Assembly line optimization research. Retrieved on June 20, 2010 from http://www.assembly-line-balancing.de.

Yeh, D. H., & Kao, H. H. (2009). A new bidirectional heuristic for the assembly line balancing problem. *Computers and Industrial Engineering, 57*(4), 1155-1160.

Pertanika J. Sci. & Technol. 20 (2): 371 - 379 (2012)

SCIENCE & TECHNOLOGY

Journal homepage: http://www.pertanika.upm.edu.my/

# Groundwater from Fractured Granite and Metasedimentary Rocks in the West Coast of Peninsular Malaysia

**Nasiman Sapari[1*], Raja Zainariah Raja Azie[2] and Hisyam Jusoh[1]**

*[1]Department of Civil Engineering, Universiti Teknologi PETRONAS, Bandar Seri Iskandar, 31750 Tronoh, Perak, Malaysia*

*[2]Department of Management and Humanities, Universiti Teknologi PETRONAS, Bandar Seri Iskandar, 31750 Tronoh, Perak, Malaysia.*

## ABSTRACT

Hard rock formations consisting of granite and metasedimentary rocks in Peninsular Malaysia, have been considered to be of poor aquifers. The map of shows the area underlain by hard rock as having poor to moderate potential for groundwater production (<230m$^3$/well/day). This paper presents a finding of productive hard rock aquifers in the west coast of Peninsular Malaysia. Data from tubewell drillings carried out for industrial water supply were analyzed. It was found that the hard rocks could yield fresh water up to a maximum of 890m$^3$/well/day. The wells were between 50 m and 200 m deep. High discharge rates of groundwater above 300m$^3$/well/day were encountered from wells that penetrate major fracture zones. The hard rocks are generally fractured at various depths. Groundwater in interconnected fractures has a steady flow that sustains production during pumping tests and actual usage of the wells. This phenomenon indicates that the groundwater is being recharged by infiltration of rainwater through the overlying weathered rocks and soils. Tubewells in hardrock of West Coast of Peninsular Malaysia were found to have an average discharge rates of 343m$^3$/well/day. However, deep tubewells penetrated only weathered granite, are generally non productive (<70m$^3$/well/day). Limited fracture openings and restricted recharge areas are likely to be the reason for the low discharge. Clay particles in fractures were observed to be the factor for the low success rate and poor quality of the water particularly in metasedimentary areas.

**Keywords: Discharge rates, groundwater, granite, sedimentary rocks, tubewells, usage**

*Article history:*
Received: 8 April 2011
Accepted: 21 April 2011

*Email addresses:*
nasiman@petronas.com.my (Nasiman Sapari),
raja_zainariah@yahoo.com (Raja Zainariah Raja Azie),
hisyam.jusoh@yahoo.com (Hisyam Jusoh)
*Corresponding Author

## INTRODUCTION

Groundwater in Malaysia is an important resource that can supplement the increasing demand of fresh water for various uses (Mohamed *et al*., 2009). Although groundwater has been used for many centuries, the usage

ISSN: 0128-7680 

is still limited to shallow unconfined aquifers using dug wells (Ang, 1994). Exploitation of groundwater from shallow aquifers is also very common in small islands (Aris *et al*., 2009). In Malaysia, deep tubewells in coarse sand aquifers were developed in the past 30 years for water supply of coastal towns, such as Kota Bharu (Sofner, 1989). The quality of the water is often described by the mineral composition, turbidity, colour, taste and odour. Iron and manganese, which are usually present in groundwater as divalent ions ($Fe^{2+}$ and $Mn^{2+}$), are considered as contaminants mainly because of their organoleptic properties (Ellis *et al*., 2000). Other contaminants in groundwater may include ammonium, arsenic and phosphate. Fortunately, the method of treatment for the removal of these contaminants is available (Katsoyiannis & Zouboulis, 2004).

Recent development of tubewell drilling in Malaysia is driven by the expansion of industries and population growth in remote areas where connection to water supply mains is not available. Alternatively, groundwater becomes an attractive source of water supply. However, many of the factories are located in the areas that are underlain by hard rocks, where porosity and permeability is known to be very low (GSDM, 1992). However, fractured rocks have been reported to have relatively high hydraulic conductivity of between 0.001 to 10 m/day (Bouwer, 1979). It is important to note that the hard rocks in Malaysia have a wide distribution covering almost 90% of the country, particularly in undulating and hilly topography areas. The search for groundwater in these areas began in the mid eighties after the country experienced a long dry period in the early eighties (GSDM, 1987). Some initial studies of groundwater in fractured granite show that several industries in Malaysia have exploited the water for various uses (Sapari *et al*., 2010). This paper presents the findings of a study on the availability of groundwater in hard rocks in Malaysia. The objective of this study was to access the suitability of groundwater as an alternative source for the water supply to remote communities and industries. In addition, the quality of groundwater and its usage by industries were also examined.

## METHOD OF STUDY

The method of the study involves observation of drilling operations and analysis of water samples from the tubewells. One hundred and thirty six tubewells, drilled for industrial and drinking water supply in the west coast of Peninsular Malaysia, were examined in this study (see Fig.1). The tubewells typically penetrated though the soil or loose quaternary alluvium, weathered rocks and hard rocks until reaching the fractured zones that produce water in the hard unweathered part of the rock. The upper parts of the wells were provided with steel casings of 355 mm diameter while PVC pipe casings of 200 mm were used in the lower part when the wells reached the medium and hard rock. The drilling might reach a maximum depth of around 200 m unless a fractured zone that produces sufficient water with a minimum production rate of 100 $m^3$/day was encountered.

Three types of drilling methods were used, namely, Rotary Drilling with water circulation, Air Percussion Rotary and Air-Foam Rotary. The drilling by water circulation using the mud of bentonite or polimer was used for the upper soft residual soil and loose alluvium or weathered bedrock where the size of the well is 350 mm in diameter.

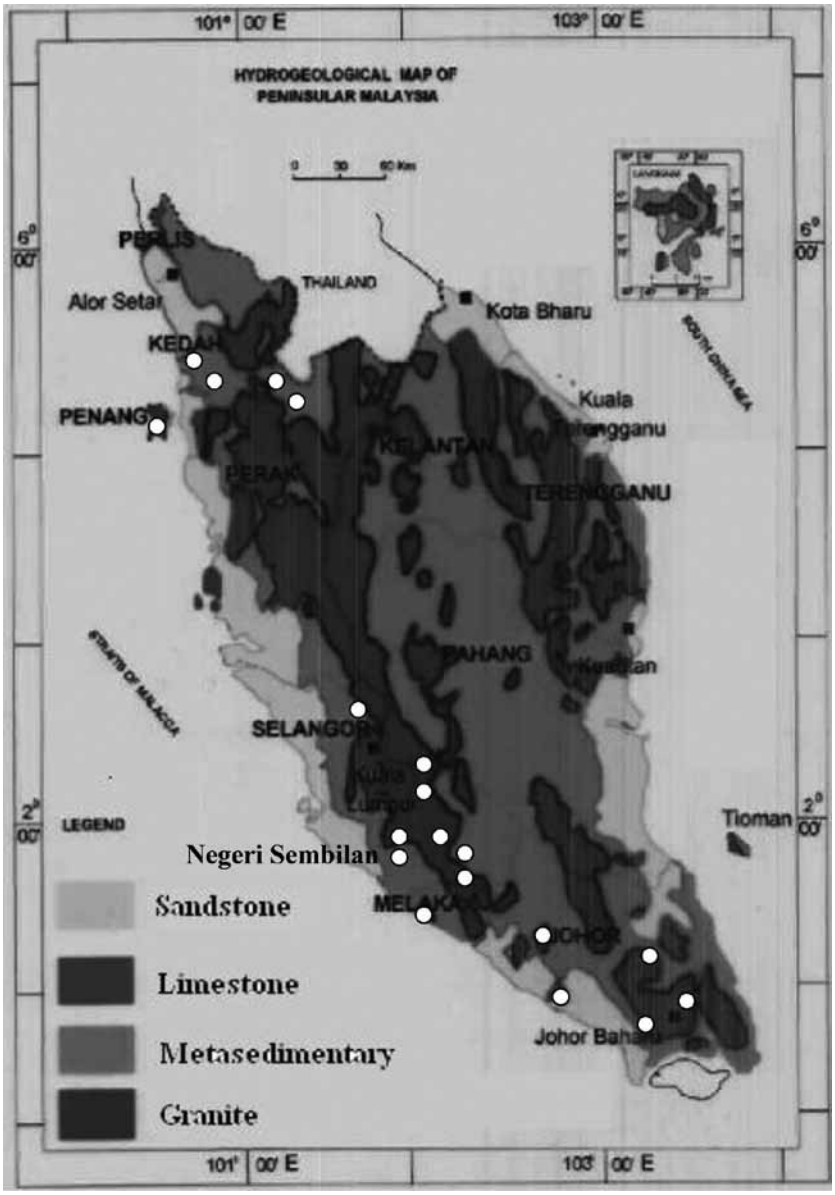


Fig.1: Location of wells and the study area in West Coast of Peninsular Malaysia

Meanwhile, the air percussion rotary drilling method was used for drilling in the medium hard of the semi-weathered and unweathered sections of the rock. Air compressor generating 1.7 MPa was used during drilling to bring the rock chips to the surface of the ground. In this section of the borehole, the size is 210 mm in diameter. The tubewells that met the required discharge rate were developed into production wells. The development was carried out by airlift method throughout the entire length of the borehole by blowing compressed air at two meter intervals from the top of the screen section downward to the bottom of the tubewell, and then upward again to the top of the top screen section. Development operation lasted for

more 6 hours or until the air-lifted water was clear and sand free. A pumping test was also conducted on the developed wells. Both step drawdown and constant discharge rate methods were used to determine the optimum yield of the wells. The discharge rate was determined by measuring the height of the water flow over a 90° V-notch weir using Equation (1):

$$Q = 1.34H^{2.48} \quad (1)$$

where,
Q = discharge rate, $m^3$/day.
H = vertical distance from the crest of weir to the free water surface, m

The water samples were collected during the pumping tests for water quality analysis according to the Standard Method (APHA, 1981). The analyzed parameters include pH, major cations ($Ca^{2+}$, $Mg^{2+}$, $Na^+$ and $K^+$), major anions ($HCO^-_3$, $SO^{2-}_4$ and $Cl^-$), conductivity, total dissolved solids, iron, manganese, hardness. The characteristics of the developed wells were recorded in terms of their discharge rate, water quality and the intended use. The locations of the wells were also recorded which are often limited by the boundary of the land owned by the industry, except for the government wells. In fact, the site were located randomly based on the availability of the land space within the boundary of the property that belonged to the industry.

## RESULTS AND DISCUSSION

The results derived from the drilling operations are shown in Fig.2 whereby the depth of the successful wells varies from 29 to 201 m with an average of 149 m. From one hundred and thirty six drilling records examined, one hundred and three were found to be successfully developed into production wells, with a minimum flow rate of 100 $m^3$/ day. Thus, the success rate of the drilling operation was 75 percent.

The maximum yield obtained from the wells was around 890 $m^3$/day, and the average from 128 wells was 349 $m^3$/day. The average drawdown during the pumping test was 40 to 50 m.

### *Water Quality*

The results from the water quality analysis for the total dissolved solids (TDS) are shown in Fig.3. The results indicate that 67% of the wells in hard rocks produce water with total dissolved solids between 101 and 200 mg/L. At this TDS level, the water can be classified as fresh water according to Hem (1970) and Bouwer (1979). Therefore, the water is suitable for various uses including agriculture, industry and domestic water supply.

A detail analysis carried out on ions content in the water samples from the wells in Selangor, Melaka, Kedah and Negeri Sembilan is shown in the bar diagram below (*see* Fig.4). The water sample from Selangor is found to be Sodium Bicarbonate while the water from Melaka, Kedah and Negeri Sembilan is Calcium Bicarbonate type. There are minor differences between the four states in terms of the cations content. Calcium and magnesium were higher in the water samples taken from Kedah's and Melaka's tubewells, while higher iron was found in the water samples from Negeri Sembilan. The average combined content of calcium and magnesium in

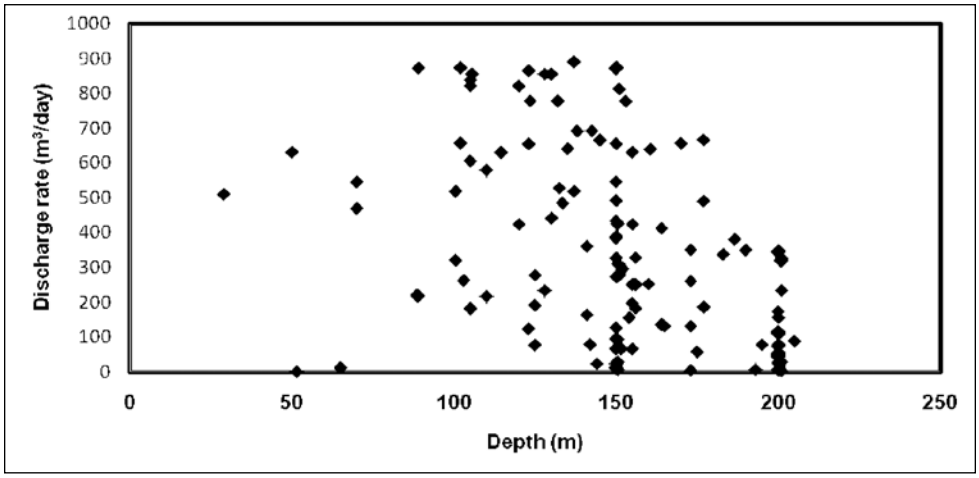


Fig.2: The depth of the wells and their optimum yield

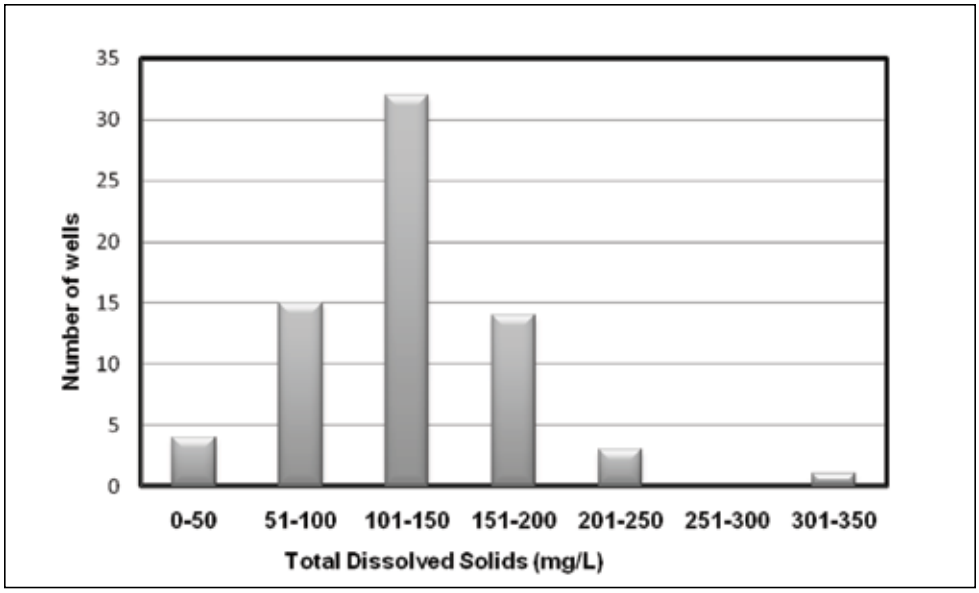


Fig.3: The total number of wells and the TDS levels (from 69 wells)

the groundwater from Melaka and Kedah was 1.86 meq/L and 1.65 meq/L, respectively. The average content of calcium for the groundwater from Penang and Johor was 0.11 meq/L and 1.59 meq/L, respectively. The water from Johor however contained higher potassium with an average of 0.79 meq/L, while the water from Penang had only 0.07 meq/L.

The results for the hardness analysis of the water sample from 52 wells, including the wells from hard rocks, are shown in Fig.5. The level ranges from 9.01 mg/L to 353 mg/L, with an average value of 76.18 mg/L.

The average water hardness indicates a moderate hardness, 48% of the wells produced soft water with hardness less than 61 mg/L. Only twenty four of the wells produced hard

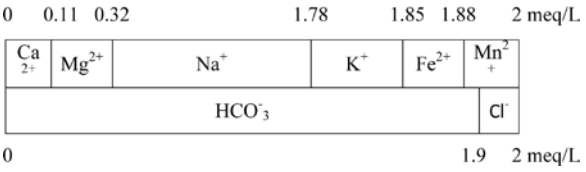


(a)

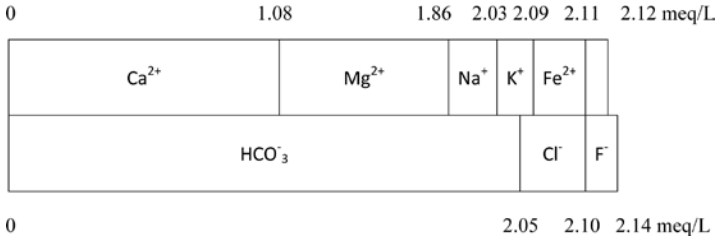


(b)

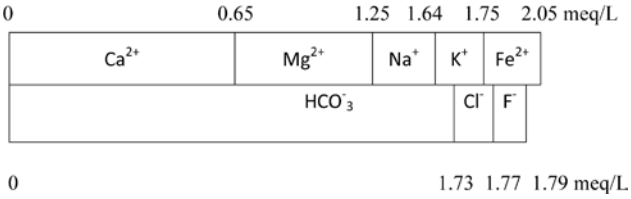


(c)

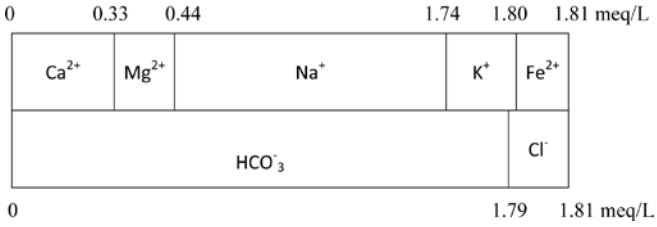


(d)

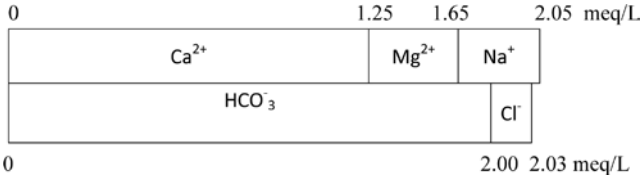


(e)

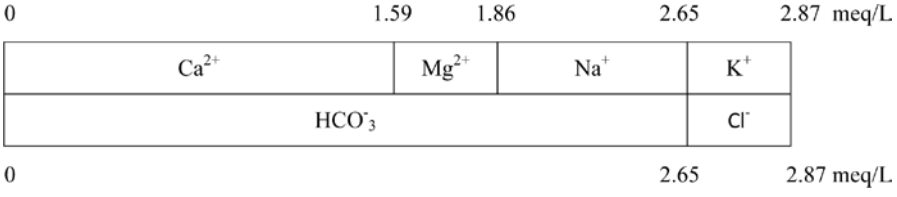


(f)

Fig.4: A Bar Diagram of the water; (a) Johor; (b) Melaka; (c) Negeri Sembilan; (d) Selangor; (e) Kedah; and (f) Penang

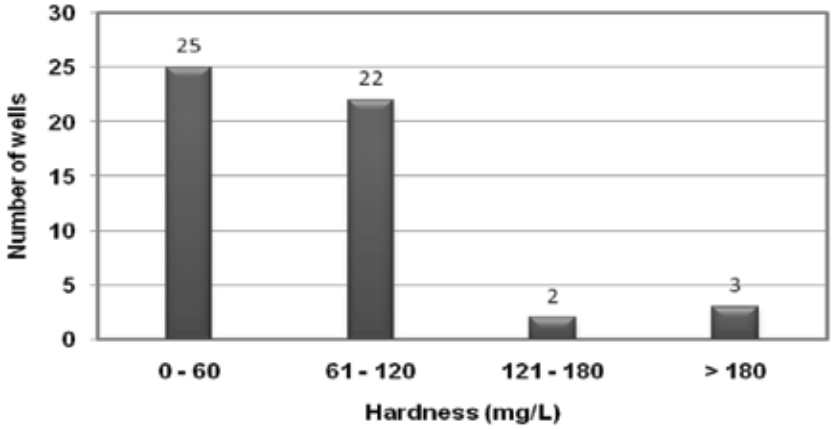


Fig.5: The number of wells and the hardness levels of the water from 52 wells

groundwater with hardness level up to 180 mg/L, and three wells produced very hard water with hardness level up to 350 mg/L.

The results of the analysis conducted on iron content are shown in Fig.6. The concentration of the total iron varies from undetectable level to as high as 14.8 mg/L. The average iron content from 59 wells is 1.81 mg/L. Therefore, treatment for iron removal is necessary prior to usage. However, about 42% of the wells contain iron less than the WHO's drinking water standard of 0.3 mg/L (Rowe *et al*., 1985). As shown in Fig.6, the distribution of the iron content in the water from different wells does not show any correlation with the depth of the wells. The treatment method currently used by the industries is adsorption by granular activated carbon or impregnated sand materials. The adsorption capacity of activated carbon for Fe(II) and Mn(II) were 3.6010 and 2.5451 mg/g, respectively (Jusoh *et al.*, 2005).

*Water Usage*

The usage of groundwater from the successfully developed wells is shown in Table 1. The locations of the industries are distributed all over the Peninsular. The presence of groundwater in fractured hard rocks will potentially fulfil the demand for water by various industries and

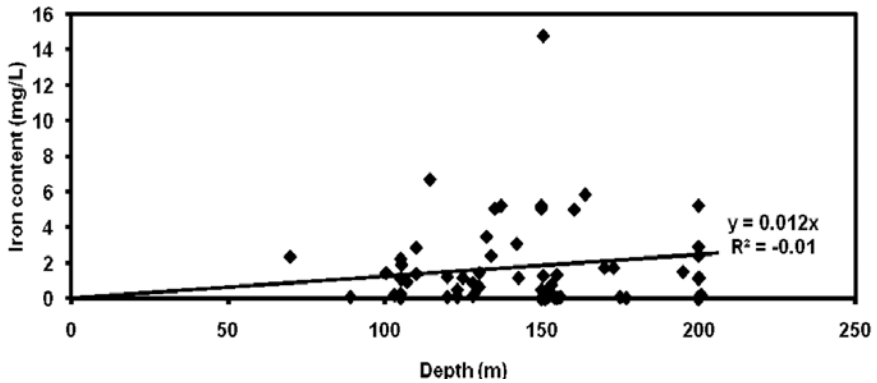


Fig.6: The concentration of total iron in the water samples from 59 wells of hard rocks

the rural communities. The advantage of using groundwater is that it is available at the site without the need of transporting and extensive piping system. The highest usage of groundwater is in manufacturing and construction industries followed by agriculture and domestic water supply. The manufacturing sector that consumes high quantity of water includes paper and textile industries. As drinking water supply, groundwater is used for domestic purposes and mineral water bottling. In other sectors, latex processing plant and golf course are the main consumers of groundwater.

Table 1: The number of wells from hard rocks and their uses

| Classification of usage* | Number of wells | Percentage (%) |
|---|---|---|
| Agriculture | 19 | 19 |
| Domestic | 15 | 15 |
| Industrial | 62 | 60 |
| Monitoring | 3 | 3 |
| Natural mineral water/bottled drinking water | 3 | 3 |
| Total | 102 | 100 |

*The classification of usage is based on the hydrogeological map, JMG (2008).

## SUMMARY AND CONCLUSION

Groundwater in interconnected fractured granite and metasedimentary rocks in Malaysia has a steady flow that sustains production during pumping test and actual usage of the wells. The depth of the wells varies from 21 to 201 m with an average of 149 m. The average yield from the wells is 349 $m^3$/day. The water is generally fresh water with TDS levels between 100 and 150 mg/L. The hardness of the water is also low, i.e. around 60 mg/L or less. Only about 9% of the wells produced hard water with hardness levels over 120 mg/L. The average iron content of the groundwater is 1.81 mg/L. In addition 42% of the wells contain iron lower than the WHO's drinking water standard of 0.3 mg/L. Groundwater in fractured hard rocks is available in almost every place underlain by the rocks. All hard rocks in Malaysia are fractured and they receive a high rate of recharge from rainwater infiltration. The readily available groundwater has supported the development of industries and domestic water supply in the remote areas and the industries include manufacturing, agriculture and mineral water bottling. In conclusion, groundwater from fractured hard rocks has high potential to be further exploited for water supply.

## REFERENCES

Ang, N. K. (1994). Hydrologic Framework and Groundwater Resources Utilisation in Peninsula Malaysia. *Proceedings of Groundwater Forum. No. 4*, Geological Society of Malaysia, 11th, January 1994, 1.1-1.5

APHA. (1981). *Standard Methods for the Examination of Water and Wastewater* (15th ed.). Washington D.C.: American Public Health Association.

Aris, A. Z., Mohd Harun Abdullah, & Sarva Mangala Praveena (2009). Evolution of groundwater chemistry in the shallow aquifer of a small tropical island in Sabah, Malaysia. *Sains Malaysiana, 38*(6), 805–812.

Bouwer, H. (1979). *Groundwater Hydrology.* Kogakusha, Japan: McGraw-Hill.

Ellis, D., Bouchard, C., & Lantagne, G. (2000). Removal of iron and manganese from groundwater by oxidation and microfiltration. *Desalination,* ***130***, 255 – 264.

Geological Survey Department of Malaysia, GDSM. (1992). *Potential of Groundwater Resources in Malaysia and Recommendation for their Planned Development*. Report No. CRU 4/1992, department of Geological Survey, Kuala Lumpur.

Geological Survey Department of Malaysia, GDSM. (1987). Groundwater Resource Study of Seri Gading Area, Johor & Rembau-Tampin-Gemas Ara, Negeri Sembilan: Fourth Malaysian Plan (1981-1985) Project Report Department of Geological Survey, Kuala Lumpur.

JMG. (2008). *Hydrogeological Map of Peninsular Malaysia* (1st ed.) Director General Minerals and Geoscience Department, Malaysia.

Jusoh, A.b., Cheng,W. H., Low,W. M., Ali, N., & Megat Mohd Noor, M. J. (2005). Study on the removal of iron and manganese in groundwater by granular activated carbon. *Desalination 182*, 347 – 353.

Katsoyiannis, I. A., Zikoudi, A., & Hug, S. J. (2008). Arsenic removal from groundwaters containing iron, ammonium, manganese and phosphate: A case study from treatment unit in northern Greece. *Desalination, 224*, 330-339.

Mohamed, A. F., Wan Yaacob, W. Z., Taha, M. R., & Samsudin, A. R., (2009). Groundwater and Soil Vulnerability in the Langat Basin Malaysia. *European Journal of Scientific Research*, *27*(4), 628-635.

Peavy, H. S, Rowe, D. R., & Tchobanoglous, G. (1985). *Environmental Engineering.* Singapore: McGraw-Hill.

Sapari, N., R. J. Raja Azie, & H. Jusoh. (2010). Groundwater in fractured granite for water supply to remote areas in Malaysia. *Water Practice & Technology 5*(2).

Sofner, B. (1989). *Groundwater Monitoring and Groundwater Protection in North Kelantan and Perlis, Malaysia* (p. 85). No. 88.2225-6, Hannover: Fed. Inst. Of Geosciences and Natural Res.

Pertanika J. Sci. & Technol. 20 (2): 381 - 399 (2012)

SCIENCE & TECHNOLOGY

Journal homepage: http://www.pertanika.upm.edu.my/

# Geospatial Water Productivity Index (WPI) for Rice

**Md Rowshon Kamal*, Mohd Amin Mohd Soom and Abdul Rashid Mohamed Shariff**

*Department of Biological and Agricultural Engineering, Faculty of Engineering, Universiti Putra Malaysia (UPM), 43400 Serdang, Selangor Darul Ehsan, Malaysia*

## ABSTRACT

A GIS-based user-interface programme was developed to compute the geospatial Water Productivity Index (WPI) of a river-fed rice irrigation scheme in Northwest Selangor, Malaysia. The spatial analysis includes irrigation blocks with sizes ranging from 20 to 300 ha. The amount of daily water use for each irrigation block was determined using irrigation delivery model and stored in the database for both main season (August to December) and off season (February to May). After cut-off of the irrigation supply, a sub-module was used to compute the total water use including rainfall for each irrigation block. The rice yield data for both seasons were obtained from DOA (Department of Agriculture, Malaysia) of the scheme. Then, the Water Productivity Index (WPI) was computed for each irrigation block and spatial thematic map was also generated. ArcObjects and Visual Basic Application (VBA) programming languages were used to structure user-interface in the ArcGIS software. The WPI, expressed in terms of crop yield per unit amount of water used (irrigation and effective rainfall), ranged from 0.02 to 0.57 kg/m$^3$ in the main season and 0.02 to 0.40 in off season among irrigation blocks, respectively. The development of the overall system and the procedure are illustrated using the data obtained from the study area. The approach could be used to depict the gaps between the existing and appropriate water management practices. Suitable interventions could be made to fill the gaps and enhance water use efficiency at the field level and also help in saving irrigation water through remedial measures in the season. The approach could be useful for irrigation managers to rectify and enhance decision-making in both the management and operation of the next irrigation season.

**Keywords: Water productivity index, spatial variability, Rice, GIS User-interface**

*Article history:*
Received: 18 April 2011
Accepted: 21 April 2011

*Email addresses:*
rowshon@yahoo.com (Md Rowshon Kamal),
amin@eng.upm.edu.my (Mohd Amin Mohd Soom),
rashid@eng.upm.edu.my (Abdul Rashid Mohamed Shariff)
*Corresponding Author

ISSN: 0128-7680 

## INTRODUCTION

Rice irrigation is the largest water-consuming sector in Malaysia, and it faces competing demands from other sectors including industrial and domestic sectors. About 70% of the available surface water resources are

consumed mostly for rice production (MOA, 2008). Due to the rapidly growing population and the competition for water in different sectors, it is imperative that the available water resources for irrigation supplies are used efficiently. A saving of 5% in irrigation water can meet 15% of water demand for the domestic and industrial sectors (Teh, 1998). A small improvement in water use for rice production would result in significant water savings for the other sectors. The present self-sufficiency level of rice production is 72% and the Government of Malaysia has targeted to achieve a self-sufficiency level of 100% by 2011. To achieve this goal, the development of arable lands for rice production and adequate irrigation supplies has to be ensured. Meanwhile, improving water productivity index through better utilization of available water resources is an option to divert the surplus irrigation water for other potential new rice growing areas. It is well known that Water Productivity Index (WPI) of rice irrigation schemes in Malaysia is low, which is usually less than 0.5. Thus, a systematic approach used to determine WPI is worthwhile to diagnose and rectify the water uses for rice production.

With the increasing population and limited water resources, the food security for future generations is at stake. In particular, the agricultural sector faces the challenge of producing more food with less water use by increasing Crop Water Productivity (Kijne *et al*., 2003). Thus, the application of water productivity analysis can provide clues for solutions to solve water management problems. Various methods for estimating water productivity at a range of scales, and for different agricultural systems were discussed by Cook *et al*. (2000). The analysis of water productivity is becoming increasingly important worldwide in light of population growth and increasing pressure on water resources (Abullaev & Molden, 2004). Water productivity analysis combines physical accounting of water with yield or economic output to give an indication of how much the value is obtained from the use of water (Molden & Shakthivadivel, 1999). In general, there are three types of crop water productivity that can be distinguished (Abullaev & Molden, 2004; Molden & Shakthivadivel, 1999; Immerzeel *et al*., 2008). A major constraint to increase food production is limited surface water availability (Aggarwal *et al*., 2000). Water productivity, a concept expressing the value or benefit derived from the use of water, includes various aspects of water management and is very relevant for arid and semi-arid regions (Kijne *et al*., 2003; Abullaev & Molden, 2004; Molden *et al*., 2001). WPI can be expressed in terms of grain yield per amount of water used.

Nowadays, proper utilization of available water resources for irrigation supplies and improvement of water productivity for irrigation schemes are the forefront issues due to the ever-increasing competition for water among the different sectors. A good irrigation depends on the ability for allocation of the available water at the proportional amount to the targeted irrigation service areas with respect to the water demands. Varying climates, soil and crop conditions, canal network, hydrological uncertainties, fluctuating flows in the river, unreliable water supply in the absence of a storage reservoir, and trade-off in water use by schemes have made the irrigation management difficult. Moreover, poor distribution of irrigation water at the tertiary level and the lack of proper monitoring of irrigation supplies have made difficult for spatial analysis of WPI. Therefore, the accounting of water use for rice irrigation is worthwhile to improve WPI for paddy farming.

Geospatial Information Systems (GIS) is an essential element for modern information techniques as it acts as the interface with the user. GIS, coupled with crop water simulation

models, can be used as a powerful tool to analyze simple or complex spatial information in the irrigation scheme since the temporal and spatial dimensions could be studied at once. GIS is defined as a means of measuring spatial and attribute data into a computerized database system, thereby allowing input, storage, retrieval and analysis of geographically referenced data (Star & Estes, 1990). The GIS capabilities to integrate spatial data from different sources, with diverse formats, constitute the main characteristics of the system (Goodchild, 1993). This paper describes a systematic approach for the determination of geospatial Water Productivity Index (WPI), defined as the mass of production per unit water use in rice production, using field observations and water allocation simulation model.

### *Study Area*

The study area is the Tanjung Karang Rice Irrigation Scheme (TAKRIS), which is located at 3°25/ - 3°45/ N latitude and 100°58/ - 101°15/ E longitude in the state of Selangor, Malaysia (see Fig.1a). The total command area of the scheme is about 18000 ha. Rice is grown two times in a year, mainly from August to January (main/wet season) and February to July (off/dry season). The Bernam River is the only source of water for the irrigation supplies, which is diverted by the Bernam River Headworks (BRH) into the feeder canal. Water is conveyed into the Tengi River and thence to the intake point of the main canal at Tengi River Headworks (TRH). The distance from BRH to TRH is about 36 km. Irrigation water is directly delivered from the main canal to the tertiary canals which are spaced at 400 m apart. A standard irrigation block has a net command area of about 50-300 ha (Fig.1b). Each row of irrigation blocks receives water in their paddy plots directly from two tertiary canals. A pump house was constructed in 1962 on the lower reaches of the Bernam River in Bagan Terap to provide water supply for approximately 1000 ha in the northern portion of the area. Nonetheless, this study did not consider the command areas under the pumping scheme because this command area is irrigated through different canal networks at a relatively higher elevation than the gravity fed paddy areas.

### *Data Collection and Database Development*

Data and related information were obtained from relevant government agencies such as the Tanjung Karang Rice Irrigation Scheme Authority (IADA) for different ISAs, the Department of Irrigation and Drainage (DID), Department of Agriculture (DOA), Department of Survey and Mapping Malaysia (JUPEM) and Malaysia Meteorological Department (MMD), as shown in Table 1. The detailed features of the irrigation scheme were obtained from the Department of Irrigation and Drainage (DID). Database development was the crucial task. All the data were properly registered and assembled in the GIS system.

## *Theoretical Considerations*

Water demand estimation is the primary consideration for the irrigation scheduling of a scheme. In Malaysia, the recommended pre-designed presaturation is 2.31 l/s/ha (20 mm/day) for one month and supplementary irrigation requirement is 1.16 l/s/ha (10 mm/day) for the rice irrigation systems. The total water requirement for rice production is about 1000–1300 mm,

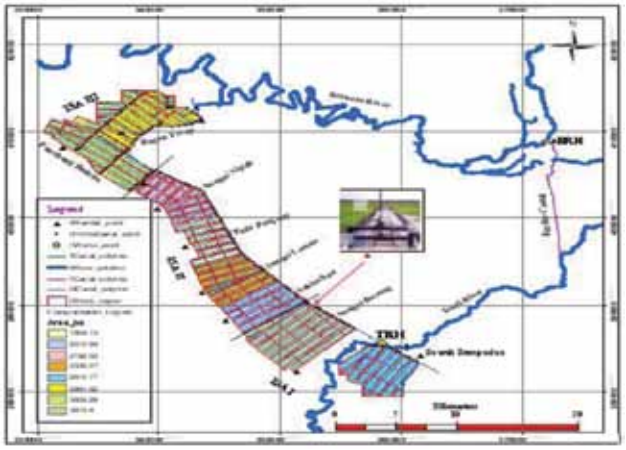

(a) Irrigation Scheme

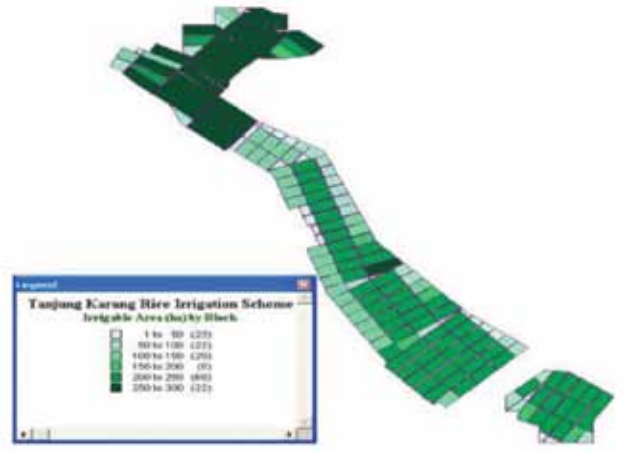


(b) Command Areas by Irrigation Block

Fig.1. Irrigation Distribution Network and Blocks of the Tanjung Karang Rice Scheme

Table 1: Required Information and Data Collected for this Study

| No. | Data type | Stations/Organization | Period of record |
|---|---|---|---|
| 1 | Daily Rainfall | 12 Stations (Dept of Irrigation and Drainage) | 1970 – 2006 |
| 2 | Daily weather events | MMD (Malaysian Meteorological Dept) | 1990 – 2006 |
| 3 | Topographic Maps | JUPEM (Malaysian Surveying Department) | Latest 1995 |
| 4 | Land use map | DOA (Dept. of Agriculture, Malaysia) | 2004 |
| 5 | Irrigation and drainage network maps | DID, Tanjung Karang Irrigation Scheme | 2004 |
| 6 | Configuration of canals and structures | DID, Tanjung Karang Irrigation Scheme | 2004 |
| 7 | Yield data | DOA, Tanjung Karang Irrigation Scheme | 2007-2008 |

depending on the characteristics of the schemes (JICA and DID, 1998). In Southeast Asia, the water requirement for pre-saturation is theoretically 150-200 mm for 2 to 4 weeks, and as high as 650–900 mm with longer duration of 24–48 days (De Datta, 1981; Rowshon, 2009).

*Water Balance Model for Paddy Field*

The field water balance provides management decisions on how the scheme ought to be operated to ensure better distribution of irrigation water. The generalized water balance equation for the paddy field can be expressed as follows:

$$WS_j = WS_{j-1} + IR_j + ER_j - ET_j - SP_j - DR_j - SR_j \quad (1)$$

Where,

$WS_j$ = ponding water depth in the field during j-th day (mm)
$WS_{j-1}$ = ponding water depth in the field during (j-1)-th day (mm)
$IR_j$ = amount of irrigation water supplied during j-th day (mm)
$ER_j$ = effective rainfall received during j-th day (mm)
$ET_j$ = crop evapotranspiration during j-th day (mm)
$SP_j$ = water lost through seepage and deep percolation loss during j-th day (cm)
$DR_j$ = drainage from paddy fields during j-th day (mm)
$SR_j$ = surface runoff from paddy fields during j-th day (mm)
j = irrigation period in (day).

*Effective Rainfall (ER)*

Effective rainfall is that portion of rainfall over the command area that potentially could contribute to the water requirements of growing rice in the field. The effective rainfall for the irrigated condition can be determined using the drainage model of the International Rice Research Institute (IRRI, 1977), as follows:

$$ER_j\left(1 - \frac{DR_j}{RF_j + IR_j}\right) * RF_j \quad (2)$$

where,

$RF_j$ = rainfall during j-th week (cm)
$DR_j$ = drainage requirement from the paddy field during j-th week (cm)

When the field water depth exceeds the maximum ponding water depth, the drainage required is:

$$DR_j = WS_j - 1 + IR_j + RF_j + ET_j - SP_j - WSmaxj \quad \text{when, } WS_j > WSmax_j \quad (3)$$

$$DR_j = WS_j - H_d \quad \text{If } WS_j > H_d \quad (4)$$

where, $H_d$ is the dike height of the paddy field in cm. A concrete box structure with flashboard or drop-board is placed at the drainage outlet of each plot to store more rainfall and maintain the desired ponding water depth as the season advances. Rainfall in excess of the flashboard

height leaves the system as surface runoff ($SR_j$).

$$SR_j = RF_j + WS_j - BH \quad (5)$$

where, BH is flashboard height in mm.

*Presaturation Irrigation Requirements*

A very large amount of water is consumed to inundate fields for pre-saturation before planting of the crop. The water required during pre-saturation period can be determined as follows:

$$SAT = \frac{IR_S + EP_S + SP + WS}{IE} \quad (6)$$

Where,

SAT = water requirement during presaturation period (mm/day)
$IR_S$ = water requirement to saturate the soil (mm/day)
$EP_s$ = evaporation loss from saturated soil surface (mm/day)
SP = seepage and percolation losses (mm/day)
WS = additional supply to maintain the initial depth of flooding (mm/day)
IE = overall irrigation efficiency

*Normal Irrigation Requirements*

The required irrigation water during the normal irrigation period shall be allocated on the basis of equation (7).

$$GIR_j = \frac{(ET_0)_j \times K_c + SP_j - ER_j}{IE} \quad (7)$$

where,

$GIR_j$ = gross irrigation water requirement (mm/day)
$(ET_0)_j$ = reference crop evapotranspiration (mm/day)
$SP_j$ = seepage-percolation loss (mm/day)
$ER_j$ = effective rainfall (mm/day)
$K_c$ = crop coefficient
IE = overall irrigation efficiency is considered to be 45% (DID and JICA, 1998).

*Irrigation Supplies for Tertiary Canals*

A GIS-integrated programme which had been developed (Rowshon *et al*., 2009) earlier was modified to determine the recommended irrigation supply for the tertiary canals as the season advances. In Tanjung Karang Rice Irrigation System, about 120 tertiary canals distribute irrigation water directly from the main canal to the paddy lots. A pair of tertiary canals passes through each row of irrigation blocks (3-5 blocks) and distributes irrigation water through the

50 mm pipe outlet for each 1.2 ha paddy lot. An empirical equation was developed to compute the recommended irrigation supply for the tertiary canals.

$$q_r = f_i \times \frac{a_i}{A} \times Q_{aV} \quad (8)$$

Where,

$q_r$ = recommended irrigation supply for tertiary canals ($m^3/s$)

$f_i$ = the operation and management factor to cater the staggered irrigation supply by one month for each ISA (for example, $f_i$ values for offtakes under ISA II and ISA III is zero in February for the off season and August for the main season so that irrigation water supplies only to ISA I and $f_i$ is zero for ISA II and ISA III)

$a_i$ = the irrigation service areas under the individual tertiary (ha)

A = total planted areas of the scheme (ha)

$Q_{av}$ = average daily available discharges for irrigation supply ($m^3/s$)

i = irrigation offtake structure number

The model can accurately recommend the irrigation supply for all the tertiary canals incorporating the actual field water demand and the available water resources as the season advances. At first, the water demand for each tertiary canal is determined. The command area for each canal is read from the GIS feature layer "Tertiary Canal*" while the other inputs are taken based on their location by ISA. After that, the proportional irrigation supplies for the tertiary canals are determined and verified with the total available discharge (*$Q_{av}$) for irrigation supply during a particular irrigation period (daily, weekly or a specified period). For the proportional allocation, the ratio of the actual planted area under each tertiary canal to the total actual planted area of the scheme is incorporated with the available water. To cover the irrigation supply for the targeted irrigation service areas throughout the scheme, the recommended irrigation supply ($q_r$) for each pair of irrigation offtakes will be normally less than or equivalent to the allowable irrigation supply (based on the available discharge for the irrigation supply). This condition must be followed to meet the recommended field water demand, unless otherwise irrigation distribution will be uneven. The prior aim must be to strengthen the regulation of the gate opening of the tertiary canals. Otherwise, some areas may not receive the right amount of irrigation supply and result in uneven allocation. As irrigation supply is staggered by one month for each ISA, the irrigation manager may adjust the irrigation supply among tertiary canals based on the priority of water demand pattern by ISA. However, the total recommended supply for all the tertiary canals must be less than $Q_{av}$ for a particular day. The recommended irrigation supply for the tertiary canals can be higher than the allowable irrigation supply when $Q_{av}$ in the main canal is sufficient to do so. However, this condition is rare during the peak water demand period. This situation can be achieved if a significant amount of rainfall is utilized as supplementary irrigation in paddy fields.

*Water Productivity Index (WPI)*

The water productivity index measures the effectiveness of the irrigation system in terms of gross rice yield and the total volume of water applied. Both the increase of rice yield per hectare and the increase of the water use efficiency are essential to improve Water Productivity Index (WPI). It is expressed as follows:

$$WPI = \frac{Y}{q} kg/m^3 \quad (9)$$

where,

Y = the specific yield, which is the yield per ha (kg/ha) for the season in the area concerned.

q = the specific supply, which is the total supply including rainfall per ha for the season in the area concerned, $m^3$/ha.

## ARCGIS-VBA USER-INTERFACE

A GIS-based user-friendly interactive system TAKRIS-SWPI (Spatial Water Productivity Index for Tanjung Karang Rice Irrigation Scheme) was developed to determine the spatial water productivity index for the rice-based system. The workflow diagram of the TAKRIS-SWPI is shown in Fig.2. TAKRIS-SWPI is an ArcGIS-VBA user-interface within the powerful ArcGIS environment which is structured with irrigation deliveries module and several sub-modules. The programme determines day-to-day irrigation supplies for the Tanjung Karang Rice Irrigation Scheme using the user-interface that allows the calculation of the spatial water productivity index after completing the irrigation season.

### *GIS User-interface Operation Procedures*

On the activation within the ArcGIS Software, the menu "TAKRIS-SWPI" appeared directly on the Menu Bar in the ArcMap Window, as shown in Fig.3. By selecting the menu item, "Open Spatial WPI (SPWI)", the programme allows viewing of the dialog wizard of the TAKRIS-SWPI, as shown in Fig.4.

### *Recommended Irrigation Supplies for the Tertiary Canals*

The module simulates the recommended irrigation supplies on a daily basis for all the tertiary canals as the season advances. A dialog window (see Fig.5) appears by clicking on the command button "Recommended Irrigation Deliveries" in Fig.4. To run the programme, the daily inputs, such as Present Standing Water Depth (SW), Recommended Standing Water Depth ($SW_{max}$ or ASW), Reference Crop Evapotranspiration (ETo), Seepage and Percolation (SP), expected daily Rainfall (RF), Crop-coefficient ($k_c$) and Irrigation Efficiency (IE), are required.

The programme allows computing the present standing water depth for each ISA using the water balance equation. This can also be obtained from field monitoring. The standing water depth can be adjusted as per the management decision for providing irrigation supplies to the priority service areas. The FAO Penman-Monteith is used for the daily inputs of ETo. The rainfall (RF) on the previous day is taken under each irrigation service area (ISA). Stochastic

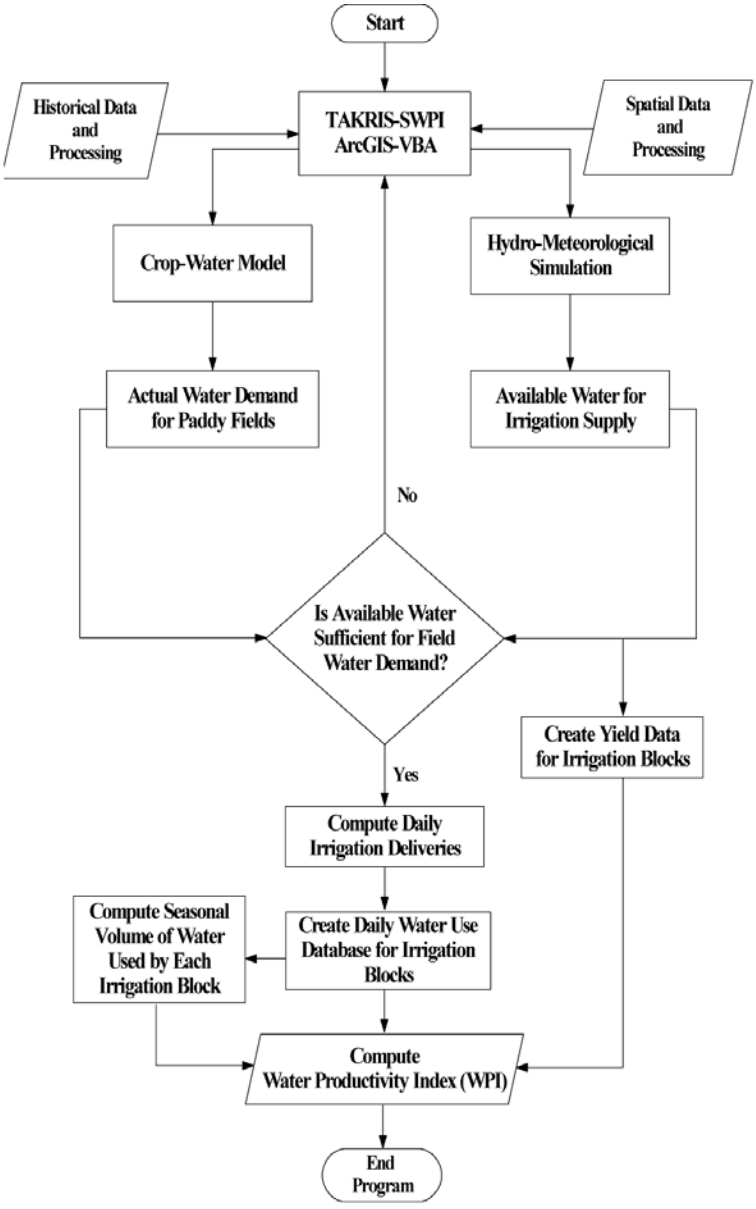


Fig.2: ArcGIS-VBA Algorithm for TAKRIS-SWPI

rainfall generation model can also be adopted in the irrigation scheduling. These values can be fed into TextBoxes by simply clicking on the Command Buttons in the sub-modules of FAO Penman-Monteith method (Allen *et al*., 1998) and the stochastic rainfall model (Fig.5).

By clicking on the command button, "Inflow at TRH" in Fig.5, the available discharge for the irrigation supplies (i.e. 26.54 $m^3/s$ on 10 November, 2008) can be estimated at the intake point of the main canal. A sub-routine for the Autoregressive model is linked with the command button "Inflow at TRH". This can be fed directly upon getting the observed data at the intake point. The installation of the real time discharges monitoring station is in progress. To ensure

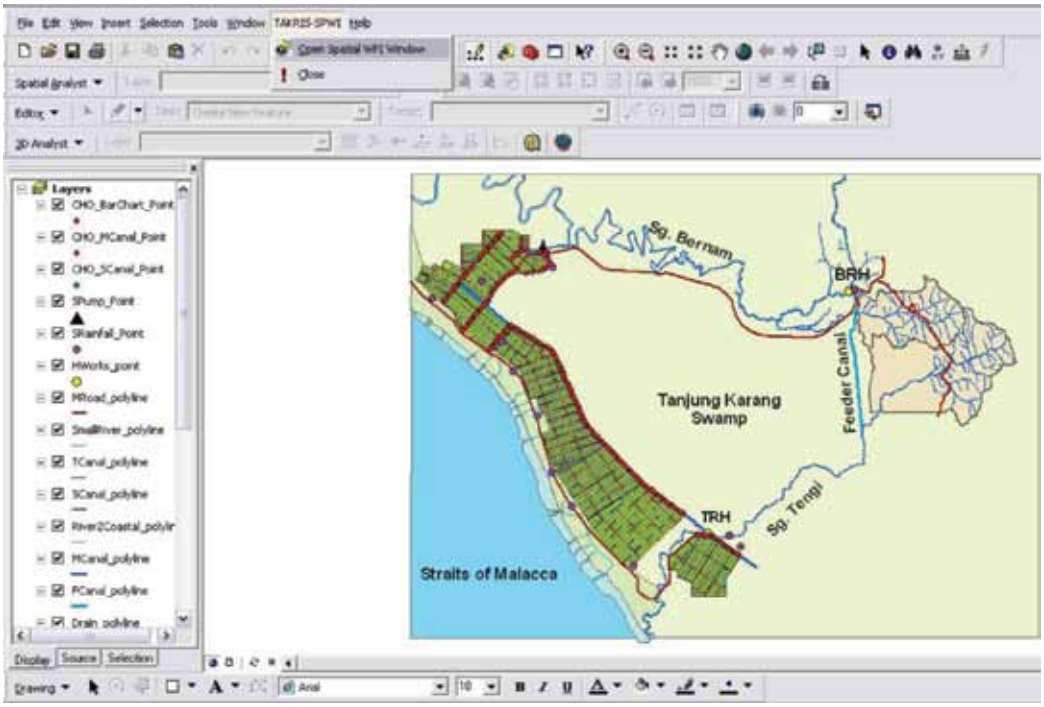


Fig.3: TAKRIS-SWPI Menu showing the Tanjung Karang Irrigation Scheme

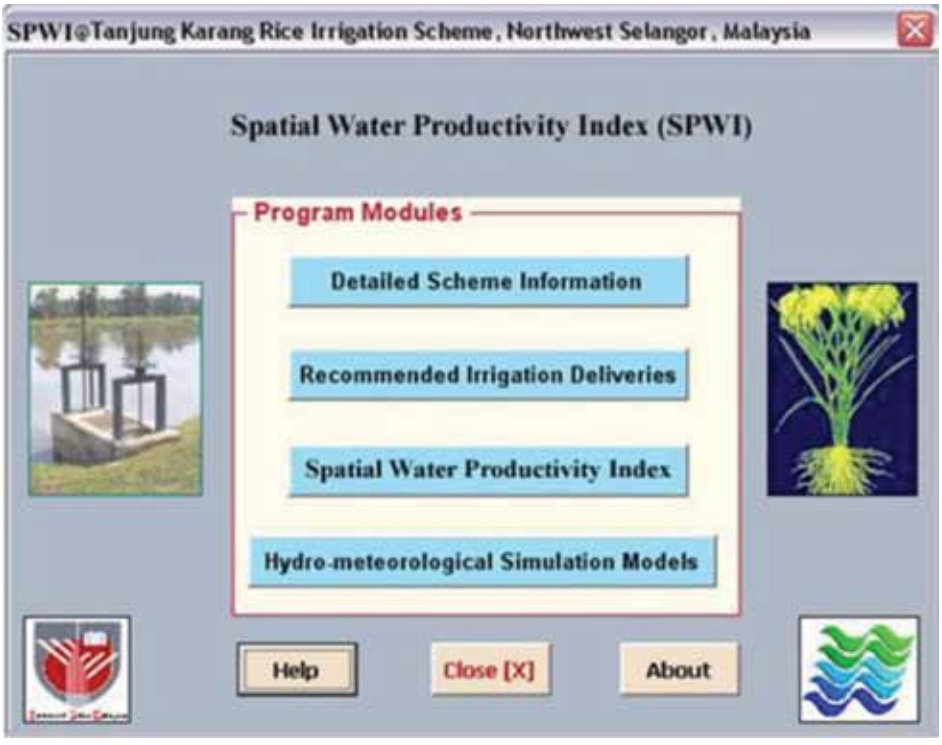


Fig.4: Dialog Wizard for Irrigation Deliveries and WPI

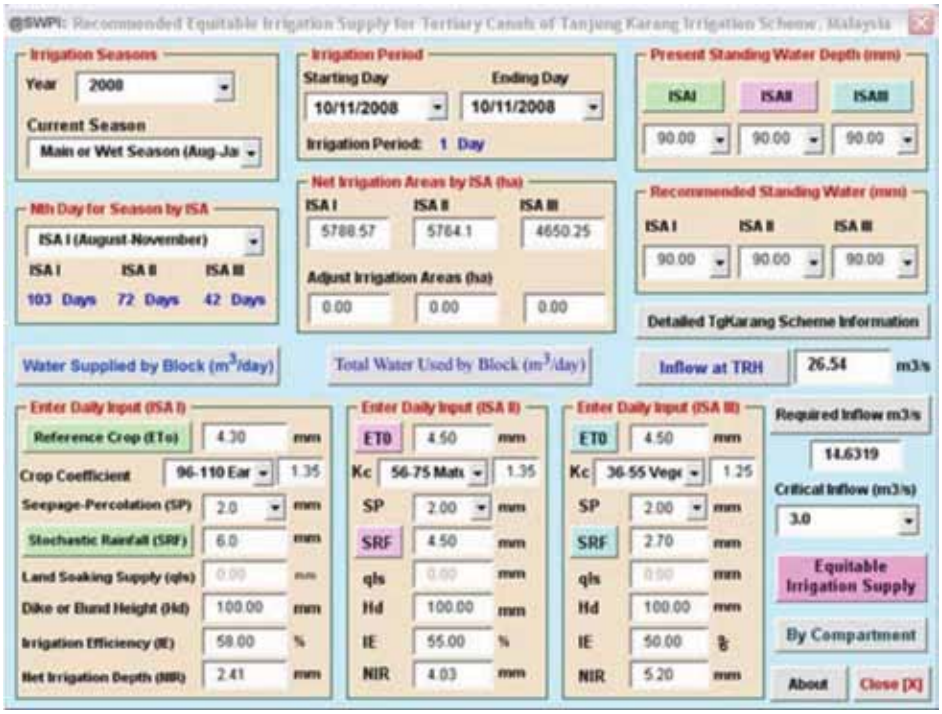


Fig.5: Dialog Wizard for Recommended and Equitable Irrigation Water Allocation by Tertiary Canals, 10 November 2008

the irrigation supply for all the tertiary canals on a particular day, the total recommended irrigation supply should not exceed the total available discharge i.e. 14.63 < 26.54 $m^3/s$. This condition can ensure an adequate irrigation supply for the targeted service areas. The total required discharge for the recommended supply is computed and displayed in the TextBox (i.e. 14.63 $m^3/s$) while changing the values of parameters in Dialog Wizard. The programme allows irrigation supply to the areas with priority by optimizing the input parameters. This decision is dependent on several factors including ponding water depth, utilization of rainfall, crop growth period and intermittent agricultural practices. After checking and adjusting the inputs, the daily recommended supplies for the tertiary canals are simulated. After this, the irrigation supply by block is computed by the command button "Water Supply by Block ($m^3$/day)" and then the total water used (Irrigation and Rainfall) by each irrigation block is computed and stored in the database by the command button "Total Water used by Block ($m^3$/day)".

*Reference Crop Evapotranspiration (ETo) Calculation*

The FAO Penman-Monteith method was used to compute the daily reference crop evapotranspiration (Allen *et al*., 1998). A sub-routine which allows the irrigation managers to compute the daily Reference Crop Evapotranspiration (ETo) was developed based on the available meteorological data for a particular day. The system allows for storing all the inputs and outputs into the MS Access database.

*Geospatial Water Productivity Index (PWI)*

A step-by-step calculation of the spatial water productivity index is shown in Fig.6. A dialog window as the one shown in Fig.7 appears by clicking on the command button "Spatial Water Productivity Index" in Fig.4. The "General Information of the Scheme" helps to explore scheme information such as irrigation date and irrigation command areas under Block, Compartment, Irrigation Service Area and Irrigation Season. An easy update system of the associated database keeps the system to be always updated in respect of the real field situation.

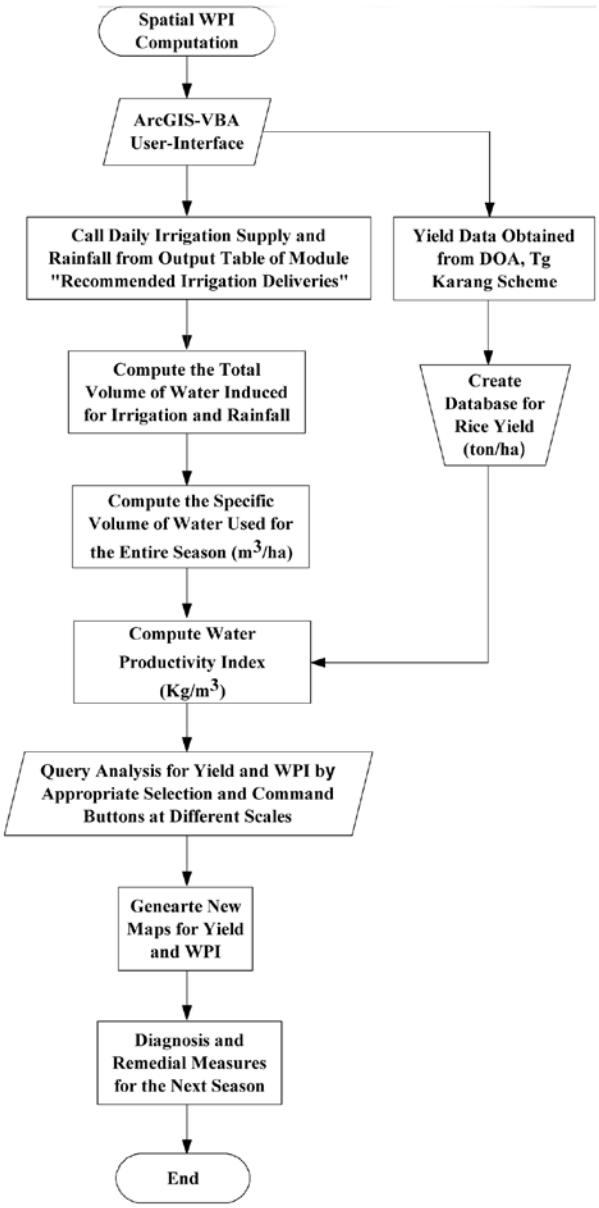


Fig.6: ArcGIS-VBA Algorithm for Spatial Water Productivity Index Calculation

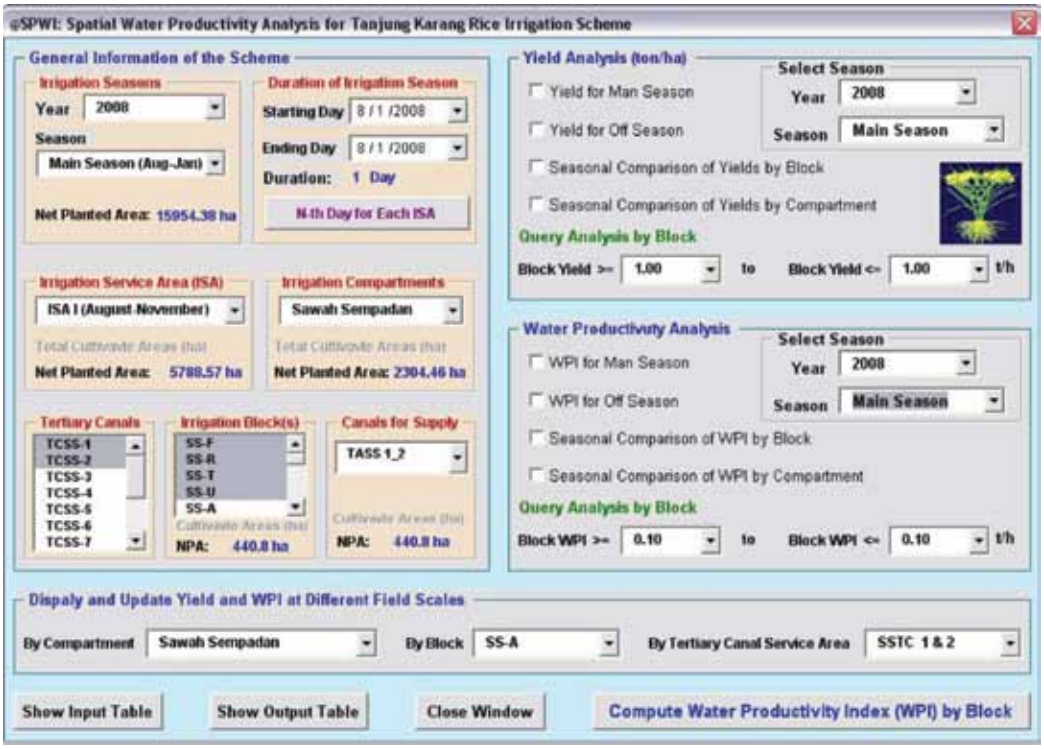


Fig.7: Dialog Wizard for Computing Spatial Water Productivity Index (SPWI)

The water productivity index is one of the important performance indicators which describe the relationship between water use and yield. The programme provides information for the scheme at different scales, i.e. irrigation block (50-300 ha), irrigation service area under each tertiary canal (2-5 irrigation blocks), irrigation compartments (8 compartments) and the scheme. After developing a proper database on the basic inputs by irrigation block, the water productivity index (WPI) and yield can be computed and analyzed at different scales. The command button "Compute Water Productivity Index (PWI) by Block" computes the spatial WPI for irrigation blocks. The user needs to select the appropriate items and options for viewing the results from Fig.10. Many command buttons shown in the parts, "Yield Analysis (tonnes/ha)" and "Water Productivity Analysis", are available to analyze the spatial rice yield and WPI. The other part, "Display and Update Yield and WPI at Different Scales", allows updating of data and provides yield and WPI information for each compartment, block and irrigation blocks (2 - 5), which are usually under two Tertiary Canals. The entire information can be displayed using the command buttons "Show Input Table" and "Show Output Table".

## RESULTS AND DISCUSSION

### *Simulation of the Recommended Daily Irrigation Deliveries*

To simulate the recommended supplies for the equitable water allocation, the ratio of the actual planted area under each tertiary canal to the total actual planted area of the scheme is

incorporated with the available discharge for irrigation supply and the actual water demand. To cover the irrigation supply for the targeted service areas of the scheme, the recommended equitable irrigation supply through each irrigation off-take structure should be less than or equivalent to the allowable irrigation supply. An allowable irrigation supply for a particular canal is the product of the available discharge for the irrigation supply in the main canal and the ratio of the actual planted area under each tertiary canal to the total actual planted area of the scheme.

Irrigation supply can be adjusted based on the priority of water demands by the tertiary canals within ISAs. For a particular day, the total recommended supply for the scheme must be less than the available discharge for the irrigation supply in the main canal (i.e. 14.63 < 26.54 in Fig.5). Then, the recommended irrigation deliveries for the tertiary canals are shown by clicking on the command button "Equitable Irrigation Supply" at the bottom right corner in Fig.5. The output is displayed instantly as shown in Fig.8. The gate operation for the irrigation off-take structures must be strengthened to release the recommended deliveries for the tertiary canals. The results displayed in maps, tables, and graphs can help the irrigation manager to diagnose the irrigation system and take the proper decisions for the gate operations, such as on 10th November in the main season, the recommended supplies among tertiary canals with respect to the allowable and design supplies are shown in Fig.8.

The name and information can be displayed together on the screen whenever the cursor is placed over the particular object of the map layout. This facilitates the irrigation manager to

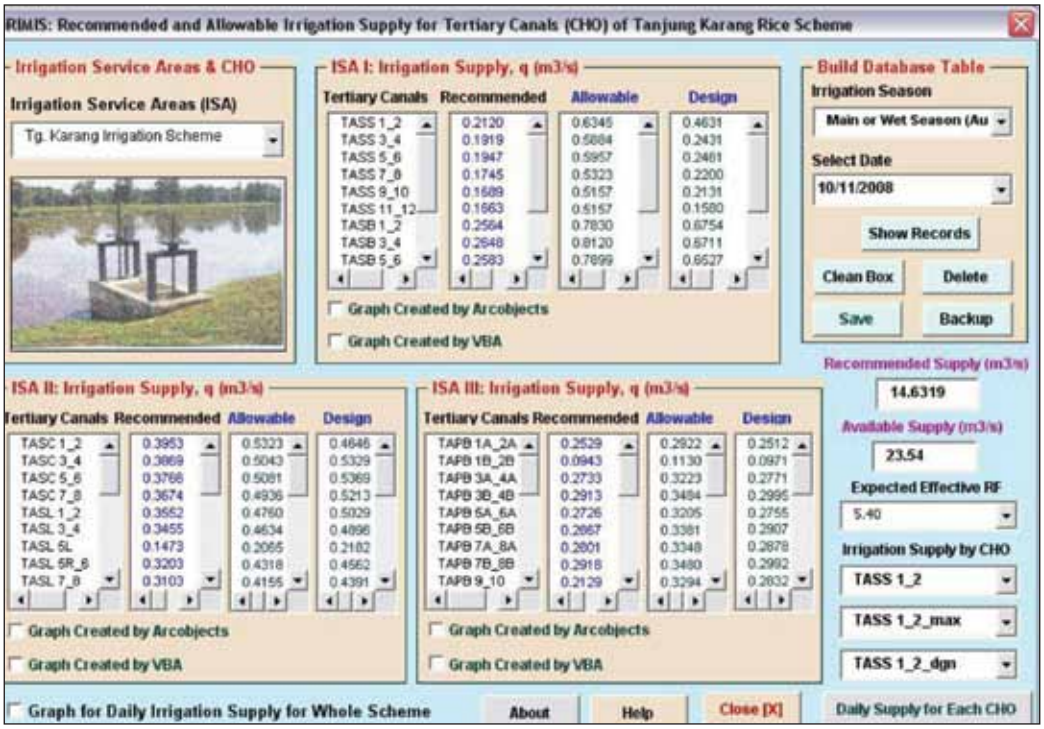


Fig.8: The Output Dialog Wizard for Recommended and Equitable Irrigation Water Allocation for all Tertiary Canals on 10 November 2008.

determine the amount of deliveries for each irrigation block and the irrigated service area. The spatial distribution of the total amount of irrigation supply throughout the irrigation blocks can be computed and displayed (*see* Fig.9) by clicking on the command button "Water Supplied by Block $m^3$/day" from Fig.5.

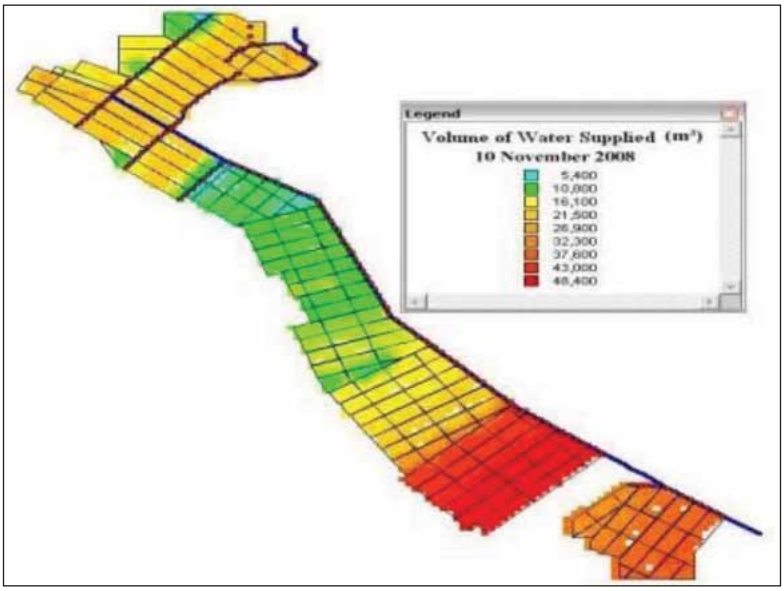


Fig.9: Volumetric Irrigation Distribution in Irrigation Blocks on 10 Nov 2008

Record keeping on the daily irrigation task in the database is essential to diagnose the irrigation distribution for each tertiary unit as the season progresses. The irrigation off-take gate at the head of the tertiary canal is called CHO (Constant Head Orifice). The programme provides tracking of seasonal irrigation supply on the daily basis for each row of the tertiary canals by clicking on the command button "Daily Supply for Each CHO" after selecting the tertiary canals in the ListBox "Irrigation Supply by CHO".

*Seasonal Yield Analysis by Irrigation Block*

The yield of the scheme for 1998-2002 obtained was around 4.47 t/ha in the off season and 4.65 t/ha in the main season, respectively. The thematic map created for the average yield obtained for the main season and the off season of the scheme in 2008 is shown in Fig.10.

*Water Productivity Index (WPI)*

The analysis for the entire irrigation season was done by summing the daily data to compute the water productivity index. The programming module can call on the database of the spatial and temporal data to produce the tabular and graphical output by SQL (Structure Query Language). The programme allows updates of the database on a random basis. The browser window displays when the user selects an option from the ListBox within the GroupBox window "Display and Update Table". The user can update information during on-going seasons

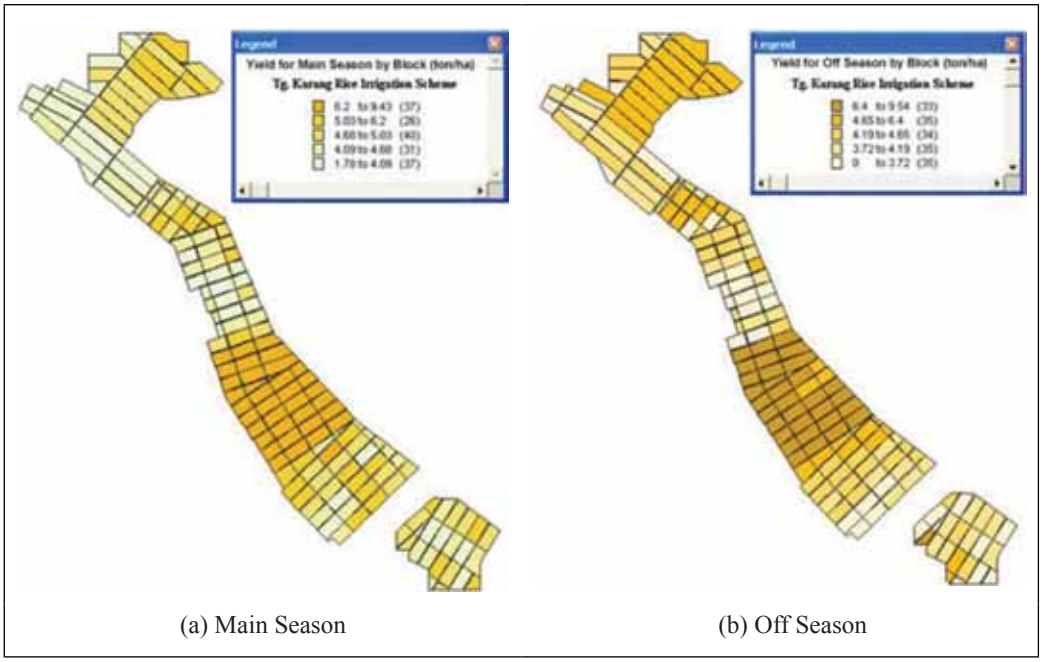


(a) Main Season (b) Off Season

Fig.10: Seasonal average rice yields by block in 2008

through options available in the dialog windows. The yield database file for an individual block is developed by season.

The water productivity index can be computed and stored in the output database using the command button "Compute Water Productivity Index (PWI) by Block" as shown in Fig.7. The computed WPI can be displayed instantly by selecting the check boxes "WPI for Main Season" and "WPI for Off Season" from Fig.7. The spatial distribution of the WPI within irrigation blocks for the main season and off season is shown in Fig.11a.

The Water Productivity Index provides a measure of the irrigation system's effectiveness in terms of gross grain yield. The values of the WPI ranged from 0.02 to 0.57 kg/m$^3$ in the main season and from 0.02 to 0.40 kg/m$^3$ in the off-season, respectively (*see* Fig.11b). The average values for the main season and off-season were found to be 0.25 and 0.21 kg/m$^3$, respectively. This is below the desirable targets of 0.30 to 0.60 kg/m$^3$. The two factors which directly affect the WPI are specific supply (m$^3$/ha) and specific yield (kg/ha). The specific supply can be reduced through utilization of rainfall. An acute shortage of the irrigation supply is the main reason for the low productivity in the off-season. The thematic map gives an excellent explanation of the spatial variation of WPI among the irrigation blocks. Meanwhile, query analysis can be done for the yield and WPI by selecting the range on the basis of irrigation block. The WPI > 0.40 for the main season can be retrieved from the database and is displayed on the irrigation blocks map, as shown in Fig.12. The highest productive irrigation blocks are shown in the highlighted area in following figure.

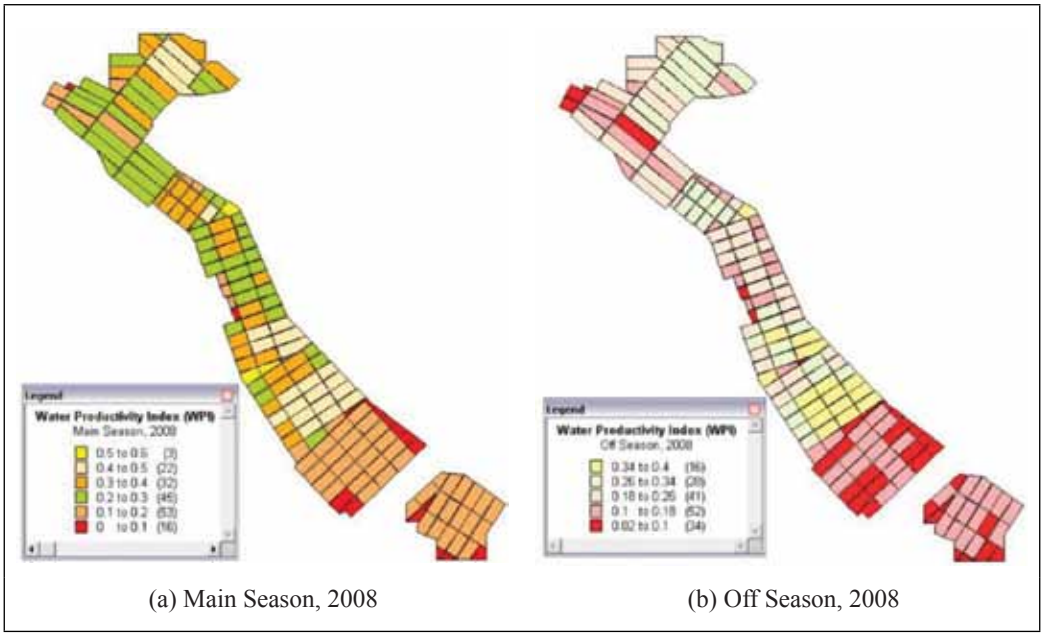


(a) Main Season, 2008 (b) Off Season, 2008

Fig.11: Seasonal Spatial Distribution of WPI for Irrigation Blocks in 2008

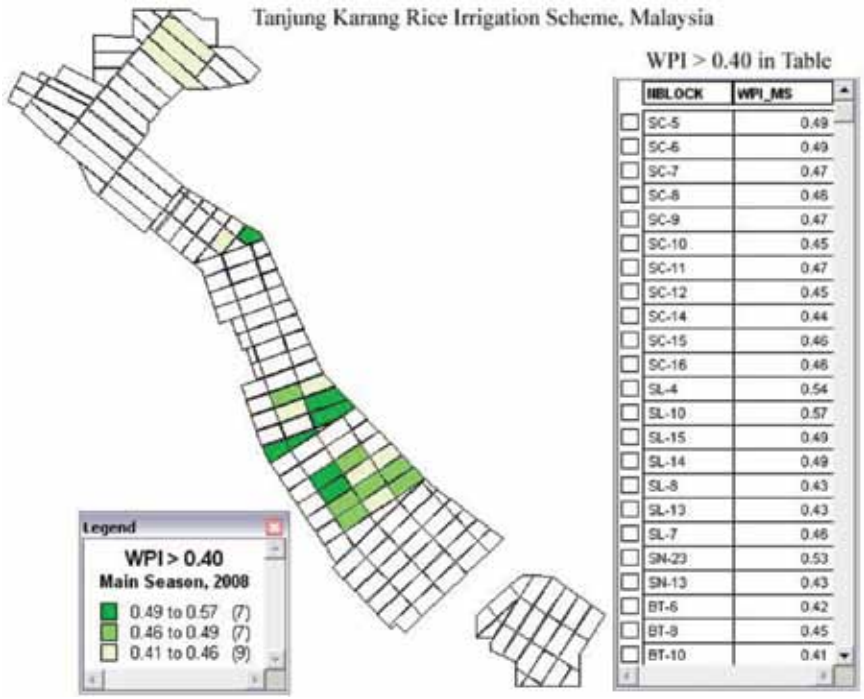


Fig.12: Irrigation Blocks where WPI > 0.40 for Main Season in 2008

## CONCLUSIONS

To get an accurate calculation of Water Productivity Index (WPI) is obviously a difficult task as it requires the calculation of the amount of water delivered or agricultural water use for each irrigation operation. It is normally calculated using the monthly or seasonal data obtained from the projects and/or various organizations. This paper focuses on a systematic computation procedure to calculate the volume of water used from the beginning to the cut-off of irrigation supply for rice production. A GIS-based user-interface programme was developed to compute and depict the spatial variation of the WPI within the irrigation blocks. There is a significant spatial variation of WPI among the irrigation blocks in every season. The temporal variability was not discussed in this paper as the programme was run to estimate the quantity of water used in rice production only for one year. This can be done after several years of running the programme. More importantly, the programme is useful to be used in determining the rate of increase or decrease of both rice production and water productivity index. The programme can be extended on the basis of the smallest scale such as each irrigation or paddy lot. There are about 17000 paddy lots of approximately 1.2 ha to 2 ha each. At the moment, it is difficult to get yield data for each paddy lot from the farmers. This programme can be used to take possible remedial measures and rectification on water management model, as well as irrigation operation to increase water productivity in the next season as the analysis of the spatial variability can clearly depict the low productive areas. This approach could be useful to procure the right information about irrigation water use for crop production and to investigate the rate of seasonal changes of water productivity index. Apparently, this useful information is probably important for the planning and decision making on water use for other water-related projects either in agriculture or other sectors. This is because the approach can depict the gaps between the existing and appropriate water management practices using the spatial variability of WPI. Suitable interventions could be made to fill the gaps and to enhance water use efficiency at field level and can also help in saving irrigation water in the forthcoming season. The analysis shows that the potential of the crop-water simulation models in considering varying soil, water, crop and climate conditions can be incorporated to determine WPI accurately. In addition, this systematic approach could be adopted for any irrigation system with the required modification.

## ACKNOWLEDGEMENTS

The authors gratefully acknowledge the research grants from the Ministry of Science, Technology and Innovation (MOSTI), and the support from Research Management Centre (RMC), Department of Biological and Agricultural Engineering, Faculty of Engineering, and the Institute of Advanced Technology (ITMA) of Universiti Putra Malaysia (UPM).

## REFERENCES

Abdullaev, I., & Molden, D. (2004). Spatial and temporal variability of water productivity in the Syr Darya Basin, Central Asia. *Water Resources Research*, *40*, W08S02.

Aggarwal, P. K., Talukdar, K. K., & Mall, R. K. (2000). Potential yields of rice–wheat system in the Indo-Gangetic plains of India. *Rice–Wheat Consortium Paper Series, 10*, 16.

Allen, R. G., Pereira, L. S., Dirk, R., & Martin, S. (1998). Crop Evapotranspiration: Guidelines for Computing Crop Water Requirements, FAO Irrigation and Drainage Paper-No 56. Rome, Italy.

Bhuiyan, S. I., Sattar, M. A., & Khan, M. A. K. (1995). Improving water use efficiency in rice irrigation through wet seeding. *Irrigat. Sci., 16*, 1–8.

Cook, S., Gichuki, F., & Turral, H. (2006). Agricultural Water Productivity: Issues, Concepts and Approaches, Basin Focal Project Working Paper No. 1.

Droogers, P., & Bastiaanssen, W. G. M. (2002). Irrigation performance using hydrological and remote sensing modelling. *J. Irrig. Drain. Eng., 128*, 11–18.

De Datta, S. K. (1981). *Water Management Practices for Rice. Principles and Practices of Rice Production*. New York: Wiley.

Goodchild, M. F. (1993). *The state of GIS for environmental problem solving. Environmental Modeling with GIS*. Oxford: Oxford University Press.

Immerzeel, W. W., Gaur, A., & Zwart, S. J. (2008). Integrating remote sensing and a process-based hydrological model to evaluate water use and productivity in a South Indian catchment. *J. Agricultural Water Management, 95*, 11–24.

IRRI. (1977). *Annual Report for 1977*. International Rice Research Institute, Los Banos, Philippines.

JICA, & DID (1998). *The study on Modernization of Irrigation Water Management System in the Granary Area of Peninsular Malaysia, Draft Final Report, Volume –II*. Annexes, March 1998, Japan International Cooperation Agency.

Kijne, J., Barker, R., & Molden, D. (2003). *Water productivity in agriculture: limits and opportunities for improvement. Comprehensive assessment of Water Management in Agriculture, Series No. 1*. Wallingford, UK: CABI press.

MOA. (Minsitry of Agriculture) (2008). *Agricultural Statistical Handbook*. Malaysia: MOA

Molden, D., & Sakthivadivel, R. (1999). Water accounting to assesses and productivity of water. *J. Water Resour. Dev., 15*(1/2), 55–72.

Molden, D., Murray-Rust, H., Sakthivadivel, R., & Makin, I. (2001). *A water productivity framework for understanding and action*. Paper presented at the Workshop on Water productivity. Wadduwa, Sri Lanka, November 12 and 13, 2001.

Rowshon, M. K., Amin, M. S. M., Lee, T. S., & Shariff, A. R. M. (2009). GIS-integrated Rice Irrigation Management System for a River-fed Scheme. *J. Water Resources Management, 23*(14), 2841-2866.

Star J., & Estes J. (1990). *Geographical Information Systems: An Introduction*. Englewood Cliffs, NJ: Prentice-Hall.

Teh, S. K. (1998). *Sustainable Rice Production*. Malaysian National Congress of Irrigation and Drainage-Annual Conference held on 13th October 1998. Alor Setar, Kedah, Malaysia.

Pertanika J. Sci. & Technol. 20 (2): 401 - 407 (2012)

SCIENCE & TECHNOLOGY

Journal homepage: http://www.pertanika.upm.edu.my/

# Synthesis of Polymeric Nanogel via Irradiation of Inverse Micelles Technique

**Yusof Hamzah[1*], Naurah Mat Isa[2] and Wan Md Zin Wan Yunus[3]**

[1]*Radiation Technology Division, Malaysian Nuclear Agency, Bangi, 43000 Kajang, Selangor, Malaysia*

[2]*Radiation Facility Division, Malaysian Nuclear Agency, Bangi, 43000 Kajang, Selangor, Malaysia*

[3]*Department of Chemistry, Faculty of Science, Universiti Putra Malaysia, 43400 Serdang, Selangor, Malaysia*

## ABSTRACT

Covalently cross-linked nanogels were prepared via irradiation of inverse micelles that had been prepared from radiation crosslinkable polymer, water, oil and surfactant. A mixture of polymer, water, heptane and sodium dioctyl sulfosuccinate (AOT) at certain compositions forms inverse micelles with the size ranging from 2 to 8 nm. The hydrophilic head of the surfactant facilitates encapsulation of water soluble polymer. If the entrapped polymer is radiation crosslinkable, it is expected that upon irradiation, polymerization shall take place in such small and confined space, leading to formation of nano-sized polymeric gel. Meanwhile, emulsion at 2 nm size was chosen for gamma irradiation process. The formation of the nano-sized discreet gel using irradiation of inverse micelles technique was proven at a dose as low as 5 kGy to obtain nanogel sized ~ 95 nm.

**Keywords: Polymer, nanogel, radiation**

## INTRODUCTION

Nanogel refers to gel that is less than 100 nm size. It is a well known fact that in this size range, almost all materials will have several advantages that are not seen in their macro form. In this case, among the advantages are large surface areas for better attachment of ligand and prolong stability in the blood stream. These advantages are useful, especially that this gel is used in the treatment of diseases which need a constant drug concentration in the blood (Hashida *et al*., 1996).

The methods used to synthesize such materials can be categorized into two. The first is the classical chemistry routes (McAllister *et al*., 2002; Oh *et al*., 2008; Vinagradov *et al*., 2002) and the radiation route (Ulanski *et*

*Article history:*
Received: 25 July 2011
Accepted: 13 January 2012

*Email addresses:*
m_yusof@nuclearmalaysia.gov.my (Yusof Hamzah),
naurah@nuclearmalaysia.gov.my (Naura Mat Isa),
wanzin@science.upm.edu.my (Wan Md Zin Wan Yunus)
*Corresponding Author

ISSN: 0128-7680 

*al.,* 1999). The classical chemistry route is normally multi-steps and it involves prohibitive and harmful toxin substances which are used as initiators, additives and crosslinking agents. The radiation route, on the other hand, offers a simpler, more efficient and cleaner process (Rosiak *et al., 2002*).

When an aqueous medium is irradiated with an ionizing radiation, absorption of the energy from the irradiation source will occur, and this will then lead to the formation of hydroxyl radicals, hydrogen atoms and solvated electrons in the medium. Out of the three species, hydroxyl radical is known to be responsible for abstracting hydrogen atom from macromolecules (Alexander *et al.,* 1957). This species may react with crosslinkable polymeric macromolecules to create active sites. When two or more of these macromolecules with active sites are in close proximity, the combination may take place and thus form 3D covalent links between the chains (known as the intermolecular crosslinking). This will finally lead to wall-to-wall gelation (macrogel). If the combination process proceeds in a confined space such as in a micelle, discreet gel is expected to form. Polymerization in such a confined space will result in the formation of single gel particle, and normally, the size of the gel formed has a dependency on the size of the micelle used. In this work, the use of inverse micelles from AOT was demonstrated as nanoreactor to produce polyethylene glycol diacrylate (PEGDA) nanogel.

## MATERIALS AND METHODS

### *Materials*

PEGDA, with an average molecular weight of around 700, AOT and n-heptane (99.5%) were purchased from Sigma Aldrich. PEGDA, AOT and n-heptane were used without further purification. Ultrapure water was used throughout the research.

### *Ternary Diagram*

Inverse micelles were formed by adding AOT into a series of PEGDA and n-heptane mixture until clear micro emulsions were formed. Suitable conditions for microemulsions formation were identified through systematic mapping of ternary phase diagrams. The ternary phase diagram of the PEGDA in n heptane microemulsion system is shown in Fig.1. The area which is covered by the black dotted lines represents the single-phase transparent microemulsion. In this work, the formulations are taken from the lower right part of the ternary diagram, where it is hypothetically known to yield clear single-phase inverse micelles that are smaller than 100 nm (Calvo *et al.,* 1997).

### *Preparation of Emulsion*

Emulsions were prepared by dissolution of PEGDA in ultrapure water, stirring and filtering it with 0.45 μm (Minisart, Sartorius). After that, 10 ml of PEGDA was added into 100ml of n-heptane containing 0.05 to 0.25 of AOT. The size of emulsion formed was measured using dynamic light scattering and the smallest size of emulsion was found to be 2 nm, and the emulsion of this particular size was chosen for electron beam irradiation process.

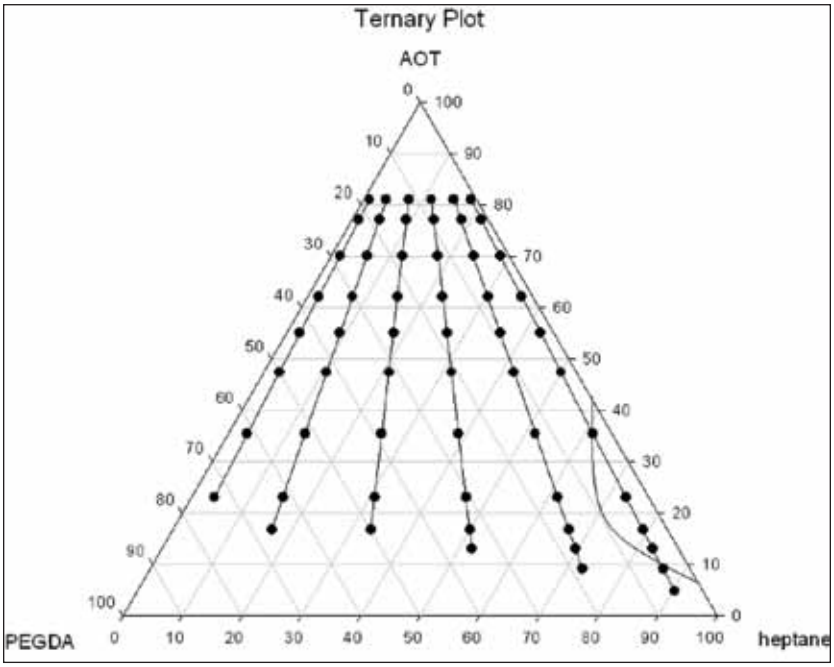


Fig.1: Ternary plot diagram PEGDA/AOT/n-heptane with the hypothetical single phase region containing W/O micelles represented by the curve

*Preparation of Nanoparticle*

The PEGDA solution (10%) was prepared by dissolving the polymer in ultrapure water by stirring overnight at room temperature. 10 ml of the PEGDA solution was added into 100 ml of n-heptane containing 0.15 M of AOT. The mixture was then irradiated at 1, 3, 5, 10, 15, 20 and 30 kGy with 3 MeV of voltage and 5 mA of beam current. All the mixtures were saturated with argon gas prior to the irradiation. The nanogel formed during the irradiation process was then recovered by evaporating n-heptane using a rotary evaporator and precipitating the dry mass with an acetone methanol (9:1) solution. The precipitate was then washed 5 times with the acetone alcohol solution to remove the excess of AOT. After the washing process, the precipitate was solubilised in ultrapure water, followed by dialysis using 12 kD cut off dialysis membrane (Spectrum) and was finally lyophilized.

*Dynamic Light Scattering Studies*

Dynamic light scattering (DLS) studies were done using DLS spectrometer of Nanophox from Sympatec GmbH (Germany) with a 10 mWatt HeNe laser beam at a wavelength of 632.8 nm at 90$^{o}$ scattering angle at room temperature. Prior to the measurement, the lyophilized nanogel was resolubilized in ultrapure water and filtered with 0.22 μm pore size filter (millipore). The 3D cross correlation of the function of the scattering intensity was analyzed using a cumulant analysis to obtain the hydrodynamic diameter, $D_h$, and the dispersity information for the particles.

## RESULTS AND DISCUSSION

AOT is a surfactant with hydrophilic head with two hydrocarbon tails (*see* Fig.2a) and simplified in this article as in Fig.2b for ease of depiction. It has been reported elsewhere that dissolution of AOT, at a critical micellar concentration in non-polar solvent such as n-heptane, forms a thermodynamically stable inverse microemulsion (Ming *et al.,* 1998). In water-oil mixture, the hydrophilic heads of the surfactant are oriented inward, thus entrapping aqueous cores, whereas the non-polar groups or the tails are extended outwards into the hydrophobic phase. This condition makes each microemulsion a suitable template for polymerization of water soluble crosslinkable polymer such as PEGDA (Fig.3a). Microemulsion with a narrow size distribution in the range of 2 nm was observed by DLS upon addition of 10% PEGDA into 0.15 M AOT in n-heptane. By decreasing the amount of AOT for the same system, a larger size of microemulsion was observed. This particular trend is consistent with the data obtained for acrylamide in the AOT system (Candau *et al.,* 1984; Shervani *et al.,* 2000). The size increase of the microemulsion was observed with an increase in the amount of AOT. Upon irradiation on such ternary system, energy imparted will be absorbed by the oil phase producing excess of electron, which will be scavenged by the micelles in the system producing solvated electron, $e^-_{aq}$ (Joshi *et al.,* 2003; Gebicki *et al.,* 2000) and hydroxyl radical by direct radiolysis of the water core surrounded by AOT (Joshi *et al.,* 2003). The unstable hydroxyl radical will react with the entrapped PEGDA to form macroradicals through hydrogen abstraction (Fig.3b). The macroradicals will then undergo combination (Fig.3c) within the micro emulsion forming nanogel (Fig.3d). It was observed that the size of the nanogel increased with the increasing dose (*see* Table 1). This could be due to the diffusion of micelles that leads to a combination of macroradicals from different micelles during longer irradiation period for higher doses.

Table 1: The effect of irradiation dose on the particle size

| Dose (kGy) | Size (nm) ± error (nm) |
|---|---|
| 0 | 0 |
| 1 | 0 |
| 3 | 0 |
| 5 | 95.8 ± 1.3 |
| 10 | 276.8±60.5 |
| 15 | 368.7±50.6 |
| 20 | 409.1±47.6 |
| 30 | 461.4±54.9 |

## CONCLUSIONS

Polymeric nanogel can be synthesized via irradiation of inverse micelles. The inverse micelles with size of 2 nm can be used to entrap radiation crosslinkable polymer. The formation of the nanosized discreet gel has proven that inverse micelles can be utilized as a nanosized reactor in synthesizing covalently cross-linked nanosized gel.

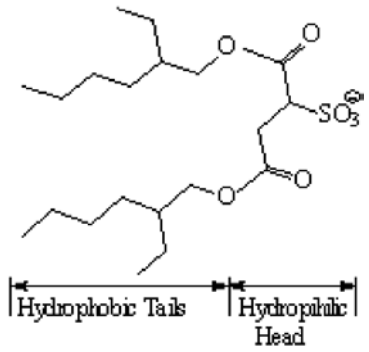


Fig.2(a): Molecular structure of AOT

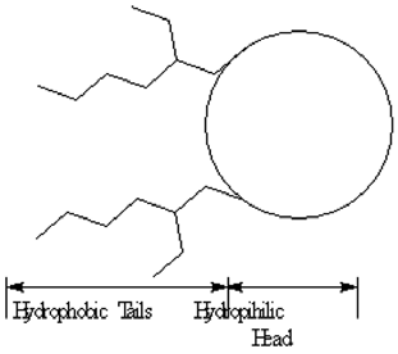


Fig.2(b): A simplified molecular structure for AOT with hydrophilic head and hydrocarbon tails

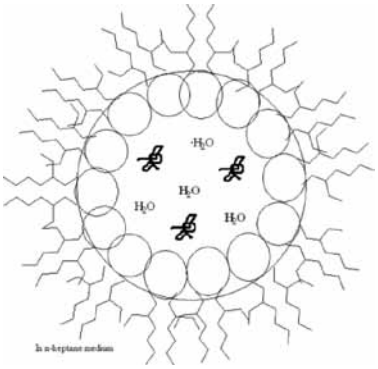

Fig.3(a): Microemulsions formed above critical micelle concentration, with the heads of the surfactant oriented inwards to the water phase and the tails are extended outwards into the oil phase.

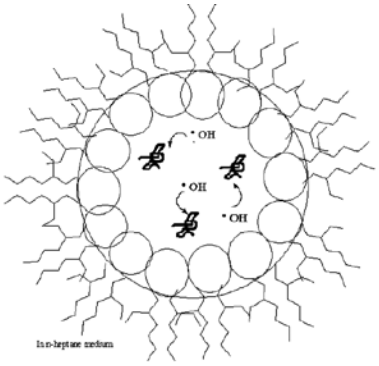

Fig.3(b): The PEGDA polymerization initiation in the micelle by hydroxyl radicals produced by irradiation.

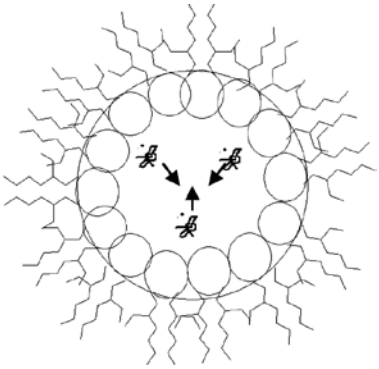

Fig.3(c): The PEGDA macroradicals combination to produce polymer networks.

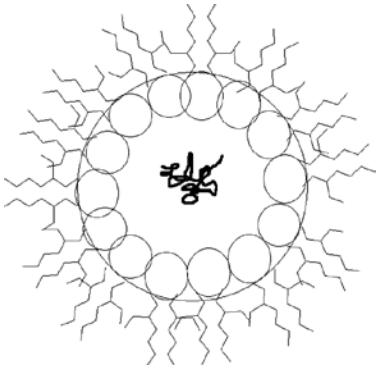

Fig.3(d): Nanogel particle produced

## ACKNOWLEDGEMENTS

The authors are grateful to the IAEA for providing aid in term of Coordinated Research Programme meetings (Research Agreement No. 15464). This project was funded by the Government of Malaysia through RMK 9.

## REFERENCES

Alexander, P., & Charlesby, A. (1957). Effect of x rays and gamma rays on synthetic polymers in aqueous solution. *Journal of Polymer Science, 23*, 355-375.

Bellocq, N. C., Pun, S. H., Jensen, G. S., & Davis, M. E. (2003). Transferrin-containing, cyclodextrin polymer-based particles for tumor-targeted gene delivery. *Bioconjugate Chemistry, 14*, 1122–1132.

Calvo, P., Lopez, C. R., Vila-Jato, J. L., & Alonso M. J. (1997). Chitosan and chitosan/ethylene oxide-propylene oxide block copolymer nanoparticles as novel carriers for proteins and vaccines. *Pharmceutical Research, 14*, 1431–1436.

Candau, F., Leong, Y. S., Pouyet, G., & Candau, S. (1984). Inverse microemulsion polymerization of acrylamide: Characterization of the water-in-oil microemulsions and the final latex. *Journal of Colloid and Interface Science, 101*, 167-183.

Gebicki, J. L., & Bednarek, P. (2000). Electron processes in AOT reverse micelles. Part 2. Influence of oil phase. Pulse radiolysis study. *Journal of Molecular Structure, 555*, 227–234.

Hashida, M., Nishikawa, M., & Takakura, Y. (1990) . *Receptor-mediated cell specific delivery of drugs to the liver and kidney*. Tokyo, Japan: Springer-Verlag.

Joshi, R., & Mukherjee, T. (2003). Hydrated electrons in water-in-oil microemulsion: a pulse radiolysis study. *Radiation Physics and Chemistry, 66*, 397–402.

Kim, S. H., Jeong, J. H., Chun, K. W., & Park, T. G. (2005). Target-specific cellular uptake of PLGA nanoparticles coated with poly (L-lysine)–poly(ethylene glycol)–folate conjugate. *Langmuir, 21*, 8852-8857.

Kohler, N., Sun, C., Wang, J., & Zhang, M. (2005) . Methotrexate-modified superparamagnetic nanoparticles and their intracellular uptake into human cancer cells. *Langmuir*, *21*, 8858–8864.

McAllister, K., Sazani, P., Adam, M., Cho, M. J., Rubinstein, M., Samuski, R. J., & DeSimone, J. M. (2002). Polymeric nanogels produced via inverse microemulsion polymerization as potential gene and anti sense delivery agent. *Journal of the American Chemical Society*, *124*, 15198-15207.

Ming, W., Jones, F. N., & Fu, S. K. (1998). Synthesis of nanosize poly(methyl methacrylate) microlatexes with high polymer content by a modified microemulsion polymerization. *Polymer Bulletin*, *40*, 749–756.

Moghimi, S. M., Hunter, A. C., & Murray, J. C. (2001). Long circulating and target specific nanoparticles: theory to practice. *Pharmacological Review*, *53*, 283-318.

Oh, J. K., Drumright, R., Daniel, J. S., & Matyjaszewski, K. (2008). The development of microgels/ nanogels for drug delivery applications. *Progress in Polymer Science*, *33*, 448-477.

Rosiak, J. M., Janik, I., Kadlubowski, S., Kozicki, M., Kujawa, P., Stasica, P., & Ulanski, P. (2002). *IAEA-TECDOC*-1324, 5-47.

Shervani, Z., & Ikushima, Y. (2000). Determination of hydrodynamic radius of AOT reverse micelles prepared in near-critical propane. *Colloids and Surfaces A: Physicochemical and Engineering Aspects*, *164*, 307–313.

Stolnik, S., Illum, L., & Davis, S. S. (1995). Long circulating microparticulate drug carriers. *Advance Drug Delivery Review*, *16*,195-214.

Ulanski, P., & Rosiak, J. M. (1999). The use of radiation technique in the synthesis of polymeric nanogels. *Nuclear Instruments and Methods in Physics Research B*, *151*, 356-360.

Vinagradov, S. V., Bronich, T. K., & Kabanov, A. V. (2002). Nanosized cationic hydrogels for drug delivery: preparation, properties and interactions with cells. *Advanced Drug Delivery Reviews*, *54*, 135-147.

Pertanika J. Sci. & Technol. 20 (2): 409 - 414 (2012)

SCIENCE & TECHNOLOGY

Journal homepage: http://www.pertanika.upm.edu.my/

# Effects of Alkali Treatments on the Tensile Properties of Pineapple Leaf Fibre Reinforced High Impact Polystyrene Composites

**J. P. Siregar[1,2*], S. M. Sapuan[1], M. Z. A. Rahman[3] and H. M. D. K. Zaman[4]**

*[1]Department of Mechanical and Manufacturing Engineering, Faculty of Engineering, Universiti Putra Malaysia, 43400 Serdang, Selangor, Malaysia*

*[2]Department of Mechanical Engineering, Universitas Malahayati, Kemiling, Bandar Lampung, Indonesia*

*[3]Department of Chemistry, Faculty of Science Engineering, Universiti Putra Malaysia, 43400 Serdang, Selangor, Malaysia*

*[4]Radiation Processing Technology Division, Malaysia Nuclear Agency Bangi, 43000 Kajang, Selangor, Malaysia*

## ABSTRACT

A study on the effects of alkali treatment and compatibilising agent on the tensile properties of pineapple leaf fibre (PALF) reinforced high impact polystyrene (HIPS) composite is presented in this paper. The tensile properties of natural fibre reinforced polymer composites are mainly influenced by the interfacial adhesion between the matrix and the fibres. In this study, several chemical modifications were employed to improve the interfacial matrix-fibre bonding and this resulted in the enhancement of tensile properties of the composites. In this study, the surface modification of pineapple fibre with alkali treatments and compatibilizer were used to improve the adhesion between hydrophilic pineapple fibre and hydrophobic polymer matrix. There are two concentrations of NaOH treatments and compatibilizer used in this study, namely, 2 and 4 wt. %. The results show that the alkali treated fibre and the addition of compatibilising agent in PALF/HIPS composites have improved the tensile strength and tensile modulus of the composites.

**Keywords: Pineapple leaf fibre, high impact polystyrene, compatibilising agent, alkali treatment**

*Article history:*
Received: 28 July 2011
Accepted: 13 January 2012

*Email addresses:*
januarjasmine@yahoo.com (J. P. Siregar),
sapuan@eng.upm.edu.my (S. M. Sapuan),
mzaki@science.upm.edu.my (M. Z. A. Rahman),
khairul@mint.gov.my (H. M. D. K. Zaman)
*Corresponding Author

## INTRODUCTION

The properties of the composites depend on the matrix, fibres and their interfacial bonding. The adhesion between the reinforcing fibres and the matrix in the composite materials plays an important role in the materials (Alawar *et al.,* 2009). The inherent differences between the highly polar natural fibres and the non-

ISSN: 0128-7680 

polar polymer matrix can result in difficulties in the dispersion of fibres, along with poor fibre-matrix interactions (Gassan & Gutowski, 2000). This is one of the significant drawbacks in utilizing natural fibre to reinforce polymer composites.

This problem can be overcome by treating these natural fibres with suitable chemicals to decrease the hydrophilic hydroxyl groups on the surface of fibres. Chemicals such as alkaline (Gomes *et al*., 2007), silane (Abdelmouleh *et al*., 2007) and compatibilising agent (Bledzki & Gassan, 1999) can react with hydrophilic hydroxyl groups of the fibre and thus improve the hydrophobic characteristics and facilitate a better bonding with the matrix. Many studies have been carried out using the chemical treatments of natural fibres to improve the mechanical properties of composites. It was found that tensile and flexural strengths of the bagasse fibre composites pre-treated with 1% NaOH increased by 14 and 16%, respectively, as compared to the untreated fibre composites (Cao *et al*., 2006). The addition of compatibilising agents, such as maleic anhydride grafted polypropylene (MAPP), has been shown to be one of the most suitable coupling agents available for use in natural fibre reinforced polypropylene composites (Lu *et al*., 2000). It consists of long polymer chains with a MA functional group grafted onto one end. In more specific, MAPP acts as a bridge between the non-polar polypropylene matrix and the polar fibres by chemically bonding with the cellulose fibres through the MA groups, and bonding to the matrix by means of the polymer chain entanglement. This study aimed to investigate the effects of alkaline and compatibilising agent treatment on the tensile properties of PALF/HIPS composites.

## MATERIALS AND METHODS

### *Materials*

The pineapple leaf fibres (*Ananas comosus*) were obtained from Pemalang, Central Java, Indonesia. The size of the pineapple leaf fibres was used in this research was 10-40 mesh. The high impact polystyrene (HIPS) used as the polymer matrix was Idemitsu PS HT 50, which was supplied by the Petrochemical (M) Sdn. Bhd., Pasir Gudang, Johor, Malaysia. The poly(styrene-*co*-maleic anhydride) (PScoMa) was used as a compatibilising agent. Sodium hydroxide (NaOH) was used in the surface modification of the pineapple leaf fibres.

### *Alkali (NaOH) Treatment*

The short pineapple leaf fibres were soaked in two different concentrations (namely, 2% and 4%) of the NaOH solutions in a water bath for 1 hour at room temperature. The ratio of the

Table 1: Denotation of the sample composites

| Sample | Material |
|---|---|
| Untreated | 50% fibre + 50% HIPS |
| PScoMA2 | 50% fibre + 48% HIPS + 2% PScoMA |
| PScoMA4 | 50% fibre + 46% HIPS + 4% PScoMA |
| Alkali2 | Treated fibre with 2% NaOH (50% fibre + 50% HIPS) |
| Alkali4 | Treated fibre with 4% NaOH (50% fibre + 50% HIPS) |

fibres to the solution was 1:20 (w/v). These specific concentrations were selected according to the previous work reported by George *et al.* (1998) and Jacob and Thomas (2004). After the treatment, the fibres were washed, rinsed several times with distilled water, and then dried in an oven at 80°C for 24 hours.

*Compatibilising Agent*

There were two different weight concentrations (2% and 4%) of the compatibilising agent. The weight of the short PALF, which was 50% of the total formulation, was kept constant while the ratio of HIPS and compatibilising agent were varied (Table 1).

*Composite Manufacturing*

The pineapple fibres were incorporated into the HIPS matrix using a Brabender Plasticorder intensive mixer, model PL2000-6 at 165°C. The mixing process was performed in the following order: First, the HIPS and compatibilising agent were mixed for 2 minutes and the screw speed was set at 50 rpm. Afterward, PALF was added into the mixing chamber for 10 minutes. The total time for the mixing process was 12 minutes. The resulting material was then compressed in the mould using a Carver laboratory press at 165°C for 5 minutes, after undergoing the process of pre-heating for 5 minutes at the same temperature. This was followed by a cooling process of 5 minutes and the final result of the composites was formed into sheets.

*Tensile Testing*

In this study, the tensile test was carried out following the ASTM D638-03: Standard Method for Tensile Properties of Plastics. The specimens were tested using the Universal Instron model 4301 testing machine fitted with a 1kN load cell and operated at cross-head speed of 1mm/min. Seven specimens were tested to failure and the results obtained from the five specimens were used to calculate the average tensile value.

## RESULTS AND DISCUSSION

*Tensile Testing*

The influence of the alkali treatment of PALF and the addition of compatibilising agent on the tensile strength of PALF/HIPS composites are shown in Fig.1. The tensile strength of untreated PALF/HIPS composites is only 23 MPa. Incorporating untreated PALF fibres in the polymer HIPS matrix results in a creation of weak interfacial region due to incompatible non polar hydrophobic HIPS and polar hydrophilic PALF fibres. This weak interfacial region may result in the reduction of efficient stress transfer from the matrix to the reinforcement fibre, and thus reducing the tensile strength of the PALF/HIPS composites. Natural fibres also exhibit a poor resistant to moisture, which leads to high water absorption, and this subsequently results in poor tensile properties of the natural fibre reinforced composites.

The addition of compatibilising agent of 2 wt. % of PScoMA has increased the tensile strength of composites by about 34 MPa. This particular treatment has brought improvement

around 48% as compared to the untreated ones. Meanwhile, the tensile strength of the composites increases up to 36 MPa with the increase in the PScoMA content, i.e. from 2 wt. % to 4 wt. %. Improvement in the tensile strength is attributed to the increased adhesion between the PALF fibres and HIPS that facilitates better stress transfer through bonding to PALF fibres. Arbelaiz *et al.* (2005) used MAPP, Epolene E43 and G3003 to treat flax fibre reinforced polypropylene composites. Their results showed that 5 and 10 wt. % compatibilizers for E43 and G3003 were the optimum doses as the tensile strength increased by about 42% and 58%, respectively.

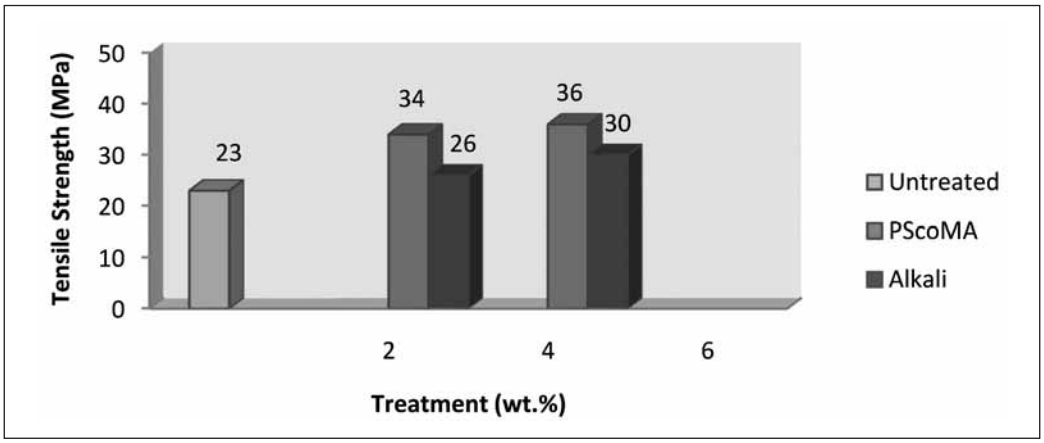


Fig.1: The effect of treatments on the tensile strength of PALF/HIPS composites

The effects of the alkali treatments (2 and 4%) on PALF fibre in the tensile strength were examined using the treated fibre (50 wt. %) composites. The NaOH treatment of the PALF fibres improved the tensile strength of the PALF/HIPS composites. Similarly, the tensile strength of the PALF/HIPS composites improved with 2 and 4% NaOH treatments by 12 and 24%, respectively, as compared to the untreated fibre composites. Rout *et al*. (2001) observed that the enhancement in the tensile strength with alkali treated fibre composites was attributed to the improved wetting of alkali treated fibre with the matrix. In particular, the alkali treatment improves the natural fibre-matrix adhesion due to the removal of natural and artificial impurities (Bisanda, 2000). The removal of impurities and waxy substances from the fibre surface and the creation of a rougher topography after alkalization resulted in a better bonding between the fibre and the matrix polymer in a composite by providing additional sites for mechanical interlocking (Mwaikambo & Ansell, 2003).

Tensile modulus is a measure of rigidity of the material (Bachtiar *et al*., 2008). Fig.2 shows that the tensile modulus of the untreated fibre composites is about 824 MPa. The addition of the compatibilising agent from 2 wt. % to 4 wt. % of PScoMA has increased the tensile modulus of composites from 1125 MPa up to 1222 MPa. The treatment of 4 wt. % PScoMA has increased the tensile modulus by 48% as compared to that of the untreated composites. This improvement could be related to a better dispersion of the fibres in polymer matrix (Sanadi *et al.,* 1997). The chemical composition of the compatibilising agent allows them to react with the fibre surface to form a bridge of chemical bonds between the fibre and matrix.

Most researchers found that these treatments are effective and have shown a better interfacial bonding. Meanwhile, the tensile modulus of the composites was observed as 1197 MPa and 1284 MPa in the 2 and 4% alkali treated samples, respectively. Thus, it can be concluded that the composites containing 4% of the NaOH treated fibres have slightly higher tensile modulus as compared to the untreated fibre composites and the composites containing 4% PScoMA treated fibre.

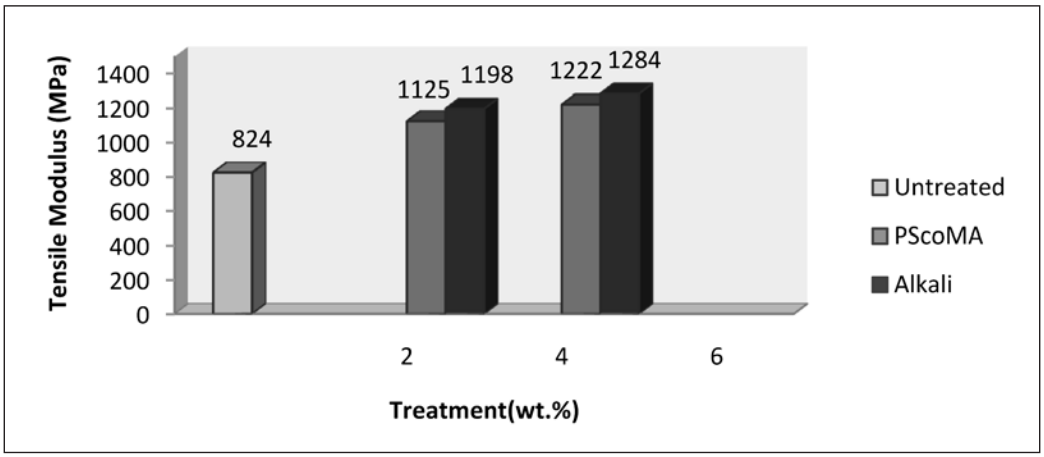


Fig.2: The effect of treatments on the tensile modulus of PALF/HIPS composites

## CONCLUSSIONS

The effects of the treatments on the pineapple leaf fibre reinforced high impact polystyrene composites were studied in the current work. The results obtained revealed that the use of alkali treatment and poly(styrene-co-maleic anhydride) compatibilising agent resulted in improved tensile properties of the PALF/HIPS composites. In particular, the composites containing compatibilising agent of 4% PScoMA appeared to be significantly stronger than the untreated fibre composites and also the composites containing NaOH treated fibre.

## ACKNOWLEDGMENTS

The authors wish to thank the Ministry of Higher Education Malaysia for funding the research through Fundamental Research Grant Scheme (FRGS) number 5523413. We also wish to thank the staff of the Malaysian Nuclear Agency, Selangor, Malaysia, for the support they gave us in carrying out this research.

## REFERENCES

Abdelmouleh, M., Boufi, S., Belgacem, M. N., & Dufresne, A. (2007). Short natural-fibre reinforced polyethylene and natural rubber composites: Effect of silane coupling agents and fibre loading. *Composites Science Technology, 67*, 1627-1639.

Alawar, A., Hamed, A. H., & Al Kaabi, K. (2009). Characterization of treated date palm trees fibres as composite reinforcement. *Composites Part B, 40*, 601-606.

Arbelaiz, A., Fernández, B., Ramos, J. A., Retegi, A., Llano-Ponte, R., & Mondragon I, (2005). Mechanical properties of short flax fibre bundle/polypropylene composites: Influence of matrix/fibre modification, fibre content, water uptake and recycling. *Composites Science and Technology, 65*, 1582-1592.

Bachtiar, D., Sapuan, S. M., & Hamdan, M. M. (2008). The effect of alkaline treatments on tensile properties of sugar palm fibre reinforced epoxy composites. *Materials & Design, 7*, 1285-1290.

Bisanda, E. T. N. (2000). The effect of alkali treatment on adhesion characteristics of sisal fibres. *Applied Composite Materials, 7*, 331-339.

Bledzki, A. K., & Gassan, J. (1999). Composites reinforced with cellulose based fibres. *Progress in Polymer Science*, *24*, 221-274.

Cao, Y., Shibata S., & Fukumoto, I. (2006). Mechanical properties of biodegradable composites reinforced with bagasse fibre before and after alkali treatments. *Composites Part A: Applied Science and Manufacturing, 37*, 423-429.

Gassan, J. & Gutowski, V. S. (2000). Effects of corona discharge and UV treatment on the properties of jute-fibre epoxy composites. *Composites Science and Technology*, *60*, 2857-2863.

George, J., Bhagawan, S. S., & Thomas, S. (1998). Improved interactions in chemically modified pineapple leaf fibre reinforced polyethylene composites. *Composite Interface, 5*, 201-223.

Gomes, A., Matsuo, T., Goda, K., & Ohgi, J. (2007). Development and effect of alkali treatment on tensile properties of curaua fibre green composites. *Composites Part A: Applied Science and Manufacturing*, *38*, 1811-1820.

Jacob, M., Thomas, S., & Varughese, K. T. (2004). Mechanical properties of sisal/oil palm hybrid fibre reinforced natural rubber composites. *Composites Science and Technology, 64*, 955-965.

Lu, J. Z., Wu, Q., & McNabb, H. S. (2000). Chemical coupling in wood fibre and polymer composites: a review of coupling agents and treatments. *Wood Fibre Science*, *32*, 88–104.

Mwaikambo, L. Y., & Ansell, M. P. (2003). Hemp fibre reinforced cashew nut shell liquid composites. *Composites Science and Technology, 63*, 1297-1305.

Rahman, M. M., & Khan, M. A. (2007). Surface treatment of coir (*Cocos nucifera*) fibres and its influence on the fibres physico-mechanical properties. *Composites Science and Technology 67*, 2369-2376.

Rout, J., Misra, M., Tripathy, S. S., Nayak, S. K., & Mohanty, A. K. (2001). The influence of fibre treatment on the performance of coir-polyester composites. *Composites Science Technology, 61*, 1303–1310.

Sanadi, A. R., Caulfield, D. F., & Jacobson, R. E. (1997). Agro-fibre /thermoplastic composites, in Paper and composites from agro-based resources, CRC Lewis Publishers, 377-401.

Pertanika J. Sci. & Technol. 20 (2): 415 - 423 (2012)

SCIENCE & TECHNOLOGY

Journal homepage: http://www.pertanika.upm.edu.my/

# Effects of Composition Parameters on Tensile and Thermal Properties of Abaca Fibre Reinforced High Impact Polystyrene Composites

**E. H. Agung[1*], S. M. Sapuan[2], M. M. Hamdan[3], H. M. D. K. Zaman[4] and U. Mustofa[1]**

[1]*Faculty of Engineering, Universitas Malahayati, Kemiling, 35153 Bandar Lampung, Indonesia*

[2]*Department of Mechanical and Manufacturing Engineering, Faculty of Engineering, Universiti Putra Malaysia, 43400 Serdang, Selangor, Malaysia*

[3]*Department of Mechanical Engineering, Faculty of Engineering, Universiti Pertahanan Nasional Malaysia, Kem Sungai Besi, 57000 Kuala Lumpur, Malaysia*

[4]*Radiation Technology, Malaysia Nuclear Agency, Bangi, 43000 Kajang, Selangor Darul Ehsan, Malaysia*

## ABSTRACT

The properties of fibre-reinforced composites are dependent not only on the strength of the reinforcement fibre but also on the distribution of fibre strength and the composition of the chemicals or additives addition within the composites. In this study, the tensile properties of abaca fibre reinforced high impact polystyrene (HIPS) composites, which had been produced with the parameters of fibre loading (30,40,50 wt.%), coupling agent maleic anhydride (MAH) (1,2,3 wt%) and impact modifier (4,5,6 wt.%) were measured. The optimum amount of MAH is 3% and the impact modifier is 6% and these give the best tensile properties. Meanwhile, Differential Scanning Calorimetry (DSC) was used to study the thermal behaviour within the optimum conditions of the composites. In this research, glass transitions temperature (Tg) of neat HIPS occurred below the Tg of the optimum condition of composites as the temperature of an amorphous state. The endothermic peak of the composites was in the range of 430-435$^0$C, including neat HIPS. It was observed that enthalpy of the abaca fibre reinforced HIPS composites yielded below the neat HIPS of 748.79 J/g.

*Article history:*
Received: 28 July 2011
Accepted: 13 January 2012

*Email addresses:*
efriyo@malahayati.ac.id (E. H. Agung),
sapuan@eng.upm.edu.my (S. M. Sapuan),
megat@upnm.edu.my (M. M. Hamdan),
khairul@mint.gov.my (H. M. D. K. Zaman),
alfa_usman@yahoo.com (U. Mustofa)
*Corresponding Author

**Keywords: Tensile properties, Differential Scanning Calorimetry (DSC), abaca fibre, Maelic Anhydride (MAH), impact modifier, High Impact Polystyrene (HIPS)**

## INTRODUCTION

Generally, some types of polymers have been used as matrices for natural fibre composites

ISSN: 0128-7680 

including polyethylene (PE), polystyrene (PS) and polypropylene (PP). These polymers have a different affinity towards the fibre due to the difference in their chemical structures. Joseph *et al*. (1996) reported that sisal/LDPE (low density polypropylene) composites released a better reinforcing effect because of the high matrix ductility and high strength/modulus ratio of sisal as compared to that of the LDPE matrix. The properties of the composites depend on those of the individual components and on their interfacial compatibility. Since thermoplastics such as polyethylene (PE), polystyrene (PS) and polypropylene (PP) are hydrophobic and have poor miscibility, chemical addition was needed to improve and facilitate the interaction between thermoplastics and reinforcing filler. Lee *et al*. (2005) and Lei *et al*. (2006) reported that the miscibility between nanoclay and PE or PP could be improved by the addition of compatibilizers such as MAPE, MAPP or carboxylated PE.

The majority of natural fibres, as a function of cellulose fibres and lignin, have low degradation temperatures (~200°C), making them inadequate for processing temperature above 200°C (Pracella *et al*., 2006). Nair *et al*. (2001) reported that the *Tg* values of polystyrene composites reinforced with short sisal fibres are lower than that of the unreinforced PS and may be attributed to the presence of some residual solvents in the composites. To solve the processing of natural fibre composites, it is necessary to promote polymer modification with polar groups (such as maleic anhydride, stearic acid or glycidyl methacrylate) to enhance the adhesion between the matrix and the composite components. The coupling agent more often used for this application is a polyethylene copolymer grafted with maleic anhydride (Keener *et al*., 2004). In this paper, the investigation of tensile properties resulted in an optimum condition of composites, meanwhile thermal behaviour within the optimum condition from abaca fibre reinforced HIPS composites at glass transition and crystallization processes was clearly observed. Commercial HIPS were used for a comparator to the natural fibre composites. The DSC methods were used in evaluating the basic thermal parameters of the optimum condition of abaca fibre reinforced HIPS composites.

## EXPERIMENTAL

### *Materials*

Abaca (*Musa textilis Nee*) fibres are produced by Ridaka Hand Craft, Pekalongan, Central Java, Indonesia. High impact polystyrene (HIPS), Idemitsu PS HT 50, density 1.04 g/cm$^3$, and melt index of 4.0g/10 min were obtained from Petrochemical (M) Sdn. Bhd., Malaysia. Maleic anhydride (MAH), (polystyrene-block-poly(ethylene-ran-butylene)-block-polystyrene-graft-maleic anhydride) was supplied by Sigma Aldrich Malaysia (M) Sdn. Bhd., Malaysia. Impact modifier, a styrene butadiene styrene (SBS) copolymer rubber (Cyclo resin), was supplied by PT. Wahana Makmur Kencana, Jakarta, Indonesia.

### *Formulation of the Samples*

The composites in this research were formulated with the response surface methodology – Box-Behnken design (BBD). Tensile properties are the responses of three factors to be determined and these three factors are designated as $X_1$ (abaca fibre), $X_2$ [maelic anhydride (MAH)] and

$X_3$ [impact modifier (IM)] within three levels, which were coded as +1, 0, −1 for high, intermediate and low values, respectively, as shown in Table 1.

Table 1: Levels and code of variables for Box Benhken design (BBD)

| Variables | Symbol | | Coded Levels | | |
|---|---|---|---|---|---|
| | Uncoded | Coded | -1 | 0 | +1 |
| Abaca | $X_1$ | $x_1$ | 30 | 40 | 50 |
| MAH | $X_2$ | $x_2$ | 1 | 2 | 3 |
| IM | $X_3$ | $x_3$ | 4 | 5 | 6 |

## METHODS

### *Composite Fabrication*

The abaca fibres were dried under the sunlight between 27 and 30$^0$C for four days. The dried abaca fibres were cut into 2 – 3 mm by means of an electronic cutting machine. Based on the proportion of the abaca fibre, maelic anhydride (MAH) and impact modifier were incorporated into the neat HIPS. The processing of the abaca fibre reinforced HIPS composites were accomplished using a rolling machine, as shown in Fig.1. The working temperature of the rolling machine was kept approximately 200$^0$C while the speed was also maintained at the slow rate. The process was continued until all the materials were well-mixed and they produced the sheets of abaca fibre reinforced HIPS composites with an average of 1mm thickness.

Fig.1: Producing abaca fibre reinforced HIPS composites using a rolling machine

### *Tensile Test*

Tensile testing of the specimens was performed according to ASTM D 638-98 on a universal test machine (Instron, model 556) at ambient temperature (27$^0$C). The strain rate was 50 mm/min with a gauge length of 60 mm. The values reported were the average of the three samples tested.

### *Differential Scanning Calorimetry (DSC)*

The characterization of a material requires the use of Differential Scanning Calorimetry analysis. The DSC analysis obtained quantitative and qualitative data concerning the net heat

changes as a thermal behaviour. The samples used for the DSC analysis were cut from the sheet of the composite in order to have a weight that ranges from 10-14 mg. A Mettler-Toledo DSC model 822 was used to determine the thermal behaviour. The temperature was programmed for heating from 25°C to 500°C, with a heating rate of 10°C $min^{-1}$ under nitrogen atmosphere.

## RESULTS AND DISCUSSION

### *Tensile Strength*

The properties of the matrix and fibres, as well as processing conditions, are very important in achieving good mechanical properties of the composites. The strength parameter is more sensitive to the matrix properties, whereas the modulus is dependent on the fibres' properties. The positive or negative effect of the application of natural fibres reinforced matrix composites is important. Meanwhile, the variables of filler or additive will improve the mechanical performance of the matrix composites. This research on the abaca fibre reinforced high impact polystyrene clearly indicates the relationship between dependent and independent variables of the tensile strength and tensile modulus which were studied in the experimental design. The effects of the response variables are demonstrated using the model in Equations 1 and 2 for tensile strength, as follows:

$$\hat{y} = 11.23 - 0.025X_1 + 0.43X_2 + 0.071X_3 - 1.15X_1^2 + 0.35X_2^2 + 1.80X_3^2 + 0.47X_1X_2 + 1.79X_1X_3 + 0.93X_2X_3 \quad (1)$$

and for the tensile modulus, model equation is:

$$\hat{y} = 1.25 + 5.345x10^{-3}X_1 + 0.05X_2 + 4.44x10^{-3}X_3 - 0.16X_1^2 - 0.026X_2^2 + 0.12X_3^2 + 0.029X_1X_2 + 0.16X_1X_3 + 0.092X_2X_3 \quad (2)$$

By contour plots, the effects of each variable with their interactions on the abaca fibre reinforced HIPS composites at one fixed level of variable (medium level) impact modifier are shown in Fig.2 and Fig.3.

The plots described in Fig.2 indicate that the tensile strength of abaca fibre reinforced HIPS composites to the saddle point curve and that two high values (the maximum of up to 12.28 MPa) at the area of abaca loading which are close to 45 wt% and 30 wt%. The graph of the tensile strength starts to decrease but then increases when the loading of the abaca fibre is close to 45 wt% and 30 wt%. In this condition, the impact modifier deals with the area close to 4.5 wt% and 5.5 wt%. This response exposes the minimum point as the effect of the impact modifier (IM) and Maelic Anhydride (MAH), while the abaca fibre is loading in level (40 wt. %).

The case of tensile modulus was studied based on the interaction effects; the abaca fibre and impact modifier also reflected the saddle point graph effect illustrated in Fig.3. The plot describes that the minimum yield of tensile modulus reflects the interaction between the impact modifier (IM) and maelic anhydride that is close to area 1.16 GPa. Upon studying the coefficient values of the tensile strength and tensile modulus, the variable $X_1$ ($\beta_1 = 0.1837$ and 0.0312) was found to be higher than the variables $X_1$ and $X_3$, indicating that it contributed the most in predicting the properties of the abaca fibre reinforced HIPS composites. Meanwhile,

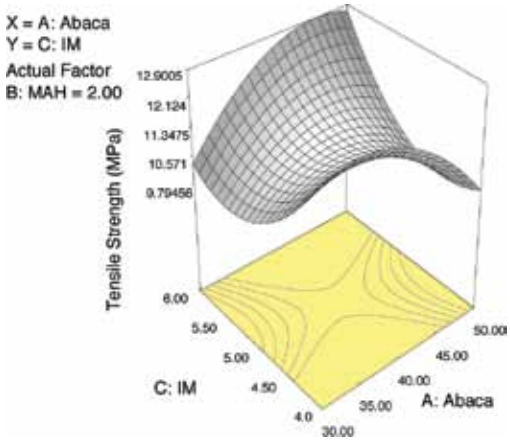


Fig.2: Response surface 3D plots showing the effect of abaca fibres and Impact Modifier for tensile strength (GPa)

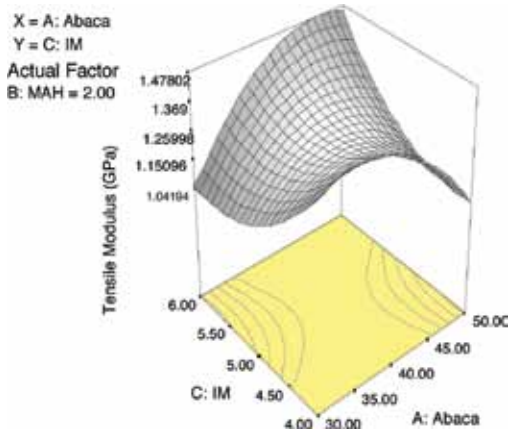


Fig.3: Response surface 3D plots showing the effect of MAH and Impact Modifier for Tensile modulus (GPa)

the interaction between $X_1$ and $X_3$ provides a more real impact for the yields. It means that abaca fibres are highly influenced by impact modifier (IM).

*The Optimum Condition of the Composites and the DSC Analysis*

Optimum conditions were solutions within the applications due to tensile and thermal properties of the abaca fibre reinforced HIPS composites. Discussion on the account of this particular situation was necessary to identify a compromise zone where the experimental responses satisfied the specifications to achieve the proposed aims. In order to choose the best coordinates of an acceptable compromise, desirability function was taken on. The acceptable values of desirability function were the values closed to one (100%). In this research, the tensile properties of the abaca fibre reinforced HIPS composite compromised on the parameters of the abaca fibre (36.76 wt.%), maelic anhydride (3 wt%) and impact modifier (4 wt.%), and this condition dealt with 77% desirability. Table 2 shows the predicted optimization experiments of the tensile properties as prepared by BBD that referred to the actual parameters of composites.

The reviewed optimization of the composites presented in Table 3 explains the condition thermal properties, tensile properties and desirability function. This research predicted the parameter of abaca fibre, maleic anhydride and impact modifier compiled optimum of the tensile properties within desirability function and summarized by composites A, B and C.

Fig.4 shows the DSC scan of the abaca fibre reinforced HIPS composites. The compositions of the abaca fibre reinforced HIPS composites (A, B, and C) may influence the energetic terms correlated with the difference of *Tg*. The glass transition (Tg) occurs over a wide temperature range (Thirta et al., 2005) as shown in Table 3 and depicted in Fig.4; Tg is determined by the region of the onset and midpoint temperature. The specimen of the abaca fibre reinforced HIPS composites with the differences of composition at 1 wt.% and 3 wt.% of maleic anhydride, respectively, resulted in a difference of *Tg*. The difference of *Tg* was ~ $34^0$C, and thus, it summarized that maleic anhydride should play a dominant role in controlling the amorphous

Table 2: Predicted optimization experiments of that tensile strength as prepared by Box-Behnken design (BBD) referred to the actual composition of composites

| No | Abaca | MAH | IM | Tensile Strength | Tensile Modulus | Desirability |
|---|---|---|---|---|---|---|
| | wt% | wt% | wt% | MPa | GPa | |
| 1 | 40 | 3.00 | 4.00 | 12.288 | 1.314 | 0.77 |
| 2 | 40 | 3.00 | 6.00 | 12.876 | 1.512 | 0.77 |
| 3 | 40 | 3.00 | 4.00 | 12.201 | 1.306 | 0.76 |
| 4 | 40 | 1.00 | 6.00 | 12.840 | 1.264 | 0.64 |
| 5 | 40 | 1.00 | 6.00 | 12.842 | 1.270 | 0.64 |
| 6 | 40 | 1.00 | 4.00 | 13.306 | 1.431 | 0.61 |
| 7 | 40 | 1.00 | 4.00 | 13.268 | 1.426 | 0.61 |
| 8 | 40 | 1.00 | 4.00 | 13.263 | 1.425 | 0.61 |

MAH: Maleic Anhydride; IM: Impact Modifier

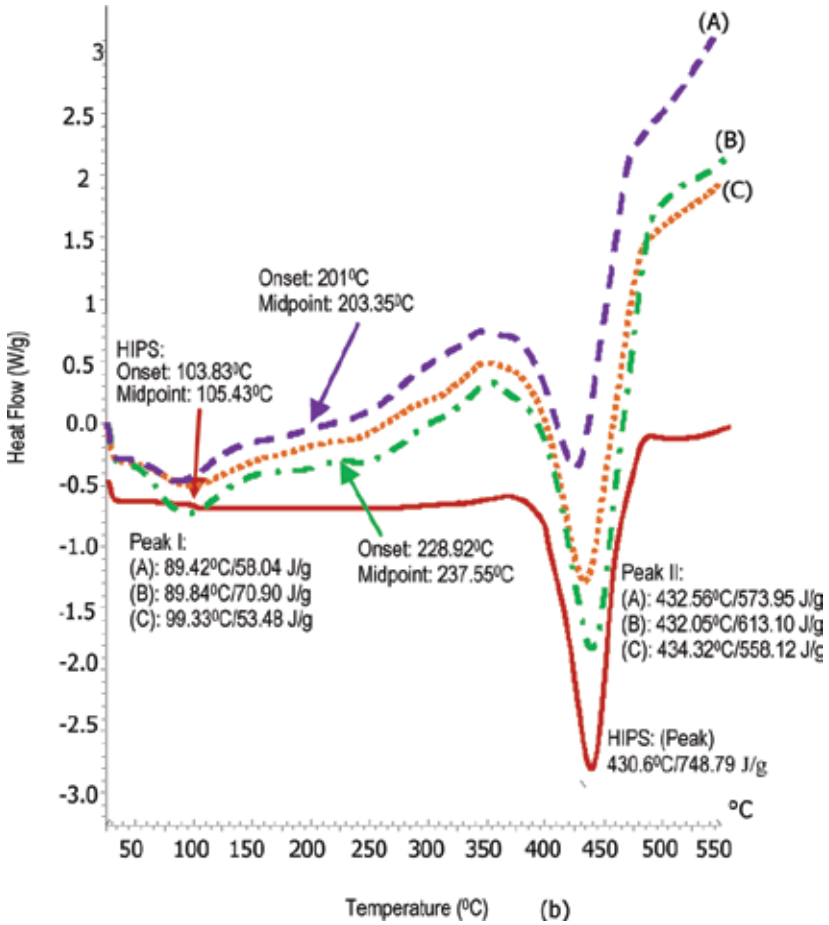


Fig.4: The DSC scan of the optimum condition of abaca fibre reinforced HIPS composites (compositions A, B, and C)

Table 3: Results of the tensile and thermal (DSC analysis) properties for the abaca fibre reinforced HIPS composites (formulations A, B and C) within the desirability function

| Composition of | THERMAL PROPERTIES | | | | | | MECHANICAL PROPERTIES | | |
|---|---|---|---|---|---|---|---|---|---|
| | Glass Transition Tg (°C) | | Endoterm Temp (°C) | | Entalphy (J/g) | | Tensile Strength | Tensile Modulus | Desirability |
| | Onset Temp | Mid-point Temp | Peak I | Peak II | ΔH Peak I | ΔH Peak II | MPa | GPa | |
| Abaca reinforced HIPS composites (A) with composition | | | | | | | 13.306 | 1.431 | 0.61 |
| Abaca (40 wt.%) | 201.00 | 203.35 | 89.42 | 432.56 | 58.04 | 573.95 | 13.268 | 1.426 | 0.61 |
| Maleic anhydride (1 wt.%) | | | | | | | 13.263 | 1.425 | 0.61 |
| Impact modifier (4 wt.%) | | | | | | | | | |
| Abaca reinforced HIPS composites (B) with composition | | | | | | | 12.288 | 1.314 | 0.77 |
| Abaca (40 wt.%) | 228.92 | 237.55 | 89.84 | 432.05 | 70.90 | 613.10 | 12.201 | 1.306 | 0.76 |
| Maleic anhydride (3 wt.%) | | | | | | | | | |
| Impact modifier (4 wt.%) | | | | | | | | | |
| Abaca reinforced HIPS composites (C) with composition | | | | | | | | | |
| Abaca (40 wt.%) | - | - | 99.33 | 434.32 | 53.48 | 558.12 | 12.786 | 1.512 | 0.77 |
| Maleic anhydride (3 wt.%) | | | | | | | | | |
| Impact modifier (6 wt.%) | | | | | | | | | |
| High Impact Polystyrene | 103.83 | 105.43 | - | 430.60 | - | 748.79 | - | - | - |

or glass transition state of the abaca fibre reinforced HIPS composites. The composition (C) of the abaca fibre reinforced HIPS composites was less free and the molecules underwent crosslinking. When compared with neat HIPS, the *Tg* of the abaca fibre reinforced HIPS composites (A and B) increased by 97.92$^0$C and 132.12$^0$C, respectively.

The heating thermograms of the abaca fibre reinforced HIPS composites (A, B, and C) represent the one peak correlated with the glass transition state and another peak in the endothermic due to crystallization state. The first peak of the abaca fibre reinforced HIPS composites were on 89.42$^0$C (A), 89.84$^0$C (B), and 99.33$^0$C (C), respectively, as shown in Table 3. This peak normally attributed to the release of the absorbed moisture related to humidity on the surface from the fibres. As the natural fibres are hydrophilic, a water desorption peak was observed around 100$^0$C (Huda & Drzal, 2008). In this study, the highest enthalpy of the abaca fibre reinforced HIPS composites (B) at the transition temperature was 70.90 J/g. Based on the highest enthalpy, the enthalpy increased by 12.86 J/g by adding 2 wt% of the maleic anhydride but decreased by 17.48 J/g by adding 2 wt% impact modifier.

The second endothermic peak of the abaca fibre reinforced HIPS composites in the range of 430-435$^0$C in the DSC curves (Fig.4) determined the dehydration of the composites. An endothermic of HIPS was also in the same range. It gave the indication that the heating rates (polymer degradation) of the composites and neat HIPS felt within the same range of temperatures. Taking composition B as a reference, with enthalpy (613.10 J/g) of abaca fibre reinforced HIPS composites, the enthalpy of (A) increased by 39.15 J/g and (C) and decreased by 54.98 J/g, respectively.

## CONCLUSION

By utilizing the Box-Benhken design of experiments, the MAH and impact modifier have been shown to improve the tensile strength and tensile modulus properties of the composites by enhancing the adhesion between the fibres and HIPS. In this study, the predicted parameters of the abaca fibres were ~40 wt%, MAH (~3 wt.%) and Impact Modifier (~6 wt%) represented for the optimum tensile properties due to desirability function. Through DSC scan, the first peak of the composites (A, B, C) revealed that the absorbed moisture release to humidity on the surface of the fibres to be below ~100$^0$C, whereas the *Tg* of optimum conditions (A, B, and C) of the abaca fibre reinforced HIPS composites were above of neat HIPS. Scanning by DSC also resulted in the peak temperature of endothermic in the range between 430-435$^0$C, including neat HIPS. The second enthalpy of the abaca fibre reinforced HIPS composites yielded less neat HIPS of 748.79 J/g.

## ACKNOWLEDGEMENTS

The authors are thankful to Universitas Malahayati, Lampung, Indonesia for the financial support. The authors also wish to acknowledgement the assistance from PT. Tara Plastic Indonesia and Radiation Technology, and Malaysian Nuclear Agency, Bangi, Malaysia for providing and testing materials for this study.

## REFERENCES

Huda, M. S., & Drzal, T. L. (2008). Properties and performance of natural-fibre composites. In K.L. Pickering. England: Woodhead Publishing Ltd.

Joseph, K., Varghese, S., Kalaprasad, G. Thomas, S., Prasannakumari, L., Koshy, P., & Pavithran, C. (1996). Influence of interfacial adhesion on the mechanical properties and fracture behaviour of short sisal fibre reinforced polymer composites. *European Polymer Journal, 32*, 1243 -1250.

Keener, T. J., Stuart, R. K., & Brown, T. K. (2004). Maleated coupling agents for natural fibre composites. *Composites (Part A),* 35, 357-362.

Lee, S. U., Oh, I. H., Lee, J. H., Choi, K. Y., & Lee, S. G. (2005). Preparation and characterization of polyethylene/montmorillonite nanocomposites. *Polymer*, *3*, 271–276.

Lei, Y., Wu, Q., & Clemons, C. M. (2006). Preparation and properties of recycled HDPE/clay Hybrids. *Journal of Applied Polymer Science*, *103*, 3056–3063.

Nair, K. C. M., Thomas, S., & Groeninck, G. (2001). Thermal and dynamic mechanical analysis of polystyrene composites reinforced with short sisal fibres. *Composites Science and Technology, 61*, 2519-2529.

Pracella, M., Chionna, D., Anguillesi, I., Kulinski, Z., & Piorkowska, E. (2006). Functionalization, compatibilization and properties of polypropylene composites with hemp fibres. *Composites Science and Technology, 66*, 2218 – 2230.

Thirta, V., Lehman, R., & Nosker, T. (2005). Glass Transition Phenomena in Melt-Processed Polystyrene/ Polypropylene Blends. *Polymer Engineering and Science*, 1187-1193.

Pertanika J. Sci. & Technol. 20 (2): 425 - 433 (2012)

SCIENCE & TECHNOLOGY

Journal homepage: http://www.pertanika.upm.edu.my/

# Preparation and Characterization of Hydrogels from Grafting of Vinyl Pyrrolidone onto Carboxymethyl Cellulose

**Ahmad, M. B.[1*], Hashim, K. B.[2], Mohd Yazid, N.[1], and Zainuddin, N.[1]**

[1]*Department of Chemistry, Faculty of Science, Universiti Putra Malaysia, 43400 Serdang, Selangor, Malaysia*

[2]*Polymer Technology Division, Malaysian Nuclear Agency, Bangi, 43000 Kajang, Selangor, Malaysia*

## ABSTRACT

In this work, hydrogels were prepared from carboxymethyl cellulose (CMC) and 1-vinyl-2-pyrrolidone (VP) by Electron Beam irradiation in the presence of N,N'-methylenebisacrylamide (BIS) as a crosslinking agent. The parameters studied include stirring time and percentage of crosslinking agent. Hydrogels were characterized using Fourier Transform Infrared (FTIR) spectroscopy and Scanning Electron Microscopy (SEM). VP and BIS were found be effective as reinforcement materials to improve the properties of CMC. Meanwhile, the optimum conditions were 5% BIS and 3 hours of stirring time. The gel fraction increased when irradiation dose was increased. FTIR confirmed the crosslinking reaction between CMC and VP after the irradiation process by using BIS as the crosslinking agent. TGA thermograms showed changes in the thermal properties of CMC-VP hydrogels in the presence of different amounts of BIS.

**Keywords: EB irradiation, crosslinker, carboxymethyl cellulose, vinyl pyrrolidone, hydrogels**

## INTRODUCTION

Hydrogels are special class of cross-linked polymers which can be prepared using different polymerization techniques. Using the radiation technology, polymerization procedure, the crosslinking structure and also cross-linked density of the hydrogels could be easily controlled (Sahiner *et al*., 2005). Electron beam irradiation has many advantages including a relatively short processing time, in-line processing, high effectiveness, low equipment cost, and increased available energy (Choi *et al*., 2008). The advantage of hydrogel formation by radiation-induced crosslinking is that the process can be done in water under mild conditions (i.e. room temperature and physiological pH) (Hennink & van

*Article history:*
Received: 28 July 2011
Accepted: 13 January 2012

*Email addresses:*
mansorahmad@science.upm.edu.my (Ahmad, M. B.),
kbhashim@nuclearmalaysia.gov.my (Hashim, K. B.),
ifahyazid@gmail.com (Mohd Yazid, N.),
hazlin@science.upm.edu.my (Zainuddin, N.)
*Corresponding Author

ISSN: 0128-7680 

Nostrum, 2002). Therefore, radiation method is an excellent tool for fabrication of materials for wound dressing, drug delivery and biomedical applications.

Hydrogels are used for a variety of applications such as biomaterials, controlled release devices and superabsorbent materials. Hydrogels derived from natural polymers, such as polysaccharides and poly(amino acids), are desirable from the viewpoint of environmental conscious technology (Zhao *et al*., 2008).

The use of polysaccharides alone is hampered due to the high solubility in aqueous medium leading to premature release of drug (Nizam El-Din *et al*., 2010). CMC is similar with other natural cellulosic polymers and a degradable polymer which can be crosslinked to form a hydrogel. However, CMC hydrogels have very poor mechanical strength which limits their applications. The synthetic polymer is used to overcome the disadvantages of CMC. The uncross-linked homopolymers poly(vinyl pyrrolidone) (PVP) is a water-soluble material that has been extensively used as a blood plasma extender, and currently serves as an additive in a variety of pharmaceutical products.

In this work, hydrogels were prepared using carboxymethyl cellulose (CMC), 1-vinyl-2-pyrrolidone (VP) and N,N'-methylenebisacrylamide (BIS). The effects of stirring, irradiation dose and amount of crosslinking agent were also studied. The hydrogels were analyzed using Fourier Transform Infrared (FTIR) spectroscopy and Scanning Electron Microscopy (SEM).

## MATERIALS AND METHODS

### *Materials*

Sodium salt CMC with a degree of substitution (DS) 1.2 and MW 250 000 were supplied by Acros Organic, New Jersey, US. VP (assay 97%) and BIS, as cross-linking agent were supplied by Fluka Chemicals, Buchs, Belgium. 2,2-dimethoxy-2-phenylacetophenone (DMPA), purity 99% was used as photo initiator agent was purchased from Acros Organic, New Jersey, US. Deionised water was also used throughout the experiment.

### *Preparation of the Hydrogels*

The samples were prepared according to previous study (Ibrahim *et al*., 2007) by dissolving the CMC in 100 ml deionised water and leave it overnight. Then VP and BIS were added into the solution and stirred to form homogeneous pastes. The total polymer weight was 20 g. The homogeneous pastes were then transferred into a plastic mould which was then inserted into a plastic bag. The plastic bag, together with the plastic mould and paste, was vacuum-sealed to remove air. The irradiation of the paste-like mixture was carried out via electron beam irradiation. An electron beam accelerator EPS 3000 with beam current of 10 mA and acceleration energy of 2 MeV was used for irradiation of the sample from 5 to 25 kGy. The effect of stirring time was studied on the samples with ratio CMC:VP 50:50 and 5% BIS. The samples were stirred for about 1 to 5 hours to form a homogeneous mixture, and irradiated at 10 kGy and 20 kGy. The effect of the crosslinking agent on the mixture was studied by varying the percentages of BIS, i.e. between 3 to 7% of the total weight of monomer at the optimum stirring time.

*Determination of Gel Fraction and Swelling Behaviour of the Hydrogels*

The percentage of the gel content was determined using the method used by Yoshii *et al*. (2003). The irradiated hydrogels were first weighed, loaded in a tea bag and soaked in distilled water for 48 hours. The soluble parts, namely uncross-linked CMC and VP, were extracted into the water during this period and the cross-linked hydrogels remained inside the tea bag. The samples were then dried at 60°C until a constant weight was obtained. The percentage of the gel content was calculated using the following equation:

$$\text{Percentage of the gel content (\%)} = (W_d/W_i) \times 100 \quad (1)$$

where $W_d$ and $W_i$ are the weight of the insoluble parts after extraction with water and the weight of the initial dried hydrogels after irradiation, respectively.

Meanwhile, swelling ratio was measured by swelling the hydrogels in deionised water at room temperature. The amount of the water absorbed was reported as a function of soaking period.

*Characterization of the Hydrogels*

The characterization of the hydrogels was carried out using Fourier Transform Infrared (FTIR) spectroscopy and Scanning Electron Microscopy (SEM).

## RESULTS AND DISCUSSION

*The Effect of Stirring Time on Gel Fraction*

Fig.1 shows the effect of stirring time on the gel fraction of CMC: VP (50:50) at 10 and 20 kGy with 5% BIS. It shows that the gel fraction for both doses increases with stirring time. This means prolonging the stirring time gives higher homogeneity of CMC and VP mixture. The optimum gel fraction was obtained at 3 hours stirring time and remained constant. On the contrary, extending the stirring time does not contribute to higher gel fraction since it may cause oxidation process towards VP.

*The Effect of Crosslinking Agent on Gel Fraction*

The effect of crosslinking agent, BIS, on the composition CMC:VP (50:50) at 10 and 20 kGy with 3 hour stirring time is shown in Fig.2. The gel fraction for 10 and 20 kGy increases with the increase in the amount of the crosslinking agent and reaches the maximum value at 5% of BIS. The preliminary result showed that there was no formation of hydrogels obtained at 1 and 2% of BIS. Meanwhile, the gel fraction increases rapidly from 3 to 5% of BIS where the maximum crosslink is at 5% of BIS, but with no significant increase at 6% and 7% of BIS. In addition, the gel fraction at 20 kGy is higher than 10 kGy due to the increase in the degree of crosslinking. The use of the crosslinking agents *in situ* with electron beam radiation in the preparation of hydrogels has been discussed in a previous study (Ibrahim *et al*., 2007).

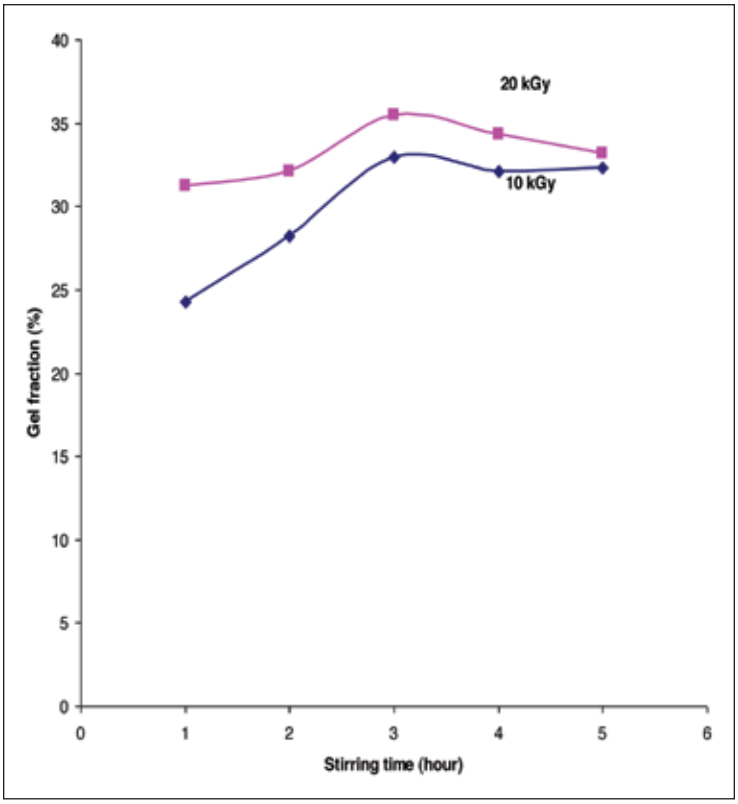


Fig.1: The effect of stirring time on gel fraction at composition CMC:VP (50:50) at 10 and 20 kGy

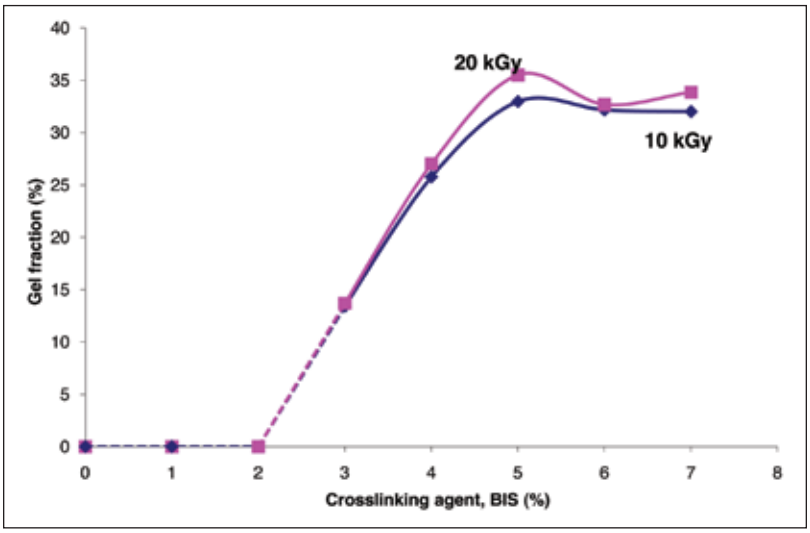


Fig.2: The effect of crosslinking agent on gel fraction at composition CMC:VP (50:50) at 10 and 20 kGy with 3 hours of stirring time

*The Effect of Stirring Time on Swelling Behaviour*

The effect of stirring time on the swelling behaviour of composition CMC:VP (50:50) at 10 and 20 kGy with 5% BIS is illustrated in Fig.3. The degree of swelling decreases with the increase in the stirring time up to 3 hours before levelling off. The degree of swelling for hydrogels irradiated at 10 kGy is higher than for those at 20 kGy, which is related to the degree of crosslinking.

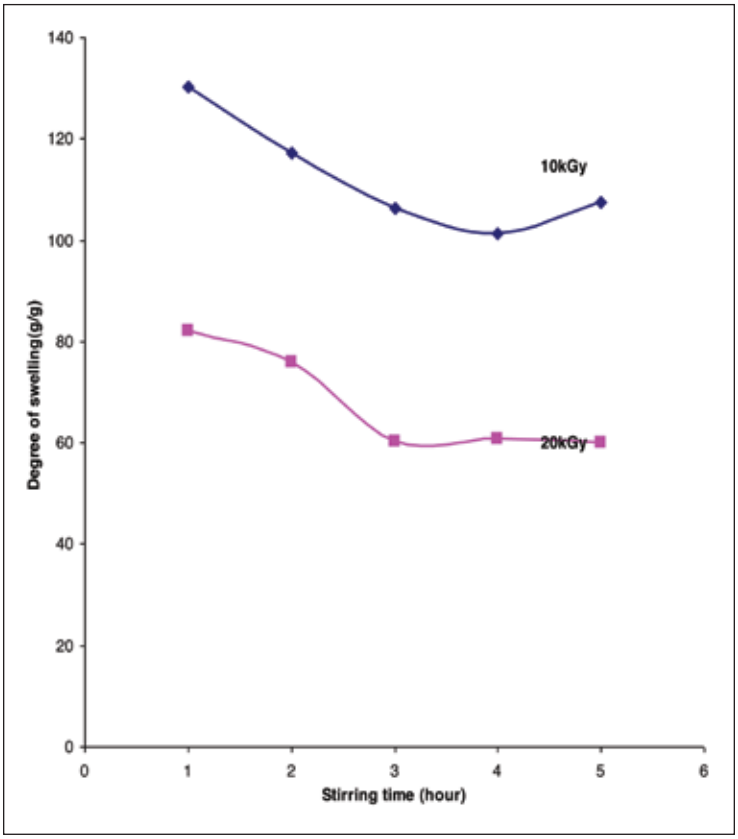


Fig.3: The effect of stirring time on swelling behaviour at composition CMC:VP (50:50) at 10 and 20 kGy with 5% BIS

*The Effect of Crosslinking Agent on Swelling Behaviour*

The effects of crosslinking agent on the swelling behaviour of 50:50 (CMC:VP) hydrogels at 10 and 20 kGy with the optimum stirring time (3 hours) are shown in Fig.4. There is no hydrogel formed at 1- 2% BIS and the maximum degree of swelling is obtained at 3% of BIS. When the amount of the crosslinking agent increases, the crosslink density also increases, and this leads to a more compact polymeric network, reduces the pore size and consequently decreases the amount of water uptake (Pourjavadi *et al*., 2006; Singh *et al*., 2007).

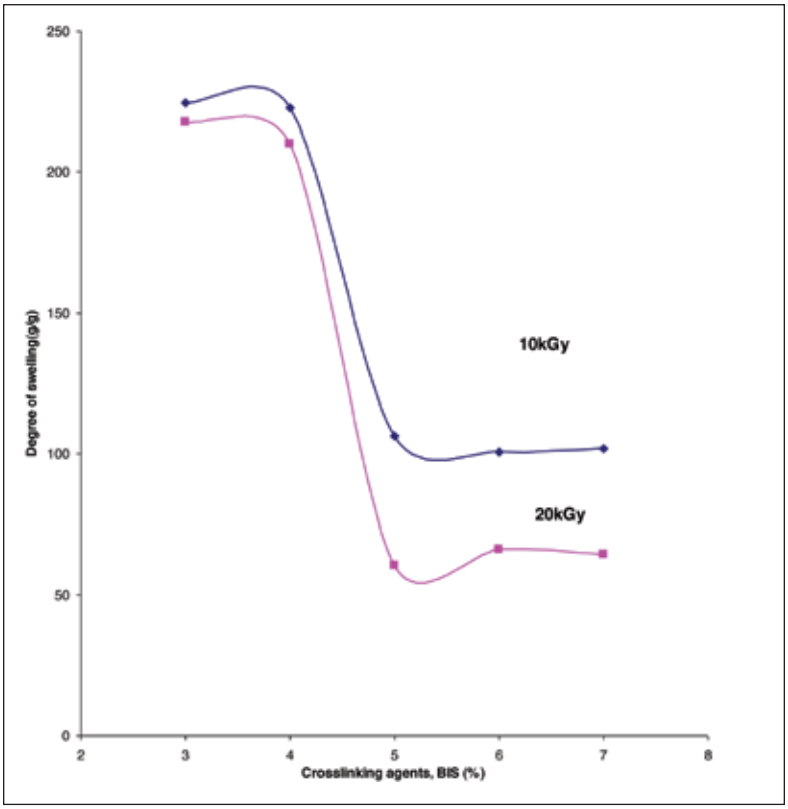


Fig.4: The effect of the crosslinking agent on swelling behaviour at composition CMC:VP (50:50) at 10 and 20 kGy with 3 hours of stirring time

*Fourier Transform Infrared Spectroscopy*

Fig.5 shows the FT-IR spectra of CMC hydrogels at 10 kGy, CMC, VP, CMC:VP (50:50) without BIS at 10 kGy and CMC:VP (50:50) with BIS at 10 kGy. For all the spectra, a broad band occurs at 3000-3500 $cm^{-1}$ and it corresponds to the O-H stretching vibration of hydroxyl group and molecules of water in all the samples. The characteristic absorption band of CMC hydrogels is similar to pure CMC, which is at 1587 $cm^{-1}$, due to the peak assigned by C=O stretching vibration of the carbonyl group (COO-) group. The intensity of the hydrogen bonding of CMC increases as a result of the polymerization of PVP, as indicated by the very wide broad absorption band at 3000-3500 $cm^{-1}$. The formation of the hydrogen bonding between the carboxylic and with the non-substituted hydroxyl group of cellulose molecule has been shown to be directly due to the crosslinking reaction between CMC and VP (Taleb *et al*., 2009).

*Morphology Study*

Fig.6 shows the SEM micrographs of the fracture surface cross-section of (a) CMC hydrogels at 10 kGy, (b) CMC:VP (50:50) at 10 kGy, and (c) CMC:VP (50:50) at 20 kGy for 400x magnification at the optimum condition. The morphology of the hydrogels confirms the higher swelling behaviour of the hydrogels at 10 kGy as compared to hydrogels at 20 kGy, as shown

previously. The average pore sizes for CMC hydrogels (a) and (b) are 64.77 $\mu$m, 65.18 $\mu$m and (c) 49.01 $\mu$m, respectively. The decrease in the pores size may be due to the higher degree of crosslinking at a higher irradiation dose.

When the pores in contact with water molecules are small, the water-uptake capacity will be reduced. This finding also confirms the result of gel fraction, whereby the gel fraction increases with the increase of irradiation dose. It was also found that CMC:VP hydrogels

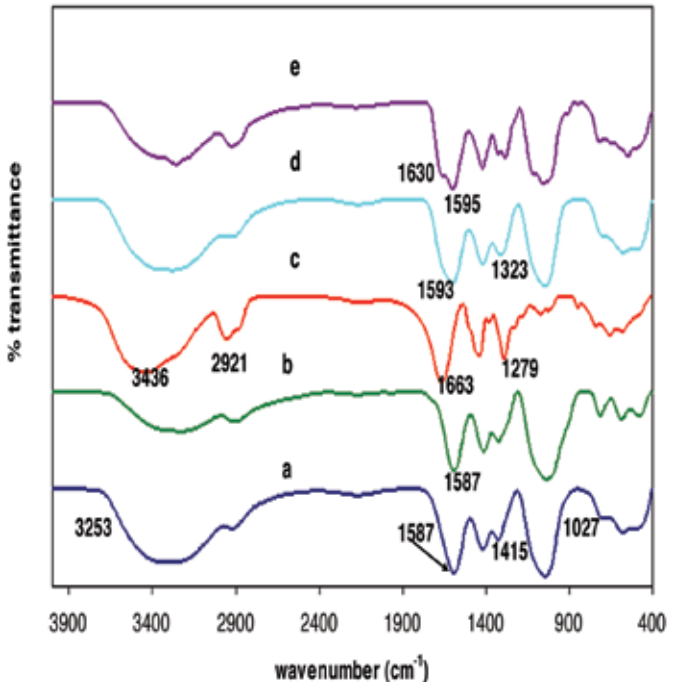


Fig.5: The FT-IR spectra of (a) CMC hydrogels at 10 kGy, (b) CMC, (c) VP, (d) CMC:VP (50:50) without BIS at 10 kGy and (e) CMC:VP (50:50) with BIS at 10 kGy

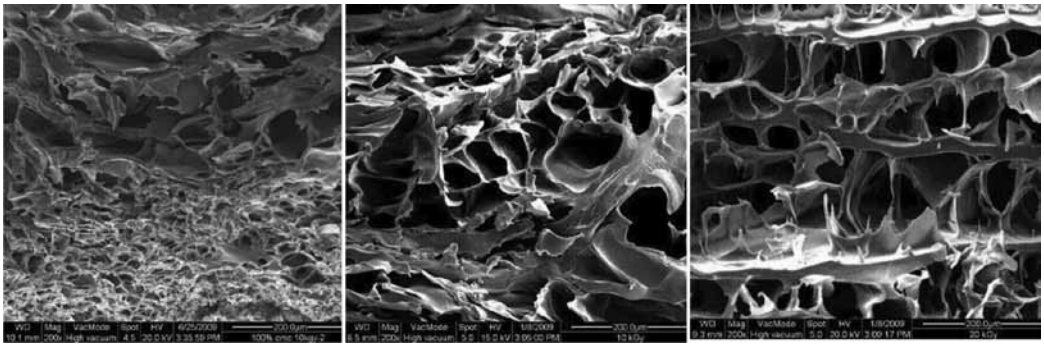

Fig.6: The SEM micrographs of the fracture surface cross-section of (a) CMC hydrogels at 10 kGy, (b) CMC:VP (50:50) at 10 kGy and (c) CMC:VP (50:50) at 20 kGy with 3 hours of stirring and 5% of BIS, 200x magnification

have more homogeneous distribution of pores and uniform pore size than CMC hydrogels. It is also assumed that the presence of VP in the formulation contributes to the homogeneity and uniformity of the morphology of the hydrogels.

## CONCLUSIONS

This study revealed the potential for VP and BIS as reinforcement materials to increase the properties of CMC. The optimum amount of BIS as a crosslinking agent to increase the gel fraction was 5%. Meanwhile, the optimum stirring time was 3 hours. The gel fraction was found to increase with irradiation dose. FTIR confirmed the crosslinking reaction between CMC and VP via irradiation technique and BIS as the crosslinking agent.

## ACKNOWLEDGEMENTS

The authors gratefully acknowledge the assistance of the technical officers from the Department of Chemistry, UPM and Malaysian Nuclear Agency. The authors would also like to acknowledge the financial support from the Ministry of Higher Education (FRGS: Vot no. 5523144) and the Ministry of Science, Technology and Innovation for the sponsorship through the National Science Fellowship.

## REFERENCES

Choi, J-I., Lee, H-S., Kim, J-H., Lee, K-W., Chung, Y-J., Byun, M-W., & Lee, J-W. (2008). Effect of electron beam irradiation on the viscosity of carboxymethylcellulose solution. *Nuclear Instruments and Methods in Physics Research Section B: Beam Interactions with Materials and Atoms, 266,* 5068-5071.

Hennink, W. E., & van Nostrum, C. F. (2002). Novel crosslinking methods to design hydrogels. *Advanced Drug Delivery Reviews, 54*, 13-36.

Ibrahim S. M., El Salmawi K. M., & Zahran A. H. (2007). Synthesis of crosslinked superabsorbent carboxymethyl cellulose/acrylamide hydrogels through electron-beam irradiation. *Journal of Applied Polymer Science, 104*, 2003-2008.

Nizam El-Din H. M., Abd Alla S. G., & El-Naggar A. W. M. (2010). Swelling and drug release properties of acrylamide/carboxymethyl cellulose networks formed by gamma irradiation. *Radiation Physics and Chemistry, 79*, 725-730.

Pourjavadi, A., Barzegar, S., & Mahdavinia, G. R. (2006). MBA-crosslinked Na-Alg/CMC as a smart full-polysaccharide superabsorbent hydrogels. *Carbohydrate Polymers, 66*, 386-395.

Sahiner, N., MalcI, S., ÇelikbIçak, Ö., Kantoglu, Ö., & Salih, B. (2005). Radiation synthesis and characterization of new hydrogels based on acrylamide copolymers cross-linked with 1-allyl-2-thiourea. *Radiation Physics and Chemistry, 74*, 76-85.

Singh, D., Choudhary, V., & Koul, V. (2007). Radiation synthesis of interpenetrating polymer networks based on N-vinyl pyrrolidone -acrylic acid copolymer and gelatin. I. Swelling, morphology, and thermal characterization for biomedical applications. *Journal of Applied Polymer Science, 104*, 1456-1463.

Taleb M. F. A., El-Mohdy, H. L. A., & El-Rehim, H. A. A. (2009). Radiation preparation of PVA/CMC copolymers and their application in removal of dyes. *Journal of Hazardous Materials, 168*, 68-75.

Yoshii, F., Zhao, L., Wach, R. A., Nagasawa, N., Mitomo, H., & Kume, T. (2003). Hydrogels of polysaccharide derivatives crosslinked with irradiation at paste-like condition. *Nuclear Instruments and Methods in Physics Research Section B: Beam Interactions with Materials and Atoms Ionizing Radiation and Polymers, 208,* 320-324.

Zhao, L., Mitomo, H., & Yosh, F. (2008). Synthesis of pH-Sensitive and Biodegradable CM-Cellulose/ Chitosan Polyampholytic Hydrogels with Electron Beam Irradiation. *J. Bioact. Compat. Polym., 23*, 319-333.

Pertanika J. Sci. & Technol. 20 (2): 435 - 444 (2012)

SCIENCE & TECHNOLOGY

Journal homepage: http://www.pertanika.upm.edu.my/

# UV-Curable Palm Oil Based-Urethane Acrylate/Clay Nanocomposites

**A. M. Salih[1,2]*, Wan Md. Zin Wan Yunus[3], Khairul Zaman Mohd Dahlan[4], Mohd Hilmi Mahmood[4] and Mansor Ahmad[1]**

*[1] Department of Chemistry, Faculty of Science, Universiti Putra Malaysia, 43400 Serdang, Selangor, Malaysia*

*[2]Department of Radiation Processing, Sudan Atomic Energy Commission, Khartoum P.O. Box 3001, Khartoum, Sudan*

*[3]Department of Chemistry, Centre for Defence Foundation Studies, National Defence University of Malaysia, 57000, Sungai Besi Camp, Kuala Lumpur, Malaysia*

*[4]Radiation Processing Technology Division, Malaysian Nuclear Malaysia, Bangi, 43000 Kajang, Selangor*

## ABSTRACT

Synthesis of palm oil based-urethane acrylate (POBUA) resins was carried out by acrylation of epoxidized palm oil (EPOP) using acrylic acid in the presence of a catalyst and followed by isocyanation to obtain the POBUA. Using the monomer as a diluent in the formulation, 4% of photoinitiator and incorporation of organoclay (1-5% wt), nanocomposites were obtained upon UV irradiation. The X-ray Diffractory XRD study revealed that the nanocomposites obtained were of the exfoliation type. The presence of the clay improved the hardness and did not affect the thermal stability. Similarly, it increased the glass transition temperature Tg but reduced the modulus as the clay content was increased. The improvement of the tensile strength was only obtained when the clay concentration was 5 phr.

**Keywords: Nanocomposites, Palm oil based-resin, urethane acrylate, UV-curing**

*Article history:*
Received: 27 July 2011
Accepted: 13 January 2012

*Email addresses:*
ashraf.msalih@gmail.com (A. M. Salih),
wanmdzin@upnm.edu.my (Wan Md. Zin Wan Yunus),
khairul@nuclearmalaysia.gov.my (Khairul Zaman Mohd Dahlan),
hilmi@nuclearmalaysia.gov.my (Mohd Hilmi Mahmood),
mansorahmad@gmail.com (Mansor Ahmad)
*Corresponding author

## INTRODUCTION

Vegetable oils are attractive raw materials for many industrial applications as they are renewable resources and can be produced in large quantities at a competitive cost. Moreover they are biodegradable compounds, and can therefore be classified as environmentally friendly products (Perepelkin, 2005; Galià *et al*., 2009). UV-curable resins are useful for

ISSN: 0128-7680 

many applications due to their fast curing and solvent free characteristics, low energy and temperature requirements (Decker, 1996). At present, polymer-clay nanocomposites have attracted a great deal of researchers' attention and many studies have been conducted on this area (Djouani *et al*., 2010; Jayabalan *et al*., 2009). Compared to their conventional counterparts, nanocomposites display excellent thermal stability and mechanical properties when a small amount of filler was incorporated into a polymer matrix (Keller *et al*., 2004).

Preparation of UV cured nanocomposites has been described by Decker *et al.* (2002). The absence of diffraction peak in the XRD patterns of the nanocomposites indicated that they were of exfoliation type (Decker *et al*., 2002). Intensive investigation on the preparation and characterization of urethane acrylate-clay nanocomposites has been done by Uhl *et al.* (2004). The authors reported that the mechanical properties of the nanocomposites improved, but the thermal stability of these polymer systems was found to be not affected by the addition of the clay (Uhl *et al*., 2004).

It has been reported that clay-based nanocomposite coatings cured by UV light were obtained by incorporating clay up to 10 wt% and using different dispersion methods. In more specific, both the mechanical and optical properties of the nanocomposite coating were found to be strongly affected by the quality of the clay dispersion (Landry *et al*., 2009). In addition, the nanocomposite coatings cured by UV were also compared to the electron beam radiation curing. The UV cured coatings were found to have a better abrasion resistance and the hardness increased as the curing dose increased due to the increase of the cross linking density (Nik Salleh *et al*., 2010). This report describes the preparation and characterization of palm oil based-urethane acrylate-clay nanocomposites.

## MATERIALS AND METHODS

### *Materials*

Epoxidized palm oil (EPOP) with oxirane-oxygen value of 3% per gram (Intermed Sdn. Bhd) was used as a raw material to produce palm oil based resin. Meanwhile, acrylic acid (99%, Aldrich) was used in the acrylation reaction of EPOP to synthesize epoxidized palm oil acrylate (EPOLA). Triethylamine (TEA) and 4-methoxyphenol (4-mp) were supplied by Aldrich Chemical Co. Inc, USA. Toluene 2, 4- diisocyanate (TDI) (80% Aldrich) and acrylate monomer (i.e., hydroxyl ethylacrylate or HEA) were used to prepare palm oil based-urethane acrylate prepolymer (POBUA). In the formulation of the UV-curable coating and nanocomposite films, trimethylopropane triacrylate (TMPTA) and tripropylene glycol diacrylate (TPGDA) (Radcure specialties) were used as monomer diluents for POBUA. Darocure ® 1173 (D-1173) was supplied by CIBA Corporation and used as received. Sodium montmorillonite treated with octadecyamine was used as a filler to prepare the nanocomposites.

### *Synthesis of EPOLA*

Epoxidized palm oil (EPOP), triethylamine and 4-mp (0.25% wt) were mixed in a reaction flask that was equipped with a condenser and stirrer for 1 h at 40ºC. Acrylic acid was introduced into the mixture (mole ratio 1:1 to EPOP). The mixture was then heated to 110ºC. The reaction

was followed by measuring the acid value of the reaction mixture. The reaction was terminated when the acid value was less than 15 mg KOH per gram resin (Hussin & Hilmi, 1990).

*Synthesis of POBUA*

EPOLA was added to a reaction flask fitted with a condenser and a stirrer, and then mixed with 4-mp (1% wt) for 1 h at 40º C. TDI was introduced to the mixture and heated up to 70ºC. Later, HEA was added into the reaction mixture (in mole ratio of 1:1 to EPOLA) and the temperature was kept below 90ºC. Synthesis was followed by FTIR spectroscopy to monitor the disappearance of the absorption peak at 2280 $cm^{-1}$ which indicates the presence of the isocyanate (NCO) group. Fig.1 shows the steps involved in the synthesis.

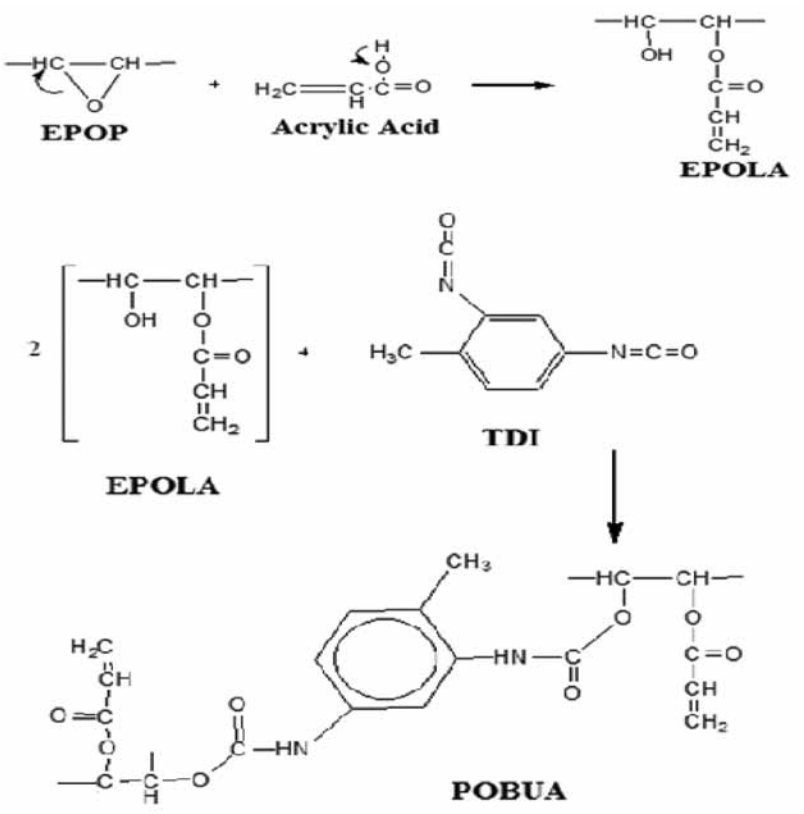


Fig.1: Reaction scheme of palm oil based resin synthesis

*Formulation of the UV-nanocomposite Films*

Table 1 shows the formulation of the POBUA-organoclay nanocomposites. POBUA was mixed with the monomers (TMPTA and TPGDA) and the organoclay, dispersed by stirring and followed by sonication for 30 min at 25ºC. After mixing with the photointiator (4% wt.), the mixture was polymerized in an aluminium mould to obtain a polymer film with a thickness of approximately 1 mm or on a glass substrate to produce a film with a thickness of about 80μm.

*UV-Curing of the Films*

Samples were exposed to UV radiation using an 80 Watt/cm, medium mercury lamp at 5 m/min, with an approximate 1.2 s exposure time.

Table 1: Formulation of the UV-curable nanocomposites films

| Sample | POBUA/g | TPGDA/Phr* | TMPTA/ phr | D1173/phr | O-clay/phr |
|---|---|---|---|---|---|
| 1 | 15 .00 | 40.00 | 15.00 | 4.00 | 1.00 |
| 2 | 15.00 | 40.00 | 15.00 | 4.00 | 3.00 |
| 3 | 15.00 | 40.00 | 15.00 | 4.00 | 5.00 |
| 4 | 15.00 | 40.00 | 15.00 | 4.00 | 0 |

*phr – parts per hundred resin

*Testing*

Measurement of oxirane oxygen content in EPOP and EPOLA samples was done using A.O.C.S Tentative Method Cd 9-57, 1963. Acid value determination (ASTM 974 method) was done by titrating one gram of the resin dissolved in 10 ml acetone. A few drops of phenol red indicator were added and then titrated with 0.1 N KOH and acid values were calculated using the following formula:

$$Av = mg\ KOH/1g\ of\ resin = 5.61 \times f \times v/ w \quad [1]$$

Where f = the factor
v = volume of KOH solution
w = weight of resin sample in grams.

Viscosity of the resins was determined using a Brookfield viscometer model RVTDV-IICP at 25ºC. The molecular weight of resins and POBUA oligomer was determined by GPC (Tosoh made GPC, model HLC-8020). The functional group of the resins and cured films was determined by FTIR spectrophotometer (Perkin Elmer Spectrum 2000).

Meanwhile, the thermal stability of the nanocomposite films was analysed by TGA (Perkin Elmer model TGA 7) and the glass transition temperature of the cured films was determined by DSC (Shimadzu DSC-60). X-ray diffraction test was also carried out using a Shimadzu XRD 6000 diffractometer with Cu-Kα radiation (λ=0.15406 nm). The samples were scanned from 2 to 10º theta at 1º/min.

Universal Tester Machine (Instron) was used to determine the mechanical properties of the cured samples (ASTM 1822 L), while the hardness of the cured films was studied using a pendulum hardness tester (Konig method). The cured films of a known weight ($W_1$) in SUS 304 stainless steel wire-mesh filter size # 100 was Soxhlet extracted for 16 h using acetone

as a solvent, dried in a vacuum oven and weighed ($W_2$) until a constant weight was obtained. Gel percentages were calculated as follows:

$$Gel\% = W_2 x 100 / W_1 \quad [2]$$

## RESULTS AND DISCUSSION

### *Synthesis of EPOLA*

Acrylation reaction was followed by the acid value titration. The acid values before and after 16 hours of the reaction were 51 mg and 10 mg KOH/g, respectively, and this indicated that EPOLA had been successfully obtained. Table 2 shows some properties of EPOP and EPOLA.

Table 2: Properties of EPOP and EPOLA.

| Resin | Viscosity/cps at 25ºC | Mw g/mole | $O_x$-$O_2$ % per mole |
|---|---|---|---|
| EPOP | 240 | 1664 | 3.0 |
| EPOLA | 1500 | 2197 | 0.2 |

The decrease in oxirane oxygen percentage, i.e. from 3% in EPOP to less than 1% in EPOLA, was due to the degradation of the oxirane rings in the acrylation reaction.

Fig.1 shows the FTIR spectra of EPOP and EPOLA. The absence of the absorption peak at 840 $cm^{-1}$ in the EPOLA spectrum, which corresponds to the asymmetric bend of oxirane ring and the appearance of peaks at 810 and 1630 cm-1 which indicate the presence of CH out of plane deformation and C=C stretching respectively in the acrylate group of EPOLA, showed that the acrylation of EPOP was successfully carried out. The same observations were also reported by Hussin and Hilmi (1990).

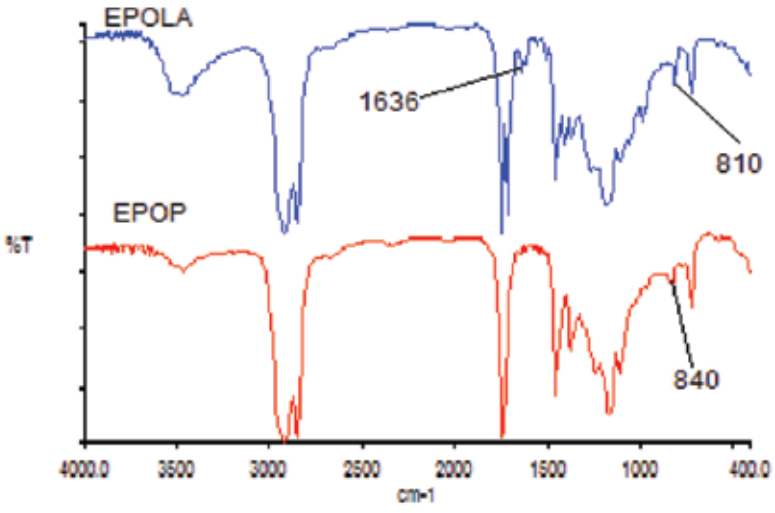


Fig.2: FTIR spectrum of EPOP and EPOLA

Fig.3 displays the FTIR spectra of the reaction mixture from several stages of the synthesis. The disappearance of the absorption peak of the NCO group at 2286 $cm^{-1}$ indicates the isocyanation reaction with OH, which decreases (as shown by 3456 $cm^{-1}$peak) as the urethane linkage is formed. The molecular weight of POBUA, as characterized by GPC, is around 4500 g/mole with the viscosity of about 700 cps at 25ºC.

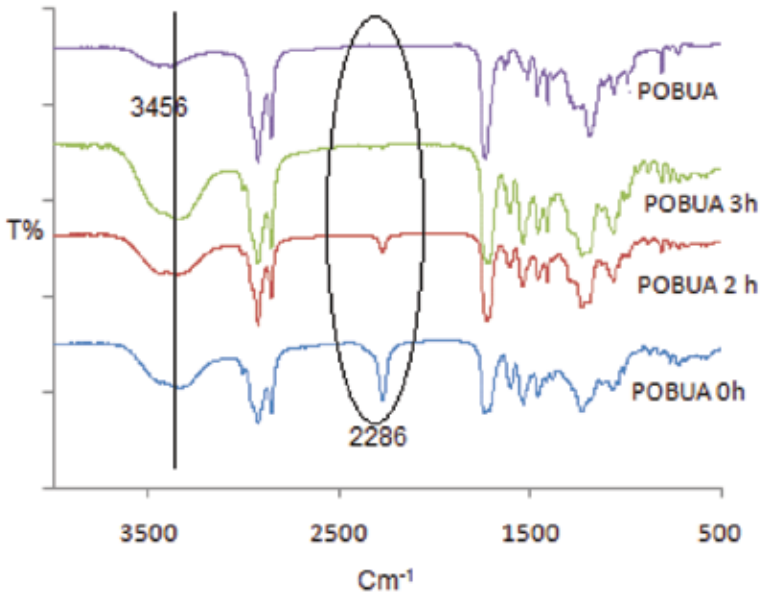


Fig.3: FTIR spectrum of POBUA at different stages during synthesis

*Nanocomposite Films*

Exfoliated nanocomposites can be obtained if the silicate layers of the clay are completely separated and randomly distributed in a polymer matrix (Keller *et al*., 2004). The disappearance of the Bragg diffraction peaks in the composite XRD patterns (Fig.4) indicates that the clay layers in the composite have been exfoliated.

The mechanical properties of the nanocomposites were investigated through tensile strength measurements. Fig.5 shows the dependence of the tensile strength and Young`s moduli on the clay concentration. The presence of 5 phr of the clay slightly improves the tensile value but reduces the modulus. The DSC results shown in Fig.6 indicate that the glass transition temperature (Tg) has shifted to higher values as the percentage of clay loaded in the nanocomposite films is increased, which is in agreement with the previous reports by Uhl *et al*. (2004) and Uhl *et al*. (2006).

Fig.7 shows the thermograms of the film samples. It was observed that there was no significant effect of clay content on the thermal stability of these polymer composites (Uhl *et al*., 2004). Meanwhile, the crosslinking density of these composites is more than 80% and increases as the organoclay content is increased, indicating the formation of a strong linkage between the polymer chains and the filler particles. Similarly, the pendulum hardness also increases with the increase in the percentage of the organoclay added (*see* Fig.8).

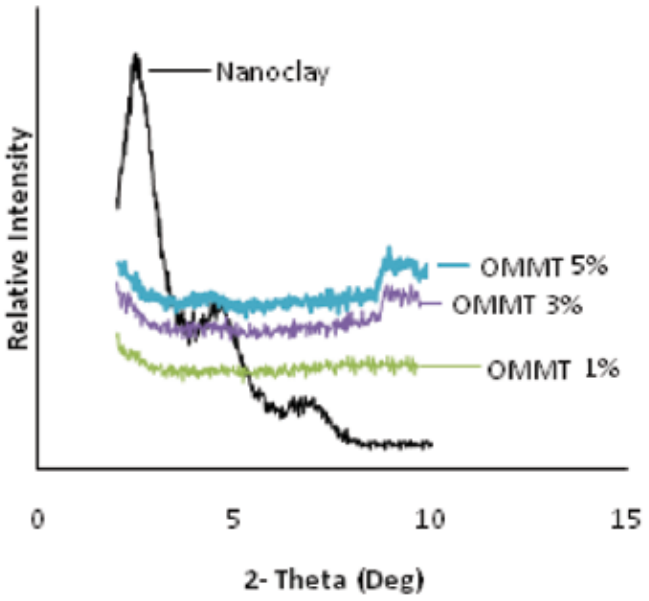


Fig.4: The XRD pattern of POBUA-clay nanocomposites

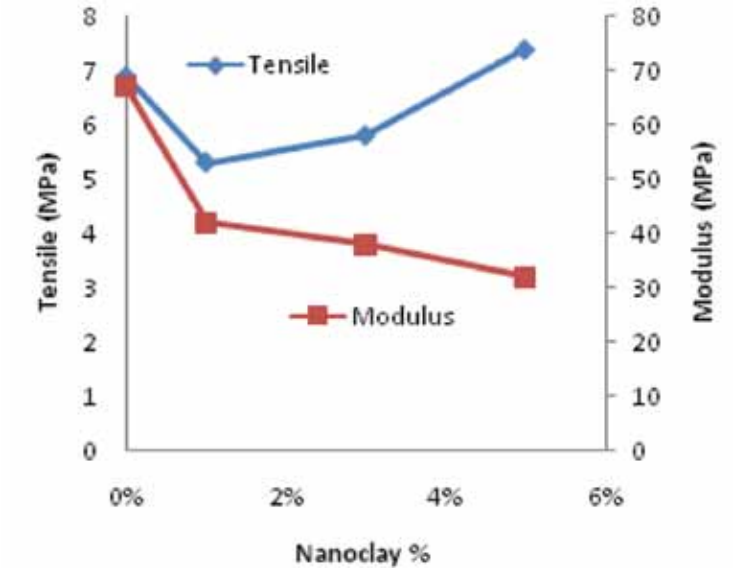


Fig.5: Mechanical properties vs. organoclay (%)

## CONCLUSIONS

Palm oil based polyurethane acrylate nanocomposites were successfully prepared. The presence of the clay improves the hardness, $T_g$, and crosslinking density, but it also reduces the modulus. Higher tensile strength could only be obtained when the clay concentration reached 5wt%.

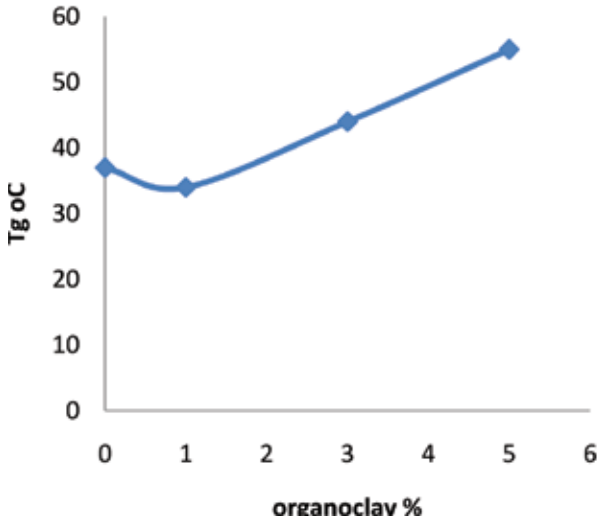


Fig.6: The dependence of the glass transition temperature on the wt% of organoclay

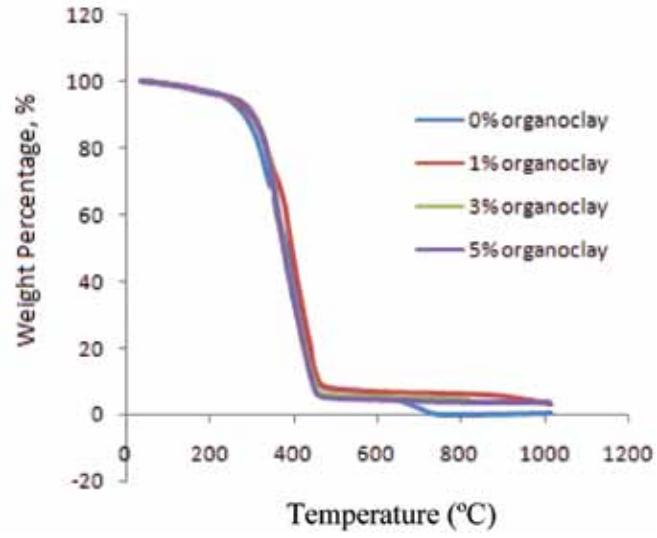


Fig.7: TGA thermogarms of the nanocomposites films

## ACKNOWLEDGEMENTS

The authors would like to thank Malaysian Nuclear Agency (MNA) for supporting this study and special thanks go to Radiation processing division staff and assistants. Special acknowledgement is also extended Prof. Sabu Thomas from the School of Chemical Sciences, Mahatma Gandhi University, India and Prof. Dean C. Webster from the Department of Coatings and Polymeric Materials, North Dakota State University, USA for their advice and assistance.

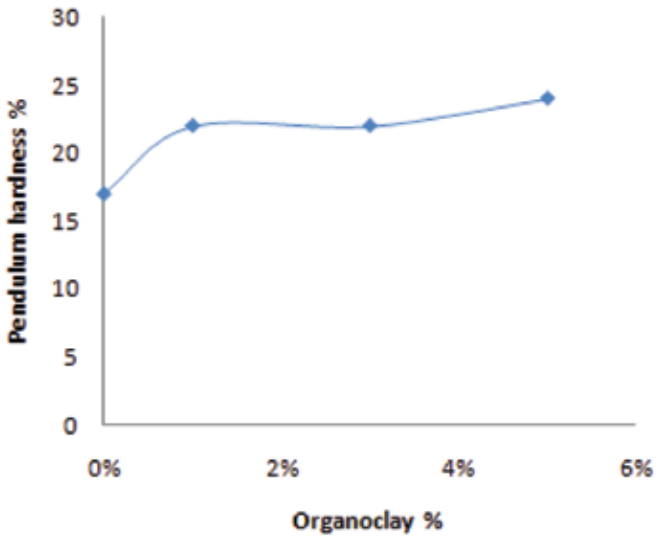


Fig.8: Pendulum hardness percentage Vs. Organoclay (wt.%)

## REFERENCES

Decker, C. (1996). Photoinitiated crosslinking polymerisation. *Progress in Polymer Science, 21*(4), 593-650.

Decker, C., Zahouily, K., Keller, L., Benfarhi, S., Bendaikha, T., & Baron, J. (2002). Ultrafast synthesis of bentonite-acrylate nanocomposite materials by UV-radiation curing. *Journal of Materials Science,* 37(22), 4831-4838.

Djouani, F., Herbst, F., Chehimi, M. M., & Benzarti, K. (2010). Synthesis, characterization and reinforcing properties of novel, reactive clay/poly(glycidyl methacrylate) nanocomposites. *Construction and Building Materials, 25*(2), 424-431.

Galià, M., de Espinosa, L. M., Ronda, J. C., Lligadas, G., & Cádiz, V. (2009). Vegetable oil-based thermosetting polymers. *European Journal of Lipid Science and Technology, 112*(1), 87-96.

Hussin, M. N., & Hilmi, M. M. (1990). The use of Epoxidised palm oil (EPOP) for the synthesis of Radiation curable resins1. Synthesis of Epoxidised RBD palm olien acyrlate. *Japanese Society of Nuclear Medicine, 8*(2), 149-155.

Jayabalan, M., Shalumon, K. T., Mitha, M. K., Ganesan, K., & Epple, M. (2009). Effect of hydroxyapatite on the biodegradation and biomechanical stability of polyester nanocomposites for orthopaedic applications. *Acta Biomaterialia, 6*(3), 763-775.

Keller, L., Decker, C., Zahouily, K., Benfarhi, S., Le Meins, J. M., & Miehe-Brendle, J. (2004). Synthesis of polymer nanocomposites by UV-curing of organoclay-acrylic resins. *Polymer, 45*(22), 7437-7447.

Landry, V., Blanchet, P., and Riedl, B. (2009). Mechanical and optical properties of clay-based nanocomposites coatings for wood flooring. *Progress in Organic Coatings, 67*(4), 381-388.

Nik Salleh, N.G., Firdaus Yhaya, M., Hassan, A., Abu Bakar, A., and Mokhtar, M. (2010). Effect of UV/EB radiation dosages on the properties of nanocomposite coatings. *Radiation physics and chemistry, 80*(2), 136-141.

Perepelkin, K. (2005). Polymeric materials of the future based on renewable plant resources and biotechnologies: Fibres, films, plastics. *Fibre Chemistry, 37*(6), 417-430.

Uhl, F.M., Davuluri, S.P., Wong, S.-C., and Webster, D.C. (2004). Organically modified montmorillonites in UV curable urethane acrylate films. *Polymer, 45*(18), 6175-6187.

Uhl, F.M., Webster, D.C., Davuluri, S.P. & Wong, S.-C. (2006). UV curable epoxy acrylate-clay nanocomposites. *European Polymer Journal, 42*(10), 2596-2605.

# Pertanika Journal of Science & Technology

## Subject Index for Volume 20 (1) & (2) 2012

# Pertanika Journal of Science & Technology

## Author Index for Volume 20 (1) & (2) 2012

# REFEREES FOR THE PERTANIKA JOURNAL OF SCIENCE AND TECHNOLOGY VOL. 20 (2) JUL. 2012

The Editorial Board of the Journal of Science and Technology wishes to thank the following for acting as referees for manuscripts published in this issue of JST.

Adem Kilicman
*(UPM, Malaysia)*

Ahmad Ramli Saad
*(USM, Malaysia)*

Amu Therwath
*(Université Paris, France)*

Bala Ramudu Paramkusam
*(Institute of Technology – Banaras Hindu University, India)*

Biswa Mohan Biswal
*(USM, Malaysia)*

BT Hang Tuah Baharudin
*(UPM, Malaysia)*

Chan Ngai Weng
*(USM, Malaysia)*

Dandi Bachtiar
*(UPM, Malaysia)*

Edi Syams Zainudin
*(UPM, Malaysia)*

Hasfalina Che Man
*(UPM, Malaysia)*

Izani Md Ismail
*(USM, Malaysia)*

Jayanthi Arasan
*(UPM, Malaysia)*

Khalina Abdan
*(UPM, Malaysia)*

M. Abdul Maleque
*(Multimedia University, Malaysia)*

Maheswar Maharana
*(Indira Gandhi Institute of Technology, India)*

Mohamad Ridzwan Ishak
*(UPM, Malaysia)*

Mohamed Abd Rahman
*(International Islamic University Malaysia, Malaysia)*

Mohamed Ansari M. Nainar
*(Universiti Tenaga Nasional, Malaysia)*

Mohamed Azwan Mohamed Zawawi
*(UPM, Malaysia)*

Mohd Noriznan Mokhtar
*(UPM, Malaysia)*

Mohd Sapuan Salit
*(UPM, Malaysia)*

Napsiah Ismail
*(UPM, Malaysia)*

Nazlina Ibrahim
*(UKM, Malaysia)*

Norman Mariun
*(UPM, Malaysia)*

Riza Wirawan
*(UPM, Malaysia)*

Rozita Omar
*(UPM, Malaysia)*

Rozita Rosli
*(UPM, Malaysia)*

Safian Sharif
*(UTM, Malaysia)*

Sahari Japar
*(UPM, Malaysia)*

Salmiaton Ali
*(UPM, Malaysia)*

Saroje Kumar Sarkar
*(UPM, Malaysia)*

Shafreeza Sobri
*(UPM, Malaysia)*

Sharmala Devi Sakaran
*(UM, Malaysia)*

Siti Khairunniza Bejo
*(UPM, Malaysia)*

Siti Mazlina Mustapa Kamal
*(UPM, Malaysia)*

Thamer Ahmed Mohamed
*(UPM, Malaysia)*

Wan Nor Azmin Sulaiman
*(UPM, Malaysia)*

Yong Zulina Zubairi
*(UM, Malaysia)*

***Note:***
*UPM – Universiti Putra Malaysia*
*UKM – Universiti Kebangsaan Malaysia*
*USM – Universiti Sains Malaysia*
*UTM – Universiti Teknologi Malaysia*
*UM – Universiti Malaya*


## Special Acknowledgement

The **JST Editorial Board** gratefully acknowledges the assistance of **Doreen Dillah**, who served as the English language editor for this issue.

# *Pertanika*

*Our goal is to bring high quality research to the widest possible audience*

**Journal of Science & Technology**

## INSTRUCTIONS TO AUTHORS

(Manuscript Preparation & Submission Guidelines)

Revised: July 2012

*We aim for excellence, sustained by a responsible and professional approach to journal publishing.*
*We value and support our authors in the research community.*

Please read the guidelines and follow these instructions carefully; doing so will ensure that the publication of your manuscript is as rapid and efficient as possible. The Editorial Board reserves the right to return manuscripts that are not prepared in accordance with these guidelines.

## About the Journal

*Pertanika* is an international peer-reviewed journal devoted to the publication of original papers, and it serves as a forum for practical approaches to improving quality in issues pertaining to tropical agriculture and its related fields. *Pertanika* began publication in 1978 as Journal of Tropical Agricultural Science. In 1992, a decision was made to streamline *Pertanika* into three journals to meet the need for specialised journals in areas of study aligned with the interdisciplinary strengths of the university. The revamped Journal of Science and Technology (JST) is now focusing on research in science and engineering, and its related fields. Other *Pertanika* series include Journal of Tropical Agricultural Science (JTAS); and Journal of Social Sciences and Humanities (JSSH).

JST is published in **English** and it is open to authors around the world regardless of the nationality. It is currently published two times a year i.e. in **January** and **July**.

### Goal of *Pertanika*

Our goal is to bring the highest quality research to the widest possible audience.

### Quality

We aim for excellence, sustained by a responsible and professional approach to journal publishing. Submissions are guaranteed to receive a decision within 12 weeks. The elapsed time from submission to publication for the articles averages 5-6 months.

### Indexing of *Pertanika*

Pertanika is now over 33 years old; this accumulated knowledge has resulted in Pertanika journals being indexed in SCOPUS (Elsevier), EBSCO, DOAJ, AGRICOLA, and CABI etc. JST is indexed in SCOPUS, EBSCO, DOAJ and ISC.

### Future vision

We are continuously improving access to our journal archives, content, and research services. We have the drive to realise exciting new horizons that will benefit not only the academic community, but society itself.

We also have views on the future of our journals. The emergence of the online medium as the predominant vehicle for the 'consumption' and distribution of much academic research will be the ultimate instrument in the dissemination of the research news to our scientists and readers.

## Aims and Scope

*Pertanika* Journal of Science and Technology aims to provide a forum for high quality research related to science and engineering research. Areas relevant to the scope of the journal include: *bioinformatics, bioscience, biotechnology and bio-molecular sciences, chemistry, computer science, ecology, engineering, engineering design, environmental control and management, mathematics and statistics, medicine and health sciences, nanotechnology, physics, safety and emergency management*, and related fields of study.

## Editorial Statement

*Pertanika* is the official journal of Universiti Putra Malaysia. The abbreviation for *Pertanika* Journal of Science & Technology is *Pertanika J. Sci. Technol.*

## Guidelines for Authors

**Publication policies**

*Pertanika* policy prohibits an author from submitting the same manuscript for concurrent consideration by two or more publications. It prohibits as well publication of any manuscript that has already been published either in whole or substantial part elsewhere. It also does not permit publication of manuscript that has been published in full in Proceedings. Please refer to Pertanika's **Code of Ethics** for full details.

**Editorial process**

Authors are notified on receipt of a manuscript and upon the editorial decision regarding publication.

*Manuscript review*: Manuscripts deemed suitable for publication are sent to the Editorial Board members and/or other reviewers. We encourage authors to suggest the names of possible reviewers. Notification of the editorial decision is usually provided within to eight to ten weeks from the receipt of manuscript. Publication of solicited manuscripts is not guaranteed. In most cases, manuscripts are accepted conditionally, pending an author's revision of the material.

*Author approval*: Authors are responsible for all statements in articles, including changes made by editors. The liaison author must be available for consultation with an editor of *The Journal* to answer questions during the editorial process and to approve the edited copy. Authors receive edited typescript (not galley proofs) for final approval. Changes **cannot** be made to the copy after the edited version has been approved.

**Manuscript preparation**

*Pertanika* accepts submission of mainly four types of manuscripts. Each manuscript is classified as **regular** or **original** articles, **short communications**, **reviews**, and proposals for **special issues**. Articles must be in **English** and they must be competently written and argued in clear and concise grammatical English. Acceptable English usage and syntax are expected. Do not use slang, jargon, or obscure abbreviations or phrasing. Metric measurement is preferred; equivalent English measurement may be included in parentheses. Always provide the complete form of an acronym/abbreviation the first time it is presented in the text. Contributors are strongly recommended to have the manuscript checked by a colleague with ample experience in writing English manuscripts or an English language editor.

Linguistically hopeless manuscripts will be rejected straightaway (e.g., when the language is so poor that one cannot be sure of what the authors really mean). This process, taken by authors before submission, will greatly facilitate reviewing, and thus publication if the content is acceptable.

The instructions for authors must be followed. Manuscripts not adhering to the instructions will be returned for revision without review. Authors should prepare manuscripts according to the guidelines of *Pertanika*.

**1. Regular article**

*Definition:* Full-length original empirical investigations, consisting of introduction, materials and methods, results and discussion, conclusions. Original work must provide references and an explanation on research findings that contain new and significant findings.

*Size:* Should not exceed 5000 words or 8-10 printed pages (excluding the abstract, references, tables and/or figures). One printed page is roughly equivalent to 3 type-written pages.

**2. Short communications**

*Definition:* Significant new information to readers of the Journal in a short but complete form. It is suitable for the publication of technical advance, bioinformatics or insightful findings of plant and animal development and function.

*Size:* Should not exceed 2000 words or 4 printed pages, is intended for rapid publication. They are not intended for publishing preliminary results or to be a reduced version of Regular Papers or Rapid Papers.

**3. Review article**

*Definition:* Critical evaluation of materials about current research that had already been published by organizing, integrating, and evaluating previously published materials. Re-analyses as meta-analysis and systemic reviews are encouraged. Review articles should aim to provide systemic overviews, evaluations and interpretations of research in a given field.

*Size:* Should not exceed 4000 words or 7-8 printed pages.

**4. Special issues**

*Definition:* Usually papers from research presented at a conference, seminar, congress or a symposium.

*Size:* Should not exceed 5000 words or 8-10 printed pages.

**5. Others**

*Definition:* Brief reports, case studies, comments, Letters to the Editor, and replies on previously published articles may be considered.

*Size:* Should not exceed 2000 words or up to 4 printed pages.

With few exceptions, original manuscripts should not exceed the recommended length of 6 printed pages (about 18 typed pages, double-spaced and in 12-point font, tables and figures included). Printing is expensive, and, for the Journal, postage doubles when an issue exceeds 80 pages. You can understand then that there is little room for flexibility.

Long articles reduce the Journal's possibility to accept other high-quality contributions because of its 80-page restriction. We would like to publish as many good studies as possible, not only a few lengthy ones. (And, who reads overly long articles anyway?) Therefore, in our competition, short and concise manuscripts have a definite advantage.

**Format**

The paper should be formatted in one column format with at least 4cm margins and 1.5 line spacing throughout. Authors are advised to use Times New Roman 12-point font. Be especially careful when you are inserting special characters, as those inserted in different fonts may be replaced by different characters when converted to PDF files. It is well known that 'μ' will be replaced by other characters when fonts such as 'Symbol' or 'Mincho' are used.

A maximum of eight keywords should be indicated below the abstract to describe the contents of the manuscript. Leave a blank line between each paragraph and between each entry in the list of bibliographic references. Tables should preferably be placed in the same electronic file as the text. Authors should consult a recent issue of the Journal for table layout.

Every page of the manuscript, including the title page, references, tables, etc. should be numbered. However, no reference should be made to page numbers in the text; if necessary, one may refer to sections. Underline words that should be in italics, and do not underline any other words.

We recommend that authors prepare the text as a **Microsoft Word** file.

1. Manuscripts in general should be organised in the following order:

    - **Page 1: Running title.** (Not to exceed 60 characters, counting letters and spaces). This page should **only** contain the running title of your paper. The running title is an abbreviated title used as the running head on every page of the manuscript.

      In addition, the **Subject areas m**ost relevant to the study **must be indicated on this page.** Select the appropriate subject areas from the Scope of the Journals provided in the Manuscript Submission Guide.

      A **list** of n**umber of black and white / colour figures and tables should also be indicated on this page.** Figures submitted in color will be printed in colour. See "*5. Figures & Photographs"* for details.

    - **Page 2: Author(s) and Corresponding author information.** This page should contain the **full title** of your paper with name(s) of all the authors, institutions and corresponding author's name, institution and full address (Street address, telephone number (including extension), hand phone number, fax number and e-mail address) for editorial correspondence. The names of the authors **must** be abbreviated following the international naming convention. e.g. Salleh, A.B., Tan, S.G., or Sapuan, S.M.

      **Authors' addresses.** Multiple authors with different addresses must indicate their respective addresses separately by superscript numbers:

      George Swan[1] and Nayan Kanwal[2]
      [1]Department of Biology, Faculty of Science, Duke University, Durham, North Carolina, USA.
      [2]Office of the Deputy Vice Chancellor (R&I), Universiti Putra Malaysia, Serdang, Malaysia.

    - **Page 3**: This page should **repeat** the **full title** of your paper with only the **Abstract** (the abstract should be less than 250 words for a Regular Paper and up to 100 words for a Short Communication). **Keywords** must also be provided on this page (Not more than eight keywords in alphabetical order).

    - **Page 4 and subsequent pages**: This page should begin with the **Introduction** of your article and the rest of your paper should follow from page 5 onwards.

    **Abbreviations.** Define alphabetically, other than abbreviations that can be used without definition. Words or phrases that are abbreviated in the introduction and following text should be written out in full the first time that they appear in the text, with each abbreviated form in parenthesis. Include the common name or scientific name, or both, of animal and plant materials.

    **Footnotes.** Current addresses of authors if different from heading.

2. **Text.** Regular Papers should be prepared with the headings **Introduction**, **Materials and Methods**, **Results and Discussion, Conclusions** in this order. Short Communications should be prepared according to "*8. Short Communications."* below.

3. **Tables.** All tables should be prepared in a form consistent with recent issues of *Pertanika* and should be numbered consecutively with Arabic numerals. Explanatory material should be given in the table legends and footnotes. Each

table should be prepared on a separate page. (Note that when a manuscript is accepted for publication, tables must be submitted as data - .doc, .rtf, Excel or PowerPoint file- because tables submitted as image data cannot be edited for publication.)

4. **Equations and Formulae.** These must be set up clearly and should be typed triple spaced. Numbers identifying equations should be in square brackets and placed on the right margin of the text.

5. **Figures & Photographs.** Submit an original figure or photograph. Line drawings must be clear, with high black and white contrast. Each figure or photograph should be prepared on a separate sheet and numbered consecutively with Arabic numerals. Appropriate sized numbers, letters and symbols should be used, no smaller than 2 mm in size after reduction to single column width (85 mm), 1.5-column width (120 mm) or full 2-column width (175 mm).

6. Failure to comply with these specifications will require new figures and delay in publication. For electronic figures, create your figures using applications that are capable of preparing high resolution TIFF files acceptable for publication. In general, we require **300 dpi or higher resolution for coloured and half-tone artwork** and **1200 dpi or higher for line drawings**. For review, you may attach low-resolution figures, which are still clear enough for reviewing, to keep the file of the manuscript under 5 MB. Illustrations may be produced at extra cost in colour at the discretion of the Publisher; the author could be charged Malaysian Ringgit 50 for each colour page.

7. **References.** Literature citations in the text should be made by name(s) of author(s) and year. For references with more than two authors, the name of the first author followed by *'et al*.' should be used.

   Swan and Kanwal (2007) reported that …
   The results have been interpreted (Kanwal *et al.* 2009).

   - References should be listed in alphabetical order, by the authors' last names. For the same author, or for the same set of authors, references should be arranged chronologically. If there is more than one publication in the same year for the same author(s), the letters 'a', 'b', etc., should be added to the year.

   - When the authors are more than 11, list 5 authors and then et al.

   - Do not use indentations in typing References. Use one line of space to separate each reference. The name of the journal should be written in full. For example:

     - Jalaludin, S. (1997a). Metabolizable energy of some local feeding stuff. *Tumbuh, 1,* 21-24.
     - Jalaludin, S. (1997b). The use of different vegetable oil in chicken ration. *Malayan Agriculturist, 11,* 29-31.
     - Tan, S.G., Omar, M.Y., Mahani, K.W., Rahani, M., & Selvaraj, O.S. (1994). Biochemical genetic studies on wild populations of three species of green leafhoppers *Nephotettix* from Peninsular Malaysia. *Biochemical Genetics*, *32,* 415 - 422.

   - In case of citing an author(s) who has published more than one paper in the same year, the papers should be distinguished by addition of a small letter as shown above, e.g. Jalaludin (1997a); Jalaludin (1997b).

   - Unpublished data and personal communications should not be cited as literature citations, but given in the text in parentheses. 'In press' articles that have been accepted for publication may be cited in References. Include in the citation the journal in which the 'in press' article will appear and the publication date, if a date is available.

8. **Examples of other reference citations**:

   ***Monographs***: Turner, H.N., & Yong, S.S.Y. (2006). *Quantitative Genetics in Sheep Breeding*. Ithaca: Cornell University Press.

   ***Chapter in Book***: Kanwal, N.D.S. (1992). Role of plantation crops in Papua New Guinea economy. In Angela R. McLean (Ed.), *Introduction of livestock in the Enga province PNG* (p. 221-250). United Kingdom: Oxford Press.

   ***Proceedings***: Kanwal, N.D.S. (2001). Assessing the visual impact of degraded land management with landscape design software. In Kanwal, N.D.S., & Lecoustre, P. (Eds.), *International forum for Urban Landscape Technologies* (p. 117-127). Lullier, Geneva, Switzerland: CIRAD Press.

9. **Short Communications** should include **Introduction, Materials and Methods, Results and Discussion, Conclusions** in this order. Headings should only be inserted for Materials and Methods. The abstract should be up to 100 words, as stated above. Short Communications must be 5 printed pages or less, including all references, figures and tables. References should be less than 30. A 5 page paper is usually approximately 3000 words plus four figures or tables (if each figure or table is less than 1/4 page).

   *Authors should state the total number of words (including the Abstract) in the cover letter. Manuscripts that do not fulfill these criteria will be rejected as Short Communications without review.

**STYLE OF THE MANUSCRIPT**

Manuscripts should follow the style of the latest version of the Publication Manual of the American Psychological Association (APA). The journal uses American or British spelling and authors may follow the latest edition of the Oxford Advanced Learner's Dictionary for British spellings.

**SUBMISSION OF MANUSCRIPTS**

All articles should be submitted electronically using the ScholarOne web-based system. ScholarOne, a Thomson Reuters product provides comprehensive workflow management systems for scholarly journals. For more information, go to our web page and click "**Online Submission**".

Alternatively, you may submit the electronic files (cover letter, manuscript, and the **Manuscript Submission Kit** comprising *Declaration* and *Referral* forms) via email directly to the Executive Editor. If the files are too large to email, mail a CD containing the files. The **Manuscript Submission Guide** and **Submission Kit** are available from the *Pertanika*'s home page at http://www.pertanika.upm.edu.my/ or from the Executive Editor's office upon request.

All articles submitted to the journal **must comply** with these instructions. Failure to do so will result in return of the manuscript and possible delay in publication.

Please do **not** submit manuscripts to the editor-in-chief or to any other office directly. All manuscripts must be **submitted through the executive editor's office** to be properly acknowledged and rapidly processed at the address below:

Dr. Nayan KANWAL
The Executive Editor
Pertanika Journals, UPM Press
Office of the Deputy Vice Chancellor (R&I)
IDEA Tower II, UPM-MTDC Technology Centre
Universiti Putra Malaysia
43400 UPM, Serdang, Selangor
Malaysia
E-mail: ndeeps@admin.upm.edu.my; tel: + 603-8947 1622.
or visit our website at http://www.pertanika.upm.edu.my/ for further information.

Authors should retain copies of submitted manuscripts and correspondence, as materials can not be returned. Authors are required to inform the Executive Editor of any change of address which occurs whilst their papers are in the process of publication.

**Cover letter**

All submissions must be accompanied by a cover letter detailing what you are submitting. Papers are accepted for publication in the journal on the understanding that the article is original and the content has not been published or submitted for publication elsewhere. This must be stated in the cover letter.

The cover letter must also contain an acknowledgement that all authors have contributed significantly, and that all authors are in agreement with the content of the manuscript.

The cover letter of the paper should contain (i) the title; (ii) the full names of the authors; (iii) the addresses of the institutions at which the work was carried out together with (iv) the full postal and email address, plus facsimile and telephone numbers of the author to whom correspondence about the manuscript should be sent. The present address of any author, if different from that where the work was carried out, should be supplied in a footnote.

As articles are double-blind reviewed, material that might identify authorship of the paper should be placed on a cover sheet.

**Peer review**

*Pertanika* follows a **double-blind peer-review** process. Peer reviewers are experts chosen by journal editors to provide written assessment of the **strengths** and **weaknesses** of written research, with the aim of improving the reporting of research and identifying the most appropriate and highest quality material for the journal.

In the peer-review process, three referees independently evaluate the scientific quality of the submitted manuscripts. Authors are encouraged to indicate in the **Referral form** using the **Manuscript Submission Kit** the names of three potential reviewers, but the editors will make the final choice. The editors are not, however, bound by these suggestions.

Manuscripts should be written so that they are intelligible to the professional reader who is not a specialist in the particular field. They should be written in a clear, concise, direct style. Where contributions are judged as acceptable for publication on the basis of content, the Editor reserves the right to modify the typescripts to eliminate ambiguity and repetition and improve communication between author and reader. If extensive alterations are required, the manuscript will be returned to the author for revision.

**The Journal's review process**

What happens to a manuscript once it is submitted to *Pertanika*? Typically, there are seven steps to the editorial review process:

1. The executive editor and the editorial board examine the paper to determine whether it is appropriate for the journal and should be reviewed. If not appropriate, the manuscript is rejected outright and the author is informed.

2. The executive editor sends the article-identifying information having been removed, to three reviewers. Typically, one of these is from the Journal's editorial board. Others are specialists in the subject matter represented by the article. The executive editor asks them to complete the review in three weeks and encloses two forms: (a) referral form B and (b) reviewer's comment form along with reviewer's guidelines. Comments to authors are about the appropriateness and adequacy of the theoretical or conceptual framework, literature review, method, results and discussion, and conclusions. Reviewers often include suggestions for strengthening of the manuscript. Comments to the editor are in the nature of the significance of the work and its potential contribution to the literature.

3. The executive editor, in consultation with the editor-in-chief, examines the reviews and decides whether to reject the manuscript, invite the author(s) to revise and resubmit the manuscript, or seek additional reviews. Final acceptance or rejection rests with the Editorial Board, who reserves the right to refuse any material for publication. In rare instances, the manuscript is accepted with almost no revision. Almost without exception, reviewers' comments (to the author) are forwarded to the author. If a revision is indicated, the editor provides guidelines for attending to the reviewers' suggestions and perhaps additional advice about revising the manuscript.

4. The authors decide whether and how to address the reviewers' comments and criticisms and the editor's concerns. The authors submit a revised version of the paper to the executive editor along with specific information describing how they have answered' the concerns of the reviewers and the editor.

5. The executive editor sends the revised paper out for review. Typically, at least one of the original reviewers will be asked to examine the article.

6. When the reviewers have completed their work, the executive editor in consultation with the editorial board and the editor-in-chief examine their comments and decide whether the paper is ready to be published, needs another round of revisions, or should be rejected.

7. If the decision is to accept, the paper is sent to that Press and the article should appear in print in approximately three months. The Publisher ensures that the paper adheres to the correct style (in-text citations, the reference list, and tables are typical areas of concern, clarity, and grammar). The authors are asked to respond to any queries by the Publisher. Following these corrections, page proofs are mailed to the corresponding authors for their final approval. At this point, only essential changes are accepted. Finally, the article appears in the pages of the Journal and is posted on-line.

**English language editing**

Pertanika **emphasizes** on the linguistic accuracy of every manuscript published. Thus all authors are required to get their manuscripts edited by **professional English language editors**. Author(s) **must provide a certificate** confirming that their manuscripts have been adequately edited. A proof from a recognised editing service should be submitted together with the cover letter at the time of submitting a manuscript to Pertanika**. All costs will be borne by the author(s)**.

This step, taken by authors before submission, will greatly facilitate reviewing, and thus publication if the content is acceptable.

## Author material archive policy

Authors who require the return of any submitted material that is rejected for publication in the journal should indicate on the cover letter. If no indication is given, that author's material should be returned, the Editorial Office will dispose of all hardcopy and electronic material.

**Copyright**

Authors publishing the Journal will be asked to sign a declaration form. In signing the form, it is assumed that authors have obtained permission to use any copyrighted or previously published material. All authors must read and agree to the conditions outlined in the form, and must sign the form or agree that the corresponding author can sign on their behalf. Articles cannot be published until a signed form has been received.

**Lag time**

A decision on acceptance or rejection of a manuscript is reached in 3 to 4 months (average 14 weeks). The elapsed time from submission to publication for the articles averages 5-6 months.

**Hardcopies of the Journals and off prints**

Under the Journal's open access initiative, authors can choose to download free material (via PDF link) from any of the journal issues from Pertanika's website. Under "Browse Journals" you will see a link entitled "Current Issues" or "Archives". Here you will get access to all back-issues from 1978 onwards.

The **corresponding author** for all articles will receive one complimentary hardcopy of the journal in which his/her articles is published. In addition, 20 off prints of the full text of their article will also be provided. Additional copies of the journals may be purchased by writing to the executive editor.

# Pertanika

*Our goal is to bring high quality research to the widest possible audience*

Pertanika is an international peer-reviewed leading journal in Malaysia which began publication in 1978. The journal publishes in three different areas — Journal of Tropical Agricultural Science (JTAS); Journal of Science and Technology (JST); and Journal of Social Sciences and Humanities (JSSH).

**JTAS** is devoted to the publication of original papers that serve as a forum for practical approaches to improving quality in issues pertaining to tropical agricultural research or related fields of study. It is published four times a year in **February**, **May**, **August** and **November**.

**JST** caters for science and engineering research or related fields of study. It is published twice a year in **January** and **July**.

**JSSH** deals in research or theories in social sciences and humanities research with a focus on emerging issues pertaining to the social and behavioural sciences as well as the humanities, particularly in the Asia Pacific region. It is published four times a year in **March**, **June**, **September** and **December**.

## Why should you publish in *Pertanika* Journals?

### Benefits to Authors

**PROFILE:** Our journals are circulated in large numbers all over Malaysia, and beyond in Southeast Asia. Recently, we have widened our circulation to other overseas countries as well. We will ensure that your work reaches the widest possible audience in print and online, through our wide publicity campaigns held frequently, and through our constantly developing electronic initiatives via Pertanika online submission system backed by Thomson Reuters.

**QUALITY:** Our journals' reputation for quality is unsurpassed ensuring that the originality, authority and accuracy of your work will be fully recognised. Each manuscript submitted to Pertanika undergoes a rigid **originality check**. Our double-blind peer refereeing procedures are fair and open, and we aim to help authors develop and improve their work. *Pertanika* JTAS is now over 33 years old; this accumulated knowledge has resulted in Pertanika being indexed in SCOPUS (Elsevier), EBSCO, DOAJ, CABI and AGRICOLA.

**AUTHOR SERVICES:** We provide a rapid response service to all our authors, with dedicated support staff for each journal, and a point of contact throughout the refereeing and production processes. Our aim is to ensure that the production process is as smooth as possible, is borne out by the high number of authors who publish with us again and again.

**LAG TIME:** Submissions are guaranteed to receive a decision within **14 weeks**. The elapsed time from submission to publication for the articles averages 5-6 months. A decision of acceptance of a manuscript is reached in 3 to 4 months (average 14 weeks).


## Call for Papers

*Pertanika* invites you to explore frontiers from all fields of science and technology to social sciences and humanities. You may contribute your scientific work for publishing in UPM's hallmark journals either as a regular article, short communication, or a review article in our forthcoming issues. Papers submitted to this journal must contain original results and must not be submitted elsewhere while being evaluated for the *Pertanika* Journals.

Submissions in English should be accompanied by an abstract not exceeding 300 words. Your manuscript should be no more than 6,000 words or 10-12 printed pages, including notes and abstract. Submissions should conform to the *Pertanika* style, which is available at www.pertanika.upm.edu.my or by mail or email upon request.

Papers should be double-spaced 12 point type (Times New Roman fonts preferred). The first page should include the title of the article but no author information. Page 2 should repeat the title of the article together with the names and contact information of the corresponding author as well as all the other authors. Page 3 should contain the title of the paper and abstract only. Page 4 and subsequent pages to have the text - Acknowledgments - References - Tables - Legends to figures – Figures, etc.

Questions regarding submissions should only be directed to the Executive Editor, *Pertanika* Journals.

Remember, *Pertanika* is the resource to support you in strengthening research and research management capacity.

**An Award Winning International- Malaysian Journal**

FEB 2008

*Mail your submissions to:*

The Executive Editor
Pertanika Journals, UPM Press
Office of the DVC (R&I)
IDEA Tower II, UPM-MTDC Technology Centre
Universiti Putra Malaysia
43400 UPM, Serdang, Selangor
Malaysia

Tel: +6 03 8947 1622

ndeeps@admin.upm.edu.my
www.pertanika.upm.edu.my

***Pertanika* is Indexed in SCOPUS, EBSCO & DOAJ**

**Case Report**



**Selected Articles from World Engineering Congress 2010: Natural Resources and Green Technology**





**Selected Articles from UPM-Malaysian Nuclear Agency Symposium 2011**

Pertanika Journal of Science & Technology
Vol. 20 (2) Jul. 2012

## Contents



**Research Management Centre (RMC)**
1st Floor, IDEA Tower II
UPM-MTDC Technology Centre
Universiti Putra Malaysia
43400 UPM Serdang
Selangor Darul Ehsan
Malaysia

http://www.rmc.upm.edu.my
E-mail : ndeeps@admin.upm.edu.my
Tel : +603 8947 1622 /1620

**UPM Press**
Universiti Putra Malaysia
43400 UPM Serdang
Selangor Darul Ehsan
Malaysia

http://penerbit.upm.edu.my
E-mail : penerbit@putra.upm.edu.my
Tel : +603 8946 8855/8854
Fax : +603 8941 6172

ISSN 0128-7680
07
9 770128 768083